

# Development of high-throughput screening methods and their application to a *C. elegans* model of alpha-1 antitrypsin deficiency

Anwen Elinor Brown

A thesis submitted in partial fulfilment of the requirements for the degree of:

Doctor of Philosophy of  
University College London

2018

Primary supervisor: Professor David Lomas  
Secondary supervisor: Professor David Sattelle

I, Anwen Brown, confirm that the work presented in this thesis is my own. Where information has been derived from other sources, or work undertaken by anyone other than myself, I confirm that this has been indicated in the thesis.

## Acknowledgements

I could not have asked for a more excellent supervisory team than Professor David Lomas and Professor David Sattelle. David Lomas' positive and optimistic outlook as well as his rigorous approach to research sets the tone for the group and creates a productive working environment that is also a very happy one. Although he is surely one of the busiest people at UCL, he never fails to make time for members of the group and has certainly steered my project through some difficult times. I would first like to thank David Sattelle for his invaluable advice in preparing this thesis. His scientific knowledge and insight is as inspiring as it is constructive and his fascinating anecdotes and recalling of lyrics kept me well entertained along the way. I would also like to thank him for his continual day-to-day support over the last three years, his kindness and eagerness to help is something I will never forget. Thank you for reminding me on more than one occasion that 'all shall be well'. I am also incredibly grateful for the hard work and constant guidance of Dr Freddie Partridge, without whom this project would not have been possible. He has patiently taught me so much over the time that we have worked together; a time that has been as rewarding as it has been enjoyable. I will certainly miss our brainstorming and wild hypothesising sessions.

In addition to excellent supervision, I was fortunate to be part of a research group consisting of great colleagues who evolved into wonderful friends. I would like to particularly thank Dr James Irving for his helpful advice and his ability to answer almost any question posed to him, Dr Riccardo Ronzoni for his precise practical advice and for some excellent tiramisus, and Dr Nina Heyer-Chauhan for her hard work keeping the lab running and taking care of us on a day-to-day basis. An enormous thanks has to go to Emma Elliston and Alistair Jagger, two of the best colleagues and friends I could have imagined meeting during my time at UCL. They have been there from day one with constant encouragement, advice and a lot of laughter. Thank you, Alistair for that first falcon tube on my first day in the lab, for saying it like it is and for

always staying for one more. Thank you, Emma for inspiring me, caring about whatever's going on in and out of the lab and for being the best co-social rep CRB has ever seen. Thank you to all the other lab members over the three years, particularly Jing He who was instrumental in helping to set up the RNAi screen and was a great pleasure to work with. I would also like to thank the wider UCL Respiratory group for a truly supportive and pleasant working environment, with special thanks to Dr Manuela Plate and Greg Contento for their help setting up the qPCR experiments.

Aside from the support I have gratefully received from colleagues at UCL, neither this PhD nor any of my education would have been possible without the continual guidance, financial help and love from my wonderful family. Thank you to Mam, for your un-ending emotional support and for being proud of me whatever I do; Dad, am dy gymorth TG ac am fod yn barod i wneud bron unrhywbeth drosto fi; and Eleri, for being the loveliest sister and best friend anyone could ever ask for, your positivity and care know no bounds. Grandma and Grandad, thank you for your generosity, for helping me with somewhere to live and for your constant words of encouragement.

A special thanks must also go to Lewis Brayshaw, who is a continual source of energy, optimism and strength in my life. Thank you for being there for every up and down of this PhD and helping with either a celebration or a plan of action at the appropriate time.

Lastly, I would like to thank the Rosetrees Trust for their generous support of this work. I am also very grateful to Mrs Jenny Arrow for helping to fund my project in memory of her husband, Mr Tony Arrow. I hope that in some way this work will contribute to the field of AATD research and advance insight into the disease.

## Abstract

Alpha-1 antitrypsin deficiency (AATD) is a genetic disorder which involves the toxic aggregation of misfolded mutant alpha-1 antitrypsin (AAT) protein, within the endoplasmic reticulum of hepatocytes, where it is synthesised. AAT is a protease inhibitor, which regulates lung tissue turnover. Loss of AAT protection in the lung leads to pulmonary disease (COPD and emphysema), and accumulation of mutant AAT in the liver can lead to inflammation, cirrhosis and hepatocellular carcinoma. Current treatments are limited to liver transplantation and symptomatic relief, meaning there is an urgent need for novel therapies. This thesis study aimed to recapitulate the liver component of AATD in the genetic model organism *C. elegans*. The transgenic worm expressed the mutant form of the protein (ZAAT) in the muscle, which gave rise to a growth/motility deficient phenotype. The mutant phenotype was characterised using the in-house automated high-throughput imaging system INVertebrate Automated Phenotyping Platform (INVAPP). The capabilities of this system as a high-throughput screening tool are illustrated using nematode growth and motility and by screening of an open source (Pathogen Box) small molecule library on *C. elegans*. Hits included auranofin, currently indicated for rheumatoid arthritis, isradipine and tolfenpyrad.

The powerful combination of the worm model of AATD displaying a growth/motility deficient phenotype and the ability to quantify this phenotype using the INVAPP imaging system allowed the development of high-throughput screening protocols to search for novel modifiers of AATD. Three such screens were developed and carried out in this study. A drug library screen was undertaken to search for small molecules which rescue the transgenic worm movement deficiency phenotype. A high-throughput genome-wide RNAi screen was performed for 2 of the 6 chromosomes of *C. elegans*. A chemically-induced forward genetic screen was also undertaken to search for novel genetic modifiers of the mutant phenotype. Preliminary hits from the screens were investigated and validated for their relevance to AATD.

## Impact statement

The work presented in this thesis study includes demonstrating the capabilities of a novel high-throughput nematode imaging system, characterising a newly generated *C. elegans* model of alpha-1 antitrypsin deficiency (AATD) and developing and performing three new screening strategies on the worm model of AATD to search for chemical and genetic modifiers of disease.

The applications of the novel high-throughput imaging system, INVertebrate Automated Phenotyping Platform (INVAPP) are two-fold. First, its use in screening of nematodes for new anthelmintic compounds was demonstrated by screening an open source library of small molecules and identifying compounds with such properties. Parasitic nematodes infect hundreds of millions of people and their livestock worldwide, therefore a system which is able to screen for anti-parasitic compounds rapidly is likely to prove extremely useful in drug discovery for these often neglected tropical diseases. Secondly, its use in chemical and genetic screening on nematode models of human disease could prove extremely valuable in the search for new therapies. Diseases which have been modelled in *C. elegans* include Parkinson's disease, spinal muscular atrophy, Huntington's disease and Alzheimer's disease. Phenotypic screening of worm models of disease has proved fruitful in bringing treatments to clinical trials, thus the high-throughput nature of INVAPP provides a valuable opportunity to broaden the scope and speed up the search for novel modifiers of disease. Indeed, there has already been considerable industrial interest in using the imaging system to test compounds on nematode models of human disease, which could result in an advantageous collaboration between the research group and a large pharmaceutical company. A scientific article outlining the capabilities of INVAPP has also been published in the International Journal of Parasitology, Drugs and Drug Resistance (2018) 8(1):8-21.

The full characterisation of a new *C. elegans* model of AATD offers great potential in elucidating key disease mechanisms and contributing to the wider research area of protein misfolding diseases. Such a model could also prove useful in the quest for the identification of small molecules or candidate drug targets with the potential to ameliorate disease. The development of three screening methods including a small molecule screen, a whole genome RNAi knock down screen and a forward mutagenesis screen using the worm model of AATD, provides the platform from which it is possible to discover such novel chemical or genetic modifiers of disease. Modifiers could then be evaluated for their clinical relevance and, where appropriate, be taken forward for testing in higher order animals or potentially in humans. Additionally, small molecules identified from *in vitro* screening or designed based on structural information from the alpha-1 antitrypsin protein can be rapidly tested on the *C. elegans* model of AATD. This facilitates the acquisition of *in vivo* data with relative ease and at low cost compared with often challenging mouse experiments. Taken together, the development of INVAPP, the *C. elegans* model of AATD and three screening strategies could (a) expand our understanding of this and other diseases, and (b) lead to the discovery of novel therapies for AATD, other diseases and the control of pathogens.

## List of associated publications

2,4-Diaminothieno[3,2-d]pyrimidines, a new class of anthelmintic with activity against adult and egg stages of whipworm.

Partridge FA, Forman R, Willis NJ, Bataille CJR, Murphy EA, Brown AE, Heyer-Chauhan N, Marinić B, Sowood DJC, Wynne GM, Else KJ, Russell AJ, Sattelle DB.

*PLoS Negl Trop Dis.* (2018) **12**(7)

An automated high-throughput system for phenotypic screening of chemical libraries on *C. elegans* and parasitic nematodes.

Partridge FA, Brown AE, Buckingham SD, Willis NJ, Wynne GM, Forman R, Else KJ, Morrison AA, Matthews JB, Russell AJ, Lomas DA, Sattelle DB.

*Int J Parasitol Drugs Drug Resist.* (2018) **8**(1): 8-21

Electrophoresis- and FRET-Based Measures of Serpin Polymerization.

Faull SV, Brown AE, Haq I, Irving JA.

*Methods Mol Biol.* (2017) **1639**: 235-248

# Contents

Abbreviations .....	15
Chapter 1 Introduction .....	16
1.1 The serine protease inhibitors and alpha-1 antitrypsin (AAT).....	16
1.2 The structure and inhibitory mechanisms of AAT .....	17
1.3 AAT polymerisation underpins alpha-1 antitrypsin deficiency.....	18
1.4 Pathology of AATD .....	21
1.5 Current treatment strategies for AATD .....	23
1.6 Molecular pathways involved in polymer accumulation .....	24
1.6.1 ERAD and UPR.....	24
1.6.2 The ER overload response.....	26
1.7 Modelling the disease AATD .....	27
1.7.1 Cellular models of AATD .....	27
1.7.2 Yeast models of AATD .....	28
1.7.3 A <i>Drosophila</i> model of familial encephalopathy with neuroserpin inclusion bodies (FENIB): a serpinopathy. ....	29
1.7.4 Murine models of AATD.....	30
1.7.5 <i>C. elegans</i> as a model organism.....	31
1.7.6 A <i>C. elegans</i> model of FENIB .....	34
1.7.7 <i>C. elegans</i> as a model of AATD.....	35
1.8 Pathways and challenges to therapies for AATD .....	37
1.8.1 Improving ZAAT folding and trafficking .....	37
1.8.2 Enhancing degradation of ZAAT polymers.....	40
1.8.3 <i>SERPINA1</i> silencing.....	40
1.8.4 Gene therapy .....	41
1.8.5 Cell therapy .....	42
1.8.6 Hypothesis.....	43
1.8.7 Aims.....	43
Chapter 2 Methods .....	45
2.1 Preparation of NGM plates .....	45
2.2 Preparation of bacterial food supply .....	45
2.3 Preparation of <i>C. elegans</i> liquid culture .....	46
2.4 Synchronisation of <i>C. elegans</i> cultures .....	46
2.5 <i>C. elegans</i> cultured in 96-well plates .....	46
2.6 Temperature shift of ZAAT <i>C. elegans</i> cultures .....	47

2.7 Crossing in mutant <i>C. elegans</i> strains to the transgenic ZAAT strain ( <i>rrf-3, fem-1</i> ) .....	47
2.8 Testing drugs/drug screen .....	48
2.9 Single worm PCR .....	49
2.10 DNA gel electrophoresis .....	50
Chapter 3 Development and validation of a novel high-throughput screening system, INVAPP/Paragon .....	51
3.1 Introduction .....	51
3.1.1 Phenotypic and target-based screening .....	51
3.1.2 Large-scale phenotypic screening with <i>C. elegans</i> .....	53
3.1.3 Automated systems for phenotypic screening of models of parasites and human disease .....	53
3.1.4 Developing a new robust motility/growth quantification system focussed on rapid, high-throughput chemical screening .....	55
3.2 Aims.....	55
3.3 Methods .....	56
3.3.1 INVAPP/Paragon system .....	56
3.3.2 <i>Caenorhabditis elegans</i> motility and growth assays.....	56
3.3.3 Pathogen box screening.....	57
3.4 Results.....	58
3.4.1 INVAPP/Paragon: a high throughput assay for quantifying nematode motility and growth.....	58
3.4.2 Validation of the INVAPP / Paragon system using existing commercial anthelmintic standards.....	61
3.4.3 Screening the Pathogen Box for compounds that affect <i>C. elegans</i> growth.....	64
3.4.4 Identification of known anthelmintic compounds by screening the Pathogen Box library in the <i>C. elegans</i> growth assay .....	65
3.4.5 Novel anthelmintics that block <i>C. elegans</i> growth .....	68
3.5 Discussion.....	71
3.5.1 A novel high-throughput imaging system for large-scale high-throughput screening .....	71
3.5.2 The imaging system was validated by screening The Pathogen Box library of compounds .....	73
3.5.3 Applications of INVAPP/Paragon to <i>C. elegans</i> models of human disease.....	75
Chapter 4 Characterisation of a novel <i>C. elegans</i> model of AATD expressing ZAAT .....	76
4.1 Introduction .....	76
4.1.1 The transformation of <i>C. elegans</i> to model human disease.....	76
4.1.2 The advantages of scorable mutant phenotypes .....	77
4.1.3 Transgenic <i>C. elegans</i> models of protein accumulation diseases.....	78

4.1.4 Limitations of <i>C. elegans</i> models of human disease .....	80
4.2 Aims.....	80
4.3 Methods .....	81
4.3.1 Purifying and polymerising human plasma derived AAT .....	81
4.3.2 Purification of mAbs from media.....	82
4.3.3 Polyacrylamide gel electrophoresis .....	82
4.3.4 <i>C. elegans</i> lysis to isolate ZAAT protein .....	83
4.3.5 Western blot analysis.....	84
4.3.6 Sandwich ELISA .....	84
4.3.7 RNAi targeting the ZAAT transgene .....	85
4.4 Results.....	86
4.4.1 Generation of novel transgenic ZAAT-expressing <i>C. elegans</i> strains.....	86
4.4.2 ZAAT transgenic <i>C. elegans</i> accumulate more ZAAT protein at higher temperatures .....	87
4.4.3 Purifying and polymerising ZAAT from human plasma for <i>in vitro</i> studies .....	88
4.4.4 ZAAT expressed by the transgenic <i>C. elegans</i> worms is recognised by a polyclonal anti-AAT antibody .....	91
4.4.5 Quantification of total and polymeric ZAAT protein within the transgenic ZAAT-expressing <i>C. elegans</i> strain .....	92
4.4.6 ZAAT transgenic <i>C. elegans</i> display growth and developmental impairment when cultured at higher temperatures .....	94
4.4.7 The motility of ZAAT transgenic <i>C. elegans</i> can be quantified and is temperature-dependent.....	96
4.4.8 A separately integrated transgenic <i>C. elegans</i> strain, Z10fem also displays temperature-dependent movement deficit .....	98
4.4.9 Attempting to knock down the ZAAT transgene by RNAi.....	100
4.4.10 Confirmation that the motility-deficient phenotype was the result of transgene expression by qPCR .....	103
4.5 Discussion.....	105
4.5.1 A newly generated transgenic <i>C. elegans</i> model of AATD.....	105
4.5.2 The temperature-dependent effects and the molecular basis of toxicity.....	107
4.5.3 The ZAAT worm strain motility deficiency is screenable and has good potential for use in high-throughput screening.....	108
Chapter 5 Development of a small molecule screen using the <i>C. elegans</i> ZAAT strain.....	110
5.1 Introduction .....	110
5.1.1 <i>C. elegans</i> and small molecule treatments .....	110
5.1.2 The development of small molecule screening using <i>C. elegans</i> .....	111

5.1.3 The successes of small molecule screening using <i>C. elegans</i> models of human disease .....	112
5.1.4 Previous small molecule screening on a <i>C. elegans</i> model of AATD .....	114
5.2 Aims.....	114
5.3 Results.....	115
5.3.1 Seeding the correct amount of <i>E. coli</i> to each well is important for worm culture and imaging.....	115
5.3.2 The time point at which the temperature of ZAAT worm culture is changed affects motility .....	116
5.3.3 The presence of progeny in the well affects the environment of the well but does not affect the movement index .....	118
5.3.4 Crossing <i>fem-1</i> strain into the ZAAT-expressing <i>C. elegans</i> strain.....	120
5.3.5 Temperature selection for the screen .....	121
5.3.6 The screen was performed robustly, however no small molecule hits were detected .....	121
5.4 Discussion.....	123
5.4.1 The development of the small molecule screen.....	123
5.4.2 The small molecule screen failed to detect any hit compounds but has potential for use in a larger-scale screen of a bigger library.....	125
Chapter 6 Whole genome RNAi screening on the transgenic ZAAT <i>C. elegans</i> strain.....	127
6.1 Introduction .....	127
6.1.1 Reverse mutagenesis .....	127
6.1.2 Mechanisms of RNAi: Exploiting endogenous RNAi pathways .....	127
6.1.3 Mechanisms of RNAi: Systemic and heritable RNAi .....	129
6.1.4 Methods of RNAi in <i>C. elegans</i> .....	130
6.1.5 RNAi as a whole genome screening method .....	131
6.2 Aims.....	133
6.3 Methods .....	134
6.3.1 RNAi screen .....	134
6.4 Results.....	136
6.4.1 Crossing in <i>rrf-3</i> .....	136
6.4.2 Z3RF displays a decrease in growth/motility when cultured at higher temperatures .....	138
6.4.3 RNAi feeding protocol method development.....	139
6.4.4 Confirmation of functional RNAi by the detection of dumpy phenotype worms in the screen.....	139
6.4.5 The primary RNAi screen of <i>C. elegans</i> chromosomes I and II identified a number hit genes .....	140

6.4.6 Analysis of the hit genes from the RNAi screen did not reveal any common pathways but did reveal a set of genes with gene ontology terms enriched against the background of chromosomes I and II.....	145
6.4.7 The correlation between hit genes from this RNAi screen and published RNAi screens of <i>C. elegans</i> models of AATD and other protein misfolding disease.....	151
6.4.8 Investigating human orthologs for the improving and worsening hit genes.....	152
6.4.9 Predicting hit gene product biomolecular and chemical interactions.....	152
6.5 Discussion.....	156
6.5.1 Developing the novel high-throughput genome-wide RNAi screen .....	156
6.5.2 Hit genes from a primary screen of chromosomes I and II with the caveat of required re-screening .....	157
6.5.3 The originality of this whole genome RNAi screen and its future applications .....	160
Chapter 7 Forward mutagenesis using the transgenic ZAAT <i>C. elegans</i> strain .....	161
7.1 Introduction .....	161
7.1.1 Forward mutagenesis.....	161
7.1.2 Forward mutagenesis as a screening method .....	161
7.1.3 Forward mutagenesis screen design.....	162
7.1.4 Types of mutagenic agents suitable for use in large-scale genetic screening .....	164
7.1.5 Mapping the mutations .....	165
7.1.6 Forward mutagenesis screening using a <i>C. elegans</i> model of human disease .....	167
7.2 Aims.....	168
7.3 Methods .....	169
7.3.1 EMS mutagenesis.....	169
7.3.2 RT-qPCR.....	172
7.4 Results.....	174
7.4.1 Selected EMS mutants display an improved growth/motility phenotype at higher temperatures compared with Z AAT-expressing worms .....	174
7.4.2 EMS-induced mutant strains display a decrease in fluorescent ZAAT accumulation .....	175
7.4.3 Measuring ZAAT transgene expression in the candidate mutant strains .....	177
7.5 Discussion.....	182
7.5.1 The forward mutagenesis screening protocol for ZAAT worms was robust and capable of identifying mutants with an improved motility phenotype .....	182
7.5.2 Limitations of the forward screen.....	182
7.5.3 Future applications of the novel forward mutagenic screen on ZAAT-expressing <i>C. elegans</i> .....	184
Chapter 8 Final conclusions and future perspectives .....	185
8.1 The urgent need for novel treatments for AATD .....	185

8.2 The capabilities of the INVAPP/Paragon system for large scale chemical and genetic screening.....	185
8.3 A novel <i>C. elegans</i> model of AATD.....	186
8.4 Library-scale chemical screening of a <i>C. elegans</i> model of AATD.....	186
8.5 Genome-scale RNAi screening of a <i>C. elegans</i> model of AATD .....	187
8.6 A forward genetic screen applied to a <i>C. elegans</i> model of AATD .....	187
8.7 Cell and gene therapy for AATD.....	188
8.8 Conclusions .....	189
Bibliography .....	190
Supplementary Table 1 .....	211
Supplementary Table 2 .....	214
Supplementary Table 3 .....	215

## Abbreviations

2C1	Polymer-specific monoclonal antibody
3C11	Monomer and polymer-recognising monoclonal antibody
AAT	Alpha-1 antitrypsin
AATD	Alpha-1 antitrypsin deficiency
AD	Alzheimer's disease
COPD	Chronic obstructive pulmonary disease
CRISPR	Clustered regularly interspaced short palindromic repeats
ELISA	Enzyme-linked immunosorbent assay
EMS	Ethyl methanesulfonate
ER	Endoplasmic reticulum
ERAD	Endoplasmic reticulum-associated degradation
FENIB	Familial encephalopathy with neuroserpin inclusion bodies
FPS	Frames per second
GO	Gene ontology
GPCR	G-protein coupled receptor
GSEA	Gene set enrichment analysis
HD	Huntington's disease
hiPSCs	Human induced pluripotent stem cells
HSP	Heat shock protein
INVAPP	INVertebrate Automated Phenotyping Platform
IPTG	Isopropyl $\beta$ -D-1-thiogalactopyranoside
mAb	Monoclonal antibody
MMV	Medicine for Malaria Venture
MWCO	Molecular weight cut off
N2	Wild type <i>C. elegans</i>
NGM	Nematode growth medium
NHK	Null Hong Kong AAT variant
PAGE	Polyacrylamide gel electrophoresis
PBS	Phosphate buffered saline
PCR	Polymerase chain reaction
PD	Parkinson's disease
PDB	Protein data bank
RCL	Reactive centre loop
RFP	Red fluorescent protein
SDS	Sodium dodecyl sulphate
Serpin	Serine protease inhibitor
SMA	Spinal muscular atrophy
UPR	Unfolded protein response
UV	Ultraviolet

# Chapter 1 Introduction

## 1.1 The serine protease inhibitors and alpha-1 antitrypsin (AAT)

The serine protease inhibitor (serpin) superfamily is present in both eukaryotes and prokaryotes and consists of around 500 intracellular and extracellular proteins, with the majority acting as proteinase inhibitors [1]. Inhibitory serpins regulate complex biological cascades such as blood clotting (by thrombin and factor Xa), fibrinolysis (by plasminogen activator inhibitor-1) and inflammation (by alpha-1 antitrypsin, AAT) [2]. Non-inhibitory serpins include the endoplasmic reticulum (ER)-localised heat shock protein (HSP)47 [3] and cortisol-binding globulin, a hormone-transporting protein expressed in the liver [4].

AAT is the archetypal member of the serpin superfamily; its conserved structure, consisting of three  $\beta$ -sheets and nine  $\alpha$ -helices, allows it to inhibit a wide range of proteinases including trypsin, chymotrypsin, cathepsin G, plasmin, thrombin and plasminogen [5]; however its main physiological target is neutrophil elastase [6]. It is a 394 residue, 52KDa glycoprotein, encoded by the *SERPINA1* gene and produced predominantly in hepatocytes [7]. It is also present in lung [8] and gut [9] epithelia, neutrophils [10] and alveolar macrophages [11]. It is the most abundant circulating serpin; a normal healthy human produces more than 2g of AAT per day resulting in a serum concentration of approximately 2mg/ml [12]. AAT is expressed with a secretion tag containing hydrophobic residues therefore targeting it to the ER for folding and glycan addition prior to secretion [13].

Wild type (M)AAT is secreted from hepatocytes into the circulation [14], from where it enters the lung and performs its main antiprotease function. There, it regulates the proteolytic effects of neutrophil elastase, protecting pulmonary tissue from destruction due to excessive elastin degradation [6].

## 1.2 The structure and inhibitory mechanisms of AAT

The AAT molecule (shown in Figure 1.1) contains 9  $\alpha$ -helices (termed A-I) and 3  $\beta$ -sheets (termed A-C) with the large  $\beta$ -sheet A defining the front face of the molecule. Analogous to other serpins, AAT uses a suicide-trapping mechanism to inhibit enzymes as opposed to the simple non-covalent lock and key mechanism employed by other proteinase inhibitors [15]. The suicide-trapping mechanism requires the serpin to remain in a metastable 'active state' which is readily able to change conformation and allow the transfer of energy to the proteinase which traps the enzyme in a catalytically unfavourable conformation [16]. The transition from this active state to a more stable confirmation during the suicide inhibition demands a major conformational change involving the exposed reactive centre loop (RCL) and major  $\beta$ -sheet A; a feature common to most serpins [2].

In AAT, the exposed RCL allows the docking of neutrophil elastase. Cleavage of the RCL apical peptide bond follows. Elastase becomes covalently bound to the adjacent residue forming a covalent serpin-proteinase complex. AAT then switches from a stressed to a relaxed form, which modifies the configuration of the complex thereby translocating the elastase to the opposite pole of the AAT molecule [17]. Simultaneously, the cleaved reactive loop inserts as an extra central  $\beta$ -strand within an underlying  $\beta$ -pleated sheet (sheet A). This thermodynamically favourable conformational change traps and distorts the catalytic machinery of the enzyme, rendering it unable to regenerate [17] (Figure 1.2A). The protein-enzyme complex is cleared from the circulation by the liver via uptake by lipoprotein receptors on hepatocytes [18].

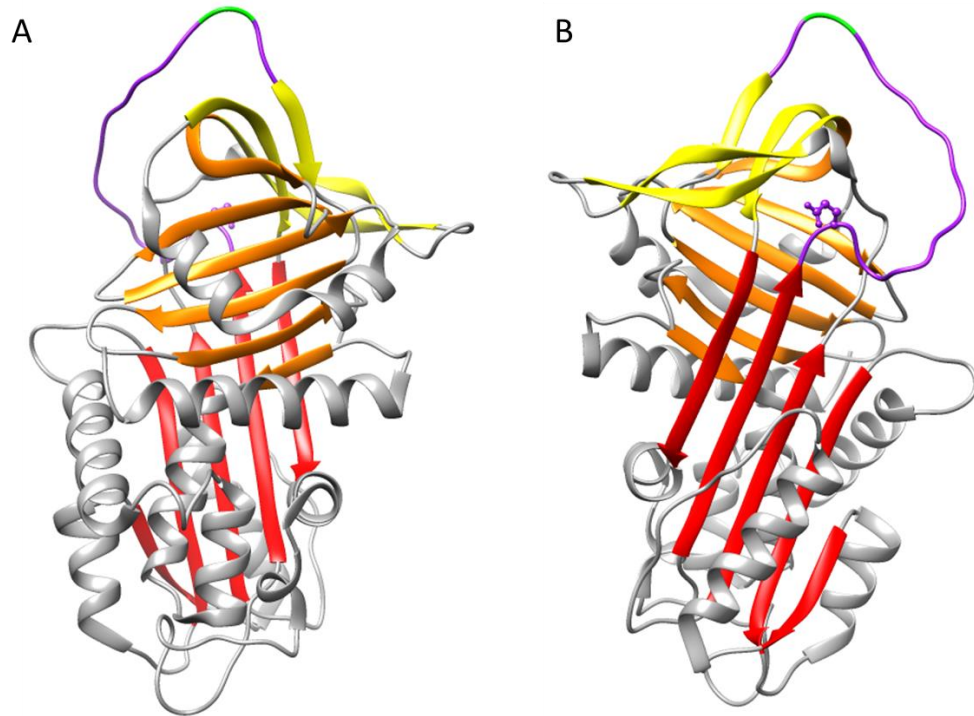


**Figure 1.1.** The structure of alpha-1 antitrypsin (AAT). (A) View from the back of the molecule. (B) View from the front of the molecule.  $\beta$ -sheets are shown in red, orange and yellow; the reactive centre loop is shown in purple with the cleavage site in green. The position of the Z mutation is represented by the ball and stick. The shutter region is the hydrophobic core of the protein located behind  $\beta$ -sheet A. Structure generated using the software Chimera [19] based on PDB structure 1QLP [20].

### 1.3 AAT polymerisation underpins alpha-1 antitrypsin deficiency

The serpinopathy alpha-1 antitrypsin deficiency (AATD) is caused by point mutations in the *SERPINA1* gene and is inherited in an autosomal recessive pattern. It was first described by Laurell and Eriksson (1963), who observed the absence of the alpha-1 band when visualising serum proteins by electrophoresis [21]. Presently, over 150 mutations in *SERPINA1* have been described. The most common disease-causing allele, a glutamate to lysine substitution at position 342, is termed Z. Most patients with severe AATD (>95%) are homozygous for the Z allele, a condition which affects approximately 1 in 1600 to 1 in 2000 individuals of Northern European descent [22, 23]. The Z mutation allows the insertion of the flexible RCL from one

AAT molecule into the  $\beta$ -sheet of another to produce ordered multimeric assemblies, termed polymers, via the transient formation of an unstable intermediate ( $M^*$ ) during the initial fast phase of polymerisation [24]. The ZAAT protein polymers accumulate as insoluble aggregates which are retained within the ER of hepatocytes in diastase-resistant inclusion bodies [25]. The mechanism of polymerisation is not fully understood, though three mechanisms have been proposed and are described in Figure 1.2 (B, C and D).

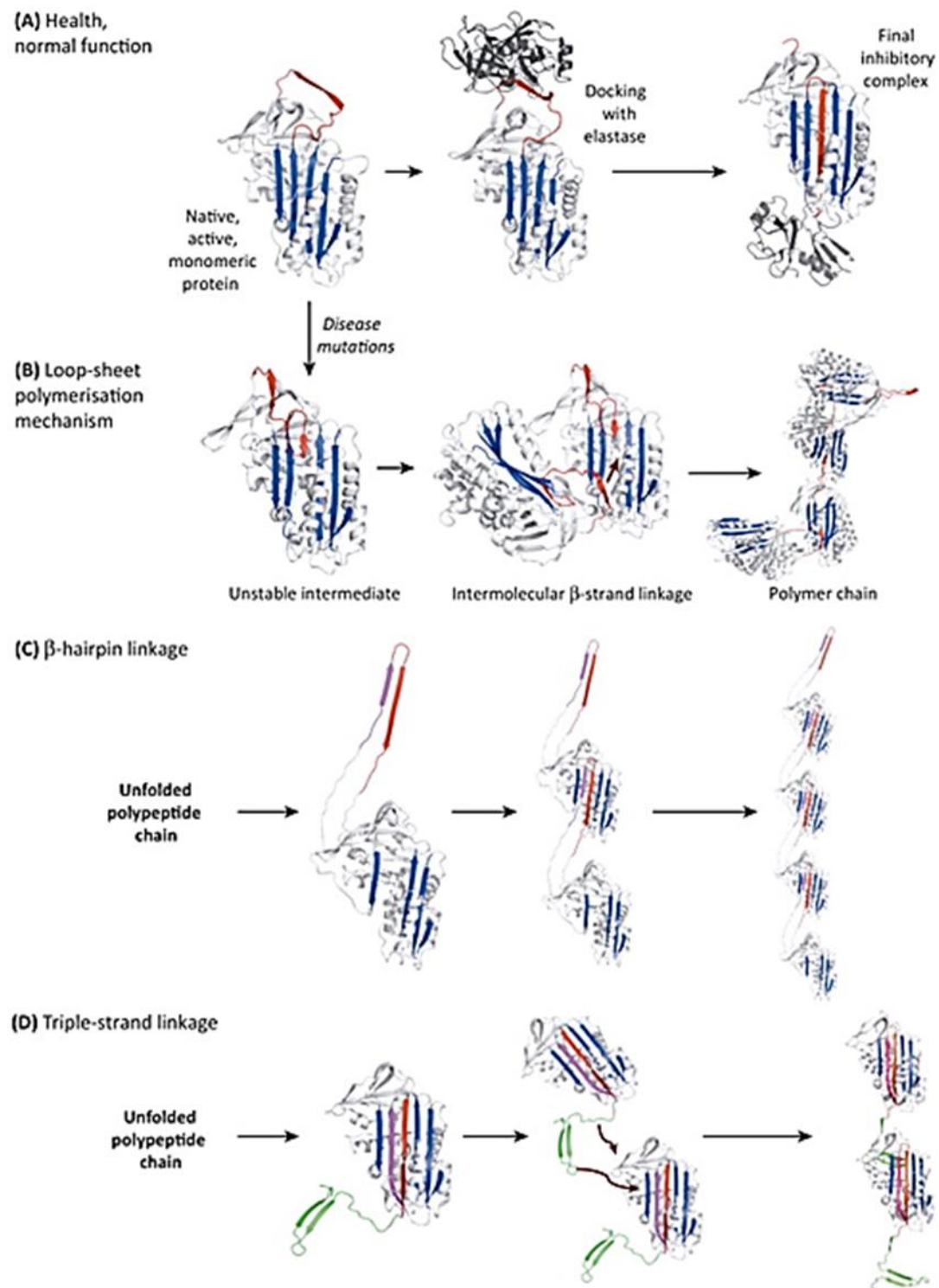


**Figure 1.2.** Structure and binding mechanisms of AAT. (A) The mechanism of AAT docking with elastase and the final inverted inhibitory complex. (B) The loop-sheet model of polymerisation suggests that the Z mutation in AAT results in the destabilisation of the top of  $\beta$ -sheet A causing the RCL to partially insert into this region. The change in overall structure makes it possible for the RCL of another AAT molecule to then insert into the lower section of the  $\beta$ -sheet [26]. (C) The beta-hairpin model is a domain swap mechanism between over 50 residues of strands 4A

and 5A. This swapping gives rise to a  $\beta$ -hairpin which is thought to insert into  $\beta$ -sheet A of another AAT molecule [27]. This mechanism is unlikely to underlie physiological polymer formation as it is not supported by electron micrograph images of polymer isolated from patients' livers [28]. (D) The C-terminal model. The intermolecular linkage involves three  $\beta$ -strands complementing  $\beta$ -sheets B and C and the expansion of  $\beta$ -sheet A to accept the RCL of another AAT molecule [29].  $\beta$ -sheet A is shown in blue and the reactive centre loop in red. Taken from Gooptu et al. (2014) [7].

Other mutations in the *SERPINA1* gene give rise to varying deficiencies of plasma AAT correlating with differing severity of disease. The S allele (Glu264Val) occurs in up to 1 in 5 Northern Europeans; S homozygotes display AAT levels approximately 60% of that of M homozygotes, though do not result in any significant clinical disease [30]. Three rarer mutations resulting in the most profound plasma deficiency and hepatic inclusions are Siiyama (Ser53Phe), Mmalton ( $\Delta$ Phe52) and King's (His334Asp) [31]. The Null Hong Kong (NHK) allele arises due to a frameshift mutation resulting in a premature stop codon at residue 334. This generates a truncated form of the protein, which is efficiently degraded in the ER. Plasma levels of AAT are consequently undetectable [32].

## 1.4 Pathology of AATD

The nature of AATD is that of a genetic "gain of function" and "loss of function" disorder. Polymer inclusion within the liver underlies the gain of function phenotype. Approximately 70% of mutant ZAAT is thought to be removed by ER-associated degradation (ERAD) [7], and approximately 10-15% folds correctly and is secreted; however, the remainder self-assembles into ordered polymers. An unknown portion of these are degraded by autophagy whereas the rest aggregate as inclusions within the ER [33]. ZAAT polymers which have been isolated from the hepatocytes of AATD patients, can be seen in Figure 1.3. The hepatotoxic polymer accumulation can cause neonatal hepatitis and predispose individuals to cirrhosis and

hepatocellular carcinoma [34]. Hepatocytes containing inclusion bodies are also more sensitive to exogenous factors, which increases cell death and limits regeneration [35]. Indeed, alcohol consumption and a high fat diet can greatly exacerbate the condition and worsen liver pathology.

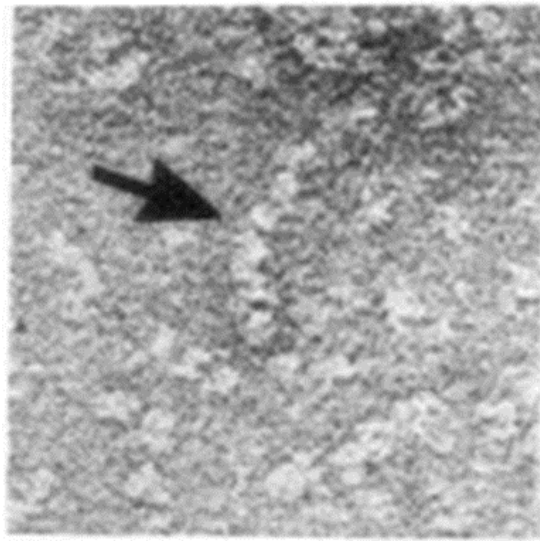


**Figure 1.3.** Polymeric ZAAT protein isolated from inclusion bodies from AATD patient hepatocytes visualised by negative stain imaging. Chains of protein polymers can be seen with their characteristic “beads-on-a-string” appearance [36]. Image adapted from Lomas et al. (1992) [25].

A decrease in circulating plasma and lung levels of functional monomeric AAT is key to the loss of function phenotype [37]. As a result of reduced anti-proteinase activity in the lung, damage to parenchyma is unregulated. Prolonged over-activity of neutrophil elastase leads to destruction of pulmonary connective tissue and loss of alveolar units. Consequently, patients commonly present with emphysema [21] or chronic obstructive pulmonary disease (COPD) [38]. The presence of pro-inflammatory polymers in the lung has also been detected by bronchoalveolar lavage [39]. Polymers in the lung have been shown to be chemotactic for neutrophils which mediate further inflammation [40]. Smoking also exacerbates pulmonary disease in AATD, due to the oxidation of key methionine residues to sulphoxides by hydrogen

peroxide, resulting in reduced anti-neutrophil elastase activity [41]. Patients with AATD are also affected by asthma, granulomatosis with polyangiitis and panniculitis [42].

## 1.5 Current treatment strategies for AATD

Currently, as there is no AATD-specific therapy, treatment of patients is aimed at controlling symptoms or treating the presenting condition e.g. emphysema or COPD regardless of the underlying cause [30]. Interventions can include smoking cessation to prevent disease progression [43], inhalation of bronchodilators and corticosteroids, vaccinations against influenza and pneumonia and oral corticosteroid and antibiotic use during periods of disease exacerbation. Lung volume reduction surgery can prove beneficial in some cases, although improvements in lung function and exercise capacity tend to be short term [44]. Lung transplantation is considered an option for individuals with end-stage emphysema; AATD patients accounted for 3.2% of lung transplants in 2009 in the International Society for Heart and Lung Transplantation Registry. Post-operative survival rates are comparable with patients who do not have AATD [30].

Given that a decrease in circulating functional AAT is the basis of lung disease associated with AATD, one therapy involves augmenting plasma protein levels via intravenous (IV) infusion of MAAT isolated from donor plasma. Weekly doses of 60mg/kg of MAAT are transfused into AATD patients to maintain plasma levels above a “protective threshold” of 80mg/dL [45]. AAT replacement therapy is only licensed in certain countries to prevent progression of lung disease and therapeutic preparations are available for example in the USA and Spain [46]. IV infusions of AAT are well tolerated with low levels of reported side effects, however unfortunately, there is limited evidence that replacement therapy in fact provides any clinical benefit to AATD patients [47]. Consequently, it is not offered as a therapy in the UK.

Liver and lung function of AATD patients is continually monitored and if severe cirrhosis has developed, liver transplantation is considered, and indeed is sometimes the only therapeutic

option [48]. AATD patients account for 1% of all adult liver transplants and 3% of paediatric liver transplants, with good survival rates comparable to those of general liver transplantation [49]. Interestingly, the transplanted liver continues to produce AAT levels of the donor [50], which can also result in the improvement in lung function by the effective control of pulmonary neutrophil elastase degradation [51].

## 1.6 Molecular pathways involved in polymer accumulation

### 1.6.1 ERAD and UPR

Normally, misfolded protein accumulated within the ER will activate the unfolded protein response (UPR), as is the case with the NHK variant of AAT [32]. The triggering mechanism of the UPR is disputed, however it is thought that increased levels of misfolded proteins sequester the heat shock protein-70 chaperone BiP away from the ER stress sensor molecules protein kinase R-like endoplasmic reticulum kinase (PERK), inositol requiring enzyme 1 (IRE1) and activating transcription factor 6 (ATF6), thus releasing them from an inhibitory interaction [52, 53]. The purpose of the UPR is to clear proteins which are already misfolded and prevent misfolding of newly synthesised ones. The UPR adaptive measures include transcription of ER chaperone genes to promote correct folding along with genes implicated in ER-associated degradation (ERAD) [54]. ERAD causes degradation of misfolded proteins via the ubiquitin-proteasome system. It involves retrotranslocation of the protein to the cytosol where the proteasome resides. Substrates of this process are selected based on their residence time within the ER; cycles of sugar moiety modifications identify proteins that have been retained in the ER too long. ER  $\alpha$ -1,2 mannosidase I (ERManI) trims mannose residues from N-glycan groups of AAT to trigger a signal for degradation [55]. A large proportion (around 70%) of mutant monomeric AAT is removed by ERAD (Figure 1.4). The rate of ZAAT folding is slower than that of M, potentially due to the point mutation, and so would be susceptible to a residence time-based ERAD mechanism [56]. Alternatively, the non-native conformation of the

intermediate protein prior to polymerisation could be targeted by ER quality control systems [28]. An unknown amount of polymerogenic AAT is degraded via autophagy [57], which is able to degrade much larger structures, such as polymers (Figure 1.4). Numerous autophagosomes were detected in mouse livers expressing ZAAT and in liver biopsies from AATD patients [58]. Protective degradation pathways are however not inexhaustible, and cells overwhelmed by misfolded ER proteins undergo the last resort of the UPR: apoptosis [59]. Indeed, the accumulation of ZAAT polymers has been shown to induce cell death [35].

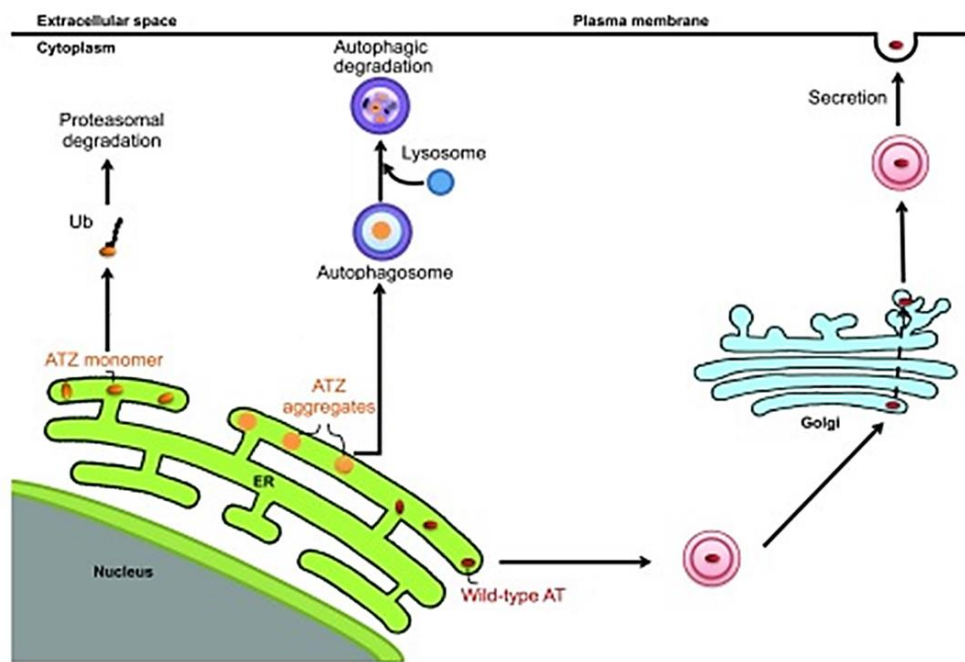


**Figure 1.4.** Secretion and degradation pathways of AAT. Wild type MAAT protein folds normally and efficiently traffics through the Golgi before secretion into the blood plasma. Soluble monomeric mutant ZAAT protein is secreted from the ER and is thought to be degraded by the proteasome via ERAD. Some polymeric mutant ZAAT protein is degraded via autophagy whereas the rest aggregates and accumulates within the ER. Figure adapted from Ghouse et al. (2014) [48]

Curiously, cell line and transgenic mouse studies have shown that accumulation of polymeric ZAAT in the ER is not associated with UPR activation [33]. In contrast, accumulation of

truncated, non-polymerogenic mutant AAT (e.g. NHK variant) in the ER does induce the UPR [60]. The fact that polymers are structurally ordered molecules rather than misfolded disorganised proteins could in part explain the lack of UPR activation, however further elucidation of the mechanism is required.

Retention of polymerogenic ZAAT alone is not sufficient to trigger the UPR, however the stress of a 'second hit' such as glucose depletion, tunicamycin or the presence of another misfolded protein causes hypersensitivity of cells to ER stress. This can in turn lead to a more marked UPR activation [61]. It has been shown in cell models and in ZAAT patient liver cells that the accumulation of polymerogenic ZAAT causes gross morphological changes to the structure of the ER [62]. However, the relationship between morphology and molecular mechanisms of ER stress and the UPR is not resolved. There is still much to be learned about the details of this 'second hit' phenomenon and its full repercussions on the cell.

### 1.6.2 The ER overload response

Some mutant forms of AAT such as the NHK allele do indeed cause ER stress, however, intriguingly, the Z polymeric form of AAT induces little or no ER stress. In the absence of ER stress and UPR activation, the build-up of misfolded protein within the ER leads to an event termed the ER-overload response. The ER-overload response is distinct from the UPR in that it occurs when misfolded proteins accumulate and distend the ER [63]. NF- $\kappa$ B is a hallmark of the ER-overload response and its constitutive activation has been observed in cell models of ZAAT ER-accumulation [61]. The mechanism by which NF- $\kappa$ B is activated is not known, however a pathway distinct from the UPR mediated by calcium has been implicated [63]. The ER-overload response ensues the release of the cytokines interlukin-6 (IL-6) and IL-8, both of which are known mediators of acute and chronic inflammation [61]. These pro-inflammatory cytokines could play a key role in the pathology of lung and liver damage in AATD, though the events leading to liver damage remain to be determined.

## 1.7 Modelling the disease AATD

### 1.7.1 Cellular models of AATD

The use of cellular models in AAT research has been informative with regard to polymer accumulation resulting from mutant forms of AAT. Utilising cell lines such as HEK, CHO or COS-7 transfected with M, Z or other disease-causing mutations has provided key information on degradation pathways involved in disease (as previously discussed), the mechanisms of cellular stress and potential injury and also on the kinetics of AAT synthesis and secretion [64]. Human induced pluripotent stem cells (hiPSCs) provide an excellent opportunity to model AATD on a cellular level as they allow the expression of proteins of interest from endogenous promoters. Fibroblasts isolated from the skin of AATD patients have been used to generate patient-specific hiPSC lines. The lines were differentiated into ‘hepatocyte-like cells’ using a novel protocol where pluripotency was initiated by a chemically defined medium containing olyvinyl alcohol, activin, FGF2, BMP-4 and a PI3K inhibitor. Differentiation was induced by incubation with growth factors and cytokines. The resulting cells were capable of albumin secretion and cytochrome P450 metabolism and recapitulated the key cellular feature of AATD: the aggregation of polymerised ZAAT within the ER [65]. The same study showed that the cells could be re-programmed to genetically correct the Z mutation [66]. Furthermore, when implanted into the livers of mice, the hiPSCs integrated into the organ and functioned as mature healthy human hepatocytes. Not only does this aid in the understanding of cell line-specific polymer accumulation and proteotoxicity, it also potentially paves the way to a personalised approach of novel cellular therapeutics [67]. However, the challenge with regards to hiPSCs as a potential therapy is to obtain cells that are more like the fully-differentiated hepatocyte and which are safe to use in humans [68].

### 1.7.2 Yeast models of AATD

A transgenic AATD model was created using the budding yeast, *Saccharomyces cerevisiae*, engineered to express human AAT protein [69]. The model implicated a role of the ERAD degradation pathway in the disposal of mutant ZAAT by implicating a process requiring the proteasome [70] and the hsp70 homologue BiP/Kar2p [71]. A forward genetic screen using the mutagenizing agent ethyl methane sulfonate (EMS) was performed using the yeast model of AATD to search for mutations resulting in defective ZAAT protein degradation. The screen involved a colony-blot immunoassay to identify mutant strains which accumulate high levels of ZAAT. The screen identified 30 mutants which were deficient in degradation [72]. One interesting mutant, *add3* was caused by a mutation in *VPS30/ATG6*, which encodes a component of a PI3K involved in the regulation of membrane trafficking and an essential role in autophagy [56]. Mutations in the autophagy specific PI3K gene, *ATG14* cause the accumulation of ZAAT aggregates within the ER and also constitutive activation of the UPR. Deletions in genes known to be involved in the UPR were tested in the same AAT colony-blot immunoassay screen and 6 additional mutants were identified in several genes not previously associated with protein degradation [73]. One such mutant implicated the protein *add66p*, a cytoplasmic protein that interacts with *Pba1p* and associates with proteasome precursors, facilitating the assembly and function of the proteasome [74]. *Add66p* and *ire1* deletion double mutants were found to be hypersensitive to the UPR-inducer dithiothreitol (DTT) [75]. Thus, both autophagy and the proteasome are implicated in ZAAT degradation.

A yeast screen, using cellular toxicity, instead of protein accumulation as a readout, addressed the question of how accumulation of ZAAT protein leads to cell damage and death. The *S. cerevisiae* genome-wide deletion library was screened to search for mutants which specifically restricted growth of ZAAT-expressing but not MAAT-expressing or empty vector control yeast [76]. Five out of the 31 genes identified in the screen had human orthologues. Some of the

genes were previously associated with AATD degradation, such as the ERAD-associated E3 ubiquitin ligase *HRD1*, known to aid clearance of misfolded ZAAT protein and hence protect against toxicity [77, 78]. The cellular protective roles of other genes, such as the mitochondrial ribosomal component, *MRPL1*, are not yet known, but could lead to the elucidation of novel mechanisms involved in cellular injury downstream of mutant ZAAT accumulation.

As valuable as cellular-based AATD models are, there are of course limitations with regard to recapitulating a disease, which affects multiple systems in a whole organism. The crucial involvement of other cell types, tissues and organs cannot be addressed fully using cell models of disease. This can pose problems when attempting to translate drug candidates identified from *in vitro* studies into efficacious *in vivo* therapies. Insights into drug toxicity, pharmacokinetics and pharmacodynamics cannot be derived from *in vitro* studies. In order to better represent AATD, the use of animal models of disease is crucial.

### 1.7.3 A *Drosophila* model of familial encephalopathy with neuroserpin inclusion bodies (FENIB): a serpinopathy.

FENIB is a serpinopathy that results in the intracellular accumulation of the protease inhibitor neuroserpin in inclusions known as Collin's bodies within neuronal cells [79]. It is an autosomal dominant dementia, where the aggregation of neuroserpin polymers causes neuronal cell death and results in cognitive deficits [80]. *Drosophila* was selected as a model organism for FENIB due to its close genetic orthology to humans, up to 70%, [81] as well as its fast and inexpensive culture in a laboratory setting. The relative ease of generating transgenic strains of *Drosophila* expressing human wild type and mutant serpins using the tissue-targeting GAL4-UAS system is a key advantage of the fruit fly [82]. Human serpins expressed in the fly eye or brain have given rise to distinct phenotypes which include degenerative behavioural changes, developmental deficits and biochemical irregularities. Deficits in climbing correlating with levels of accumulation of neuroserpin polymers in the eye and brain were observed after

eclosion. Interestingly, there was no observed difference in median survival of flies expressing wild type, mutant or control neuroserpin [83]. This model reported a correlation between polymer load and neurological disease *in vivo*; however, the subtlety of the climbing phenotype and *Drosophila* culture methods could limit its usefulness for high-throughput chemical and genetic screening. Another disadvantage to working with *Drosophila* is that mutant strains cannot be frozen and retrieved [84].

#### 1.7.4 Murine models of AATD

The first transgenic mouse expressing human ZAAT, known as the PiZ mouse, was generated in the late 1980's. It was created by cloning a 14.4kb fragment of DNA that codes for the human ZAAT gene with 2kb of flanking 3' and 5' genomic sequences into the germline of mice [85]. The mice were shown to synthesise human AAT in the liver, accumulate hepatic intracellular ZAAT polymer within the rough ER and secrete low levels of protein into the circulation; all features seen in the human disease state [86]. The mice also expressed high levels of human ZAAT in the kidney leading to the observation that the endogenous mouse gene is also expressed in the kidney [85].

The mouse is an attractive model organism for human disease studies due to its strong genetic and physiological overlap with humans. However, mice are very expensive to maintain, there are strict controls on using them for research purposes, their generation time and life span are long and they are not amenable to high-throughput genetic or chemical screens [87]. There are concerns over use of the PiZ mouse, as it contains multiple copies of the human gene in each cell. This overexpression of the mutant protein means it is an exaggerated model of polymer accumulation [88]. Liver disease in PiZ mice has been broadly characterised and has been found to recapitulate several features of human disease such as the development of fibrosis and hepatocellular carcinoma [35, 89, 90]. However, as mice express an endogenous murine AAT, they do not develop the pulmonary component of the disorder, making their use

limited to the study of liver disease in AATD. The mouse model has been valuable for a number of small molecule studies including the testing of autophagy-enhancing compounds for effects on hepatic fibrosis [91] as well as for gene therapy testing where mice were treated with viral vectors containing siRNAs to inhibit transcription or translation of the mutant gene [92].

A group led by Professor Christian Mueller recently resolved the problem of endogenous murine AAT activity inhibiting the study of lung disease associated with AATD in mouse models. Mice have five AAT genes, and the group succeeded in creating a quintuple mouse knock out of all five genes using Clustered Regularly Interspaced Palindromic Repeats/Cascade9 (CRISPR/Cas9)-mediated genome editing. CRISPR and CRISPR-associated (Cas9) genes function in adaptive immunity in select bacteria and archaea to protect against invading genetic material. The invading DNA is cut into fragments and is incorporated into a CRISPR locus. The loci are transcribed and processed to generate small RNAs which are used to guide effector endonucleases that target the invading DNA based on sequence complementarity [93]. The AAT-null mouse model phenotype included absent hepatic and circulating AAT which in turn resulted in pulmonary tissue destruction and emphysema due to unregulated damage by neutrophil elastase [94]. The recapitulation of the pulmonary component of the disorder in a mouse model paves the way for preclinical studies to ameliorate lung disease in AATD. Interestingly, the group is now turning its attention to developing a ferret model of AATD (funded by a New Foundation Grant). Ferrets only have one AAT gene and their lung physiology is more similar to that of a human. The collaboration involved Professor John Engelhardt who also developed a ferret model of cystic fibrosis [95].

### 1.7.5 *C. elegans* as a model organism

*Caenorhabditis elegans* (*C. elegans*) is a non-parasitic nematode worm found worldwide. It was chosen as a model for biological research in the early 1960's by Sydney Brenner [96]. *C. elegans* has been studied extensively with regard to its genetics and development. It was the

first complex eukaryote to have its genome sequenced and although each individual has only around 1000 cells, remarkably up to 80% of its genes have homologues in humans. The transparency of the worm has facilitated detailed studies of its anatomy (shown in Figure 1.5) and physiology and its complete cell lineage has been described [97]. It is the only complex organism for which the entire cell lineage is known. For this work, Horvitz, Sulston and Brenner were awarded The Nobel Prize in Physiology or Medicine in 2002. The nervous system of *C. elegans* is also the only one for which a complete synaptic wiring diagram is available [98] facilitating studies on neural signalling and nervous and neuromuscular disorders. Numerous biochemical signal transduction pathways are at least partially conserved between the worm and humans [99]; with some pathways highly conserved, such as the transforming growth factor- $\beta$  pathway (TGF- $\beta$ ) [100]. *C. elegans* are easy to culture and maintain in a laboratory setting, they have a rapid life cycle (approximately 3 days from egg to adult), a short lifespan (~20 days) and feed on bacteria (typically *E. coli* in a laboratory setting). Their small size (1mm) means ease of storage and a simple dissecting microscope is sufficient for visualisation. Their hermaphroditic reproduction, known as selfing, gives rise to genetically-identical progeny and mutant strains can be preserved and revived from freezing in glycerol; features facilitating genetic studies.

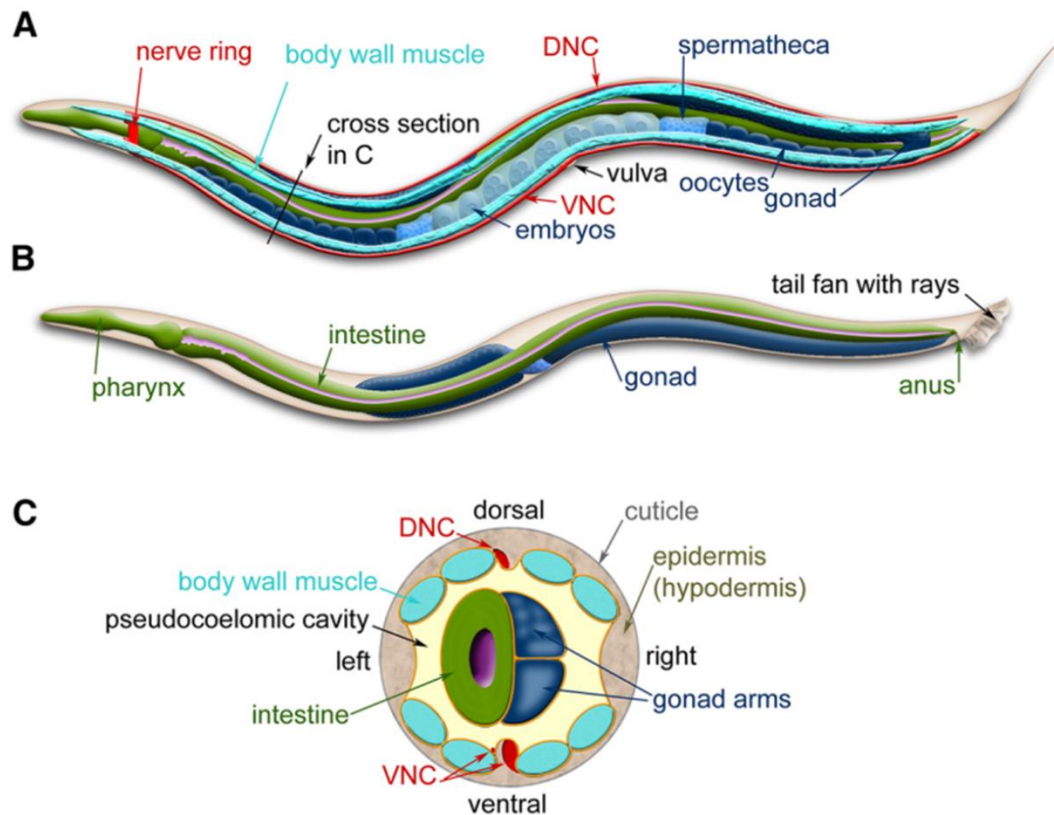


**Figure 1.5.** The anatomy of *C. elegans*. Major anatomical features of a hermaphrodite (A) and a male (B). (A) The dorsal nerve cord (DNC) and ventral nerve cord (VNC) span the entire length of the worm from the nerve ring. Worm body wall muscle runs along the length of the animal; two out of four muscle quadrants are shown. (B) The nervous system and muscles are not shown in this image; the intestinal system can be seen running all the way from the mouth (and pharynx) to the anus. (C) Cross-section through the anterior region of the *C. elegans* hermaphrodite (marked with a black line in A) showing the cuticle and epidermis surrounding the four muscle quadrants with the intestine and gonad residing within the pseudocoelomic cavity. Image taken from The WormBook [101].

The major attribute of the worm in the study of human disorders is the ease of which its genome can be manipulated. The creation of transgenic strains can reflect a host of disease states in an intact multicellular organism. Genetic changes can give rise to scorable phenotypes and behaviours which lend themselves to automated phenotyping technology [102, 103].

Worms can be treated with drugs or small molecules and this coupled with their other

attributes make them amenable to high-throughput compound screening. There are however limitations to using *C. elegans* as a molecular research tool and one such concern relates to its innate physical and enzymatic defences which allow for survival in the environment. The worm is somewhat inaccessible to some pharmacological molecules, meaning that high concentrations of drugs are often required to observe changes in phenotype [104]. However, it is possible to create strains, which have an increased permeability to small molecules [105]. Taken together, *C. elegans* is an organism of about the right level of complexity to provide molecular insight into multicellular life, and complemented by its ease of maintenance and use in a research setting, it is an excellent tool for modelling human disease.

### 1.7.6 A *C. elegans* model of FENIB

*C. elegans* has been used to study a large number of human diseases, including proteostasis mechanisms in protein misfolding and accumulation disorders [106]. One such disease is FENIB. In one study, a nematode model for FENIB was described where a homologous mutation of the endogenous *C. elegans* serpin, *srp-2* was expressed in the worm with the aim of capturing the ER proteotoxicity resulting from mutant neuroserpin accumulation [107]. The authors proposed that the accumulation occurs in the lumen of the ER and that it recapitulates phenotypic and biochemical features of the human disease, most notably, altered UPR signalling. However, this study was directly contradicted by claims that SRP-2 lacks an N-terminal signal peptide meaning it is instead a member of the intracellular serpin family. Using an ER-colocalisation marker and confocal imaging, it was suggested that wild type SRP-2 localised to the cytosol rather than the ER. It was also shown that an aggregation-prone *srp-2* mutant formed intracellular inclusions also in the cytosol [108]. Sequence analysis suggests that *srp-2* is not a functional homolog of neuroserpin and therefore *srp-2* mutants are not a suitable model for the proteotoxicity observed in FENIB. These studies highlight the

importance of caution in using endogenous genes and proteins to model human disease, as they may fail to recapitulate key biochemical mechanisms.

### 1.7.7 *C. elegans* as a model of AATD

The genetic tractability of *C. elegans* has allowed the elucidation of key information on biochemical pathways, cellular involvement and molecular interactions in AATD [109]. *C. elegans* lack an endogenous AAT serpin but do express nine intracellular serpin proteins, however only SRP-1, SRP-2, SRP-3, SRP-6 and SRP-7 are translated as full length proteins capable of protease inhibitory activity, with the rest transcribed as pseudogenes or non-inhibitory variants [108]. A *C. elegans* model of AATD has been generated, and transgenic worms have been shown to express wild type and mutant AAT in intestinal cells. The transgene is driven by the *nhx-2* promoter and contains an N-terminal signal peptide linked to GFP, cDNA of M or ZAAT and a pharyngeal RFP co-expression marker. The model expressing ZAAT was found to accumulate fluorescent spots indicating ZAAT aggregation within intestinal cell ER whereas the model expressing MAAT displayed diffuse cytoplasmic fluorescence suggesting that it had been secreted from the ER [109, 110]. ZAAT accumulation resulted in several worm deficiency phenotypes, including growth, brood and lifespan decrease when compared to wild type strains or strains expressing MAAT protein. Interestingly, the abnormal phenotypes had a temperature-dependent effect within the range 16-27°C, with greater penetrance at higher temperatures. The involvement of ERAD and autophagy in the degradation of ZAAT were implicated by knocking out components of each pathway in the worm model of AATD and observing changes in fluorescence accumulation [109].

Using these transgenic strains, large-scale screening was undertaken in order to search for modifiers of ZAAT fluorescent protein accumulation. Genome-wide RNAi screens have identified novel candidate drug targets and molecules which act on them (discussed further in chapter 6) [111] and drug screens have found novel hit molecules that modulate polymer

accumulation [110]. The drug screen identified two such compounds: fluphenazine and carbemazapine [112] which were further tested in mouse models of AATD, with carbamazepine currently being evaluated in a clinical trial.

This *C. elegans* model expressing mutant AAT has also been used to link stress and aging pathways with protein misfolding diseases, such as AATD. The aging component of conformational disease is thought to result from a progressive loss of ability to activate the UPR (or the heat shock response (HSR)) [113]. The insulin/insulin-like growth factor 1 signalling (IIS) pathway has been implicated in the regulation of cellular stress resistance and proteotoxicity associated with AATD, probably due to its influence on UPR, autophagy and ERAD. In the *C. elegans* model of AATD, reducing the IIS pathway was shown to significantly decrease misfolded AAT accumulation and led to reduced proteotoxicity as demonstrated by rescued mutant phenotypes. It was also shown by means of a cyclohexamide chase approach that the half-life of misfolded protein in *daf-2* (the major receptor in the IIS pathway) mutants was significantly shorter than in wild type worms. This enhanced protein clearance was not blocked by RNAi knockdown of autophagy or ERAD pathway components, suggesting that IIS might clear misfolded protein via an unidentified mechanism [109]. Reducing the IIS pathway results in the activation of three downstream transcription factors: DAF-16/FOXO, HSF-1 and SKN-1/NRF [114]. Hyperactivation of these factors can lead to resistance to stress, therefore small molecules which act on them could be useful in protein misfolding disorders such as AATD. The usefulness of this transgenic worm is unquestionable, however mutant and rescued phenotype evaluation relies solely on observable GFP signal as a measure of polymer accumulation. It provides little or no whole-organism functional read out.

*C. elegans* models of other mutant AAT variants were also generated, including two polymerogenic variants: Mmalton and Siiyama, which both possess mutations on helix B known to facilitate the mobility of the shutter region. Both mutations are associated with

hepatic inclusions, low plasma levels and polymer formation; however, Mmalton retains its inhibitory activity against neutrophil elastase. An S AAT variant *C. elegans* model was also generated. The S mutation is found in helix G and is associated with a reduction in plasma levels and inhibitory activity; it also forms polymers upon heating *in vitro*. Two null AAT variants were also expressed in worm models: the NHK and Saar alleles, which produce truncated proteins that are efficiently degraded and are associated with only deficiency phenotypes. All strains expressed the protein tagged with GFP in intestinal cells. The Mmalton and Siiyama variant worm models displayed fluorescent accumulation patterns comparable to that of the ZAAT-expressing strain. The S allele model displayed cytoplasmic fluorescence with some aggregation; however, neither the NHK nor the Saar variant worm models displayed any intracellular fluorescent protein accumulation. All variant strains displayed some phenotypic abnormalities such as slow growth, and the Siiyama and Mmalton models displayed shorter lifespans. Interestingly, the lifespans of S, Saar and NHK variant models were unaffected. Knock down assays of pathway components revealed a key role of ERAD in the degradation of AAT protein in all strains but of autophagy in only ZAAT, Mmalton and Siiyama, suggesting that autophagy is not involved in the degradation of S, Saar and NHK variants of AAT [115].

## 1.8 Pathways and challenges to therapies for AATD

### 1.8.1 Improving ZAAT folding and trafficking

A structure-based drug development approach has been employed where drug-like small molecules are designed to prevent polymerisation of the mutant ZAAT protein and theoretically improve its potential for secretion. These small molecules target a surface hydrophobic cavity in the ZAAT molecule for allosteric blockage of the conformational transition that underpins polymer formation. The cavity is open in the native molecule but is filled during the formation of the  $\beta$ -sheet linkages during polymerisation. Lead molecules were found to block AAT inhibitory function and prevent ZAAT polymerisation *in vitro* and

additionally increased clearance of ZAAT in cell models of AATD [116]. Peptides targeting the RCL of AAT have also been tested and were shown to increase the rate of secretion of ZAAT in a cell model of disease and to decrease the ZAAT-accumulation-dependent release of PERK-dependent NF- $\kappa$ B, IL-6, IL-8 and calnexin [117]. It is important to note however, that none of these small molecules have been tested on animal models of disease, and so their *in vivo* safety and clinical efficacy remain to be elucidated. Furthermore, designing small molecules which block polymerisation of ZAAT without affecting the inhibitory activity of the molecule, will be key to identifying a therapeutically-relevant treatment.

Chemical chaperones, which are thought to generally improve the intracellular folding environment and as a result allow the correction of cellular mislocalisation of certain mutant proteins, have been considered as a potential therapeutic class for AATD. Unlike pharmacological chaperones which bind and stabilise proteins in a substrate-specific way, chemical chaperones are able to facilitate the folding and trafficking of multiple misfolded proteins non-specifically [118]. Two such compounds, glycerol and 4-phenylbutyric acid (PBA), generated a substantial increase in the secretion of ZAAT in a cell model of AATD [119]. Oral administration of PBA also resulted in increased circulating levels of human ZAAT in a mouse model of AATD. However, a pilot study of ten patients with liver disease treated with PBA for 14 days did not result in increased serum levels of AAT [120]. The length of treatment duration or the need for prohibitively large doses of PBA were cited as potential reasons for this disappointing result. However, the promising cell and animal model data could mean that modified PBA formulations could improve treatment efficacy for patients.

More recently, a drug with similar chemical properties to PBA, suberoylanilide hydroxamic acid (SAHA), resulted in increased ZAAT secretion in two cell models of AATD. The mechanism was thought to occur by modulating a calnexin-sensitive proteostasis pathway via inhibition of the histone deacetylase HDAC7 [121]. SAHA has not yet been tested *in vivo* and indeed, there are

concerns over some of its other properties. It has been shown to cause a substantial increase in the synthesis of ZAAT through a transcriptional activation mechanism. It is therefore not known whether the increase in secretion is simply the result of increased synthesis. Therapeutic usefulness of SAHA is questionable, as a drug which causes an increase in ZAAT synthesis is likely to exacerbate mutant protein accumulation and resulting proteotoxicity.

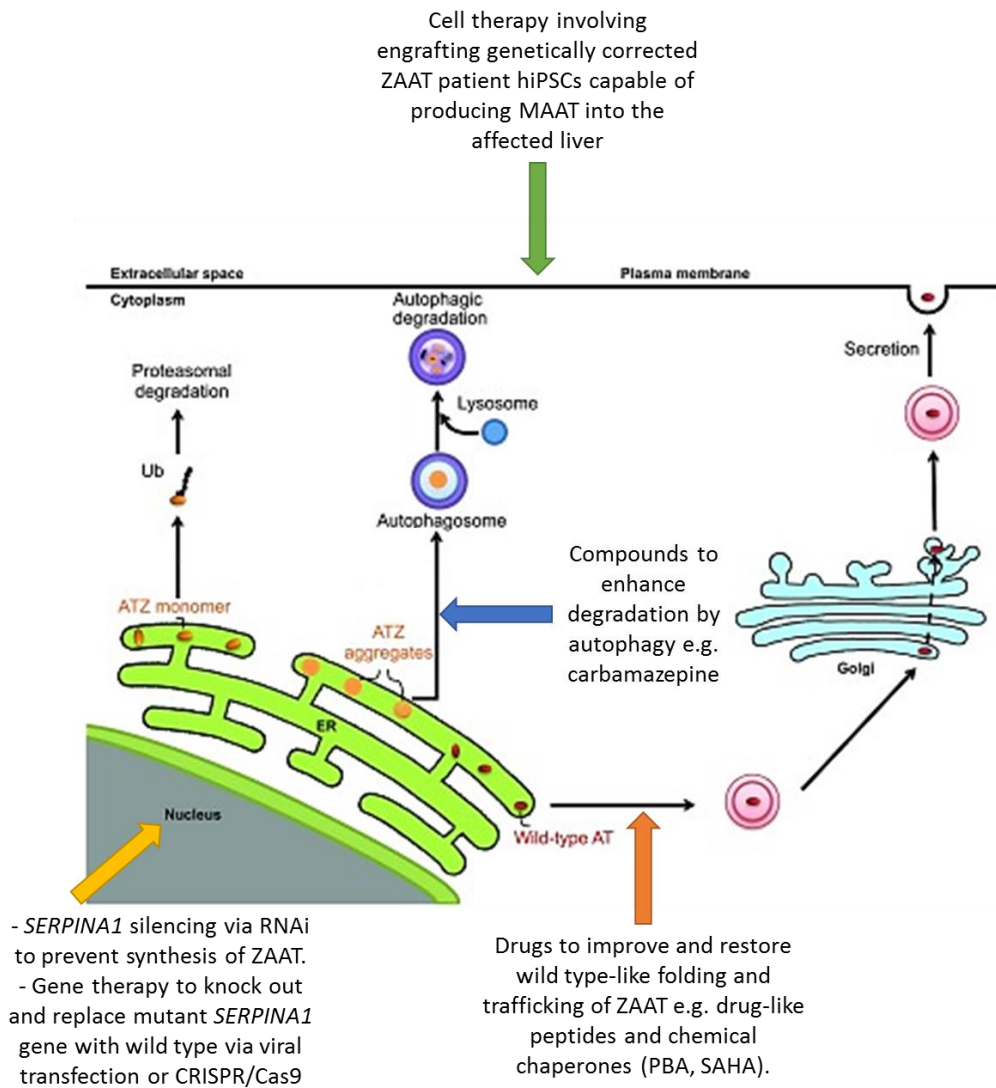


**Figure 1.6.** Possible therapeutic approaches in AATD indicated by arrows. (Yellow arrow) Targeting ZAAT transcription involves silencing the *SERPINA1* gene by use of siRNAs or replacing it with a wild type gene via gene therapy or CRISPR/Cas9. (Orange arrow) Use of small molecules aimed at improving the folding and trafficking of ZAAT include drug-like peptides and chemical chaperones. (Blue arrow) Increasing ZAAT polymer degradation via compounds which enhance autophagy, for example carbamazepine. (Green arrow) Replacement of diseased hepatocytes

for healthy ones. Cell therapy involves using AATD patient iPSCs corrected genetically to produce wild type MAAT. Cells are engrafted into diseased livers where they supersede the native liver and secrete functional MAAT. Figure modified from Ghouse et al. (2014) [48]

### 1.8.2 Enhancing degradation of ZAAT polymers

Autophagy is known to play a key role in the degradation of ZAAT polymers [57]; thus the targeting of autophagic pathways represents a novel strategy to treat the hepatic inclusions associated with liver disease. *In vitro* and mouse model studies have shown that enhanced macro-autophagy can lower the ZAAT hepatic polymer load and can also reduce liver injury [122, 123]. Drugs which are known to enhance autophagy such as: rapamycin, carbamazepine, along with a genetic approach used to augment the expression of key autophagy regulators, have been shown to reduce intracellular accumulation of ZAAT and consequent proteotoxicity in mouse and *C. elegans* models of AATD [91, 112, 124]. However, in some cases, large doses of the drugs were necessary to observe an effect. A phase II trial led by Professor David Perlmutter looking at the efficacy and safety of carbamazepine in patients with severe liver disease is due to end in 2020 (NIH, clinicaltrials.gov). The results will be of interest as it is possible that up-regulating a ubiquitous mechanism such as autophagy may have multiple off-target effects.

### 1.8.3 *SERPINA1* silencing

RNA interfering (RNAi) technology is being used as an approach to target the synthesis of mutant ZAAT in order to prevent the accumulation of toxic polymers within hepatocytes. A *SERPINA1* small interfering RNA (siRNA) delivered to the PiZ mouse model of AATD revealed complete reversal of liver injury associated with disease [125]. Alnylam Pharmaceuticals (Cambridge, Massachusetts, USA) undertook a phase I/II clinical trial to analyse the safety of an siRNA therapy called ALN-AAT which targeted ZAAT synthesis with the aim of ameliorating liver injury associated with AATD. Despite initially promising results, the trial was terminated in March 2018 due to the observation of asymptomatic, transiently elevated liver enzymes in a

subset of study individuals (NIH, clinicaltrials.gov). A major consideration with *SERPINA1* gene silencing therapies, is that it would prevent all AAT production, potentially improving liver disease but greatly exacerbating lung disease. In order to correct for this, siRNA therapy would have to be used in conjunction with another therapy such as gene therapy or augmentation therapy to ensure supplementation of circulating and pulmonary functional AAT. The recent FDA approval for Patisiran (Alnylam), an RNAi therapy for transthyretin or amyloidosis in 2018 lends confidence to the possibility of a safe efficacious RNAi therapy for AATD.

#### 1.8.4 Gene therapy

Gene therapy involves replacing defective or non-functional genes within a cell by transfection so that the treated cell consequently functions normally. Transfection vectors are usually of viral origin and commonly used strategies include retroviral, adenoviral and adeno-associated viral systems [126]. This type of treatment has the most potential for a genetic disease such as AATD, as it addresses both the gain-of-function and the loss-of-function components of AATD in order to ameliorate liver and lung disease. One study used an adeno-associated virus encoding a short-hairpin RNA to silence endogenous ZAAT gene expression together with a codon-optimised wild type MAAT transgene cassette to treat mouse models of AATD. Mutant ZAAT mRNA was reduced in the mouse liver and serum by 95%, effectively reversing liver pathology. Concurrently, a 13- to 30- fold increase in circulating MAAT was observed in the same mice [127]. Another study employed a recombinant adeno-associated viral vector encoding microRNA to silence endogenous ZAAT expression delivered alongside a microRNA-resistant wild type MAAT gene to treat the PiZ mouse model of AATD. Serum ZAAT levels were reduced by an average of 80% and knock down was also observed in the liver. Simultaneous increased levels of serum MAAT were again observed in the mouse models which also displayed improved liver profiles [92]. These results show the potential for gene therapy as a treatment for AATD, indeed one such therapy reached phase II in a trial [128], however

improvements to the design and delivery of the viral vectors were required to achieve therapeutic serum levels of MAAT.

More recently, CRISPR/Cas9 technology has been employed to correct the genetic mutation in the livers of mouse models of AATD. The CRISPR/Cas9 system is endogenous to bacterial strains and confers protection against invading viruses or plasmids. It constitutes one of the most powerful genome technologies currently available to researchers and has great potential for use in genetic disorders such as AATD. In one study, two adeno-associated viruses, one expressing Cas9 and another encoding an AAT guide RNA homology-directed repair template, were delivered to neonatal and adult PiZ mice. The treatment partially restored MAAT in the serum of the animals and sequencing showed the gene correction in hepatocytes [129]. Similar approaches have been employed by other groups and results appear promising, with gene correction resulting in improved liver pathology in mouse models of AATD [130, 131]. Gene therapy using CRISPR/Cas9 to correct the ZAAT mutation could indeed prove to be an exciting avenue of clinical research in the near future, though it is not without its challenges. Important concerns over off-targeting of genome editing at non-specific loci as well as large deletions and unknown repair mechanisms post-editing leading to further DNA damage need to be addressed before it is considered as a safe human therapy [132].

### 1.8.5 Cell therapy

Cell transplantation has been proposed as a potential therapy for AATD, as transplanted hepatocytes are able to repopulate a diseased liver. Interestingly, wild type MAAT-expressing donor hepatocytes transplanted into the liver of a transgenic mouse model of AATD replaced 20-98% of the mutant host hepatocytes. Repopulation was also accelerated by injection of an adeno-vector expressing hepatocyte growth factor [133]. Due to the proliferative advantage that the transplanted hepatocytes have over the native hepatocytes and indeed their ability to

supersede the endogenous liver, this type of cellular replacement therapy could prove a plausible therapeutic option to ameliorate lung and liver disease.

Another potential treatment opportunity for AATD could be a combination of gene-targeting and cell-based therapy. As previously discussed, hiPSCs from a patient homozygous for the ZAAT mutation were shown to be corrected by a combination of zinc-finger nucleases and transposon technology. The cells were then transplanted into the liver of a mouse model of AATD where they engrafted and functioned as normal MAAT-expressing hepatocytes [66]. This strategy could prove clinically beneficial in correcting the ZAAT mutation in patients if it could be adapted for human application. It would address both the liver and the lung components of the disease and would have the added advantage of not requiring patient immunosuppression [48].

### 1.8.6 Hypothesis

The novel high-throughput automated imaging system INVAPP/Paragon, can accurately quantify nematode motility and can be used to screen compounds for anthelmintic activity. It is also possible to use the platform to screen *C. elegans* models of human disease. A novel *C. elegans* model of the genetic disease AATD which displays a movement deficient phenotype could be used to screen for chemical and genetic modifiers of disease.

### 1.8.7 Aims

1. To describe and validate the capabilities of the imaging platform INVAPP/Paragon by screening a panel of known anthelmintic compounds and a library of drugs, The Medicines for Malaria Venture Pathogen Box, on the nematode *C. elegans* for their ability to block nematode growth/movement.
2. To phenotypically and biochemically characterise a newly generated transgenic *C. elegans* strain expressing the human mutant protein ZAAT and to evaluate its

usefulness in high-throughput genetic and chemical screening using INVAPP/Paragon to search for novel modifiers of the disease AATD.

3. To develop and carry out three screening strategies using the transgenic *C. elegans* model of AATD to search for ameliorating modifiers of disease: a small molecule screen, an RNAi knock down screen and a forward chemical mutagenesis screen.

## Chapter 2 Methods

### 2.1 Preparation of NGM plates

Stock *C. elegans* strains were maintained at 20°C on nematode growth medium (NGM) agar.

NGM agar was made by first autoclaving a solution containing 3g NaCl, 17g agar, 2.5g peptone, 975ml deionised (DI) water in a 2L flask. The flask was cooled to 55°C and 1ml 1M CaCl<sub>2</sub>, 1ml 5mg/ml cholesterol in ethanol, 1ml 1M MgSO<sub>4</sub> and 25ml 1M KPO<sub>4</sub> were added. 5ml NGM agar was then poured aseptically into 60mm petri plates using a peristaltic pump. The plates were left to dry then stored at 4°C until required [96].

### 2.2 Preparation of bacterial food supply

The *E. coli* strain OP50 was used to feed *C. elegans* grown on NGM plates. OP50, a uracil auxotroph, has limited growth on NGM plates, thereby largely restricting the worms to a defined bacterial lawn. OP50 was streaked onto Lysogeny broth (LB) agar (10g Bacto-tryptone, 5g Bacto-yeast, 5g NaCl, 15g agar in 1L DI water, pH 7.5) and left to grow overnight at room temperature. A single colony was used to inoculate 100ml LB (1 litre: 10g Bacto-tryptone, 5g Bacto-yeast, 5g NaCl, DI water, pH 7 using 1M NaOH) at 37°C overnight. The OP50 solution was stored at 4°C until required. To seed the lawn, approximately 50µl of OP50 solution was placed and spread onto the NGM plates.

The *E. coli* strain HB101 (used as a food source in the liquid culture of *C. elegans*) was cultured as described with minor modifications. HB101/pUC (HB101 *E. coli* contained a plasmid encoding an ampicillin resistance gene) was selected by ampicillin (100µg/ml) addition to the LB agar. A single colony was then used to inoculate 2x 25ml starter cultures of LB+100µg/ml ampicillin. The cultures were agitated at 200rpm, 37°C for 6h before distribution between 4X 2L flasks containing 500ml terrific broth, 2ml glycerol, 100µg/ml ampicillin. The cultures were

then shaken at 200rpm, 37°C overnight. 2X 50ml portions of the cultures were centrifuged at 3059 X g, 10min and the remaining pellets frozen at -20°C until required.

### 2.3 Preparation of *C. elegans* liquid culture

To prepare the large quantities of *C. elegans* needed for chemical and genetic screens, 50ml worm cultures, were prepared following the protocol outlined in The WormBook; Maintenance of *C. elegans* [134] but using *E. coli* HB101 instead of OP50. Briefly, the S-complete components (25µl of 100mg/ml ampicillin, 50µl of 5mg/ml cholesterol in ethanol, 500µl of trace metal solution (1.86g disodium EDTA, 0.69g FeSO<sub>4</sub> • 7 H<sub>2</sub>O, 0.2g MnCl<sub>2</sub>•4 H<sub>2</sub>O, 0.29g ZnSO<sub>4</sub> • 7 H<sub>2</sub>O, 0.025g CuSO<sub>4</sub> • 5 H<sub>2</sub>O, H<sub>2</sub>O to 1 litre DI H<sub>2</sub>O), 500µl of potassium citrate, 150µl of CaCl<sub>2</sub>, 150µl of MgSO<sub>4</sub>) were added to one pellet (approximately 2g) of bacteria and the mixture made up to 50ml with S-basal (500ml: 2.9g NaCl, 0.5g K<sub>2</sub>HPO<sub>4</sub>, 3g KH<sub>2</sub>PO<sub>4</sub>). Well-fed worms were then washed off 1-2 small uncontaminated NGM plates and added to the liquid mixture. Cultures were agitated at 200rpm, 20°C.

### 2.4 Synchronisation of *C. elegans* cultures

The *C. elegans* liquid cultures were synchronised at the first larval stage (L1) using the following bleaching protocol. First, 50ml mixed stage cultures containing many adults were pelleted by centrifuging for 2min, 1195 X g and bleached with a solution prepared by combining 1.5ml 4M NaOH, 2.4ml NaOCl, 2.1ml and DI water. The mixture was repeatedly pipetted for 4min before washing 3x with 50ml S-basal medium. The eggs were incubated at a range of temperatures between 20-27°C whilst being agitated at 200rpm overnight to allow the eggs to hatch. Worm development was thereby arrested at the L1 stage until re-feeding.

### 2.5 *C. elegans* cultured in 96-well plates

To facilitate chemical and genetic screening *C. elegans* were cultured in a 96-well plate format. Larvae at the L1 stage were diluted to approximately 10-20 worms per 50µl in S-basal medium.

The components of S-complete were added to a pellet of HB101 *E. coli* which was then added to the worm culture (1:50v/v). The worm containing solution was then dispensed into 96-well plates, 50µl per well, using an automated plate dispenser. Plates were incubated at a range of temperatures (20-27°C) before imaging.

## 2.6 Temperature shift of ZAAT *C. elegans* cultures

To assess the effect of temperature on the motility of *C. elegans* when shifted to a higher temperature at different developmental stages, liquid cultures in 96-well plates were shifted from 20°C to incubation at either 25°C or 26°C at various stages of culture in flasks or 96-well plates. Initial investigation of the temperature shift involved shifting to 25°C immediately after bleaching the cultures (A) or immediately after the cultures were re-fed with *E. coli* (B). Shifting the cultures to 26°C immediately after bleaching was also investigated (C). The effect of temperature on worms cultured on agar plates was probed by picking 3 gravid adults to a fresh plate then incubating them at 20/25/26°C before imaging plates with the imaging platform on day 6 or 7. Temperature in the incubators was accurately measured using a calibrated Traceable® thermometer (VWR International).

## 2.7 Crossing in mutant *C. elegans* strains to the transgenic ZAAT strain (*rrf-3, fem-1*)

An alternative to using FUDR to prevent appearance of progeny in assay plates is to cross a strain which is sterile at higher temperatures e.g. *fem-1, rrf-3* [135] with the AAT-expressing worms. Successful crosses contain both the mutation which causes sterility at high temperatures and the AAT transgene. ZAAT-expressing male *C. elegans* (Z3 or Z10) were produced by heat shocking 40 L4 ZAAT-expressing hermaphrodites, 30°C, 3h. Males were picked from the progeny of the hermaphrodites and mated with hermaphrodites of the strain desired to be crossed in (*rrf-3, fem-1*) by placing 6 AAT-expressing males and 2 *rrf-3/fem-1* hermaphrodites on a plate and incubating at 20°C. Several days later, the plate was examined

for F1 offspring that displayed fluorescence which indicates AAT expression due to the RFP labelling of the protein. Approximately 5 fluorescent F1 hermaphrodites were selected and allowed to self-fertilise on a separate plate. 16 fluorescent F2 offspring from these individuals were selected and allowed to reach adulthood at 20°C in order to lay a number of eggs. Subsequently, the selected F2s were transferred to continue egg-laying at 25°C and their offspring observed for the sterile phenotype. Sterility was confirmed by the lack of fertility from the offspring of the F2s. Plates which contained low numbers of worms were noted and the corresponding worm strains on plates incubated at 20°C were genotyped.

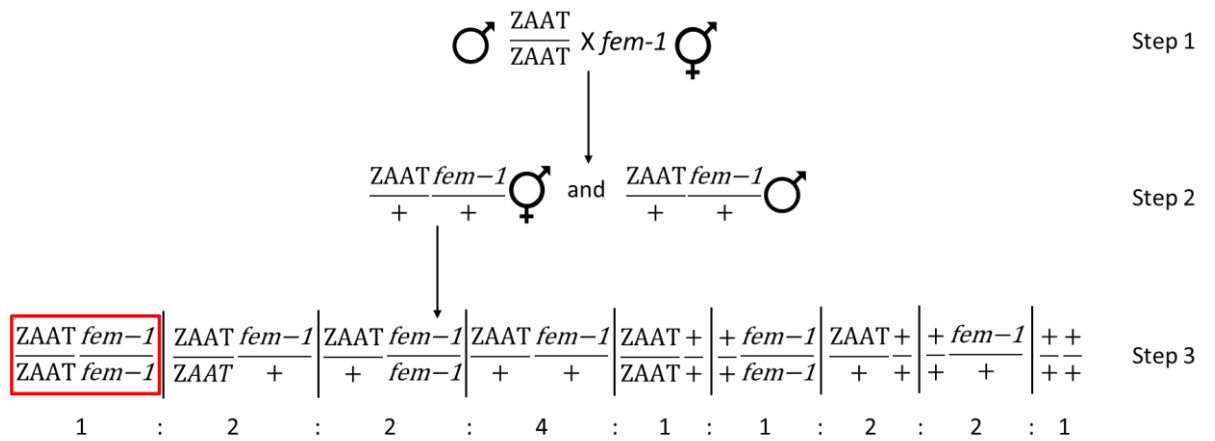


**Figure 2.1.** The crossing map of ZAAT and *fem-1* indicating the steps necessary when attempting to cross the transgenic strain ZAAT and the sterile strain *fem-1*. Male ZAAT worms are mated with *fem-1* hermaphrodites. F1 progeny of this cross which display RFP fluorescent accumulation indicative of ZAAT heterozygosity are picked and allowed to self. F2 progeny are then selected based on RFP fluorescent accumulation and genotyped for the homozygous *fem-1* mutation by sequencing.

## 2.8 Testing drugs/drug screen

*C. elegans* were grown in 50ml liquid cultures until many L1s were present. The cultures were pelleted (1195 X g, 2min, brake speed ~2) then re-suspended in 25ml S-basal. The worm solution was filtered using a 10µm filter to isolate only L1 larvae. The L1-containing solution

was then diluted to approximately 10-20 animals per 50 $\mu$ l of S-complete medium with approximately 1% w/v HB101 *E. coli*. Drug assay plates (96-well) were prepared with 49 $\mu$ l of S-basal and 1 $\mu$ l of DMSO or compound in DMSO. 50 $\mu$ l of L1 suspension was added to each well. Plates were incubated at a temperature range between 25-26°C for 7 days before imaging.

## 2.9 Single worm PCR

In order to amplify DNA from *C. elegans* strains to assess genomic DNA and identify the presence of mutations such as *rrf-3* and *fem-1*, a PCR protocol which first involves lysing a single worm, was used (modified from the Chin-Sang lab protocol: <http://post.queensu.ca/~chinsang/lab-protocols/single-worm-pcr.html>). A single gravid adult *C. elegans* worm was picked into a PCR tube containing 3 $\mu$ l of PCR buffer (95 $\mu$ l PCR reaction buffer, 5 $\mu$ l 20mg/ml (w/v) proteinase K). The tube was immediately frozen at -80°C overnight. The next day, the tube was heated (65°C, 60min) to lyse the worm and release genomic DNA. The proteinase K was inactivated by heating the tube to 95°C for 15min.

The PCR was performed following the 50 $\mu$ l reaction NEB protocol for OneTaq® 2X Master Mix (<https://www.neb.com/protocols/2012/09/06/protocol-for-onetaq-2x-master-mix-with-standard-buffer-m0482>). Briefly, the following components were added to the tube containing the lysed worm: 1 $\mu$ l of 10mM both forward and reverse primers (0.2 $\mu$ M final concentration), 25 $\mu$ l One Taq 2X Master Mix, 20 $\mu$ l nuclease-free water. Mineral oil was added to top the reaction mixture before placing in a PCR thermocycler. The PCR conditions are shown in Table 2.1.

Step	Temperature/°C	Time
Initial Denaturation	94	30s
30 Cycles	94	15-30s
	45-68	15-60s
	68	1min/kb
Final Extension	68	5min
Hold	4-10	Indefinitely

**Table 2.1.** Cycling conditions for single worm PCR protocol

## 2.10 DNA gel electrophoresis

PCR products were mixed with 3 $\mu$ l gel loading dye (6X) (NEB, Ipswich, Massachusetts) loaded into wells of agarose gels (2% agarose, 1x Tris-acetate-EDTA (TAE) buffer, 0.5% v/v ethidium bromide) in TAE buffer. A Quick-Load<sup>®</sup> 1kb DNA ladder (NEB, Ipswich, Massachusetts) was included in the first lane (5 $\mu$ l). The DNA gel was run at 65V for approximately 2h before observation under UV. Bands were excised and extracted using a MinElute<sup>®</sup> Gel Extraction Kit (Qiagen, Hilden, Germany) as per the manufacturer's protocol.

# Chapter 3 Development and validation of a novel high-throughput screening system, INVAPP/Paragon

## 3.1 Introduction

### 3.1.1 Phenotypic and target-based screening

Traditionally, drug discovery has typically engaged a phenotype-based approach where the effects of small molecules are screened on observable characteristics of an animal, tissue or cell model. As a result of rapid developments in genetics (especially the sequencing of the human genome) and molecular techniques, a target-based approach to drug screening has been deployed [136]. Once the molecular target of a disease is known, drug discovery can benefit from the use of tools such as crystallography, computational modelling, binding kinetics and biochemistry and molecular pharmacology [137]. Additionally, target-based approaches are often simpler to execute, faster, easier and less costly than phenotypic ones [138].

The development of such approaches has enabled high-throughput identification and optimisation of molecules with specific desired properties leading to the discovery of effective drugs for a number of human diseases [139]. For example, target-based approaches such as *in silico* methods and molecular interaction prediction tools [140] have been widely employed in the tuberculosis drug discovery efforts to identify novel small molecules which ameliorate disease [141]. One such drug candidate, PBTZ169 entered clinical trials (however later failed to enter phase II) [142]. Detailed molecular knowledge about G protein-coupled receptors (GPCRs) has also propelled the development of next-generation drugs such as pimavanserin, identified by a target-based approach [143]. Its target is the 5-HT2a receptor, known to be involved in psychosis [144]. The potential pitfall of target-based approaches however, are that recombinant systems often fail to capture the biological system as a whole and molecular interactions and complex mechanisms are not taken into account. This can often lead to the

fruitless pursuit of a lead compound that will ultimately fail in a whole organism system [137].

The tuberculosis drug, PTBZ169 is a classic example of this danger.

Whereas target-based approaches require some prior knowledge of disease pathways and molecular targets with potential to ameliorate disease, phenotypic screening by contrast allows for an unbiased approach to finding novel targets and compounds. Due to the complexity of many diseases, the promise of finding first-in-class drugs [139] and the development of advanced screening tools and technologies, there has been a resurgence in phenotypic screening for drug discovery. Phenotypic screening typically involves the use of cell or animal based-models with measurable phenotypes to recapitulate certain aspects of disease in large-scale chemical or genetic screens. Such screens can often be more physiologically relevant than *in vitro* target-based assays and have led to the identification of several clinically relevant drugs. For example, daclatasvir, an anti-hepatitis C virus drug, was discovered phenotypically by expressing the virus replicon in engineered human cells and scoring for clinically relevant genotypes. Daclatasvir also led to the elucidation of the previously unknown viral protein NS5A as a drug target [145]. Interestingly, drugs can even be approved for use without full elucidation of the target, as was the case with ezetimibe (Zetia). It was identified as a cholesterol absorption inhibitor in a high cholesterol mouse model and approved for use as a cholesterol-lowering drug [146]. Later, it was found that it acted on the NPC1L1 cholesterol transporter [147].

Phenotypic-based approaches are of course not without their limitations, there are still a number of obstacles in the translation from drug discovery to clinical therapy. Challenges include problematic hit validation and target elucidation and the cost of the processes involved [148]. However, it remains a powerful approach to exploit unknown or undrugged targets in diseases where mechanisms are poorly understood. Realistically, target-based and phenotypic-

based approaches should be viewed as complementary, where employment of both efforts strengthens the overall aims of drug discovery.

### 3.1.2 Large-scale phenotypic screening with *C. elegans*

The nematode *C. elegans* is a powerful genetic model organism that can be used to phenotypically recapitulate human diseases and also can be used to model parasitic organisms. These attributes are discussed in further detail in chapter 4. Large-scale phenotypic screens using *C. elegans* can be a powerful aid to drug discovery, since parameters such as growth, movement, egg laying and death can be scored. Manual scoring of such parameters has been effective and used to screen libraries of up to 67,000 compounds [149-151]. However, this approach can be slow, repetitive and laborious and may result in researcher fatigue and inaccuracies [152]. It is therefore desirable to develop automated phenotyping platforms which allow for high-throughput screening of nematodes to robustly capture sometimes subtle changes in observable phenotype or behaviour. The whole-organism phenotypic screening approach using *C. elegans* has also benefitted from the wealth of genetic knowledge surrounding the worm. The targets of small molecules, or the identification of genetic modifiers can be rapidly elucidated using powerful genetic tools, such as forward mutagenesis (utilising random mutagenic agents, discussed further in chapter 7) and reverse mutagenesis or RNAi, discussed further in chapter 6 [153].

### 3.1.3 Automated systems for phenotypic screening of models of parasites and human disease

Automated phenotyping systems offer the potential of higher throughput and greater reliability of small molecule or genetic screening. Such approaches include indirect assessment of viability by using the xCELLigence System; assessment of metabolic activity via colorimetric assays such as resazurin, MTT, and acid phosphatase activity; assessment of motor activity via

isothermal microcalorimetry and quantification of movement-related light scattering [154-158]. However, these systems are limited to cell-based or *in vitro* assays.

Imaging-based systems for the quantification of whole-organism motility or growth have also been developed. The principle of such imaging systems relies on the ability to record and measure movement of organisms such as *C. elegans* in assay plates [159]. An automated system for measuring worm swimming, or thrashing, was developed along with an algorithm which was capable of quantifying nematode movement using covariance [160]. This system facilitated large-scale chemical and genetic screening of *C. elegans* displaying phenotypes with a reduced thrashing frequency and had applications in human disease drug discovery and the search for novel anthelmintic treatments [152]. Indeed, most nematode phenotype imaging platforms are currently employed in the search for new compounds against human or plant parasites. The “WormAssay” system quantifies the motility of macroscopic parasites such as *Brugia malayi* adult worms [161]. This system has been further developed into “The Worminator”, which quantifies the motility of smaller nematode species and developmental stages and has been validated by quantifying the activity of several anthelmintics [162]. This system has a reported scan time of 30s per well, hence a throughput of around one and a quarter 6-well plates per hour. A system based on single-well imaging and thresholding of motile pixels with a throughput of around five 96-well plates per hour has also been reported [163]. Its utility has been demonstrated by the successful screening of a 522-compound kinase inhibitor library and the 400-compound Medicine for Malaria Venture Pathogen box on *Haemonchus contortus* larvae [164, 165]. A notable recently-described screen of the effects of 26,000 compounds on *Caenorhabditis elegans* growth/survival used WormScan, a system that uses a conventional flat-bed scanner to capture two frames of images of whole plates and then uses an algorithm based on the image differences to assign a value to each well that reflects motility/growth [166, 167]. This led to the identification of several compounds with previously

unreported anthelmintic activity, including compounds targeting PINK-1 and MEV-1. The authors reported a throughput of approximately 25-40 96-well plates per hour.

### 3.1.4 Developing a new robust motility/growth quantification system focussed on rapid, high-throughput chemical screening

It is clear that recent developments in phenotypic screening of parasitic and model nematodes have led to an acceleration of the discovery of potential novel anthelmintic compounds. Given the large sizes of drug-like compound libraries and the need to efficiently identify the hit compounds therein that have the potential to be developed into potent and selective anthelmintic lead molecules, it is desirable that nematode phenotypic screening be further accelerated. This study will describe the development of the Invertebrate Automated Phenotyping Platform (INVAPP) used in conjunction with the Paragon algorithm to quantify nematode motility and growth with a throughput of approximately 100 96-well plates per hour, with a robust and unbiased approach [168]. The imaging system was validated by quantifying the activity of a panel of known anthelmintics on *C. elegans*, a parasite model and then by screening, in a blinded fashion, the Medicines for Malaria Venture Pathogen Box for compounds that block or reduce nematode growth.

## 3.2 Aims

1. To describe and validate the imaging capabilities of the novel high-throughput imaging system INVAPP/Paragon.
2. To screen a panel of known anthelmintic compounds on *C. elegans* to confirm the ability of the imaging system to identify anti-parasitic drug activity.
3. To screen an open source drug library the Medicines for Malaria Venture Pathogen Box for compounds which have anthelmintic activity, denoted by a blocking in *C. elegans* growth and/or movement.

### 3.3 Methods

#### 3.3.1 INVAPP/Paragon system

The INVAPP / Paragon system consists of a fast high-resolution camera (Andor Neo, resolution 2560x2160, maximum frame rate 100 frames per second) with a line-scan lens (Pentax YF3528). Microtiter plates (96 wells) are placed in a holder built into the cabinet and imaged from below. Illumination is provided by an LED panel with acrylic diffuser. Movies were captured using  $\mu$ Manager [169]. The desirable movie frame length and duration of filming depends on the particular organism under study. To image *C. elegans*, recordings constitute 200 frames for a total of 7s. Movies were analysed using MATLAB scripts. Briefly, movies were analysed by calculating the variance through time for each pixel. The distribution of these pixel variances was then considered, and pixels whose variance was above the threshold (typically, those greater than one standard deviation away from the mean variance) were considered 'motile'. Motile pixels were then counted and assigned by well, generating a movement score for each well. The movement index is an arbitrary measurement of movement for a single well in a 96-well plate. The source code for this software has been released under the open source MIT license and is available at <https://github.com/fpartridge/invapp-paragon>. A further MATLAB script has been provided for batch processing of movies.

#### 3.3.2 *Caenorhabditis elegans* motility and growth assays

*C. elegans* strains were maintained at 20 °C on nematode growth medium (NGM) agar seeded with the *E. coli* strain OP50. To obtain worms for screening, a mixed-stage liquid culture was prepared by washing well-fed worms from one small NGM plate into a medium of 50 ml S-complete buffer with a pellet of approximately 2-3 g *E. coli* HB101. Cultures were agitated at 200 rpm, 20 °C, until there were many adults present, then synchronised at the L1 stage by bleaching. Fifty millilitre cultures were pelleted and bleaching mix (1.5 ml 4M NaOH, 2.4 ml NaOCl, 2.1 ml water) added. Mixing for 4 minutes led to the release of embryos, which were

washed three times with 50 ml S-basal medium. The cultures were incubated in 50 ml S-basal at 20 °C and agitated at 200 rpm overnight to allow eggs to hatch and arrest as a synchronous L1 population.

For the growth assay, *C. elegans* were cultured in a 96-well plate format. Synchronised L1 were diluted to approximately 20 worms per 50 µl in S complete medium with around 1% w/v HB101 *E. coli*. Assay plates were prepared with 49 µl of S-basal and 1µl of DMSO or compound in DMSO solution per well. Next, 50 µl of the L1 suspension were added to each well. Plates were incubated at 20°C before imaging using the INVAPP / Paragon system 5 days later. Prior to imaging, worm motion was stimulated mechanically by inserting and removing a 96-well PCR plate into/from the wells of the assay plate. Whole-plate 200 frame movies were recorded at 30 frames /s (7 seconds total).

For the adult motility assay, synchronised L1 were refed as a bulk 50 ml culture and cultured at 20 °C until they developed into young adults. Worms were washed in S-basal and dispensed, approximately 20 worms per well, into 96-well plates with compound dissolved in DMSO, or DMSO alone and then incubated for 3 hours. Whole-plate 200 frame movies were recorded at 30 frames /s (7 seconds total).

### 3.3.3 Pathogen box screening

The Pathogen Box library was obtained from the Medicines for Malaria Venture as 10 mM solutions in DMSO, and then diluted in DMSO to 1 mM. It was then screened in the *C. elegans* growth assay as described (final concentration 10 µM, n=5, 1% v/v final DMSO). Solid material for confirmatory screening of actives was obtained from Sigma-Aldrich (tolfenpyrad) and Santa Cruz Biotechnology (auranofin). Solid samples of MMV007920, MMV020152, MMV652003 and MMV688372 were obtained from the Medicines for Malaria Venture.

## 3.4 Results

### 3.4.1 INVAPP/Paragon: a high throughput assay for quantifying nematode motility and growth

In order to develop and test a novel assay for large-scale chemical and genetic screening on the motility and growth of diverse parasites, a high-throughput and automated system was established. The INVAPP/Paragon imaging and analysis system was developed in the Sattelle/Lomas laboratory (key contributors: Dr FA. Partridge, Prof. SD. Buckingham and Prof. DB. Sattelle). A schematic of the INVAPP hardware is shown in Figure 3.1A. This allows recording of movies of entire microplates (96 wells) at high frame rate, reducing the per plate acquisition time to 10-30 seconds. Tens of thousands of compounds or conditions can therefore be readily screened per day.

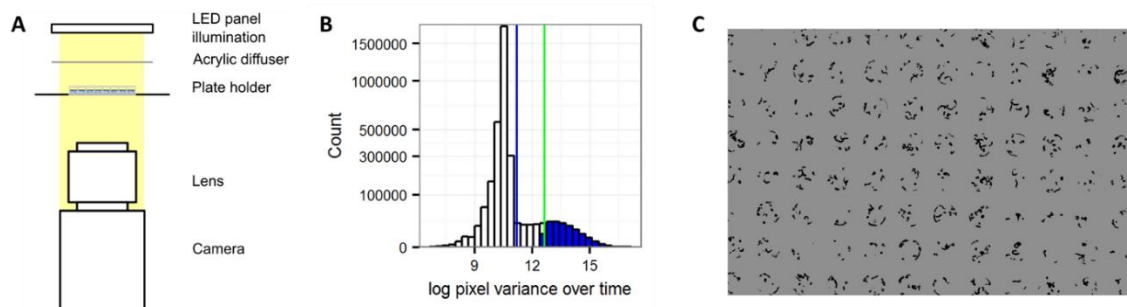


**Figure 3.1.** The INVAPP / Paragon system with its movement index algorithm is fully-automated and enables high-throughput screening. (A) Schematic of the INVAPP setup (B) Principle of the algorithm: thresholding of moving pixels by statistical analysis of variance of each pixel through time. Histogram shows the distribution of pixel variance over time. Blue vertical line indicates mean pixel variance. The green vertical line indicates mean plus standard deviation of pixel variance; the blue shaded portion of the histogram indicates pixels that exceed this threshold so are deemed to be motile. (C) Image of 96-well plate containing *C. elegans* adults processed by the INVAPP / Paragon movement index system. Dark pixels are those categorized as moving by the algorithm.

A statistical approach was taken to quantify motility. The variance through time for each pixel in the plate was calculated and the distribution of the variances examined. Pixels whose variance is greater than a threshold of the mean plus typically one standard deviation are determined to be “motile” (Figure 3.1B). An example of this thresholding model is shown in Figure 3.1C, which shows analysis of a 96-well plate containing adult *C. elegans*. Dark pixels are those that have been determined to be motile. Once the motility threshold has been applied to the data, ‘motile’ pixels are assigned by well to their plate location and counted. All analysis is fully automated via a set of MATLAB scripts, available at

<https://github.com/fpartridge/invapp-paragon>.

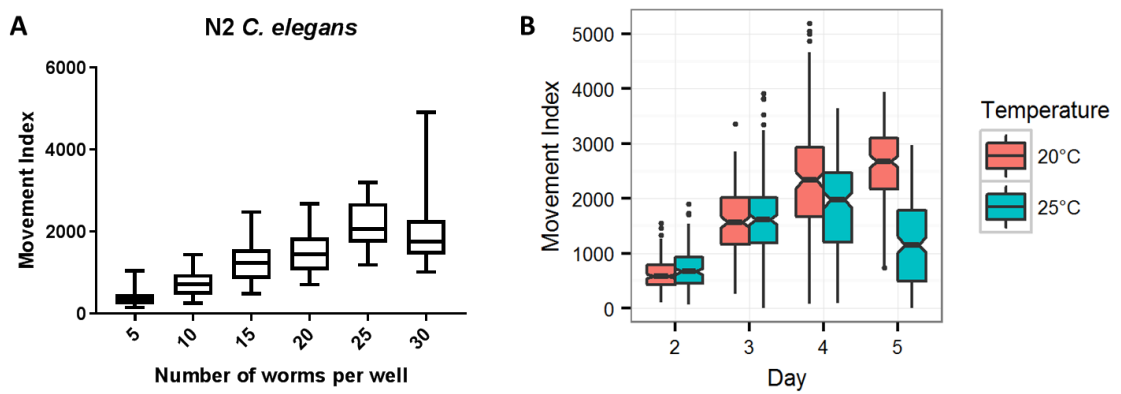


**Figure 3.2.** The INVAPP / Paragon system is able to determine motility and growth rate. (A) Increasing the number of *C. elegans* worms per well leads to increase in reported movement index. Boxplot bars indicate 95% confidence interval. (B) Movement index algorithm is able to quantify *C. elegans* growth in 96-well plates. Movement index increases with growth. Synchronized L1 population refed on day 0. Decrease in movement index in 25°C group on Day 4 reflects completion of the *C. elegans* lifecycle and exhaustion of the bacterial food source. Boxplot notches indicate 95% confidence interval, n=192.

This approach was able to determine motility. To illustrate this, plates containing a variable number of synchronized adult *C. elegans* worms were analysed. As expected, quantified

movement increased with the number of worms per well, reflecting a larger number of 'motile' pixels in the recording (Figure 3.2A).

The system was also able to quantify nematode growth. To test this, *C. elegans* were synchronised at the L1 stage, before re-feeding them in plates at two temperatures commonly used in *C. elegans* culture (20 °C and 25 °C). Plates were then analysed using INVAPP / Paragon every 24 hours. The results are shown in Figure 3.2B. The quantified movement index increases as worms develop from L1 to adult stage. The drop in motility in the 25 °C group on day 5 reflects growth of L1 progeny leading to exhaustion of the bacterial food source and starvation. Thus, INVAPP/Paragon is able to quantify nematode growth and motility. When animals are cultured in plates from L1 and imaged once several days later however, it is not possible to separate quantification of growth and motility, therefore the movement index could represent both.

When establishing a high-throughput assay it is important to consider the issue of edge effects [170]. Systematic biases across the plate are particularly common around edges. Typical causes are evaporation, which is often worse at the edges, or temperature inhomogeneity. In our assay, given that it involves imaging of whole plates, it was important to exclude the possibility of systemic bias caused by optical distortion. To address these concerns, a 1920-well *C. elegans* growth dataset was analysed. This was chosen because the long four-day incubation time gave the maximum possibility of confounding evaporation differences. Wells on the outer rows and columns of the plate were classified as being outer wells, and their quantified motility was compared to the inner wells (Figure 3.3A). There was no significant difference between these groups (Mann-Whitney-Wilcoxon test,  $P=0.77$ ), and therefore no evidence of problematic edge effects in this assay. To further exclude the possibility of assay inhomogeneity across the plate, a heat map was calculated showing average normalised motility for each well (Figure 3.3B). Again, this showed no evidence of systemic bias by plate position.

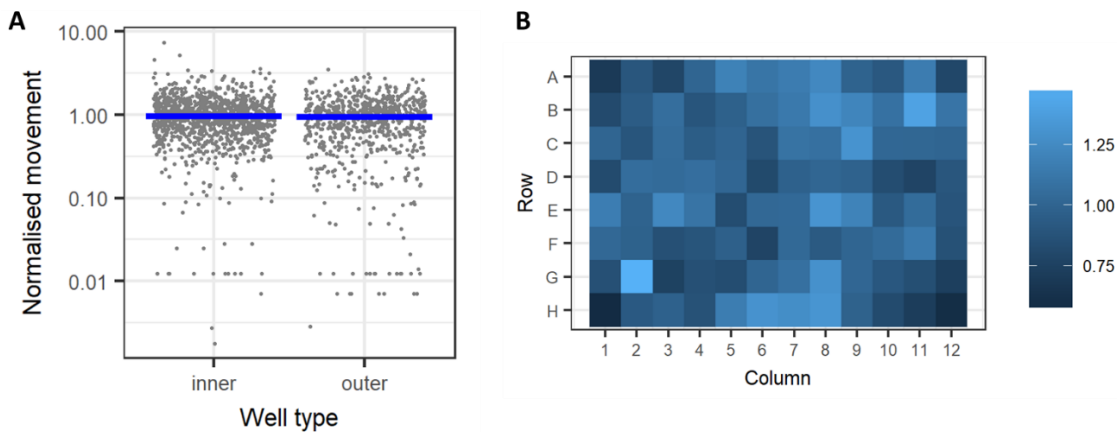


**Figure 3.3.** No systematic bias or edge effect was detected in our screening assay. (A) Absence of edge effects in this assay – analysis of a 1920-well *C. elegans* growth dataset shows no difference of the normalised movement score for 96-well plate outer edge wells (the wells found in columns 1 and 12 or rows A and H) compared to the score for inner wells (the other wells in the plate). Movement index for each well is normalised by dividing by the mean movement index for all wells of that plate. The blue bar indicates median. (B) No edge effects or other inhomogeneity across the plate – heat map shows average normalised movement index for each well location.

### 3.4.2 Validation of the INVAPP / Paragon system using existing commercial anthelmintic standards

Having set up this high-throughput, motility and growth assay, it was necessary to validate its utility by examining the effects of a panel of known anthelmintics. Nine anthelmintics were selected with a variety of reported mechanisms of action. Piperazine is a GABA agonist that acts at the neuromuscular junction [171]. Diethylcarbamazine has been proposed to have a similar mechanism, although other mechanisms including targeting host arachidonic acid metabolism are also thought to be important [172]. Levamisole, oxantel and pyrantel are nicotinic acetylcholine receptor agonists that induce spastic paralysis [173]. Mebendazole is an inhibitor of beta-tubulin polymerisation [174]. Ivermectin is a positive allosteric modulator of glutamate-gated chloride channels although other targets have also been suggested [175]. Trichlorfon is a member of the organophosphate group of acetylcholine esterase inhibitors. Praziquantel is thought to act by disrupting calcium ion homeostasis but its target is unclear

[176]. Concentration-response curves for this panel of anthelmintics were first measured in an acute treatment (3h) adult *C. elegans* assay. The results are shown in Figure 3.4. As expected, the major ion channel-targeting drugs ivermectin, levamisole, oxantel and pyrantel were active in this assay, reflecting their direct effects on worm motility.

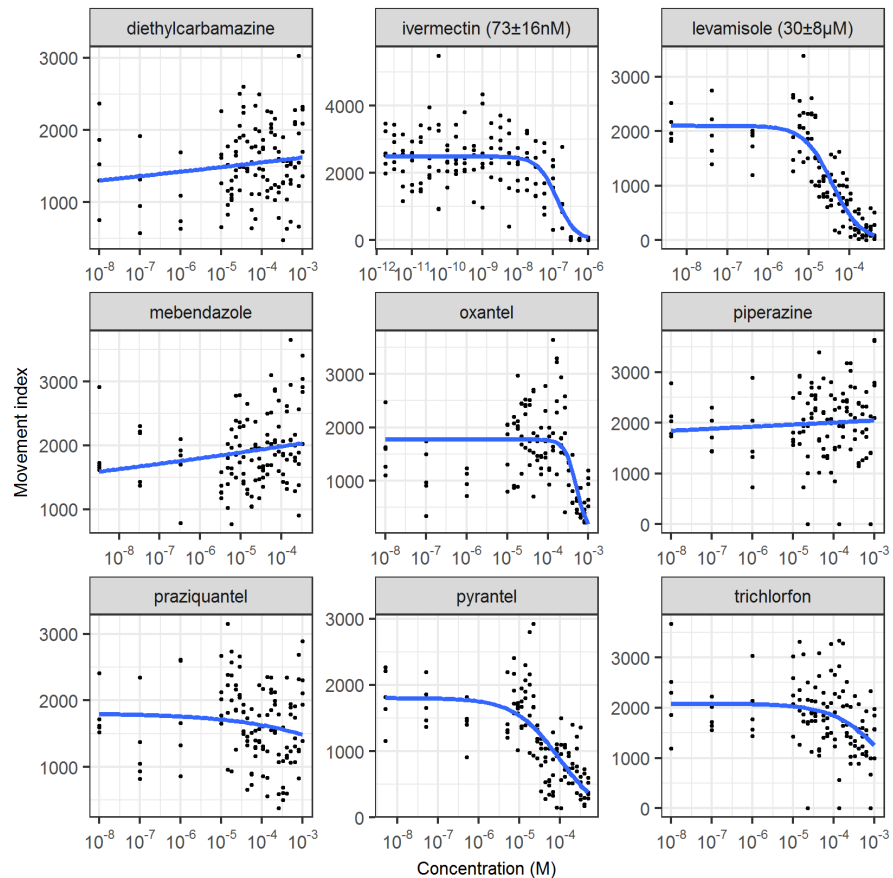


**Figure 3.4.** Determination of the effect on *C. elegans* adult motility of acute treatment (3h) with important anthelmintics, using the INVAPP/Paragon system. Each dot represents one well in the 96-well plate. Blue line fitted using the 3-parameter log-logistic model. EC<sub>50</sub> values are shown in parentheses, with standard error for this estimate calculated using *drc* [177].

The concentration-response curves for this panel of anthelmintics were then measured in a chronic treatment *C. elegans* growth assay. The results are shown in Figure 3.5. Activity was again found with ivermectin, levamisole, oxantel and pyrantel and, additionally, with mebendazole, piperazine and trichlorfon. This reflects that some anthelmintic modes of action

may not be measured in purely acute motility assays, supporting the use of assays that involve growth or development. Diethylcarbamazine and praziquantel were not active in these assay as expected. This reflects previously reported low *in vitro* activity of diethylcarbamazine and its proposed mechanism of acting on host arachidonic acid metabolism [172]. Praziquantel, used primarily to treat flukes and tapeworms, is known to have limited efficacy against nematodes [178]. Successfully demonstrating the ability of the INVAPP / Paragon system to determine the effects of known anthelmintics increased confidence in this approach.

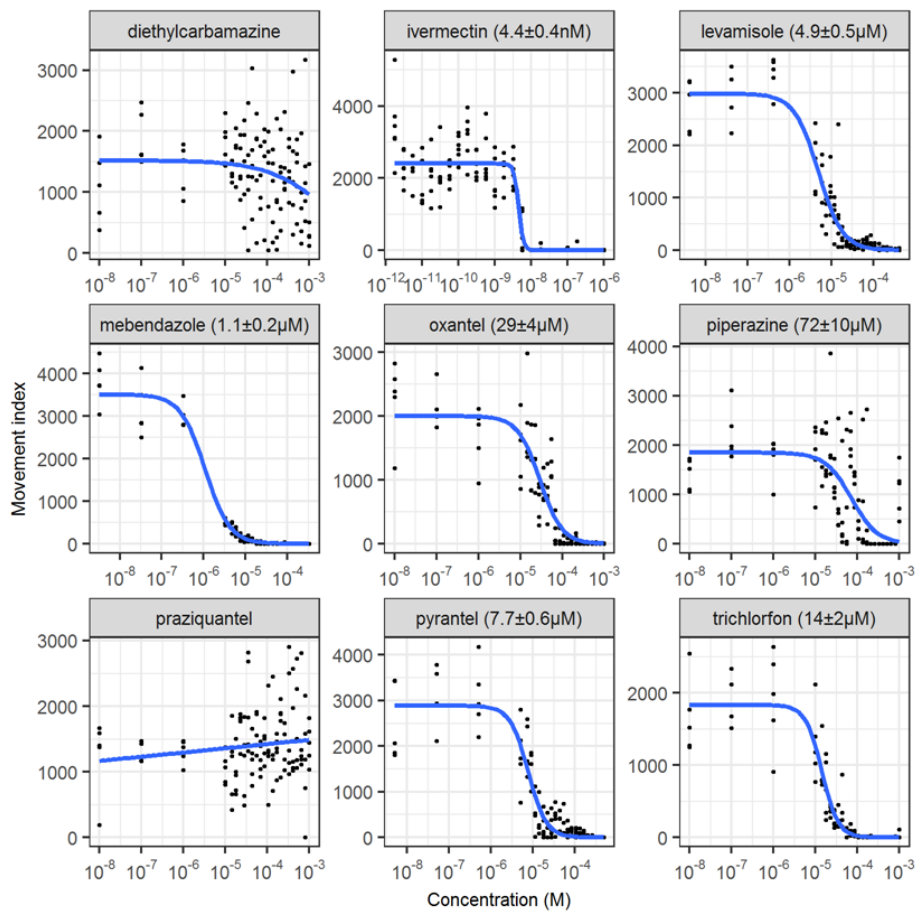


**Figure 3.5.** Determination of the effect of important on *C. elegans* growth of well-established anthelmintics using the INVAPP / Paragon system. Each dot represents one well in the 96-well plate. Blue line fitted using the 3-parameter log-logistic model. EC<sub>50</sub> values are shown in parentheses, with standard error for this estimate calculated using *drc* [177].

### 3.4.3 Screening the Pathogen Box for compounds that affect *C. elegans* growth

The INVAPP/Paragon system was then applied to the identification of novel anthelmintic small molecules. The Pathogen Box, a collection of 400 diverse drug-like molecules that are known to be active against various neglected disease pathogens (particularly, tuberculosis (or *Mycobacterium* spp.), malaria and kinetoplastid protozoa) was obtained. This library is distributed as an open-science project by the Medicines for Malaria Venture. A screen of this library for compounds affecting motility of exsheathed L3 of *H. contortus* was published recently [165], which identified the insecticide, tolfenpyrad, as active against the larvae. To complement this approach, and with the aim of identifying compounds blocking growth of nematodes as opposed to solely immobilising them, the library was screened in a blinded fashion (n=5, concentration 10  $\mu$ M) using the INVAPP / Paragon *C. elegans* growth assay. For each compound, movement index and significance (Mann-Whitney-Wilcoxon test) were calculated relative to DMSO-only control wells. A volcano plot showing the results of this screen is shown in Figure 3.6A. Compounds that reproducibly reduced growth/motility are found towards the top left of this plot. To confirm identity of the hit molecules, the top 20 putative hit compounds were retested with the same library material (n=5, concentration 10  $\mu$ M) in the same INVAPP / Paragon *C. elegans* growth assay (Figure 3.6B). A total of 18 out of 20 compounds were active ( $P < 0.05$ , Dunnett's multiple comparison test).

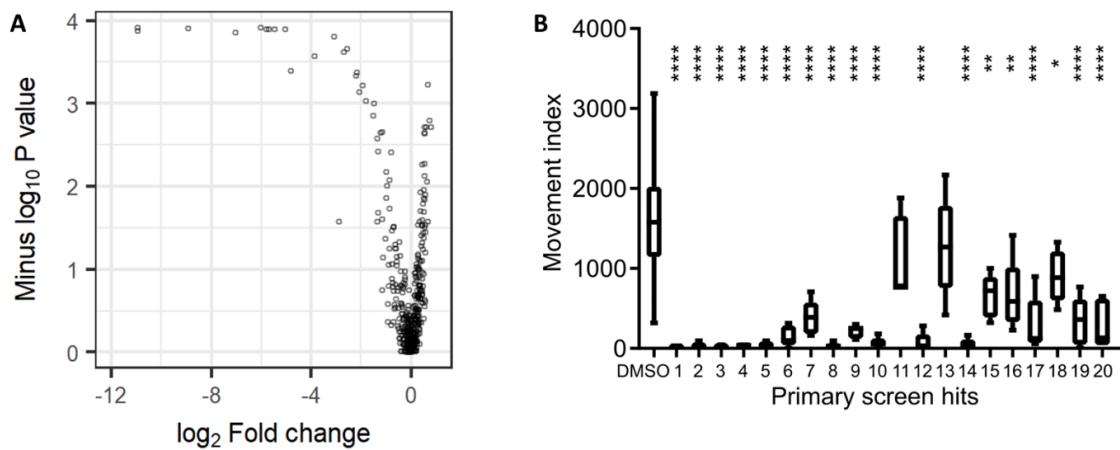


**Figure 3.6.** Screening the Pathogen Box in the *C. elegans* growth screen. (A) Volcano plot showing the results of the primary screen ( $n=5$ , concentration = 10  $\mu$ M). Each point represents one compound. Drug effect size is shown on the x axis, as log<sub>2</sub>-fold change (ratio of the median movement for the repeats of the compound to the median movement of DMSO-only wells). Statistical significance is shown on the y axis as the -log<sub>10</sub> P value in the Mann-Whitney-Wilcoxon test. A location at the top left of this plot indicates anthelmintic activity. (B) Secondary rescreen of hit compounds, in order of their activity in the primary screen, from library material. Statistical significance compared to DMSO-only control calculated by Dunnett's multiple comparison test ( $n=5$ , \* indicates  $P < 0.05$ , \*\* indicates  $P < 0.005$ , \*\*\*\* indicates  $P < 0.0005$ ).

### 3.4.4 Identification of known anthelmintic compounds by screening the Pathogen Box library in the *C. elegans* growth assay.

Known anthelmintic compounds found to be active in the primary screen were considered first (Table 3.1). Mebendazole, an anthelmintic from the benzimidazole group, acts by inhibiting microtubule synthesis.

Compound	MMV ID	PubChem CID	Hit ID	Log <sub>2</sub> fold change in growth		EC <sub>50</sub> (μM) ± standard error
				(1° screen)	(2° screen)	
Tolfenpyrad	MMV688934	10110536	1	-10.9	-10.6	0.2 ± 0.04
Auranofin	MMV688978	24199313	2	-10.9	-7.2	1.1 ± 0.3
Mebendazole	MMV003152	4030	5	-6.0	-5.7	1.1 ± 0.2
Isradipine	MMV001493	158617	16	-2.2	-1.4	1.6 ± 0.7
Tavaborole	n/a	11499245		n/a	n/a	8.6 ± 1.9

**Table 3.1** Named compounds that were active in the *C. elegans* growth screen. Log<sub>2</sub>-fold change in growth estimate compared to DMSO-only controls. EC<sub>50</sub> confidence interval is the standard error. The EC<sub>50</sub> estimate for mebendazole is from Figure 3.5.

Tolfenpyrad is a broad-spectrum acaricide and insecticide that acts as an inhibitor of complex I of the electron transport chain. It has been recently reported to reduce motility of *H. contortus* exsheathed L3 and to block L3 to L4 development of this parasite *in vitro* [165]. Activity of this compound was confirmed using solid material. As shown in Figure 3.7A, the EC<sub>50</sub> was 200 ± 40 nM. Independently identifying these known anthelmintic compounds using a blinded screening approach further validates the INVAPP/Paragon system as a robust high throughput screening approach.

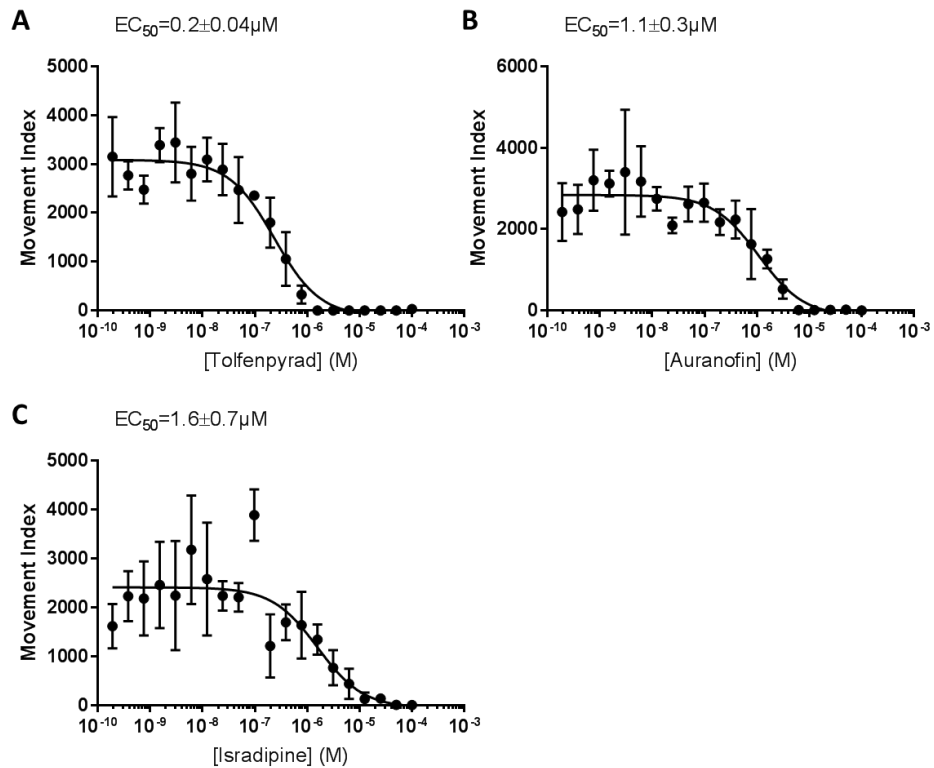


**Figure 3.7.** Re-testing known compounds identified from Pathogen Box screen in growth/motility assay. Concentration-response curves showing the activity of known anthelmintics – (A) tolfenpyrad, (B) auranofin, (C) isradipine – that were found in the Pathogen box screen retested using solid material (supplied by the Medicines for Malaria Venture) in the *C. elegans* growth assay. A concentration-response curve for mebendazole in the assay was presented in Figure 3.5. Error bars indicate standard deviation,  $n=4$ . Curve fitting was undertaken using three parameter log logistic model in Graphpad Prism v.7

Auranofin is a gold (I) compound originally developed for the treatment of rheumatoid arthritis. It has received attention for repurposing as an anti-cancer agent, with a number of clinical trials under way. It has been shown that auranofin has *in vitro* and *in vivo* activity in several models of parasitic diseases, including schistosomiasis [179], amoebiasis [180], leishmaniasis [181] and onchocerciasis [182]. A phase IIa trial of auranofin for gastrointestinal protozoal infection is ongoing. Activity of this compound was confirmed in the *C. elegans*

growth assay using solid material. As shown in Figure 3.7B, the EC<sub>50</sub> of this compound was 1.1 ± 0.3 μM.

Isradipine is an antihypertensive drug that belongs to the dihydropyridine family of L-type calcium channel blockers. A structurally related dihydropyridine, nemadipine-A, has been shown to cause growth and egg laying defects in *C. elegans* by antagonising the L-type calcium channel α1-subunit EGL-19 [183]. Activity of this compound was confirmed in the *C. elegans* growth assay using solid material. As shown in Figure 3.7C, the EC<sub>50</sub> of this compound was 1.6 ± 0.7 μM.

### 3.4.5 Novel anthelmintics that block *C. elegans* growth

Fourteen compounds without previously-described anthelmintic activity were identified in the Pathogen Box screen (Table 3.2). Four of these compounds were examined more closely. First, activity was determined, using solid material, in the *C. elegans* growth assay (Figure 3.8). The EC<sub>50</sub> values for the confirmatory assay are shown in Table 3.2. These results have been recorded in the PubChem database with Assay ID 1259335.

MMV ID	PubChem CID	Hit ID	Log <sub>2</sub> fold change in growth		EC <sub>50</sub> (μM)
			(1° screen)	(2° screen)	
MMV652003	46196110	3	-8.9	-7.6	4.3±2.5
MMV007920	721133	4	-7.0	-5.4	6.2±2.4
MMV688372	72710598	6	-5.8	-4.0	3.3±1.7
MMV675994	44222802	7	-5.7	-2.0	n.d.
MMV026550	44530521	8	-5.5	-5.9	n.d.
MMV020391	7918647	9	-5.0	-2.7	n.d.
MMV676395	54678166	10	-4.8	-4.8	n.d.
MMV020152	8880740	12	-3.1	-6.9	2.5±1.0
MMV676406	30238526	14	-2.7	-8.0	n.d.
MMV688417	58346931	15	-2.6	-1.1	n.d.
MMV688936	18589797	17	-2.2	-3.7	n.d.
MMV1028806	16387386	18	-2.1	-0.8	n.d.
MMV688888	5179236	19	-2.0	-2.1	n.d.
MMV687180	41058173	20	-1.8	-3.6	n.d.

**Table 3.2.** Compounds with previously unreported anthelmintic activity that were active in the *C. elegans* growth screen. MMV ID is the compound identifier for the Medicines for Malaria Venture. PubChem CID is the compound identifier for the PubChem database. Log<sub>2</sub> fold change in the growth estimate in the INVAPP/Paragon assay compared to DMSO-only controls.

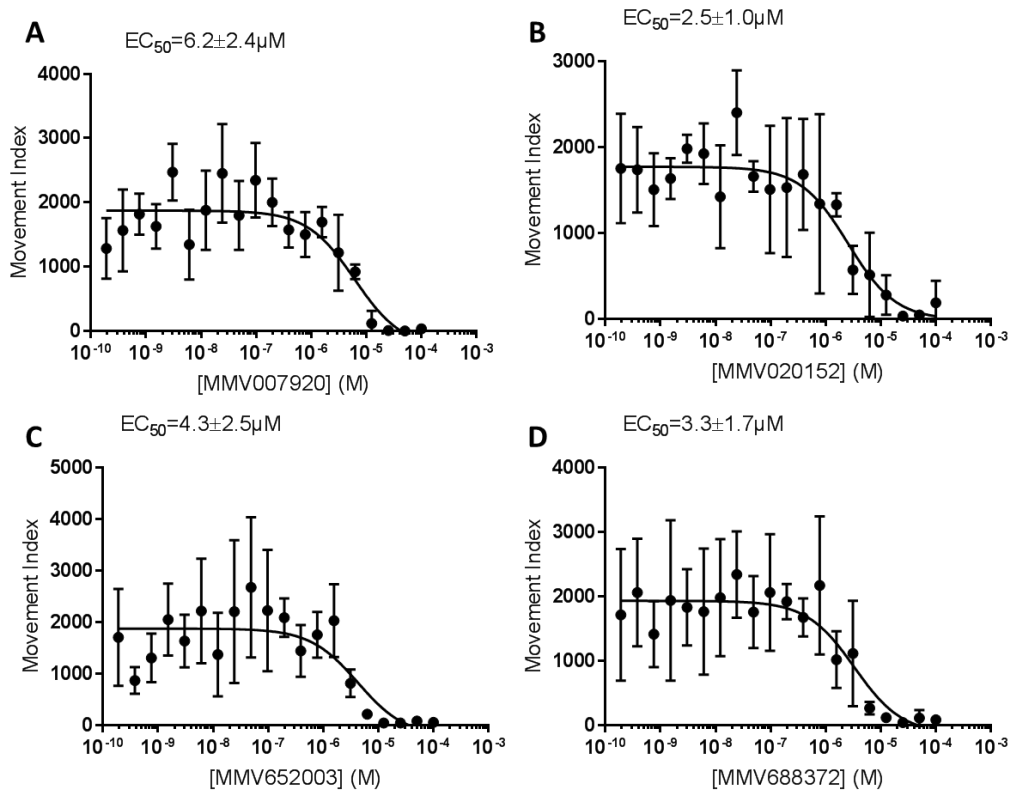


**Figure 3.8.** Concentration-response relationships for selected hit compounds in the *C. elegans* growth screen. (A) MMV007920 (B) MMV020152 (C) MMV652003 (D) MMV688372.

MMV007920 is a benzoxazole-containing compound previously identified in a screen for agents that inhibit *Plasmodium falciparum* proliferation. The target of this compound is not known but it has been suggested that some benzoxazole compounds act on beta-tubulin [184]. MMV020152 is an isoxazole-containing compound previously identified in a screen for compounds that inhibit *P. falciparum* growth. A number of other compounds also containing isoxazole motifs have been shown to have insecticidal activity [185]. MMV688372 is an imidazopyridine-containing compound that has been previously shown to have *in vivo* anti-trypanosomal activity [186].

MMV652003 is a benzoxaborole-containing compound that has also been given the identifier AN3520 in the literature. This compound has potent activity against *Trypanosoma sp.*, both *in*

*vitro*, and in murine models of human African trypanosomiasis [187]. In this context this compound has been iteratively improved leading to the identification of the close relative SCYX-7158 [188], which is currently in clinical trials. The anti-trypanosomal target of this benzoxaborole class is not known [189]. A simpler benzoxaborole compound, tavaborole, has been approved as an anti-fungal [190]. This acts by inhibiting cytoplasmic leucyl-tRNA synthetase by forming an adduct with tRNA<sup>Leu</sup> in the enzyme editing site [191]. Benzoxaborole anthelmintic agents are being developed by Anacor/Eli Lilly [192, 193]. Benzoxaborole compounds also show promise for other infectious diseases, including malaria, cryptosporidiosis, toxoplasmosis and tuberculosis, in each case acting via inhibition of leucyl-tRNA synthetase [194-196].

### 3.5 Discussion

#### 3.5.1 A novel high-throughput imaging system for large-scale high-throughput screening

The INVAPP/Paragon system, based on imaging of whole microplates and thresholding pixel variance to determine motion, is able to quantify growth and/or motility of the free-living nematode, *C. elegans* as well as parasitic nematodes[168]. A strength of this system is its high-throughput capability, typically imaging a whole plate for 5–20 s is sufficient to reliably quantify motion in all 96 wells. The advantages and disadvantages of other recently developed worm phenotypic imaging systems are outlined in Table 3.3. The capabilities of INVAPP/Paragon have been demonstrated by determining efficacy of a panel of anthelmintics in both acute motility and growth in *C. elegans* assays. The utility of the system was further demonstrated in a screen of small molecules for compounds that block or limit *C. elegans* growth. Current anthelmintic screens generally focus on motility reduction, as growth of parasitic nematodes can be difficult to model *in vitro*, with larvae failing to moult through their larval stages outside of the host. However, anthelmintic activity *in vivo* can be much

broader than inhibition of motility and thus screening compounds for their ability to inhibit *C. elegans* growth, rather than motility, represents a useful strategy to identify compounds which can subsequently be tested for growth inhibition activity *in vivo*.

Imaging system	Principle of imaging method	Advantages	Disadvantages	Reference
WormAssay/The Worminator	Camera mounted onto microscope and algorithm analyses videos to detect worm movement within the wells	<ul style="list-style-type: none"> <li>- Able to capture images of microscopic parasites and larval stages</li> <li>- Can image many different multi-well plate types</li> <li>- Amenable for use in library screening</li> <li>- Low cost</li> </ul>	<ul style="list-style-type: none"> <li>- Up to 30s imaging time per well, approximately 48mins per 96-well plate</li> </ul>	Marcellino et al. (2012) [161]; Storey et al. (2015) [162]
n/a	Camera mounted onto microscope and motile pixel thresholding interpreted as motility index to quantify worm movement	<ul style="list-style-type: none"> <li>- Able to image multi-well plates</li> <li>- Amenable for use in library screening</li> <li>- Low cost</li> </ul>	<ul style="list-style-type: none"> <li>- Up to 5s imaging per well which is approximately 1h for 1 x 96-well plates</li> </ul>	Preston et al (2015) [164]; Preston et al. (2016) [163]; Preston et al. (2016) [165]
WormScan	Flat-bed scanner captures two frames of images of whole plates and algorithm assigns value representing worm movement by comparing differences between images	<ul style="list-style-type: none"> <li>- Scans up to 4 96-well plates at once</li> <li>- Amenable for use in library screening</li> <li>- Low cost</li> </ul>	<ul style="list-style-type: none"> <li>- No dynamic high frame rate image capture</li> <li>- Takes approximately 10mins to image 4 plates</li> </ul>	Mathew et al. (2012) [166]; Mathew et al. (2016) [167]
INVAPP/Paragon	Stand-alone camera set up captures videos and algorithm	<ul style="list-style-type: none"> <li>- Captures whole plate videos of multi-</li> </ul>	<ul style="list-style-type: none"> <li>- Not currently set up for 384-well plates</li> </ul>	Buckingham et al. (2009) [160]; Partridge et

	<p>based on thresholding motile pixels quantifies worm motility</p>	<p>well plates up to 96-wells</p> <ul style="list-style-type: none"> <li>- Scans 1 x 96-well plate in 7s</li> <li>- Bespoke algorithms to quantify motility of variety of organisms</li> <li>- Amenable for use library screening in growth and motility assays</li> </ul>	<p>-Not currently adapted for continuous imaging</p>	<p>al. (2018) [168]</p>
--	---	--	--	-------------------------

Table 3.3. The advantages and disadvantages of recently developed automated nematode phenotypic imaging systems.

### 3.5.2 The imaging system was validated by screening The Pathogen Box library of compounds

The Pathogen Box, a library of a collection of 400 diverse drug-like molecules known to be active against various neglected diseases, distributed as an open-science project by the Medicines for Malaria Venture, was used in a screen against *C. elegans* growth/motility. Identifying the compounds with known anthelmintic or anti-parasitic activity mebendazole and tolfenpyrad [165] using an independent blinded screening approach serves as an important validation and supports the robustness of the screening platform. Repurposing of existing drugs for new indications is an established approach in drug discovery [197] and is particularly valuable for neglected tropical diseases as it may reduce research and development costs and speed progress to clinical trials [198]. Auranofin has recently been shown to have activity against filarial nematode infection [182]. The identification of auranofin as a compound that blocks *C. elegans* growth lends support to test repurposing of this compound for nematode infections. Isradipine, a safe and well-tolerated L-type calcium channel blocker, was also active

in the screen. Assaying the activity of isradipine in *in vivo* models of parasitic infection is a priority and could lead to re-purposing trials.

Fourteen compounds with previously undescribed anthelmintic activity were also identified in the *C. elegans* growth assay, belonging to a variety of chemical classes. These include benzoxazole and isoxazole compounds previously shown to have activity against *P. falciparum* [184, 185], and an imidazopyridine-containing compound previously shown to have *in vivo* anti-trypanosomal activity [186]. Another notable active compound was the benzoxaborole, MMV652003. Since the identification and successful progression into the clinic of the anti-fungal tavaborole, a number of benzoxaborole compounds have been reported to show potential for trypanosomiasis, malaria, cryptosporidiosis, toxoplasmosis and tuberculosis [199]. These results support the idea that some drug chemotypes can have activity against a diversity of infectious agents. Taken together these results demonstrate the potential for anthelmintic discovery using this system, with new compounds with anthelmintic activity identified by screens using the free-living nematode *C. elegans* as a parasite model.

The anthelmintic compounds identified in this study were active in a growth assay using *C. elegans*, which is typically considered a free-living nematode, although it undoubtedly has utility in anthelmintic drug discovery [149]. A critical step to support the development of these compounds will be to determine their activity on important human and animal parasitic nematodes. These compounds were inactive in a recently reported screen that determined their effects on motility of *H. contortus* xL3 [165]. It is therefore possible that their activity requires active growth of the target nematode, perhaps reflecting a target distinct from the neuromuscular system. A recent set of criteria for hit-to-lead progression in neglected infective diseases provides a useful guide to the steps that need to be taken to progress these early-stage hit compounds [200]. It will be particularly important to demonstrate activity against a

range of nematode parasites and differential sensitivity between parasite and host to support the development of a new anthelmintic.

The need for discovery of novel anthelmintic compounds for human, animal and crop parasites is clear from the global burden of such infections. Parasitic nematodes infect around one billion people, with soil transmitted *Ascaris*, hookworm and whipworm each afflicting hundreds of millions of people [201]. These diseases cause high morbidity and are closely linked with poverty in the developing world. The global impact of parasitic nematodes is worsened by their effect on livestock, equids and companion animals. Parasitic nematodes of livestock are thought to cost approximately \$10 billion annually; however increasing resistance to anthelmintics [202] and failure of eradication programs means there is an urgent need to identify new anti-parasitic treatments. Thus, the potential of large-scale high-throughput drug screening to identify such novel compounds could be a valuable contribution to this effort.

### 3.5.3 Applications of INVAPP/Paragon to *C. elegans* models of human disease

This study focused the application of the INVAPP/Paragon imaging system on investigating anthelmintic drug discovery. However, given its ability to determine growth and motility of *C. elegans* quickly and robustly, it could also be applied to the study of other human diseases modelled in *C. elegans*. It therefore constitutes a novel high-throughput imaging system that could be used for the large-scale library screening of transgenic worm models of human disease which display scorable growth/motility phenotypes, for novel chemical or genetic modifiers of disease.

# Chapter 4 Characterisation of a novel *C. elegans* model of AATD expressing ZAAT

## 4.1 Introduction

### 4.1.1 The transformation of *C. elegans* to model human disease

There are many advantages to using *C. elegans* to research human disease, as previously discussed in chapter 1, however a major strength is the capability of modifying its genome and using it to model complex human disorders. The three ways by which a *C. elegans* disease model can be generated include: (1) knocking out as a result of producing a mutant or knocking down (by RNAi) the worm homolog of a human gene involved in disease to investigate the resulting phenotype; (2) selecting a process in the worm that recapitulates cellular or molecular aspects of the disease mechanism; (3) enabling the worm to express the human gene, thereby providing a disease-associated measurable phenotype [203]. This third mode of genetic manipulation of the worm involves inserting a human gene, known as a transgene, by the method of transgenesis and is particularly useful in the study of human diseases which involve genetic component but for which there is no known worm homologue; as is the case with AAT.

Transgenesis is usually performed by microinjection of DNA into *C. elegans*. Simple transgenic DNA is injected into the distal arm of the gonad of the worm which contains a central core of cytoplasm that is shared by many germ cell nuclei [204]. Thus, DNA injected into this area can be delivered to many progeny. Microinjection of DNA by this method leads to the formation of large extrachromosomal arrays [205], however, these can be unstable and variable (animals are mosaic) and genetic information can be lost over generations. The extrachromosomal arrays can be integrated into the worm genome by irradiation (usually UV or gamma) which induces chromosomal breaks and ligation of arrays to chromosomes during DNA repair. This often results in multi-copy integration of the transgene, but this can be overcome by co-

injecting transgene DNAs with a single stranded DNA oligonucleotide [205], by using microparticle bombardment [206], by use of Mos1 transposon techniques [207] and more recently by use of the CRISPR/Cas9 system to introduce low or single copy transgene integrations. The CRISPR/Cas9 system provides the added advantage of locus-specific integration of the transgene [208].

Careful consideration is necessary when designing a transgene construct, which contains non-coding regions, the 5' flanking region with its promoter and transcriptional control regions, the 3' flanking region, the 5' untranslated region (UTR) with the functional translation site and the 3' UTR which provides a cleavage and polyadenylation signal and translational control elements. Additionally, introns are crucial as pre-mRNA splicing determines mRNA processing [209]. When generating transgenic *C. elegans* strains, it is also desirable to include a selectable co-injection genetic marker such as a specific phenotype (e.g. dumpy or roller) or a fluorescent marker [205]. This can help when attempting to identify mutants from a population.

#### 4.1.2 The advantages of scorable mutant phenotypes

Phenotypic modification can also be exploited when creating transgenic lines which model human disease. Transgenic *C. elegans* mutants can then be characterised for a specific phenotype and can be used to search for novel genetic or chemical modifiers of disease. Types of phenotypes can be wide ranging from simple fluorescent signal measurements, for example, fluorescently-labelled  $\alpha$ -synuclein expressed by a transgenic *C. elegans* model of Parkinson's disease (PD) which can be assessed in terms of its accumulation [210]; to observable physical changes, such as hyperplasia of the vulva in transgenic worm models of cancer [211]; to more complex behavioural modifications, such as defects in odourant preference associative learning observed in amyloid-beta transgenic worm models of Alzheimer's disease (AD) [212]. Measurable phenotypes can provide significant information on disease processes and pathologies and can be used to search for genes or chemicals which affect them. When these

phenotypes can be scored automatically, by high-throughput imaging methods such as the ones described in chapter 3, their use is particularly powerful in genetic or small molecule screening to search for disease alterants [159, 213].

#### 4.1.3 Transgenic *C. elegans* models of protein accumulation diseases

Transgenic worm models expressing and accumulating disease-associated proteins have provided key insight into disease mechanisms and have been used to search for novel genetic modifiers and drugs, which ameliorate disease. Examples include the tau and beta-amyloid (Abeta) accumulation models of AD; and the  $\alpha$ -synuclein accumulation model of PD.

AD is a progressive neurological disease that results in the irreversible degeneration of neurones especially in the neocortex, an area of the brain involved in higher order functions such as cognition and spatial reasoning and language [214]. Patients experience progressive dementia and current treatments are limited to symptomatic relief, meaning the need for novel therapies is great. Brains of AD patients are characterised by the accumulation of intracellular tau (a microtubule protein) neurofibrillary tangles [215] and of extracellular senile plaques composed of Abeta peptide [216]. Several transgenic *C. elegans* models of AD have been generated; one such worm strain expressed human mutant tau in all its neurones. Expression of the mutant protein caused decreased lifespan, uncoordinated movement, reduced egg laying and dumpy phenotypes in the worms resulting from axonal degeneration and progressive neuronal loss [217]. This model was used in a small molecule screen of 1120 compounds for chemical suppressors of tau-induced defects. The worm liquid thrashing assay identified 16 compounds which improved mutant swimming, and one compound, azaperone, also reduced tau aggregation in cultured human cells [218]. A number of transgenic *C. elegans* models of AD have been generated, expressing instead the toxic Abeta peptide [219]. Worm strains expressing Abeta in the muscle display varying degrees of movement defects and paralysis [220-222] and strains expressing Abeta in neurones display movement deficits and

neuronal damage (although, not all worm models display neuronal damage which is a limiting factor in their suitability) [223, 224]. Screening on such strains as these has yielded a number of small molecules capable of reducing Abeta aggregation-associated toxicity, such as the small molecule screening of the Abeta-expressing CL2006 strain identifying caffeine, bacitracin and tannic acid, which all reduced neuronal pathology [225].

PD is a progressive movement disorder characterised by symptoms of involuntary movements, muscle rigidity and balance problems due to the gradual loss of dopaminergic neurones from the substantia nigra. The cellular pathology of PD involves cytoplasmic protein inclusions called Lewy bodies which are largely composed of  $\alpha$ -synuclein, mutations in which are causatively related to PD, although the exact mechanisms are still poorly understood [226]. A transgenic *C. elegans* model of PD expressing human  $\alpha$ -synuclein labelled with yellow fluorescent protein (YFP) within the muscle was generated. Mutant worms developed an age-related  $\alpha$ -synuclein-containing inclusion phenotype which was screenable. RNAi screening was performed using this model which identified quality control and vesicle trafficking genes expressed in the ER/Golgi complex and vesicular compartments, suggesting a link between inclusion formation and cellular ageing [227]. A similar method was adopted by Hamamichi and colleagues, who expressed GFP-labelled human  $\alpha$ -synuclein in the *C. elegans* muscle. RNAi screening on this model implicated trafficking proteins, a modulator of G protein signalling and a gene thought to be involved in murine neurodegeneration [228].

Other examples include transgenic worm models expressing human mutant SOD1 and TDP-43 proteins, which are implicated in amyotrophic lateral sclerosis [229-231] and transgenic strains expressing mutant forms of *smn-1* associated with spinal muscular atrophy [232] (discussed in detail in chapter 5). Both of which have been used to further understanding of the disease pathology or to screen for novel modulators of disease [233, 234]. The *C. elegans* model of AATD previously described, is another such example. The model expresses and accumulates a

fluorescently-labelled mutant human ZAAT protein in intestinal cells and has been used in high-throughput drug and RNAi screening to search for modifiers which reduce this intracellular aggregation [109-111, 235]. These examples serve to outline the powerful combination of transgenic *C. elegans* disease modelling and the use of worms in high-throughput chemical and genetic screening to elucidate new information on human protein accumulation diseases.

#### 4.1.4 Limitations of *C. elegans* models of human disease

Modelling human diseases in transgenic *C. elegans* has many advantages and can be used to investigate disease pathology and mechanisms and to identify compounds which alter these processes, however, there are important limitations. The anatomical and molecular differences between nematode model organisms and humans do limit the utility of *C. elegans* in human disease research and clinical drug development. Such models should be viewed as complementary to cellular or *in vitro* assays rather than a replacement for higher order animal testing [236]. The usefulness of worm models remains strong particularly in the early stages of drug development such as high-throughput, genome-wide knock down or small molecule screening.

## 4.2 Aims

1. To phenotypically characterise a newly generated transgenic *C. elegans* strain expressing the human mutant protein ZAAT in terms of fluorescent protein accumulation, growth, motility and transgene expression.
2. To perform *in vitro* characterisation of the ZAAT protein expressed in the transgenic ZAAT worm strain and confirm its identity.
3. To evaluate the usefulness of the transgenic *C. elegans* model of AATD in high-throughput genetic and chemical screening studies using the INVAPP/Paragon imaging system.

## 4.3 Methods

### 4.3.1 Purifying and polymerising human plasma derived AAT

Mutant ZAAT was isolated from human blood plasma. Plasma was centrifuged at 3000 X g for 30 min at 4°C to remove any aggregates of additional plasma components. The supernatant was extracted and subjected to a second centrifugation under the same conditions. Plasma was filtered through glass fibre and cellulose acetate filters before loading onto an alpha-1 antitrypsin Select resin containing column (GE Healthcare). The packed bed agarose within the column contains camelid-derived single domain antibody which has a high affinity for AAT. The column was first washed with PBS adjusted to pH2.0 (low pH disassociates anything bound to the column) using an AKTAprime purification system (GE Healthcare), then equilibrated with binding buffer (20mM Tris, 150mM NaCl, pH7.4) at a flow rate of 3ml/min. The filtered plasma was then loaded onto the column before it was washed once again with binding buffer to remove any non-specific binding. 4ml fractions were collected by loading the elution buffer (20mM Tris, 2M MgCl<sub>2</sub>, pH7.4) through the column. Fractions containing protein were identified using absorbance at 280nm. The fractions were then pooled and dialysed overnight against 20mM Tris, pH8.0 at 4°C.

The protein sample was then subjected to ion exchange chromatography. A 5ml HiTrap Q HP™ column (GE Healthcare) was first equilibrated with washing buffer (20mM Tris, pH8.0). The dialysed protein solution was then loaded at a rate of 5ml/min before flushing washing buffer through the column once again. 4ml fractions were collected by loading elution buffer (20mM Tris, 1M NaCl, pH8.0) over a gradient of 0-100%. The fractions were then analysed using SDS denaturing and non-denaturing PAGE. Samples with the confirmed presence of monomeric ZAAT were pooled and β-mercaptoethanol (10mM final concentration) was added to reduce di-sulphide linkages and inhibit AAT dimerisation. The solution was then buffer exchanged against PBS+5% v/v glycerol using a 30,000 MWCO filtration tube (Millipore) (unless otherwise

stated, PBS was at pH7.4). Protein concentration was determined using a NanoDrop One (Thermo Fisher Scientific).

To polymerise ZAAT, the protein solution was diluted to 0.2mg/ml in PBS+5% v/v glycerol and 100µl aliquots were placed in PCR tubes. The tubes were heated at 60°C for 18h in a PTC-200 Thermal Cycler (MJ Research). The aliquots were then pooled and analysed by non-denaturing PAGE and western blot.

#### 4.3.2 Purification of mAbs from media

A 5ml protein G HiTrap column, mAb binding buffer (Thermo Fisher Scientific), mAb elution buffer (Thermo Fisher Scientific) and media supernatant containing the mAb were equilibrated to room temperature. The column was first washed with MilliQ water using the AKTAprime (GE Healthcare), then equilibrated with binding buffer at a flow rate of 3ml/min. The supernatant containing the mAb (3C11/2C1) was diluted 1:2 in binding buffer and loaded onto the column before washing with binding buffer. 3ml fractions were collected by passing elution buffer through the column. 300µl of Tris pH9 was added to the fractions containing mAb sample to neutralise the solution. The sample was then loaded onto a Q HiTrap column and washed 3X with PBS.

#### 4.3.3 Polyacrylamide gel electrophoresis

##### 4.3.3.1 SDS-PAGE

Purified protein samples or *C. elegans* lysates were examined by denaturing SDS-PAGE (sodium dodecyl sulphate-polyacrylamide gel electrophoresis) using the Nu-PAGE Bis-Tris gel system (Life Technologies (Thermo Fisher Scientific), Waltham, Massachusetts)). Briefly, 2µg of purified protein samples or 20µl of worm lysate were mixed with 1x lithium dodecyl sulphate (LDS) (a loading buffer for visualisation), DTT, 50mM, was also added when performing reducing PAGE to reduce the disulphide bond) and heated in a PTC-200 Thermal Cycler at 95°C

for 5min to denature the protein. The samples were then run on NOVEX 4-12% w/v Bis-Tris gels in NuPAGE MOPS running buffer at 200V for approximately 40min. A protein ladder (Spectra Multicolour Broad Range) was run in the first lane of the gel to allow for approximate determination of the protein band molecular weight. Protein band visualisation was achieved by staining with Instant Blue Coomassie stain (Expedeon) which was added to a tray containing the excised gel.

#### 4.3.3.2 Non-denaturing PAGE

Purified protein samples were also observed by non-denaturing PAGE using the Native PAGE gel system (Life Technologies (Thermo Fisher Scientific), Waltham, Massachusetts). The protein sample (2 $\mu$ g) was mixed with 1:4 sample buffer (50% v/v glycerol containing bromophenol blue to colour the sample). Samples were then loaded into NOVEX 4-16% w/v Bis-Tris gels and run in Native PAGE running buffer at 25 mA for approximately 40min. Bands were visualised using the Coomassie stain.

#### 4.3.4 *C. elegans* lysis to isolate ZAAT protein

Three gravid adult worms (ZAAT/N2) were picked to several large NGM plates seeded with OP50 *E. coli* bacteria. Plates were incubated at either 20°C, 24°C or 25°C until many animals were present. Worms of the same strain and experimental conditions were washed from the plates using 3X 3ml S-basal washes and collected in 50ml falcon tubes. The falcon tubes were centrifuged at 1195 x g for 2min and the supernatant discarded. The bottom 1ml worm suspension was transferred to an Eppendorf tube and 500 $\mu$ l of S-basal added to it. The Eppendorf was centrifuged at 16.1 x g for 10min and the supernatant discarded once more. 200 $\mu$ l of lysis buffer (150mM KCl, 1mM EDTA, 50mM Tris-HCl, 1 X protease inhibitor cocktail) was added to the pellet. The tubes were placed at -80°C overnight. Tubes were extracted from the freezer and the solutions were allowed to melt at room temperature. Worm suspensions were subjected to sonication at 5 microns for 15s X 2 with cooling on ice for 2min in the

interval. The samples were centrifuged at 16.1 x g at 4°C for 10min. The supernatant containing the soluble fraction was extracted and placed in a fresh Eppendorf and 200µl of lysis buffer was added to the remaining pellet. Both fractions were stored at -80°C.

#### 4.3.5 Western blot analysis

To visualise proteins using specific antibodies, the western blotting technique was employed. An SDS-PAGE or a non-denaturing PAGE was run as described above with 0.2µg purified protein per lane or with *C. elegans* lysate, 20µl. An Odyssey® One-color protein molecular weight marker (LI-COR, Lincoln, Nebraska) was included as a ladder, 2µl. The gel was transferred onto a polyvinylidene difluoride (PVDF) membrane using an Invitrogen iBlot machine (Thermo Fisher Scientific) for 7min. The membrane was soaked in phosphate buffered saline (PBS) for 10min before blocking in 5% w/v non-fat dry milk in PBS for 1h. AAT purified rabbit polyclonal antibody (1µg/ml) or 2C1 [237]. (0.1µg/ml) in blocking buffer (PBS 1X, Polysorbate 20 (Tween®20) 0.1% v/v, bovine serum albumin (BSA) 0.1% w/v, azide 0.1% w/v) were added and the membrane incubated at 4°C overnight. The next day the membrane was washed 6X 3min with PBS, Tween®20 (0.1% v/v). All steps from this point were performed in the dark. The Li-cor Odyssey IR labelled secondary anti-mouse/rabbit antibodies were added 1:10,000 in PBS-Tween® (0.1% v/v), 5% w/v milk and incubated for 1h at room temperature. The membrane was then washed 6X 5min in PBS-Tween® (0.1% v/v) and 6x 5min in PBS. The membrane was then scanned using a LI-COR Odyssey® IR reader at 169µM resolution and 2.5rfu intensity.

#### 4.3.6 Sandwich ELISA

Sandwich ELISA were performed using COSTAR 96-well EIA/RIA flat bottom plates. Assays were carried out at room temperature with 50µl final volume per well unless otherwise stated. Plates were coated with AAT purified rabbit polyclonal antibody diluted at 2µg/ml in coating buffer (PBS 1X pH 7.4) and left overnight. The plates were then washed the next day 3X 300µl

washing buffer (NaCl 0.9% w/v, Tween20 0.05% v/v) per well and blocked with 300 $\mu$ l of blocking buffer (PBS 1X, BSA 0.25% w/v, Tween20 0.05% v/v, azide 0.1% w/v) for a minimum of 1h. 100 $\mu$ l of antigen solution (purified ZAAT monomer/polymer) diluted to 500ng/ml or worm lysate in blocking buffer was then added to the first well of each row. 50 $\mu$ l of blocking buffer was added to all other wells. A 1:2 serial dilution was performed across the plates up to well 11 leaving well 12, containing blocking buffer only as a control. The plates were incubated at 4°C overnight. The next day, plates were washed, and 50 $\mu$ l of binding monoclonal antibody (2C1/3C11) was added to each well at 1 $\mu$ g/ml diluted in blocking buffer. Plates were incubated for 2.5h before washing. 50 $\mu$ l of secondary goat anti-mouse HRP labelled antibody diluted 1:2000 in blocking buffer without azide was added to each well and incubated for 1h in the dark. The plates were then washed before 50 $\mu$ l of TMB (Sigma Aldrich) substrate solution was added to each well and allowed to develop for approximately 10min in the dark. The reaction was then stopped by adding 50 $\mu$ l of 1M H<sub>2</sub>SO<sub>4</sub> to all wells. Absorbance was read at 450nm in a plate reader within 10 min of stopping the reaction.

#### 4.3.7 RNAi targeting the ZAAT transgene

To attempt the silencing of the ZAAT transgene in the mutant *C. elegans*, worms were fed with either two different bacterial clones both expressing dsRNA homologous to a section of the mutant transgene, or with L4440, an empty vector bacterial clone that produces no dsRNA. Worms were fed from the L1 stage and scored for any changes to the phenotype. Feeding was performed with the worms in liquid culture, as described by the 96-well plate culture method outlined in chapter 2, or seeded onto NGM plates, by a method outlined in chapter 6. Swimming of the worms in the liquid culture was assessed using the motility imaging platform INVAPP/Paragon after mechanically stimulating motility by inserting and removing a 96-well PCR plate into the wells on day 3. The 96-well NGM plates were flooded with 50 $\mu$ l S-basal before swimming of the worms was measured by INVAPP/Paragon on day 3.

## 4.4 Results

### 4.4.1 Generation of novel transgenic ZAAT-expressing *C. elegans* strains

In order to generate novel transgenic *C. elegans* strains expressing human ZAAT protein, a transgene was designed (by Dr Freddie Partridge and Dr Neda Motamedi-Shad) which contained a promoter in order to drive expression in the muscle tissue of the worm. The structure of the transgene construct can be seen in Figure 4.1. The construct also contained a secretion signal to ensure the protein was targeted to the ER and a TagRFP-T fluorescent label to allow a fluorescent readout of protein accumulation. This transgene construct was microinjected into the distal arm of the *C. elegans* gonad and offspring displaying fluorescent accumulation were selected and irradiated using X-ray (performed by Dr Freddie Partridge). Resulting transgenic strains were then sequenced to confirm the presence of the incorporated transgene. Several strains were separately integrated but the main two strains investigated were the ZAAT and the Z10AAT strains.



**Figure 4.1.** The transgene used to create ZAAT transgenic *C. elegans*. The construct contains a *myo-3* promoter to drive expression in worm muscle tissue; a *C. elegans* secretion signal to ensure the protein is targeted to the ER; a cDNA sequence for Z AAT and a TagRFP-T fluorescent marker in order to observe protein expression and localisation. The construct was designed by Dr Frederick Partridge and Dr Neda Motamedi-Shad.

#### 4.4.2 ZAAT transgenic *C. elegans* accumulate more ZAAT protein at higher temperatures

ZAAT expressed in transgenic *C. elegans* is labelled with the fluorescent protein TagRFP-T, which allows visualisation of the mutant ZAAT within the worm (Tag-RFP Absorption/Emission = 555nm/584nm). To compare fluorescence observed in N2, ZAAT and Z10AAT at different temperatures, 3 worms from each strain were picked to NGM plates and incubated at either 20°C, 25°C or 26°C for at least 1 week. Four offspring from each strain were picked at random and immobilised on a 3% agarose pad. Worms were imaged by bright field microscopy with an exposure of 15ms, followed by fluorescent microscopy imaging at an exposure of 150ms. As expected, no fluorescence can be seen in any N2 strain worms in Figures 4.2A-C at 20°C, 25°C or 26°C respectively. Very little fluorescence can be seen in the ZAAT strain incubated at 20°C (Figure 4.2D), but in contrast a high level of fluorescent can be seen in ZAAT worms incubated at 25°C. This suggests that the ZAAT-expressing worms are accumulating more fluorescent protein at 25°C compared with 20°C. Virtually no fluorescence is visible in the Z10AAT strain incubated at 20°C, although some fluorescence can be seen in Z10AAT worms incubated at 25°C. The level of RFP fluorescence drops for both the ZAAT and Z10AAT strains when incubated at 26°C, this is because the worms are very unhealthy at this temperature and are in fact near death. The ZAAT strain displaying the highest level of fluorescent accumulation, it was selected to be the primary strain for further experiments including setting up screening protocols for identifying modifiers of AATD.

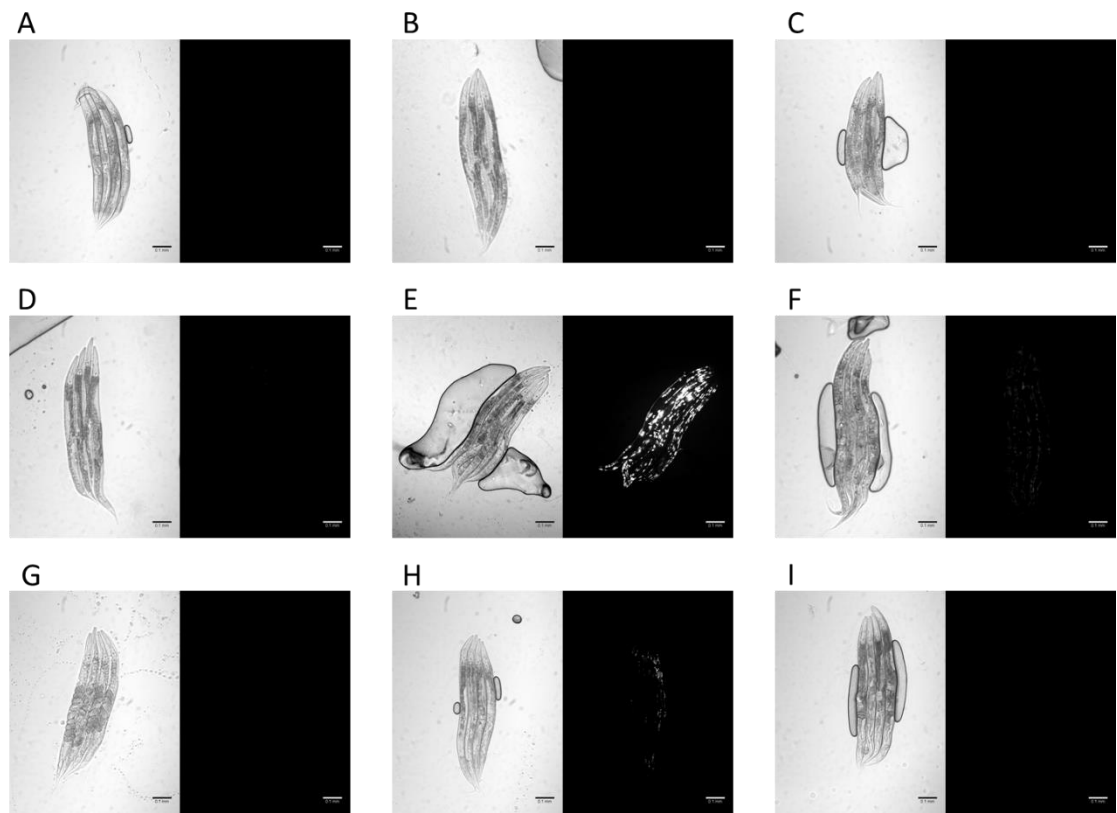


**Figure 4.2.** Bright-field and corresponding fluorescent images of N2, ZAAT and Z10AAT worm strains incubated at 20°C/25°C/26°C. Fluorescence indicates accumulation of Tag-RFP labelled ZAAT. (A-C) N2 worms incubated at 20°C, 25°C and 26°C respectively. No fluorescence is detected at any temperature. (D-F) ZAAT worms incubated at 20°C, 25°C, 26°C respectively. A higher level of fluorescence is detected in worms at 25°C compared to 20°C and lowers again at 26°C. (G-I) Z10AAT worms incubated at 20°C, 25°C and 26°C respectively. More fluorescence is detectable in worms incubated at 25°C compared with those incubated at 20°C but less detectable fluorescence in worms incubated at 26°C. Scale bar = 0.1mm.

#### 4.4.3 Purifying and polymerising ZAAT from human plasma for *in vitro* studies

In order to characterise the ZAAT expressed within the transgenic *C. elegans* ZAAT line *in vitro*, it was first necessary to isolate, prepare and purify ZAAT from human blood plasma. This purified protein could be used as a standard sample in protocols such as western blot analysis and ELISA to confirm the identity of the protein expressed in the worm model. Protein

purification from blood plasma was achieved using column chromatography. ZAAT was purified from plasma by the use of two columns. The first column contained a resin onto which was bound an antibody with high affinity for AAT. The fractions containing ZAAT (confirmed by SDS PAGE) are loaded onto a second column, an ion exchange column which separates molecules based on charge. The resulting eluent fractions were analysed by native PAGE for the presence of AAT (Figure 4.3A). Fractions containing monomer bands indicated by the blue arrow were pooled (columns 2 and 3). It is possible to induce polymerisation *in vitro* by heating monomeric AAT purified from human plasma. Polymer samples were prepared by heating monomer samples at 60°C for 18h. Polymerisation of ZAAT was confirmed by native PAGE (Figure 4.3B). Figure 4.3C confirms the final purified ZAAT monomer and polymer products on a native PAGE.

In order to characterise the ZAAT protein produced by the ZAAT-expressing transgenic *C. elegans* strains by immunochemistry, it was also necessary to purify antibodies specific for polymeric forms of ZAAT (mAb 2C1) and for monomeric and polymeric forms i.e. total protein (mAb 3C11) from hybridoma cell supernatant. Hybridoma cell lines have been generated by the Lomas group which produce antibodies specific to certain conformations of AAT [237]. Supernatant from hybridoma cells expressing either 3C11 or 2C1 was collected and purified by column chromatography using a protein G HiTrap column. Figure 4.3D shows antibody supernatant prior to purification and the resulting purified mAb after column purification for 3C11 and 2C1 respectively.

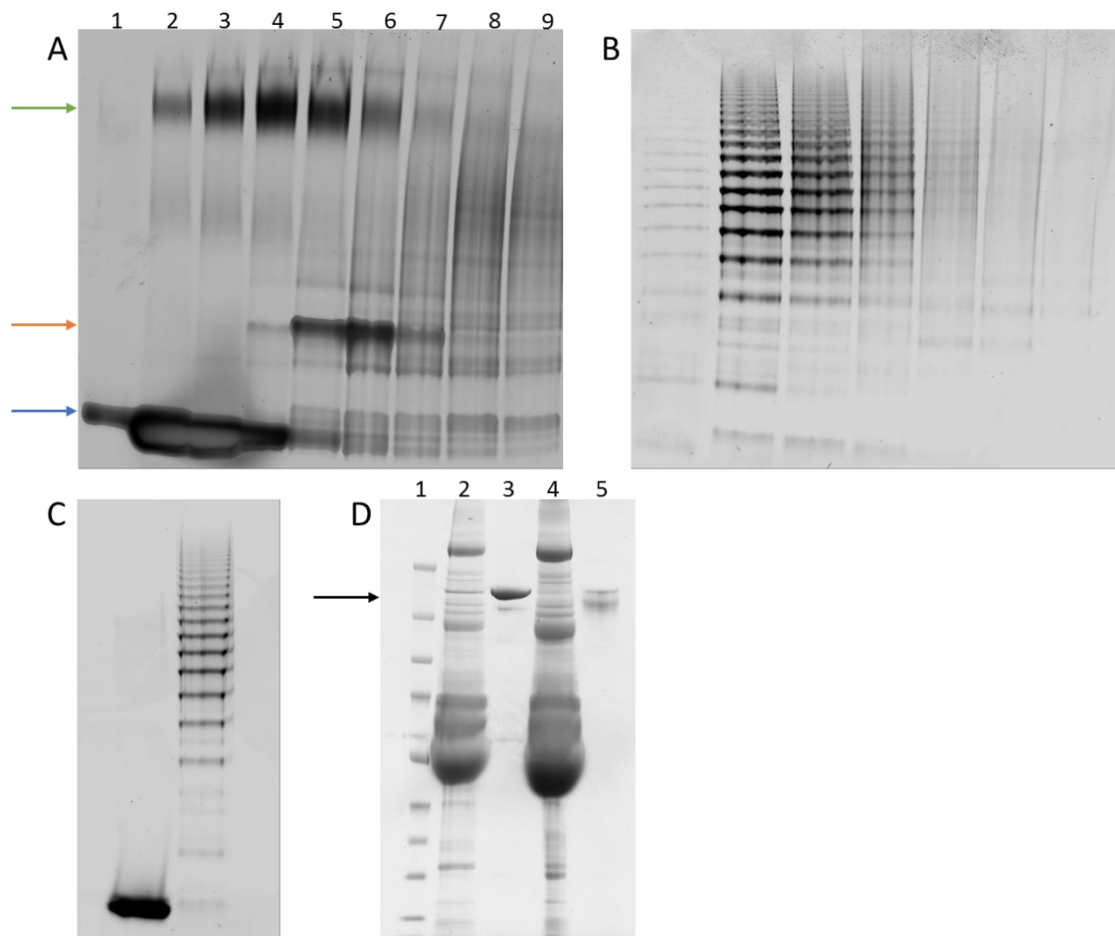


**Figure 4.3.** The purification of ZAAT from human plasma. (A) Native PAGE showing the fractions collected using the AKTApriime following purification using the alpha select resin-containing column and the Q sepharose column. The blue arrow indicates AAT monomer and the green arrow indicates an antibody bound species of AAT also present in human plasma. The orange arrow indicates ZAAT disulphide dimer species (AAT molecules can form dimers by disulphide bonding between cysteines of different molecules). The first column contains a previously purified sample of ZAAT (4 $\mu$ g) for reference. Samples from columns 2 and 3 were pooled. (B) Purified ZAAT monomer was heated at 60°C for 18h to induce polymerisation (Native PAGE) (4 $\mu$ g loaded). (C) Native PAGE showing final purified ZAAT monomer and polymer (4 $\mu$ g). (D) SDS PAGE showing the purification of 3C11 (lane 3, 2 $\mu$ g) from supernatant of hybridomas producing 3C11 (lane 2, 15 $\mu$ l) and 2C1 (lane 5, 2 $\mu$ g) from supernatant of hybridoma cells producing 2C1 (lane 4, 15 $\mu$ l).

#### 4.4.4 ZAAT expressed by the transgenic *C. elegans* worms is recognised by a polyclonal anti-AAT antibody

To confirm that the protein expressed within the ZAAT *C. elegans* strain was indeed AAT, several NGM plates of transgenic worms and N2 worms were incubated at 25°C. Worms were washed with lysis buffer and lysed by sonication. The soluble and non-soluble fractions were separated, and samples of the soluble fraction loaded in triplicate onto an SDS PAGE. The SDS PAGE gel was transferred onto a PVDF membrane and used to perform a western blot. The membrane was incubated with two antibodies: the commercially available rabbit anti-AAT polyclonal antibody (RbAT), which recognises all forms of AAT and an anti-RFP antibody to visualise the RFP in case of protein cleavage. Bands recognised by the RbAT antibody can be seen in columns 2-4 of Figure 4.4. The position of the bands is lower than expected (purified ZAAT protein was run in column 1) which is consistent with cleavage of the RFP at P1 of the reactive centre loop of AAT. RFP is attached by a linker to the C-terminal of ZAAT which is susceptible to proteolytic degradation. The bands visualised by the anti-RFP antibody can also be seen lower down in columns 2-4, confirming that the RFP has indeed been cleaved. However, the recognition of the bands containing ZAAT protein and RFP in columns 2-4 confirm that AAT-RFP is the protein being expressed in the transgenic *C. elegans* ZAAT strain. The absence of bands in columns 5-7 in Figure 4.4 confirms that this protein is not present in the wild type N2 strain.

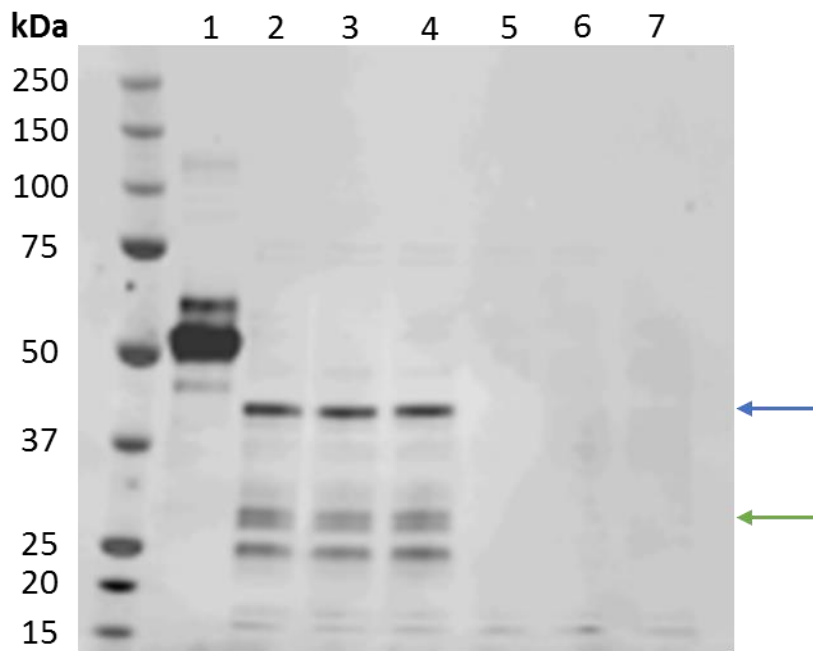


**Figure 4.4.** Visualisation of ZAAT protein in transgenic worms by western blot analysis. Western blot of a 4-12% w/v acrylamide SDS PAGE gel containing a standard sample of 0.2µg ZAAT isolated from human plasma (column 1), lysed samples of ZAAT-expressing *C. elegans* (columns 2-4) and lysed samples of N2 *C. elegans*. The western blot was incubated with two antibodies; a rabbit polyclonal anti-AAT antibody and an anti-RFP antibody. The blue arrow indicates ZAAT and the green arrow indicates RFP. The presence of bands in lanes 2-4 indicates the presence of RFP-tagged AAT in the ZAAT worm lysis and the absence of bands in lanes 5-7 suggests no AAT present in the N2 worm lysis.

#### 4.4.5 Quantification of total and polymeric ZAAT protein within the transgenic ZAAT-expressing *C. elegans* strain

In order to characterise the forms and to quantify the amount of AAT found within the transgenic *C. elegans* line, the two antibodies: 3C11 and 2C1 were used in a sandwich ELISA assay. Several plates of either N2 or ZAAT-expressing worms were incubated at 20°C or 24°C until a large number of animals were present. The worms were washed and lysed by sonication. ELISA plates were coated with the RbAT polyclonal antibody and ZAAT monomer or polymer added as standards as well as worm lysis samples (a monomer standard is used to

quantify total AAT). mAbs 3C11 or 2C1 were added as detection antibodies to visualise both monomeric and polymeric forms of ZAAT together (3C11) or only polymeric forms (2C1). Data from the sandwich ELISAs were normalised to total worm protein present in the lysed samples by Bradford assay. Standard curves in Figures 4.5A and C reveal that mAbs 3C11 and 2C1 recognise monomeric and polymeric forms of ZAAT respectively. The mAb 3C11 detected total ZAAT in the transgenic ZAAT *C. elegans* strains at 20°C and 24°C (Figure 4.5B). The levels of total protein are comparable possibly due to a balance between a higher level of polymer accumulation at 24°C but a lower level of ZAAT monomer. 3C11 did not detect total ZAAT at either temperature in the N2 strain. The mAb 2C1 has detected polymeric ZAAT in the transgenic worm strains at 20°C and 24°C, with a greater amount detected at the higher temperature (Figure 4.5D). This indicates that more polymeric ZAAT is accumulated within the ZAAT strain when the worms are cultured at a higher temperature. Virtually no polymeric ZAAT was detected in the N2 strain at either temperature. Taken together, these data confirm that the transgenic ZAAT *C. elegans* strain expresses the human ZAAT protein and accumulates more polymeric ZAAT at higher temperatures. The ELISA data shown in Figures 4.5B and D represent n=3 biological replicates.

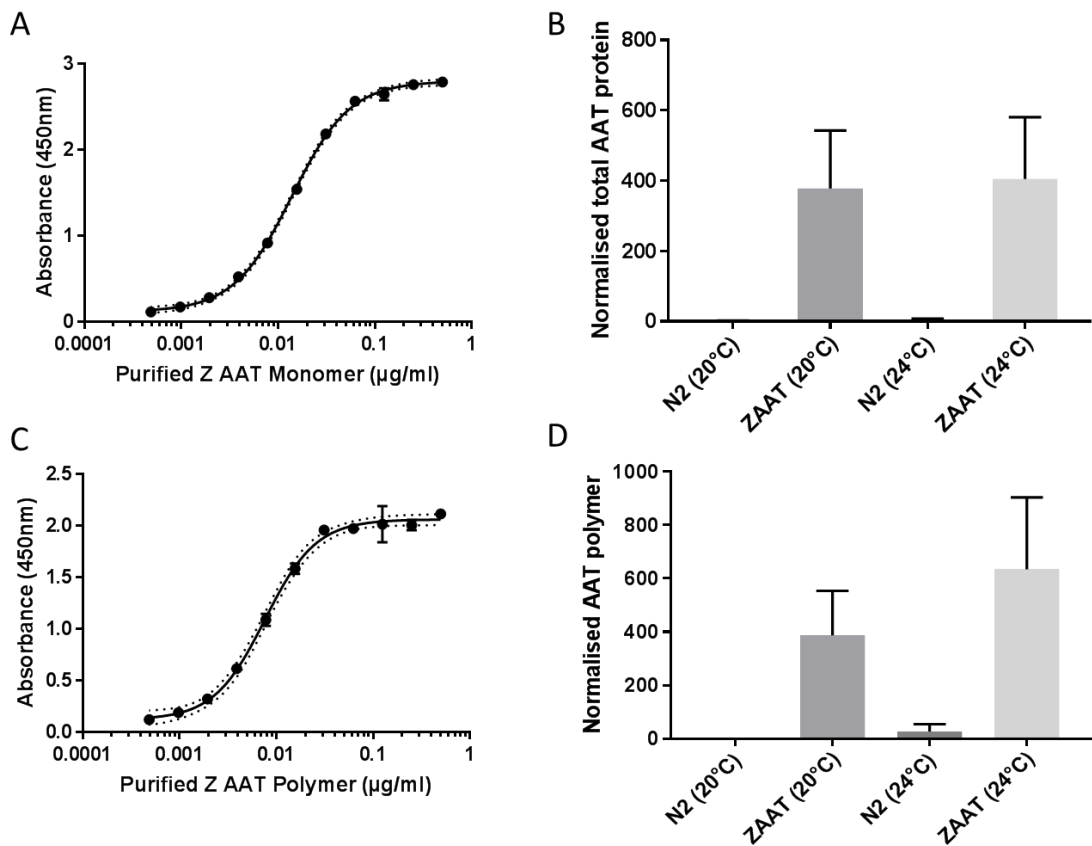


**Figure 4.5.** Quantification of ZAAT total protein and ZAAT polymer in N2 and ZAAT-expressing *C. elegans*. (A) Standard curve of ZAAT monomer recognised by the 3C11 antibody by sandwich ELISA. (B) Total (monomer and polymer) ZAAT protein levels quantified in N2 and ZAAT strains incubated at 20°C and 24°C by 3C11 sandwich ELISA and normalised to total protein by Bradford assay. (C) Standard curve of ZAAT polymer recognised by the 2C1 antibody by sandwich ELISA. (D) Polymeric ZAAT protein levels quantified in N2 and ZAAT strains incubated at 20°C and 24°C by 2C1 sandwich ELISA and normalised to total protein by Bradford assay. C and D represent n=3. Error bars in A and C represent standard deviation and dotted lines indicate 95% confidence interval. Error bars in B and D represent SEM. Plotted using GraphPad, v7.

#### 4.4.6 ZAAT transgenic *C. elegans* display growth and developmental impairment when cultured at higher temperatures

*C. elegans* are normally cultured on a lawn of bacteria on agar plates within the temperature range 15-25°C. Culturing at a higher temperature increases the speed of growth and development in wild type worms. In order to determine the effects of temperature on the rate

of growth and development, 3 gravid adult worms (N2 or ZAAT transgenic) were picked to an agar plate and incubated at variable temperatures (20/25/26°C). They were then imaged on the same day (N2 worms on day 6 and ZAAT worms on day 7). N2 *C. elegans* grew, reproduced and developed normally when incubated at all temperatures (Figures 4.6A-C), however the process was faster at 25°C and 26°C (Figures 4.6B and C respectively) compared to 20°C (Figure 4.6A). Transgenic ZAAT worms cultured at 20°C appear to grow and reproduce normally (Figure 4.6D). In contrast, ZAAT worms cultured at 25 and 26°C display a pronounced impairment of growth and/or development and/or reproduction (it is not possible to determine which aspect is being affected) when compared to those cultured at 20°C (Figures 4.6D-F). Though slower, transgenic worms cultured at 25°C do in fact reproduce and grow as some can be seen on the plate in Figure 4.6E. However, in Figure 4.6F it is apparent that most transgenic worms cultured at 26°C have failed to reproduce successfully or have died. These images show that N2 *C. elegans* grow and reproduce normally when cultured on NGM at 20, 25 and 26°C. Transgenic ZAAT *C. elegans* however, display impaired growth and reproduction when cultured at 25 and 26°C when compared with 20°C.

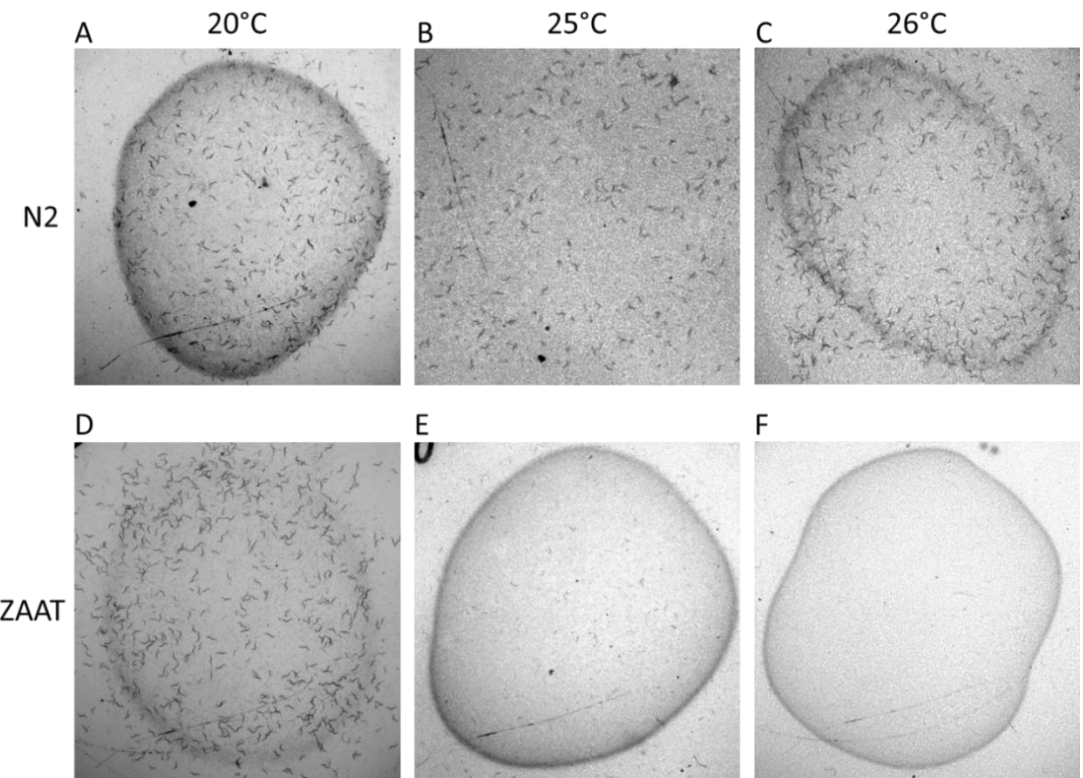


**Figure 4.6.** ZAAT transgenic worms grow and develop at a slower rate compared with N2 when cultured at different temperatures. Three *C. elegans* worms (N2 or ZAAT expressing) were picked to an NGM plate seeded with *E. coli* and incubated at different temperatures (A and D at 20°C, B and E at 25°C and C and F at 26°C) then imaged, N2 (A-C) on day 6 and Z (D-F) on day 7. (A-C) N2 *C. elegans* display an increased rate of growth and development when cultured at 25 and 26° compared to those cultured at 20°C. Development is also observed as normal. (D-F) Transgenic ZAAT expressing *C. elegans* show a marked growth or developmental deficiency when cultured at 25 and 26°C compared with culture at 20°C. A few worms can be seen on the plate at 25°C, however most worms have died at 26°C.

#### 4.4.7 The motility of ZAAT transgenic *C. elegans* can be quantified and is temperature-dependent

To explore the effect of temperature on the movement of ZAAT *C. elegans*, transgenic and wild type worms cultured in 96-well plates were incubated from bleaching at 20°C or 25°C, or at 26°C from re-feeding (Figure 5.2A, chapter 5). The plates were imaged using the INVAPP/Paragon imaging system as described in chapter 3, and the movement index

generated by the algorithm in MATLAB was plotted in GraphPad Prism. Figure 4.7A shows a significant decrease in movement in wells containing the ZAAT strain incubated at 25°C when compared with 20°C. Virtually no movement was detected in wells containing transgenic worms incubated at 26°C. N2 worms were similarly treated and no significant difference in the amount of movement was observed between plates cultured at 20, 25 and 26°C (Figure 4.7B). These results show that motility observed in wells containing ZAAT worms is considerably reduced when plates are cultured at 25°C and 26°C when compared with a control culture incubated at 20°C. Also, amount of movement in wells containing N2 worms remains unchanged when the cultures are incubated at 25°C and 26°C when compared with a control incubated at 20°C.

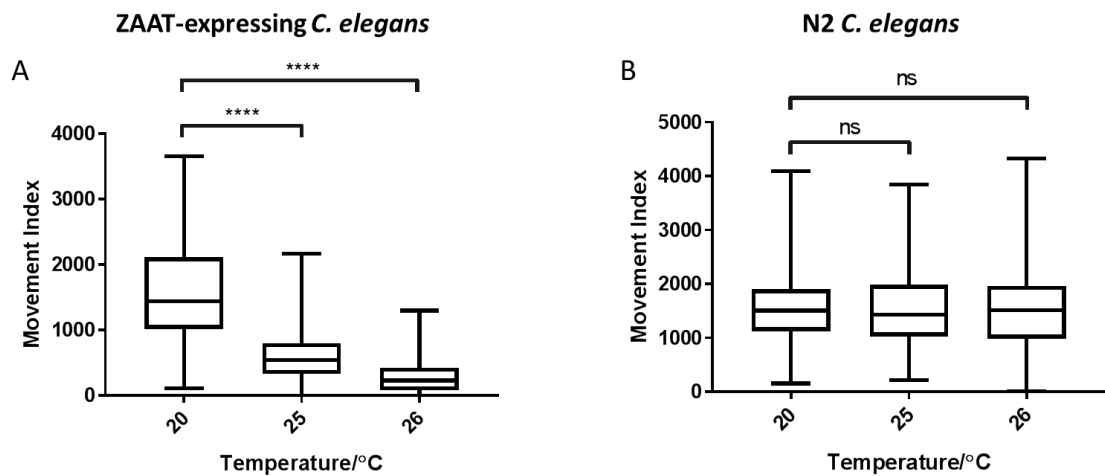


**Figure 4.7.** Motility of ZAAT transgenic *C. elegans* decreases with increasing temperature of culture incubation. (A) Movement index generated by INVAPP/Paragon imaging system of ZAAT *C. elegans* cultured in 96-well plates at 20 or 25°C from bleaching the worms (day 6) and at 26°C from re-feeding (day 7). *C. elegans* movement is reduced at 25°C compared to 20°C, and is even lower at 26°C (One-way ANOVA,  $F(2,1725)=160.4$ ,  $p<0.0001$ , followed by Tukey's multiple comparisons test, \*\*\*\*=  $P<0.0001$ ) (B) Movement index generated from imaging 96-well plates containing N2 *C. elegans* cultures incubated at 20, 25°C from bleaching (day 6) and at 26°C from re-feeding (day 7). No significant difference in movement index was detected between plates cultured at varying temperatures (One-way ANOVA,  $F(2, 1725)=0.9451$ ,  $p=0.3889$ ). Box and whiskers plot. Central line in box represents the median, the box extends from the 25<sup>th</sup> to the 75<sup>th</sup> percentiles and the whiskers indicate minimum and maximum values. Plots produced in GraphPad v7.

#### 4.4.8 A separately integrated transgenic *C. elegans* strain, Z10fem also displays temperature-dependent movement deficit

The motility of a separately injected and integrated strain of *C. elegans* expressing ZAAT (Z10fem) was investigated in order to confirm that the movement deficit observed in the ZAAT-expressing worms (Figure 4.7) was the result of transgenic integration. The integrated strain Z10 was crossed with *fem-1*, a strain which is sterile at high temperatures, as outlined in

chapter 5. The method of culture and imaging also followed the protocol that was developed for the drug screen described in chapter 5. Cultures were grown at either 25 or 26.5°C in 96-well plates from the L1 larval stage (day 1) and imaged using the INVAPP imaging system (day 7). Figure 4.8A shows that when cultured at 25°C from the L1 stage, Z10fem display a significant reduction in motility when compared with the control background strain *fem-1*. Figure 4.8B reveals that this significant temperature-dependent motility deficit is even further impaired when the cultures are incubated at 26.5°C. This result confirms that integration and expression of the ZAAT transgene has resulted in worm strains with a motility deficient phenotype.

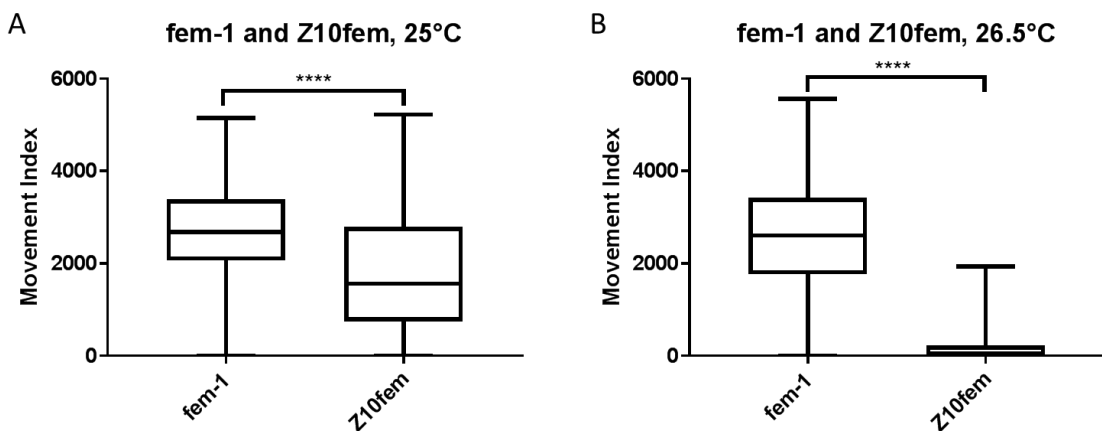


**Figure 4.8.** Motility of *Z10fem* strain decreases when incubated at higher temperatures. (A) *Z10fem* worms showed a significant decrease in motility when cultured at 25°C from L1 stage compared to the background *fem-1* strain. (Unpaired t test, \*\*\*\*= P<0.0001) (B) Very little movement was detected when *Z10fem* worms were incubated from L1 stage at 26.5°C compared with the *fem-1* strain. Cultures were started with filtered L1 worms on day 1 and imaging was performed on day 7. (Unpaired t test, \*\*\*\*= P<0.0001). Central line in box represents the median, the box extends from the 25<sup>th</sup> to the 75<sup>th</sup> percentiles and the whiskers indicate minimum and maximum values. Plots produced in GraphPad v7.

#### 4.4.9 Attempting to knock down the ZAAT transgene by RNAi

In order to further confirm that the motility deficient phenotype of the ZAAT worm strain was the result of integrated ZAAT transgene expression, RNAi knock down of the transgene was performed by three different methods: feeding on NGM agar plates, liquid feeding in 96-well plates and by the RNAi feeding protocol developed and outlined in chapter 6.

First, the effects of feeding bacterial clones containing dsRNA complementary to the TagRFP-T portion of the transgene on growth, development and reproduction were explored on NGM plates. Plates containing IPTG were seeded with either L4440 (a blank control containing no dsRNA) or with two different bacterial clones containing dsRNA. 3 gravid adult ZAAT expressing *C. elegans* were picked to plates which were incubated at 20, 25 or 26°C. The plates were all imaged on the same day 1 week later. Figures 4.9A, D and G show that transgenic ZAAT worms fed with L4440, or RNAi bacterial clones cultured at 20°C reproduced and the progeny developed and grew normally. However, Figure 4.9B, E, H and C, F, I reveal no difference in the growth and development of ZAAT worms fed the RNAi bacterial clones and incubated at 25 and 26°C respectively, when compared with the negative controls at either temperature (L4440). This suggests that the RNAi is not efficiently knocking down the mutant transgene.

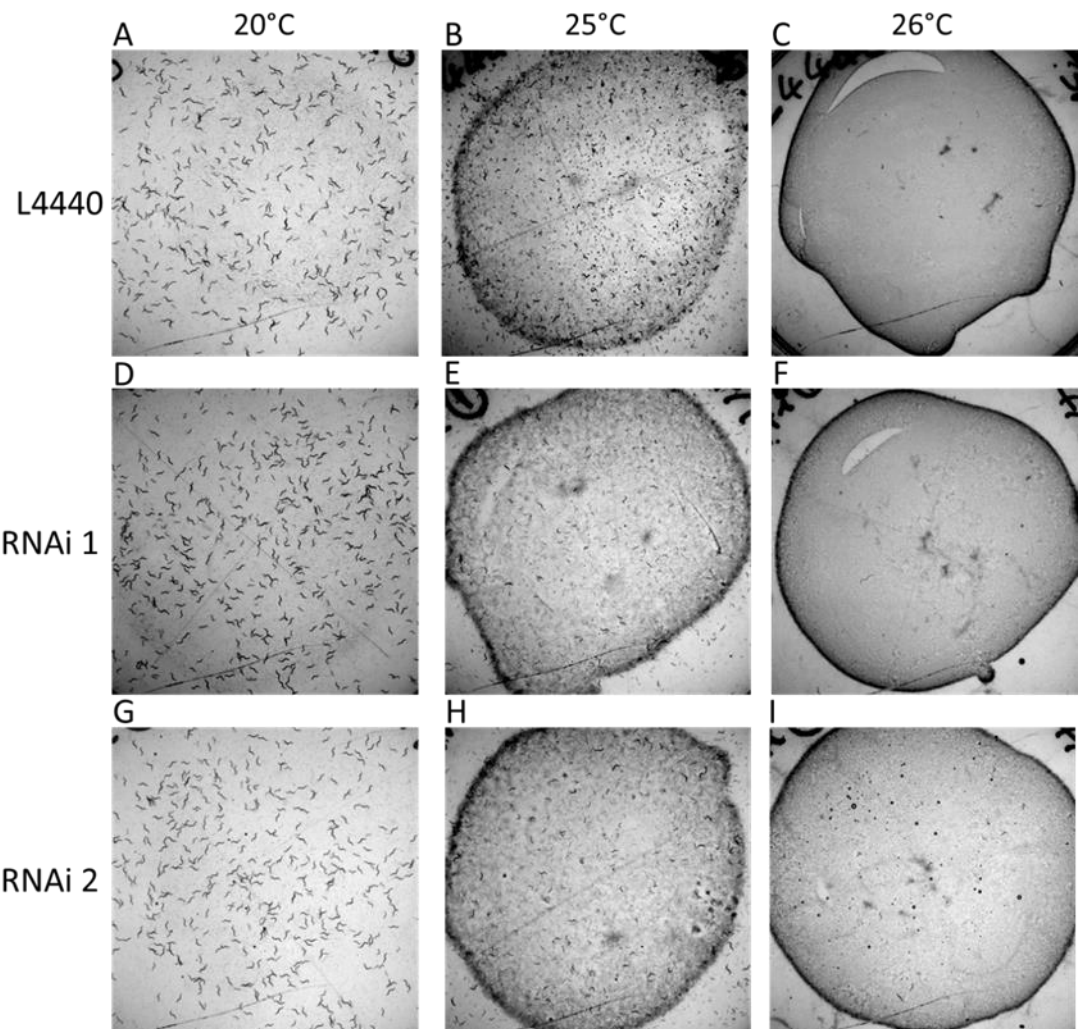


**Figure 4.9.** Three gravid adult ZAAT expressing *C. elegans* were picked to an NGM plate seeded with either L4440 (blank bacterial clone containing no dsRNA) (A-C), RNAi 1 bacterial clone (D-F) or RNAi 2 bacterial clone (G-I), containing dsRNA homologous to the Tag-RFP portion of the transgene. The plates were then incubated at 3 different temperatures: A, D and G at 20°C; B, E and H at 25°C and C, F, I at 26°C. No improvement in growth and reproduction of ZAAT worms cultured at 25 and 26°C fed either RNAi 1 or 2 when compared with the negative blank control (L4440) was observed.

The second attempt at RNAi silencing of the ZAAT transgene involved feeding the bacterial clones to liquid cultures of ZAAT-expressing worms and quantifying motility using the INVAPP/Paragon imaging system. RNAi feeding in liquid culture was performed in 96-well plates using the method outlined in chapter 3. However, instead of adding HB101 bacteria as

the food source to the worm cultures; either L4440, RNAi 1 or RNAi 2 were added instead.

Plates were incubated at either 20, 25 or 26°C and imaged using the INVAPP/Paragon system.

Figure 4.10A potentially reveals a very small improvement to the ZAAT worms' motility when fed with the dsRNA-expressing bacterial clones compared with the motility when fed with the blank L4440 control bacteria. The effect however, is neither profound nor conclusive, suggesting that efficient knock down of the transgene was not occurring. Thus, a third feeding method was attempted.

To increase the prospect of knocking down the ZAAT transgene in ZAAT *C. elegans* worms, the Z3RF strain created in chapter 6 was used in the feeding experiment. This ZAAT-expressing strain also contained a deletion mutation, *rrf-3*, which rendered it hyper-sensitive to RNAi silencing [135]. The protocol used was also the RNAi feeding protocol developed and outlined in chapter 6 for the RNAi screen. Briefly, L4440, RNAi 1 or RNAi 2 bacterial clones were seeded onto NGM agar (+IPTG) within the wells of 96-well plates. Either the control (*rrf-3*) or the Z3RF worms were dispensed onto the agar and all plates were incubated at 26.5°C for three days. Wells were flooded with S-basal and worm swimming was imaged using the INVAPP/Paragon system. No significant rescuing effect was observed on the temperature-dependent motility deficit of the Z3RF animals fed with RNAi clones expressing dsRNA complementary to the Tag-RFP portion of the transgene, compared with Z3RF worms fed with the blank L4440 clone. No effect was observed on the control *rrf-3* strain fed with any of the bacterial clones (Figure 4.10B). This data represents n=3 biological repeats. This suggests that the ZAAT transgene is not being efficiently knocked down within the transgenic strain upon feeding with bacterial clones expressing dsRNA complementary to the transgene. This could in part be due to a higher copy number of the integrated transgene than expected, as integration is a non-controlled event occurring during x-ray irradiation of worms expressing the transgene in an extra-chromosomal array.

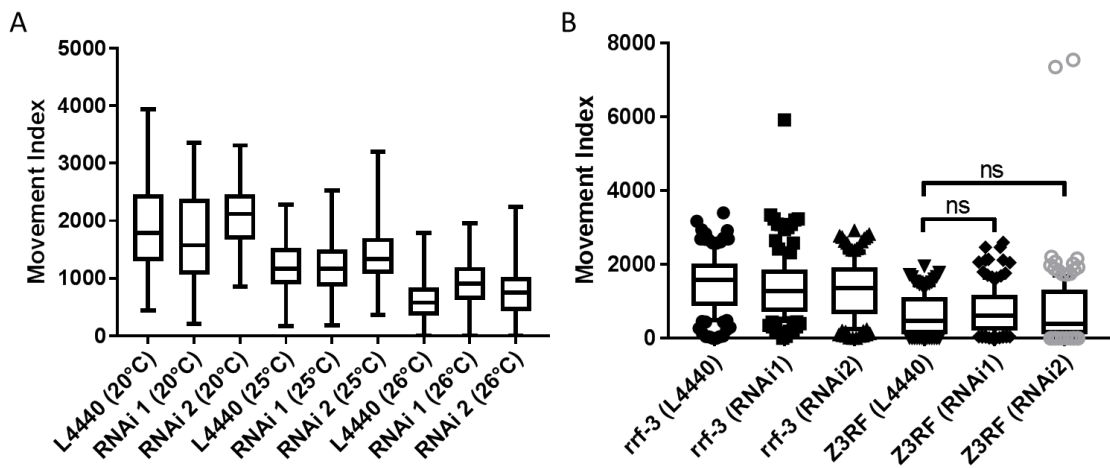


**Figure 4.10.** Efficient RNAi knock down of the ZAAT mutant transgene was not observed. (A) Two bacterial clones expressing dsRNA homologous to the transgene and a blank bacterial clone (L4440) were fed to ZAAT expressing *C. elegans* in liquid culture. Cultures were incubated at either 20°C, 25°C or 26°C. Worms were then imaged using the motility imaging platform INVAPP. A small but not complete rescue could potentially be seen. (B) Bacterial clones were fed to Z3RF and *rrf-3* (control) RNAi hypersensitive strains on NGM agar in 96-well plates. Swimming was imaged using the INVAPP system. No efficient rescue of the mutant motility deficit phenotype was captured. Data in (B) represents n=3, One-way Anova with Tukey's multiple comparison test. Central line in box represents the median, the box extends from the 25<sup>th</sup> to the 75<sup>th</sup> percentiles and the whiskers indicate minimum and maximum values. Minimum and maximum data points shown in B to highlight outliers. Produced in GraphPad v.7

#### 4.4.10 Confirmation that the motility-deficient phenotype was the result of transgene expression by qPCR

As the RNAi knock down of the ZAAT transgene in ZAAT worms was not achieved, confirmation that transgene expression (and not just disruption of the genome) was the cause of the motility impairment in the mutant strain was sought by qPCR. The second purpose of utilising this technique was to investigate whether the temperature-dependent motility deficit effect was the result of enhanced transgene expression at higher temperatures. The qPCR protocol outlined in chapter 7 was employed to measure the expression level of the inserted transgene relative to two housekeeping genes. Briefly, RNA was extracted from approximately 40

L4/adult worms and converted to cDNA. cDNA levels were quantified relative to two endogenous *C. elegans* genes: *ama-1* and *unc-15*. Figure 4.11 reveals that expression of the ZAAT transgene is indeed quantifiable within the ZAAT *C. elegans* strain. This confirms that the transgene is integrated into the worm genome and is resulting in the transcription of ZAAT protein in this strain. Interestingly, the relative expression levels of the ZAAT transgene in the strain is not significantly different between worm populations cultured at 20°C and 24°C. This also indicates that the transgene expression remains fairly constant at different temperatures, suggesting that the temperature-dependent motility impairment effects are not driven by an increase in ZAAT protein expression. Rather, the observed movement reduction phenotype could be the result of increased toxic protein accumulation within the muscle. The data in Figure 4.11 represents n=3 biological replicates.

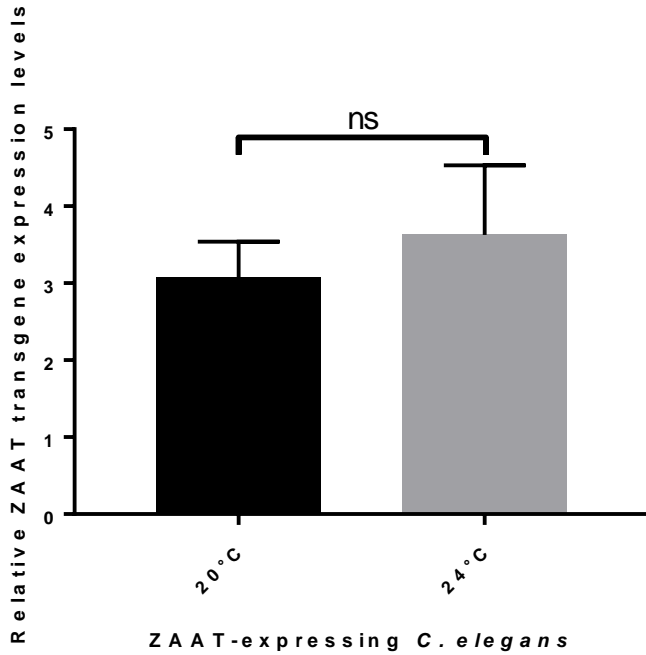


**Figure 4.11.** Expression of the ZAAT transcript is quantifiable in transgenic ZAAT-expressing worms. The expression of the inserted ZAAT transgene was quantified by qPCR. Expression was detected in worm populations cultured at 20°C and 24°C and was not significantly different across temperatures. n=3, unpaired t-test. P=0.6112. Error bars represent SEM. Plot produced in GraphPad v.7

## 4.5 Discussion

### 4.5.1 A newly generated transgenic *C. elegans* model of AATD

Properties of a novel *C. elegans* model of AATD generated to express the mutant form of ZAAT protein within the muscle of the worms have been described. Two separately integrated lines expressing the mutant protein were created: ZAAT and Z10. The accumulation of RFP fluorescently labelled ZAAT protein in the muscle of both strains can be observed in the microscopy images in Figure 4.2. Interestingly, the accumulation increases with increasing temperature. ZAAT is the more highly-expressing strain, and so it was taken forward for further investigation.

The use of human ZAAT and antibodies against monomeric and polymeric forms of AAT isolated in vitro allowed valuable characterisation of the protein expressed in the mutant *C. elegans* strain [237]. It was confirmed that the protein was indeed ZAAT by western blot and also by ELISA. The ELISA data confirmed the presence of both total (monomeric and polymeric) and polymeric forms of ZAAT expressed within the worms, and also suggested that a higher level of polymeric ZAAT protein was present in worms cultured at a higher temperature (24°C).

Phenotypic characterisation of the transgenic ZAAT-expressing worm strain revealed a significant temperature-dependent growth and/or motility deficit when cultured, with greater penetrance at higher temperatures. The motility deficit phenotype appears to be more profound than that of the *smn-1* mutant model, *cb131*, of SMA described in Sleigh *et al.* (2011), which reported a decrease in liquid thrashing rate of the worms. ZAAT worms cultured at higher temperatures displayed very little movement at all. This coincides with a more pronounced development/reproduction deficient phenotype observed in the ZAAT strain compared with the *snm-1* [234]. The ZAAT-causing motility-deficient phenotype of the transgenic worms was confirmed by motility analysis of the separately integrated ZAAT protein-expressing strain Z10fem (Z10 was crossed with *fem-1* as outlined in chapter 5). These results suggested that the worm deficiency phenotypes were caused by the toxic accumulation of mutant human ZAAT within the muscle cells. However, to confirm that these effects were indeed the result of expression of the transgene, RNAi silencing was attempted on the ZAAT transgene. Several attempts by varying methods failed to efficiently improve the growth/motility impairment in the ZAAT strain nor in the ZAAT strain crossed with the RNAi hypersensitive strain, *rrf-3* (Z3RF). This is likely due to multicopy integration of the transgene as previously discussed in the introduction [205] which can result in inefficient transgene silencing. Thus, transgene expression was confirmed by qPCR. Interestingly, transgene expression was not significantly elevated in worms cultured at a higher temperature. This

suggests that the impaired mutant phenotype is not simply the result of higher expression of the transgene, rather it is the result of increased ZAAT protein accumulation and toxicity.

#### 4.5.2 The temperature-dependent effects and the molecular basis of toxicity

The temperature-dependence of the transgenic ZAAT strain growth/motility deficiency is an interesting phenomenon. Greater penetrance of impairment phenotypes at higher temperatures suggests that the toxic effects of the accumulating ZAAT protein are more pronounced. The proposed model for this effect is that at low culture temperatures, there is little ZAAT misfolding and accumulation (due to more efficient secretion of protein) and consequently transgenic worms display normal growth and motility physiology. Whereas at higher culture temperatures, there is increased ZAAT protein misfolding possibly overwhelming of the proteostasis machinery, less secretion and more accumulation, thereby leading to an impairment in growth, development and motility. Long *et al.* (2014) observed a similar temperature-dependent negative effect on the growth, brood size and lifespan in their model of *C. elegans* expressing mutant human ZAAT in intestinal cells. These impairment phenotypes also displayed greater penetrance at higher temperatures suggesting that the temperature effect observed in the ZAAT strain described in this study was physiologically relevant and not simply an artefact [109]. It has been suggested that these temperature-dependent toxic effects are due to blocked or over-loaded ERAD-UPS and autophagy protein disposal mechanisms [238, 239] as previously discussed in chapter 1, however the precise mechanisms remain unclear.

Initially, it was thought that the temperature-dependent deficiency phenotypes observed were due to an increased expression of the ZAAT transgene in worms cultured at higher temperatures. However, qPCR results revealed that expression was not significantly different between populations of ZAAT animals cultured at 20°C and 24°C. This suggested that the

effects were not due to increased transgene expression but rather the result of physiological damage due to the misfolding and accumulation of ZAAT protein within the muscle of the worms. This was a surprising though rather exciting result, as it indicated that the *C. elegans* model was likely to be more accurately recapitulating molecular and physiological aspects of human AATD, rather than simply representing an invertebrate transgenic over-expression system. It is of course possible that sample contamination with genomic DNA occurred, however, given that DNase was used in the sample preparation, this would be unlikely. It should also be noted that a temperature-dependent phenotype impairment *C. elegans* model has particular clinical relevance, as fever in children who have AATD has been shown to increase the production and polymerisation of ZAAT, resulting in periods of more severe disease-associated pathologies [240, 241].

#### 4.5.3 The ZAAT worm strain motility deficiency is screenable and has good potential for use in high-throughput screening

The growth/motility impairment phenotype of the transgenic ZAAT-expressing worm strain is scorable using the INVAPP/Paragon imaging system described in chapter 3. When considering the suitability of a *C. elegans* phenotype for screening, the difference between wild type strains, or normal conditions and the screening strain or conditions should be great enough to allow scope for rescue phenotypes to be observed, but not so great that rescue is impossible. This effect can be defined by the Z-factor or Z-prime, a statistical measure of the effect size pertinent to a high-throughput screen [242]. This coefficient reflects both the assay signal dynamic range and the data variation associated with the signal measurements. It is not completely necessary to calculate this score for each screen intended, but the principle of determining the power of a screen is important. The success of a screen i.e. the ability to identify hits, lies in the suitability and quality of the assay, and this is largely affected by the screening phenotype and the parameters of the screening method, each of which should be carefully inspected and resolved before embarking on large-scale screens. The difference in

movement index of the ZAAT-expressing strain cultured at 20°C and 25/26°C measured by INVAPP/Paragon reveals a significantly robust growth/motility deficient phenotype which is well suited to high-throughput chemical and genetic screening. Indeed, the impaired movement phenotype observed in the ZAAT strain appears more pronounced than that observed in the *smn-1, cb131*, model of SMA. The effective use of the *cb131* strain in a chemical library screen to search for novel modifiers of disease-associated pathology [234] lends confidence to the screening possibilities using the ZAAT strain.

Finally, the growth/motility deficient phenotype of the ZAAT worm strain provides an advantage over the published *C. elegans* model of AATD described in chapter 1. The model generated and characterised for screening is evaluated by only fluorescent ZAAT accumulation as a marker of disease [109, 110], whereas the motility-impaired ZAAT model described here provides a whole organism functional read out. This allows for the investigation into the role of other biological systems, proteostasis pathways and molecular components not directly linked with protein accumulation. The powerful combination of a strong mutant motility deficient phenotype and analysis using the high-throughput imaging system INVAPP/Paragon provides an excellent platform to use this ZAAT worm model in large-scale chemical or genetic screening assays.

# Chapter 5 Development of a small molecule screen using the *C. elegans* ZAAT strain

## 5.1 Introduction

### 5.1.1 *C. elegans* and small molecule treatments

Many of the characteristics of *C. elegans* make it amenable to small molecule testing. These include the ability to model complex human diseases and characterise mutant phenotypes and the ability to monitor drug efficacy and absorption, distribution, metabolism, excretion or toxicity (ADMET) properties in a multicellular, multi-organ organism [235]. Additionally, the repertoire of genetic tools available in *C. elegans* research (such as a chemistry-to-gene EMS screens, as described in chapter 7, or a gene-to-chemistry screen, as described in chapter 6), allows the possibility of elucidating drug targets and mode of action rapidly in the early stages of drug discovery and development.

The bioavailability of a compound to the worm is an important consideration when assessing the effects of a small molecule [102]. In order for the drug to reach its target within the worm, it must first enter the body. A significant challenge to many chemical species is presented by the physical barrier of the cuticle and the intestinal lining [104]. One approach in overcoming the cuticle is the use of mutants which display disorganisation of the epidermis and cuticle layers [243]. An example of such is a deletion mutant of *bus-8*, a gene which encodes a predicted glycosyltransferase expressed in cells underlying the epidermis. Mutants displayed organisational disruption of the epidermis and cuticle layer thus resulting in increased drug sensitivity. However, they also displayed uncoordinated, skiddy movement on agar, which could limit their use in phenotypic small molecule assays [105]. It has also been shown that molecules displaying certain structural motifs are either more or less likely to be able to accumulate within the body of the worm [104]. These authors developed a freely available

computer-based model in order to predict the ability of structures to accumulate within the worm to allow a more directed approach to drug testing in *C. elegans*.

An important study which validated the efficacious action of clinically used drugs on a *C. elegans* model of disease, was the investigation using a worm model of congenital myasthenia [244]. Congenital myasthenic syndromes are a group of genetic disorders all characterised by muscle weakness and caused by mutations in the human muscle nicotinic acetylcholine receptors (nAChR) [245]. Jones and colleagues showed that the mutant *C. elegans* strain *unc-63(x26)*, with a cys-loop mutation in the nAChR subunit UNC-63, displayed a movement deficient phenotype measured by thrashing rate, which effectively recapitulated the muscle symptoms observed in congenital myasthenia. This motility impairment was partially rescued by treatment of the worms with pyridostigmine bromide and 3,4-diaminopyridine which are used to treat patients of congenital myasthenia [244]. This study confirms that drugs found to be effective in *C. elegans* models of disease could indeed be clinically relevant as potential therapies.

### 5.1.2 The development of small molecule screening using *C. elegans*

The first small molecule screen using *C. elegans* was performed in 1974 by Sydney Brenner. One hundred compounds were screened on worms on individual plates and the effects scored by eye [96]. Small scale *C. elegans* drug screens continued to be used until 2006, when the Complex Object Parametric Analyser and Sorter (COPAS™ BIOSORT, Union Biometrica) was used to sort worms into 24-well agar plates and semi-automated image acquisition employed to score a variety of phenotypes [183]. The screening of 14,100 compounds constituted the first large-scale drug screen performed using *C. elegans*, however, use of agar plates and visual scoring meant that it was still time consuming and relatively low-throughput.

The transition from low-throughput to high-throughput *C. elegans* small molecule screening was greatly facilitated by the development of an all-liquid culture workflow in a multi-well (96-

well and later 384-well) plate setting [246]. This allowed the integration of liquid handling equipment and automated imaging platforms, which increased the scope and speed of large screens. An example of a large-scale small molecule screen was the screening of 88,000 compounds on *C. elegans* lifespan. Worms were cultured with the compounds in 96- or 384-well plates for 24 days and then scored for survival by light-stimulated movement. The screen identified 48 compounds that increased lifespan by 20-60% [247, 248]. Scoring phenotypes by eye was still a laborious process, and so the development of automated image acquisition systems, as described in chapter 3 resulted in the possibility of automating every step of the screening process.

### 5.1.3 The successes of small molecule screening using *C. elegans* models of human disease

Drug screening using *C. elegans* as a model for human disease has identified a number of clinically relevant compounds, two examples of such include spinal muscular atrophy (SMA) and Parkinson's disease (PD). A worm model of SMA, a rare genetic neuromuscular disorder characterised by degeneration of lower motor neurones leading to muscle atrophy was generated. The mechanisms of pathology are unclear, but deletions and point mutations resulting in a reduced level of the survival motor neurone (SMN) protein have been implicated [232]. A substitution mutation in the *C. elegans* gene *smn-1*, resembling a point mutation in patients with a milder subset of SMA, gave rise to worms which displayed neuromuscular dysfunction. This dysfunction resulted in a slow swimming phenotype which was scorable using an automated phenotyping system. A system which as described in chapter 2, used a covariance-based predecessor of the INVAPP/Paragon imaging system [160]. The small molecule screen of a library of 1040 compounds identified three drugs which improved the mutant motility impairment and could now provide important insight into new therapies for SMA [234].

In *C. elegans* models of PD, it is possible to induce the neurotoxicity associated with disease by treatment with the organic neurotoxins 1-methyl-4-phenylpyridinium (MPP+) or 6-hydroxydopamine (6-OHDA) [249]. Both cause damage of the worm dopaminergic neurones and result in reduced mobility; a screenable phenotype. Braungart and colleagues used an MPP+ *C. elegans* model of PD to screen the efficacy of existing PD drugs to validate the worm model. Several of the known drugs did indeed improve the MPP+-induced motility impairment, confirming use of the model to screen for further small molecule treatments [250]. The 6-OHDA-induced worm model of PD was used in a compound screen of a variety of dopamine, GABA and NMDA receptor agonists and antagonists. Two dopamine D2 receptor agonists, bromocriptine and quinpirole were found to protect against toxicity induced by 6-OHDA measured by direct neuronal cell function and viability [251].

Both examples demonstrate the power of small molecule screening using *C. elegans* as a model for human disease, yet there are real challenges in translating invertebrate *in vivo* drug discovery into human therapies. In fact, only a small selection of compounds identified from worm-screens make their way to advanced stages of drug development. This is not surprising, as often costly mammalian model systems also fail to accurately predict drug effects and interactions in humans. However, *C. elegans* modelling of human disease remains particularly useful in the early stages of drug discovery, in identifying initial lead compounds which can then be followed up in higher order organisms [252]. They are also especially informative with regards to target validation and elucidation of the mode of action of small molecules. Utilising chemistry-to-gene (by forward mutagenesis, as discussed in chapter 7) or gene-to-chemistry (by reverse, RNAi knock down as described in chapter 6) screening can provide invaluable information on the identity of drug targets in *C. elegans* as well as the biomolecular systems on which they act [253].

#### 5.1.4 Previous small molecule screening on a *C. elegans* model of AATD

The *C. elegans* model of AATD which expressed and accumulated fluorescent GFP-labelled ZAAT within intestinal cells previously described in chapters 1 and 4 was used in a small molecule screen. An automated fluorescence microscopy imaging system was adapted for high content screening. An ArrayScan system was used to detect and monitor the number and intensity of fluorescent spots within the worms, indicative of mutant protein accumulation. A pilot screen of 1280 compounds of Sigma Life Science's Library of Pharmacologically Active Compounds (LOPAC®) was performed on the worm model of AATD, searching for compounds which decreased or changed the pattern of fluorescent ZAAT accumulation. Sixteen hits were selected for dose-dependent measurement and strong hits included: fluphenazine, cantharidin and pimozide [110]. Fluphenazine was taken forward for further study in cell and mouse models of AATD [112]. Again, a small molecule screen on a *C. elegans* model of AATD where scoring is based simply on fluorescent mutant protein accumulation could fail to capture compounds which exert their effect by an alternative mechanism to simply blocking accumulation. Thus, drug screening on a *C. elegans* model of AATD which displays a scorable mutant behavioural phenotype could be advantageous in capturing such compounds.

## 5.2 Aims

1. To develop a small molecule screening protocol for the ZAAT *C. elegans* worms previously characterised in chapter 4. All specific protocol details would be investigated in turn, such as worm strain, type of drug screening method, number of animals, amount of food, use of sterilisation, drug concentration, screening length and timings of temperature shift.
2. To perform a pilot screening with a small library of 960 compounds with a bias towards protein-protein interactions on the newly generated ZAAT-expressing strain. Scoring of the growth/motility impairment using the INVAPP/Paragon imaging system would

allow the screening of compounds which improved the mutant phenotype. Any hits would be considered for further testing in cell models or higher animal models of AATD.

## 5.3 Results

In developing a protocol for a small molecule screen using the ZAAT-expressing transgenic *C. elegans*, it was important to determine optimum conditions for a number of key parameters. First, the number of worms dispensed per well of 96-well plates was considered. The results which are shown in Chapter 3 revealed that approximately 10-20 worms per well was a suitable density for accurately capturing motility using the INVAPP/Paragon imaging system. As a result, this is the number selected for the small molecule screen.

### 5.3.1 Seeding the correct amount of *E. coli* to each well is important for worm culture and imaging

As part of setting up a small molecule screen using transgenic Z AAT *C. elegans*, it was necessary to develop a culturing protocol in a 96-well plate format. The reasons for this are two-fold. First, a population of worms distributed to 96-well plates are consistent and easier to manipulate e.g. shifting some to a different temperature is straightforward. Secondly, it is conducive to a high-throughput drug screen protocol where a large number of drugs are screened. An important aspect of *C. elegans* culture in a 96-well plate format is the concentration of *E. coli* food required in each well. The amount of food should be enough that the worms do not starve but not too much that they are unable to clear the wells (clearer wells are imaged better). This was investigated by seeding variable amounts of bacteria to wells containing 15-20 worms, then measuring the OD600 on day 4 of culturing. Figure 5.1 shows that lower amounts of *E. coli* added to the wells gave lower OD600 values as expected, and at day 4, there was still bacteria left in all wells including those seeded with the lowest amount (3 $\mu$ l). The OD600 data demonstrates that there is a correlation between the amount of *E. coli*

seeded into the wells and the OD600 value. It also shows that the wells seeded with lower amounts of food are clearer than those seeded with larger amounts when measured on day 4. It was therefore decided that 5 $\mu$ l of bacterial food seeded per well would be sufficient for a screen lasting up to 7 days.

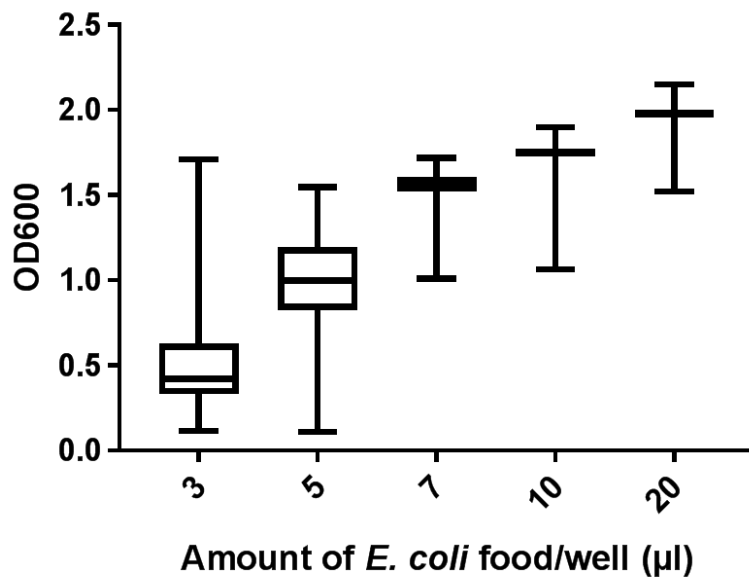


**Figure 5.1.** *C. elegans* culture adaptation to 96-well plate format: amount of food per well. OD600 readings taken on day 4 (see culture protocol in Figure 5.2) after seeding variable amounts of *E. coli* food to wells in a 96-well plate. Lower OD600 readings suggest more *E. coli* eaten by worms in the well. Box and whiskers plot, central line in box represents the median, the box extends from the 25<sup>th</sup> to the 75<sup>th</sup> percentiles and the whiskers indicate minimum and maximum values. Plots produced in GraphPad v7.

### 5.3.2 The time point at which the temperature of ZAAT worm culture is changed affects motility

N2 *C. elegans* can be cultured without issue at a temperature range between 15-25°C. To investigate whether temperature affected the motility of ZAAT expressing *C. elegans*, transgenic worms were cultured at 25°C for variable amounts of time. Standard culture of *C. elegans* is at 20°C and all cultures began at this temperature. Figure 5.2A is a schematic

demonstrating the day-by-day culturing protocol of ZAAT *C. elegans* in 96-well plates. The purple arrows in Figure 5.2A denote the time points at which 96-well culture plates were shifted from 20°C to 25°C. Culture plate A therefore was incubated at 25°C for the longest amount of time, followed by B before imaging using the platform. Control plates were incubated at 20°C throughout. Figure 5.2B reveals that plates containing ZAAT worms incubated at 25°C for the longest amount of time (shifted immediately after bleaching and allowed to hatch at 25°C) had the least amount of movement in the wells. Plates shifted to 25°C a day after re-feeding had an increased amount of movement in the wells when compared with those shifted immediately after bleaching. The movement in all test plates was reduced when compared with control. This data demonstrates that the motility impairment observed when ZAAT expressing *C. elegans* are cultured at 25°C is robust, given that shifting them to a higher temperature later in development also had an effect on movement. It also demonstrates that movement of transgenic ZAAT *C. elegans* is reduced as the time spent at 25°C increases. Therefore, it was decided that during the small molecule screen, cultures would be shifted to 25°C immediately after bleaching in order to test the compounds against a substantive motility deficit.

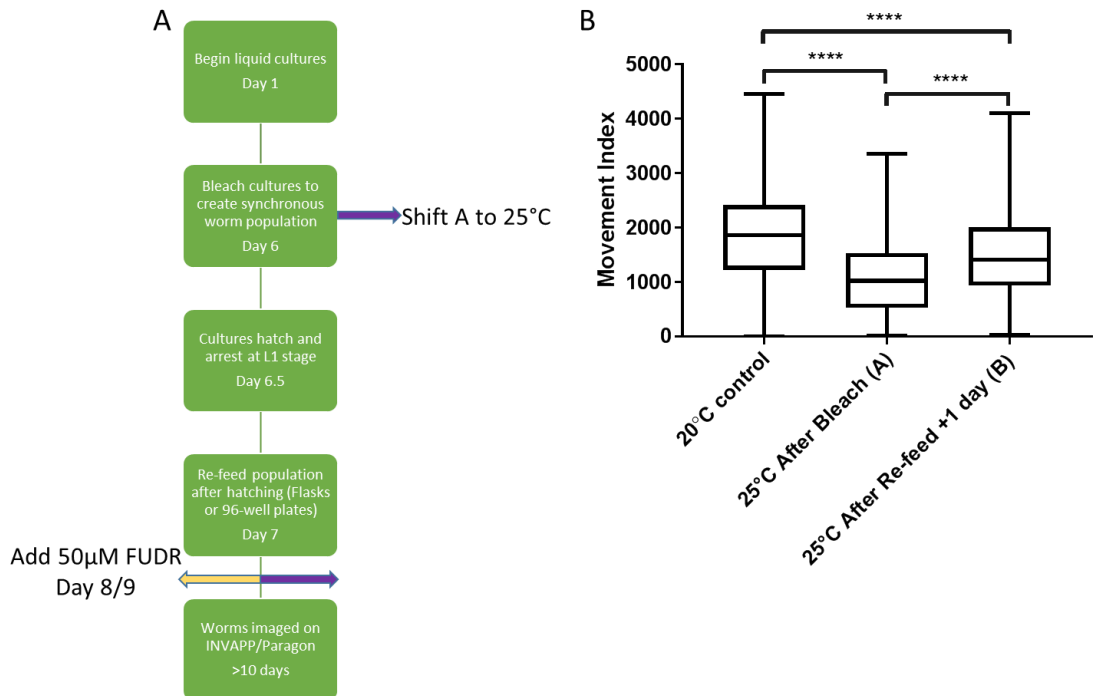


**Figure 5.2. (A) C. elegans day-by-day culture protocol in a 96-well plate format.** Purple arrows indicate shifting the cultures to incubation at 25°C. The yellow arrow indicates time point at which 50µM FUDR was added to each well (Figure 5.3). **(B)** Longer incubation of ZAAT worms at 25°C results in significantly lower movement index generated by motility imaging analysis (One-way ANOVA,  $F_2, 1725)=160.4$ ,  $p<0.0001$ ) with Tukey's multiple comparisons test,  $P = ****<0.0001$ ). Box and whiskers plot. Central line in box represents the median, the box extends from the 25<sup>th</sup> to the 75<sup>th</sup> percentiles and the whiskers indicate minimum and maximum values. Plots produced in GraphPad v7.

### 5.3.3 The presence of progeny in the well affects the environment of the well but does not affect the movement index

*C. elegans* can begin laying eggs as early as 45h after hatching (N2 at 25°C), which means progeny can be seen in the culture wells soon after seeding the plates. When present, progeny tend to dominate in the wells, they eat food faster and eventually eat the adult worms. This limits the length of time in which it is possible to image the plates to capture the motility of the adults. It was therefore necessary to explore whether addition of floxuridine (FUDR) to the wells affected the movement index of the adult worms and consequently whether preventing

hatching of progeny could lengthen the culture incubation time at 25°C before imaging. In order to prevent the hatching of progeny, 50µM FUDR was added to half of the wells in a 96-well plate culture of ZAAT worms. FUDR is an inhibitor of thymidylate synthetase which converts dUMP to dTMP (a nucleotide monomer used in DNA). It is effectively a DNA synthesis inhibitor. Added to later developmental stages of *C. elegans*, it inhibits eggs from hatching and developing without affecting the older worms. S-basal medium was added to the other half of the plates as a control. Figure 5.3A shows two examples of control wells without FUDR containing many progeny. Figure 5.3B shows two examples of wells to which FUDR was added containing no progeny. The plates were then imaged using the motility imaging platform system and analysed using the algorithm. Figure 5.3C presents the calculated movement index of wells with/without FUDR. Movement detected in wells containing FUDR is not significantly different than in wells not containing FUDR. This data demonstrates that progeny is inhibited by the presence of FUDR and that the movement index is unaffected by the presence of *C. elegans* progeny in the wells. It is therefore possible to use FUDR as a sterilising condition during the small molecule screen in order to allow a longer window in which imaging is possible.

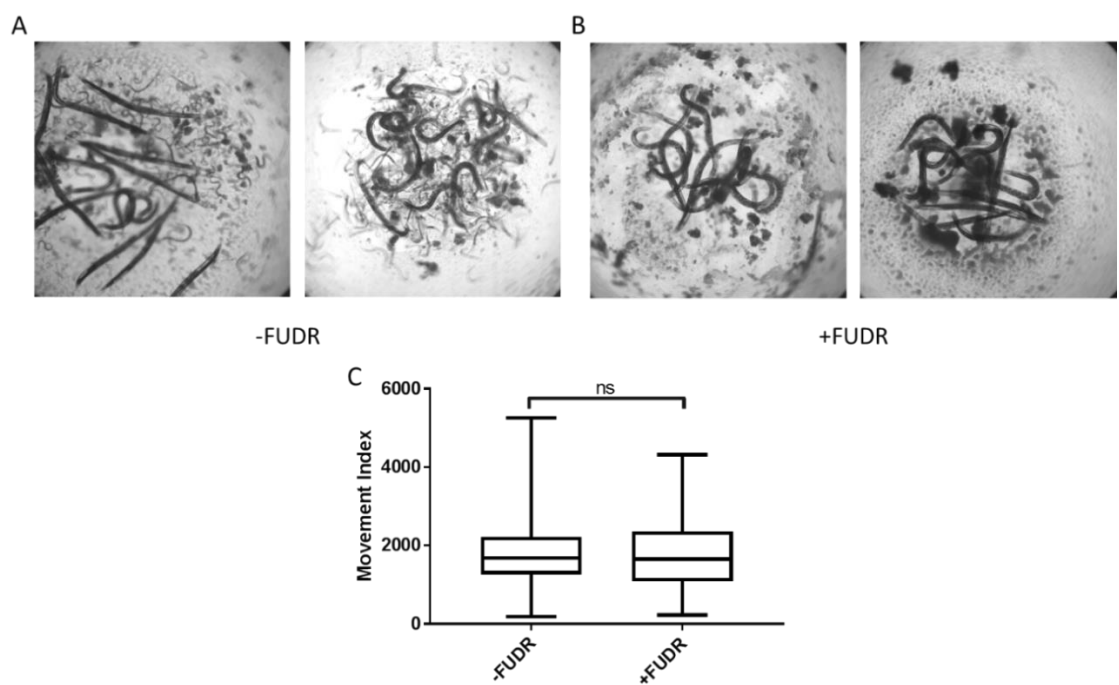


**Figure 5.3.** (A) Examples of wells where ZAAT expressing *C. elegans* were cultured in 96-well plates showing many progeny. (B) Examples of wells containing *C. elegans* cultures with the addition of 50µM FUDR, showing no progeny (imaged on the same day as A). (C) Movement index of 96-well plate cultures of *C. elegans* ± 50µM FUDR. Addition of FUDR does not significantly affect the movement index of the imaged adult worms (Unpaired t-test, n=3, p=0.8608). Box and whiskers plot. Central line in box represents the median, the box extends from the 25<sup>th</sup> to the 75<sup>th</sup> percentiles and the whiskers indicate minimum and maximum values. Plots produced in GraphPad v7.

### 5.3.4 Crossing *fem-1* strain into the ZAAT-expressing *C. elegans* strain

The use of FUDR to prevent the appearance of progeny in wells is somewhat controversial; it has been reported to improve proteostasis, increase lifespan and effect a variety of biomolecular pathways. Upon using FUDR to prevent worm progeny from hatching in the small molecule screen set up, its effects were also found to be rather variable and incredibly dependent on timing of addition. Addition at an early developmental stage for the screening worms is not desirable due to its wide-ranging effects on development, but later addition risks not accomplishing fully sterile adults and consequently the appearance of progeny in the wells. As a result, it was decided to cross into the ZAAT-expressing strain a strain which is sterile at high temperatures. The *hc17* allele of the gene *fem-1*, which is a substitution of an alanine for a glycine at position 1358, on chromosome 4 was selected [254]. This mutation results in temperature-sensitive sterility at temperatures above 25°C [254]. Figure 2.1 in chapter 2 shows the crossing method. The crossing protocol was performed twice and several of the F2 generation were inspected for the mutation. Single worm PCR was performed and the products run on a 2% w/v agarose DNA gel. Bands were excised and the DNA extracted using a gel extraction kit (Qiagen). DNA was then submitted to Source Bioscience for sequencing using the following primers: forward 5'-GAGGAAATACGG-3', reverse 5'-GAGGAAATACGA-3'.

The results of several rounds of sequencing showed that neither attempt resulted in the presence of the *fem-1* substitution mutation in any offspring. This suggests that the integrated ZAAT transgene could be near to this locus, thus preventing the recombination of *fem-1* into the strain. The cross was simultaneously performed using the Z10 strain in order to compare the two strains as previously mentioned in chapter 4, and resulted in successful double mutant strains containing the ZAAT transgene and the hc17 allele of *fem-1*.

Due to the failure of the *fem-1* X ZAAT cross, it was necessary to use a different mutation that would also ensure sterility of the worms at higher temperatures in order to be able to image at later time points. The ZAAT cross with *rrf-3* which has been described in chapter 6 for the purpose of the RNAi library screen was successful and the 3015bp deletion within the gene *rrf-3* on chromosome II also results in sterility of the double mutant worms at higher temperatures [255]. Therefore, the *rrf-3*/ZAAT worms were selected for use in the chemical library screen and were given the name Z3RF.

### 5.3.5 Temperature selection for the screen

It can be seen in Figure 6.3 of chapter 6 that Z3RF worms display a lower movement index i.e. impaired growth/movement when cultured at higher temperatures. This occurs with greater penetrance at 26°C than at 25°C and is less variable at the higher temperature. It was decided therefore to perform the small molecule screen at 26°C.

### 5.3.6 The screen was performed robustly, however no small molecule hits were detected

A library of 960 small molecules with a bias towards protein-protein interactions was obtained from collaborators at Oxford University, led by Professor Angela Russell. The library was developed based on modelling the scaffold around protein-protein interaction sites and designing small molecules whose structure has a high probability of binding within those sites. The screening of the 960-compound library was carried out using Z3RF *C. elegans* worms at

26°C. Imaging using the INVAPP system was performed 7 days after dispensing worms into the wells containing either 1% v/v DMSO or DMSO+100µM compound.

The first two columns in Figure 5.4 represent all wells from a control plate containing *rrf-3* and Z3RF respectively. A greater amount of movement was observed in wells containing the non-transgenic control *rrf-3* strain compared to wells containing Z3RF when all worms were cultured at 26°C. The third column represents all wells in the screening library plates containing Z3RF worms and 1% DMSO. As expected, very little movement has been detected in these wells due to the temperature-dependent growth/motility deficit previously characterised in these transgenic worms. The fourth column shown in Figure 5.4 represents the median movement score of each well of the small molecule library. It is clear that there have been no wells detected which display an increased movement index when compared to the DMSO-containing control wells. This means that it is unlikely that any hit compounds of utility for AATD can be identified from this small library.

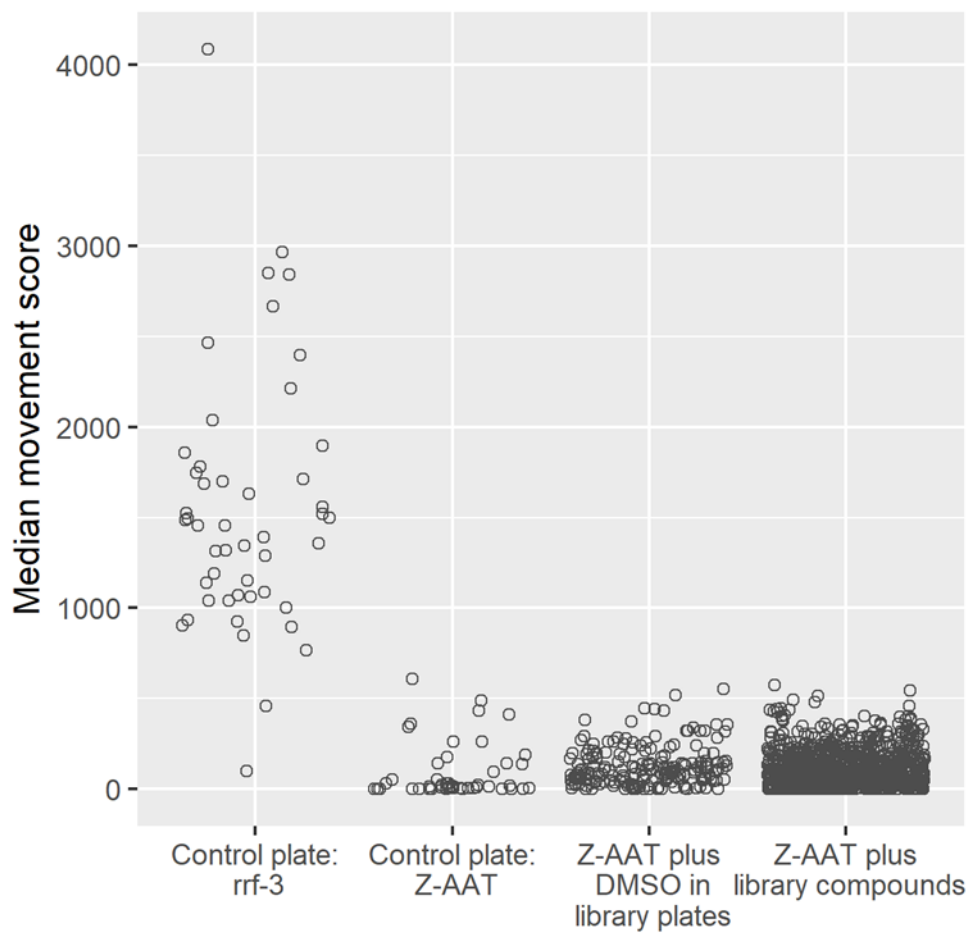


**Figure 5.4.** Screening of the 960-compound library on ZAAT *C. elegans* growth/movement. Columns 1 and 2 show the movement score for each well in a control plate containing *rrf-3* and Z3RF worms respectively. Column 3 represents wells of Z3RF worms containing 1% DMSO present in the library screening plates. Column 4 represents wells containing Z3RF worms+100 $\mu$ M compound. Each point represents the median movement score for a compound, n=3. All experiments represented on this plot were performed at 26°C. Clearly none of the compound have improved the growth/motility of the ZAAT transgenic worms.

## 5.4 Discussion

### 5.4.1 The development of the small molecule screen

In developing a novel small molecule screening protocol, there are a number of parameters requiring extensive investigation before a method is developed. The strength of a *C. elegans* drug screen lies in the detailed development of a robust method. The main aim of this study

was to adapt the culture of a ZAAT transgenic *C. elegans* line to a 96-well plate assay where the growth/motility phenotype was measurable to use in a high-throughput small molecule screen to search for novel modifiers of AATD. The screening parameters were partly developed for the drug screen using the MMV pathogen box library presented in chapter 3 and partly developed for the small molecule screen on ZAAT *C. elegans* described in this chapter.

Parameters such as the number of worms dispensed into each well and capabilities and applications of the INVAPP/Paragon imaging system and protocol are discussed in chapter 3.

Determining the correct amount of bacterial food to seed into each well was an essential step in the development of the protocol (Figure 5.1). Enough food was required to last the duration of the assay, without too much remaining at the imaging stage in order to improve image acquisition. The timeline of screening events such as bleaching was imperative for obtaining a homogenous population of worms between batches. Additionally, determining timings of the upwards shift of temperature was key to a strong, consistent growth/motility impairment phenotype (Figure 5.2). Due to the length of the protocol (1 week), it was desirable to impair the reproduction of the worms during the screen. Progeny disrupted the environment of the assay wells by consuming all the food and eventually the adults too. Sterilisation was attempted using FUDR, however results were inconsistent and use of FUDR is considered controversial [256, 257]. Crossing the *fem-1* strain, which is sterile at high temperatures into the ZAAT-expressing strain was attempted several times. It was concluded that the cross was not attainable, possibly due to the integration of the ZAAT transgene near to the *fem-1* gene location on chromosome 4. Instead, the strain generated for the RNAi screen described in chapter 6, Z3RF was selected for use in the small molecule screen. The benefits of using this strain are two-fold. First, it is sterile at high temperatures. Secondly, the strain is hypersensitive to RNAi, thus should any hits be identified during the screen, gene-to-chemistry follow up using an RNAi screen to identify the target of the small molecule would be greatly facilitated [253]. The temperature-dependent growth/motility defect of Z3RF is presented in

Figure 6.3, chapter 6. The phenotype of Z3RF was considered strong and robust and suitable for use in the small molecule screen.

An important consideration when designing a drug screen is the concentration of compound to be tested. Compounds enter the worm by ingestion and diffusion [203] however, the actual amount of drug within the worm is variable and dependent on media delivery, presence of bacteria which can metabolise molecules and penetration of the drug based on molecular structure [236]. In order to attempt to overcome these issues, compounds were added at the relatively high concentration of 100 $\mu$ M.

#### 5.4.2 The small molecule screen failed to detect any hit compounds but has potential for use in a larger-scale screen of a bigger library

The pilot screen of 960 compounds was performed according to the developed protocol, and no hit compounds rescuing mutant growth/motility were identified. However, of note, is the variability detected in the median movement index in the compound-containing wells (Figure 5.4, column 4), suggesting that the parameters investigated and resolved provide the capability of identifying hits in future screens of larger compound libraries. The lack of hit identification is not a surprising result, as small molecule screens often test several thousands of compounds before any hits are found [258-260]. The library screened was reported to contain a bias towards compounds which were thought to affect protein-protein interactions [261], however, it is only a sub-set of the full library which contains approximately 50,000 compounds. There is therefore certainly scope for testing more compounds of this nature. However, it may also be worth considering testing a larger library with no bias for any interactions, to increase the scope of the screen. The speed and ease of the screening protocol means that scaling up the number of compounds can be done with relative efficiency.

The method of drug delivery could also be modified to increase the chances of finding hit compounds. It was determined by Zheng and colleagues that drug absorption efficiency in *C.*

*elegans* increases with increasing concentration of compound; therefore, drugs could be tested at up to 150µM to observe any improved effect. It was also shown that drug concentration accumulated steadily with time reaching a peak concentration at day 1 (+24h), after which it began to gradually decrease over the course of 20 days. Given that ZAAT production within the transgenic worms is a continual process, a second addition of compound over the course of the assay could maintain a more steady concentration of the drug within the worm thus giving it a better chance of exerting its effect. Lastly, Zheng and colleagues showed that treatment of drugs alongside dead bacteria was most effective for accumulation of the drug within the worm body. Therefore feeding the assay worms with heat or UV killed bacteria could also serve to increase the concentration of compound within the animals [262].

Although the pilot small molecule screen using the transgenic mutant Z3RF strain did not identify any hits, the screening protocol developed in this study was robust. With some possible minor modifications, it certainly has great potential to be used in a larger-scale screen of a bigger library of compounds in order to identify novel modifiers of disease-associated pathologies in a *C. elegans* model of AATD.

# Chapter 6 Whole genome RNAi screening on the transgenic ZAAT *C. elegans* strain

## 6.1 Introduction

### 6.1.1 Reverse mutagenesis

Reverse genetics is the functional study of a gene which begins with the gene sequence rather than the mutant phenotype (as is the case for forward mutagenesis described in chapter 7). It was first discovered to work in animals in 1998 by Fire and Mello, that injecting double-stranded RNA (dsRNA) into *C. elegans* leads to destruction of the specific corresponding mRNA. This gene silencing process was termed RNA interference (RNAi) [263]. It was also subsequently found, that it was possible to induce RNAi in worms by soaking them in dsRNA [264] or by feeding them bacteria that expressed dsRNA [265]. Fire and Mello made two additional key discoveries which meant that RNAi would become an essential tool in *C. elegans* research. First, they showed that the effect of RNAi is systemic within the worm. Secondly, they demonstrated that it is heritable. These findings combined with the knowledge of the complete *C. elegans* genome (the first genome of a complex animal to be fully sequenced [266]), meant that rapid evaluation of gene activity as a result of loss of function by transcript knockdown was feasible for any individual gene and potentially the entire genome would now be possible. Genome-scale RNAi was later realised in *C. elegans* by Ahringer and colleagues [267].

### 6.1.2 Mechanisms of RNAi: Exploiting endogenous RNAi pathways

Gene silencing is the natural process of post-transcriptional control of gene expression regulation via interference with mRNA. During endogenous cellular RNAi, cytoplasmic dsRNA is cut by the endonuclease Dicer into double-stranded, small interfering RNA (siRNA molecules) which are approximately 20-25 nucleotides in length [268]. The siRNA binds to an RNA-Induced

Silencing Complex (RISC), a multi-protein complex, containing various Argonaute proteins [269]. The complex divides the molecules into two strands: the passenger and the guide strand. The passenger strand is degraded whilst the guide strand is integrated into an active RISC by RISC-Loading Complex (RLC) and transported to the specific complementary mRNA site [270]. Here, siRNAs base pair with their target mRNA, which is then cleaved, consequently inhibiting transcription (Figure 6.1). It is this pathway that can be exploited in *C. elegans* by introducing exogenous dsRNA into the worm to induce site specific gene silencing. This not only had consequences for gene function elucidation in *C. elegans*, but also opened the possibility of RNAi as therapeutic treatment for a number of human disorders [271-273]; including AATD, as discussed in chapter 1. This approach has recently been fully realised with the FDA approval in 2018 for Patisiran (Alnylam) for the treatment of transthyretin or amyloidosis. This is the first instance of licensing of an RNAi therapy for clinical use thus exemplifying the opportunity to exploit the RNAi pathway for therapeutic purposes.

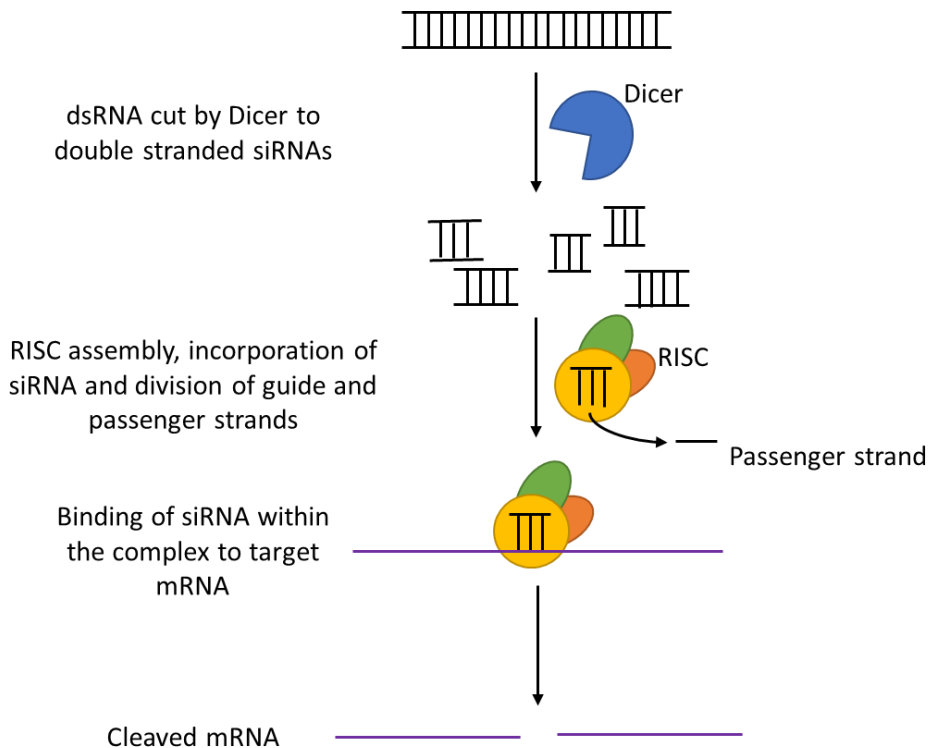


**Figure 6.1.** The mechanism of gene silencing (RNAi). Double stranded RNA (dsRNA) is cut into double stranded short interfering RNA (siRNA) molecules by the enzyme Dicer. The siRNA binds to an RNA-Induced Silencing Complex (RISC) comprised of various Argonaute proteins and is divided into two strands. The passenger strand is degraded, and the guide strand is incorporated into an active RISC complex. The complex transports the siRNA guide strand to the target mRNA where it binds and cleaves the mRNA, thus inhibiting transcription.

### 6.1.3 Mechanisms of RNAi: Systemic and heritable RNAi

Systemic RNAi is the organism-wide spread of gene silencing via the dissemination of the initial RNAi signal or its effectors. It was first observed serendipitously by Fire and colleagues when dsRNA was accidentally injected into the body cavity of the worm (the germline in the gonad being the original target) and was still found to induce whole-organism RNAi [263]. It is now known that two distinct populations of small RNAs play a role in *C. elegans* RNAi. Primary siRNAs are produced by DICER-mediated cleavage of the original dsRNA sequence, and secondary siRNAs, are produced by RNA-directed RNA Polymerase (RdRP) [274]. During

systemic RNAi, the vast majority of functional small RNAs are indeed the secondary siRNA, whose structure is characterised by RdRP initiation [275]. These secondary siRNAs amplify the RNAi mechanism throughout various tissues of the worm by uptake mechanisms which are as yet unclear, but recent studies have implicated a role of the RDE-10/RDE-11 complex upstream of the RdRPs [276].

It was also demonstrated in those first experiments by Fire and colleagues that the gene silencing in RNAi were heritable [263]. The effects were detected most strongly in the F1 generation, but have also been shown to persist into the third or fourth generation [277]. The original dsRNA is dramatically reduced over generations, thus the efficient propagation of gene silencing information must involve an amplification process such as the secondary siRNA signalling [278]. Secondary siRNAs are suspected of being inherited from the parent's gametes (sperm or eggs). Specific RdRPs which act on the germline mRNA to generate heritable siRNAs include RRF-2 and EGO-1 [279]. This process could in theory continue to further generations indefinitely, however, a dedicated regulatory system which includes a feedback loop between heritable endo-siRNAs and small RNA inheritance genes limit the extent of dsRNA-induced RNAi between generations [280]. This pathway curbs inheritance to be typically 3-5 generations in length; a duration that can be manipulated by mutating genes involved in the pathway loop such as *ppw-1* which encodes a PAZ/PIWI domain-containing protein that is a member of the Argonaute family [281].

#### 6.1.4 Methods of RNAi in *C. elegans*

There are three methods of inducing RNAi in *C. elegans* worms, injecting, soaking and feeding. The earliest RNAi experiments were performed by injecting dsRNA prepared *in vitro*, directly into the gonad (or body cavity) of the young adult hermaphrodite worms. The resulting progeny was scored for any phenotypic changes [263]. The gene silencing effects resulting from the injection method are very reliable, however the procedure can be technically difficult

and laborious. RNAi by soaking involves immersing a large number of worms in a high concentration of dsRNA solution and scoring the animals or their offspring for mutant phenotypes. This can be useful in a high-throughput setting however it does require large amounts of synthesised dsRNA [264]. RNAi by feeding involves the engineering of HT115(DE3) *E. coli* bacteria deficient in RNaseIII (an enzyme which degrades RNA), to produce high quantities of specific dsRNA segments. A bacterial construct is generated with an L4440 vector containing two bacteriophage T7 RNA polymerase promoters, which flank the multiple cloning site, where the cDNA of the gene of interest is inserted. The construct is then transformed into the *E. coli* strain HT115(DE3). The production of bacteriophage T7 polymerase from the construct is induced by addition of isopropyl  $\beta$ -D-1-thiogalactopyranoside (IPTG). As a result, the bacteria produce dsRNA specific for the gene of interest [263]. Bacterial clones are then fed to worms and RNAi is taken up into cells via the conserved transmembrane protein SID-1 which is localised to the cell periphery. Cells which do not express SID-1 are insensitive to RNAi [282]. Phenotypic scoring of the worms fed directly with the bacterial clones or their progeny is then performed depending on the developmental stage of the animals [283]. This method is the least labour intensive and most straightforward but can produce more variable silencing results.

An important consideration when designing RNAi experiments is also which strain of worm to use. It is possible to use wild type or transgenic strains to observe the effects of RNAi, however worm strains can vary in their sensitivity to RNAi. It can be pertinent to use mutant strains which display hypersensitivity to RNAi effects, such as *rrf-3* [135] and *eri-1* [284], which can also be crossed in to model strains of interest.

### 6.1.5 RNAi as a whole genome screening method

All three methods outlined above have been used effectively in large-scale RNAi screening [285-288]. RNAi by feeding is the most straightforward. However, the process of cloning the

DNA fragment from the gene of interest into a plasmid vector and then transforming it into a bacterial strain is arduous and requires significant skill in molecular biology. These obstacles were overcome, when a group led by Julie Ahringer undertook the enormous task of constructing a bacterial library of clones expressing dsRNA covering approximately 86% of the estimated 19,000 predicted genes in the *C. elegans* genome [285, 289]. The production of this commercially available library revolutionised large-scale screening of *C. elegans* genes for their role in numerous biological processes as well as in disease. The method of genome-wide RNAi screening can also be adapted to a high-throughput design which permits rapid primary gene knock down screening [267]. This has been greatly facilitated by the development of hard- and soft-ware tools for collecting and analysing data, including high-content image acquisition, as discussed in previous chapters [152, 168, 290]. The major advantage of whole genome RNAi screening is that the identity of gene targets are previously known. This greatly facilitates follow up investigation of hit genes and allows for detailed and rapid analysis of interacting genes and pathways after screening. It also means that RNAi can be used to evaluate the effects of smaller groups of candidate genes identified from database searches or for example Genome Wide Association Data (GWAS) [291, 292].

The key to a successful genome-wide RNAi screen is a specific and robust biological assay, where the phenotype of the animals to be screened is well characterised and the screening parameters are vigorously investigated with careful attention to detail [293]. Importantly, due to the variability of RNAi and inconsistency in the bacterial library, hits need to be validated in a secondary screen. To further prevent false-positive results, a second RNAi construct targeting mRNA of the same gene can serve as hit confirmation [294], or a known mutant obtained from the Caenorhabditis Genetic Centre (CGC) can be used to confirm the phenotype.

RNAi as a whole genome screening method using *C. elegans* has been used to elucidate genetic information on a number of biological mechanisms and diseases such as aging [295],

host-pathogen interactions [296], cancer drug targets [297] and neurodegenerative disease; examples of which include: Polyglutamine diseases (e.g. Huntington's disease), Parkinson's disease and Alzheimer's disease [292, 298]. It has also been used to identify novel drug targets in a *C. elegans* model of AATD, where O'Reilly and colleagues used the previously generated *C. elegans* model of AATD in a high-throughput genome-wide Ahringer library feeding screen to identify animals with a reduction in fluorescent ZAAT accumulation. Hit gene products were evaluated as drug targets; these included PI3K, TTR, ABC and OPRL-1. Eight compounds from the LOPAC library known to act on these targets were evaluated for their fluorescent ZAAT-reducing effects. Wortmannin, fluspirilene, fluoxetine and amiodarone all decreased fluorescent ZAAT accumulation in the transgenic worms and in a HeLa cell line expressing ZAAT [111]. This screen constitutes the only genome-wide RNAi screen performed on a *C. elegans* model of AATD, suggesting there is clear scope for further such studies. The ZAAT-expressing worm model used in the genome-wide RNAi screen performed by this group is also scored solely by quantification of fluorescent accumulation. It is therefore not possible to capture hits which act to improve the overall mutant phenotype by mechanisms not directly related to protein accumulation by this method.

## 6.2 Aims

1. To develop and perform a novel high-throughput genome-wide RNAi screen using the newly generated transgenic ZAAT-expressing *C. elegans* strain previously characterised in chapter 4.
2. To carefully investigate all parameters of the RNAi screen including worm strain and developmental stage, transgenic worm phenotype, RNAi delivery method, assay plate preparation, screening timetable including screening temperature and duration and scoring method using the INVAPP/Paragon imaging system.

3. To carry out the screen with two of the *C. elegans* chromosomes and search for any hit genes which improved the growth/motility deficient phenotype observed in the ZAAT-expressing transgenic worms. Analysis would be carried out on the potential hits to evaluate them for their possible role in the mechanisms of AATD.

## 6.3 Methods

### 6.3.1 RNAi screen

The RNAi screening protocol is represented schematically in Figure 6.2. NGM media was prepared as described with the addition of 25µg/ml (w/v) carbenicillin, 10µg/ml (w/v) tetracycline and 1mM Isopropyl β-D-1-thiogalactopyranoside (IPTG) and dispensed into 96-well plates, 150µl per well. Plates were allowed to cool and set for 2-3 days. 230µl of LB media containing 50µg/ml (w/v) ampicillin, 10µg/ml (w/v) tetracycline was dispensed into 96-well plates and inoculated with RNAi bacterial clones from the Ahringer library using a 96-pin replicator. Plates were incubated overnight with shaking (37°C, 200rpm).

The next day, 16µl of bacterial culture was pipetted onto the NGM within the 96-well plates and the plates allowed to dry in a laminar flow cabinet for 3h. Once dry, the plates were incubated in a humid chamber at 37°C overnight. On the same day, several plates of *C. elegans* worms (*rrf-3* and *Z3RF*) were bleached as described and allowed to hatch at 26.5°C overnight.

The following day, the 96-well NGM RNAi plates were removed from the incubator and allowed to reach room temperature. The hatched L1 *C. elegans* larvae were diluted to approximately 15-20 animals per 15µl and dispensed into the RNAi plates. The plates were dried in a laminar flow cabinet for 3h before being incubated in a humid chamber at 26.5°C for 4 days.

On day 4, the plates were removed and imaged using the INVAPP/Paragon imaging system by means of a swimming assay. 50 $\mu$ l of S-basal was dispensed into all wells and the plates imaged, 200 frames, 30 frames/s for 7s. The movies recorded were analysed using a MATLAB script.

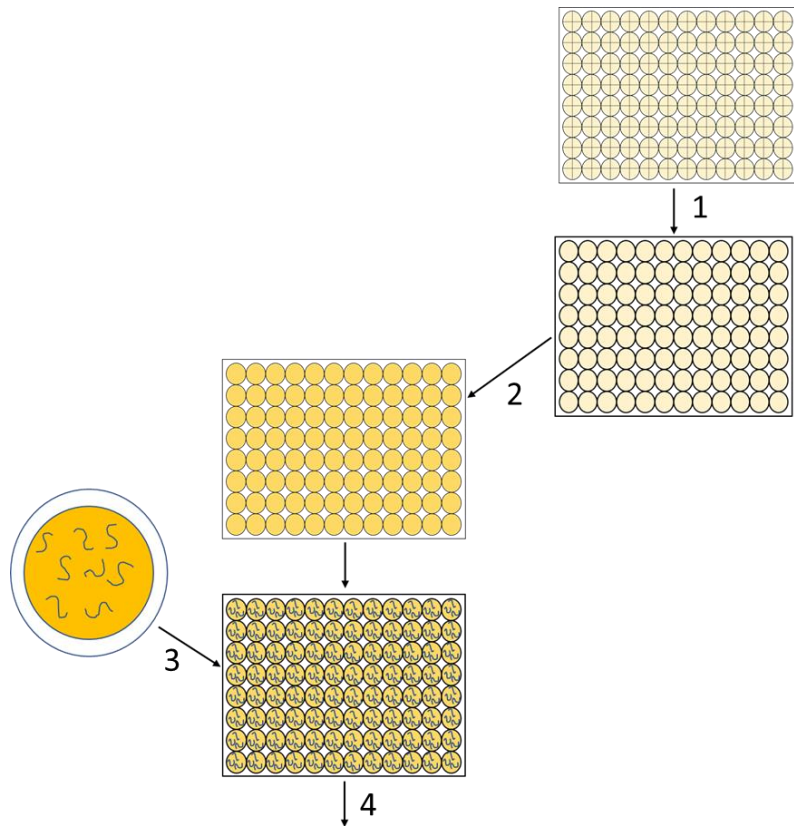


**Figure 6.2.** The *C. elegans* RNAi library screening method by feeding. (1) Bacterial clones expressing dsRNA are transferred from the Ahringer library glycerol stocks using a plastic 96-pin dispenser and used to inoculate each well of a 96-well plate containing 2X YT broth + 25 $\mu$ g/ml carbenicillin + 10 $\mu$ g/ml tetracycline. The plates are incubated at 37°C overnight with shaking (200rpm). (2) The next day, 16 $\mu$ l of bacterial cultures are seeded onto previously prepared 96-well plates containing NGM + 1mM IPTG + carbenicillin (25 $\mu$ g/ml) + tetracycline (10 $\mu$ g/ml). The plates are dried in a laminar flow hood for 3h with rotation to prevent over-drying of plates near the air flow. Once dry, plates are incubated in a humid chamber at 37°C overnight. The next day, L1 stage larval worm strains rrf-3 or Z3RF are dispensed into the plates approximately 15-20 per well. Plates are dried again in the laminar flow hood before incubation in a humid chamber at 26.5°C. Imaging is performed 3 days later using the INVAPP/Paragon imaging system.

## 6.4 Results

### 6.4.1 Crossing in *rrf-3*

In order to ensure efficiency of RNAi knock down on the ZAAT-expressing worms during the library screen, it was necessary to introduce a mutation within this strain which would render them hypersensitive to RNAi. The variant *pk1426* was selected for crossing into the ZAAT-expressing strain. This mutant variant possesses a 3015bp deletion within the gene *rrf-3* on chromosome II and results in enhanced RNAi [135, 299, 300] as well as temperature-sensitive sterility [301]. Due to its sterility at high temperatures it was also selected as the strain to be used in the small molecule library screen described in chapter 5, indeed the crossing method previously described was similarly used to cross the *rrf-3* mutation into ZAAT worms.

The F2 generation of the genetic crosses were placed at 25°C and observed for the sterile phenotype. Twelve candidate populations were then analysed by single worm PCR to detect the gene deletion using the following primers which flank a 991bp sequence of *rrf-3*: forward 5'-ATTTCTGCGATTGCGATTGG- 3'; reverse 5'- ACAC TTCCGCGTGTGATTAG -3'. The lack of a PCR product at the 991bp position indicates that the gene has been deleted (Figure 6.3A). Three of the F2 generation appeared to contain the *rrf-3* mutation (Figure 6.3B), however to confirm that the absence of a band in these lanes was not simply due to the failure of the PCR, 3 offspring of these worms were also analysed by PCR and visualised by gel electrophoresis. None of these offspring produced a PCR product band in the correct position (Figure 6.3C). Coupling this with the phenotypic evidence observed that when placing these strains at 25°C they produced little to no offspring confirmed that they contained the *rrf-3* RNAi hypersensitive deletion mutation and that they would be suitable to use in an RNAi library screen. This new strain was termed Z3RF.

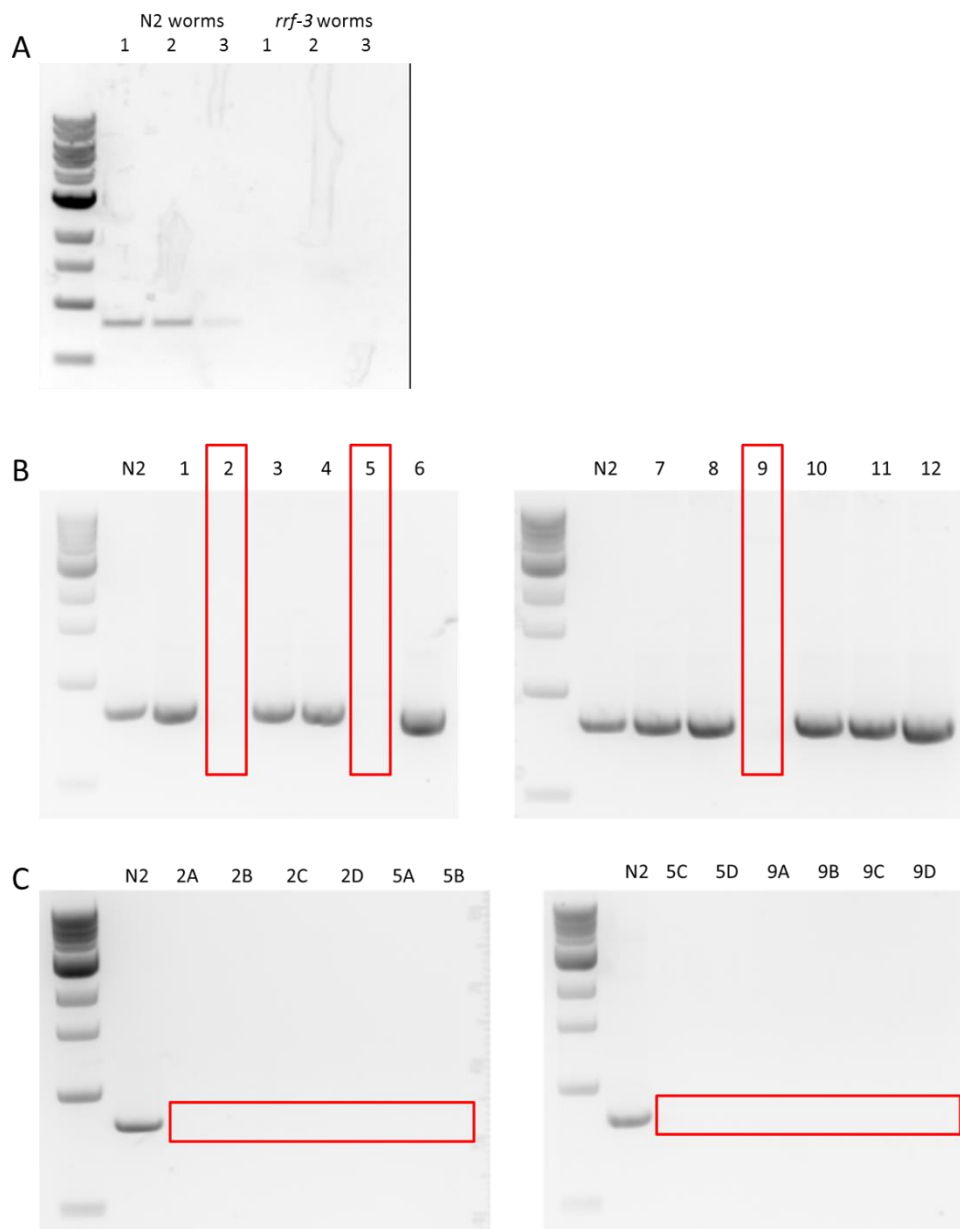


**Figure 6.3.** 2% w/v agarose gels of single worm PCR products confirming the *rrf-3* deletion mutation in resulting offspring from *rrf-3* X ZAAT genetic crosses. Single worm PCR was performed using primers which amplify the *rrf-3* gene. (A) PCR products of 3 N2 worms and 3 *rrf-3* strain worms. Bands visualised in N2 samples indicates the presence of the *rrf-3* gene; absence of PCR products in *rrf-3* worm samples indicates the *rrf-3* gene deletion mutation. (B) ZAAT males are crossed with *rrf-3* hermaphrodites and the resulting F1 progeny allowed to self, resulting in the homozygous *rrf-3* mutation in certain F2 offspring. PCR products from the F2 generation of the genetic crosses are visualised along with an N2 control. Worms 2, 5 and 9 appear to contain the deletion in *rrf-3*. (C) To confirm that these worms contain the *rrf-3* mutation, PCR products of 3 offspring from each worm identified as containing the mutation in (B) are visualised.

#### 6.4.2 Z3RF displays a decrease in growth/motility when cultured at higher temperatures

After successfully crossing the ZAAT strain with *rrf-3*, it was necessary to re-test the temperature-dependent motility deficit phenotype observed previously with the ZAAT strain. Liquid cultures of Z3RF and *rrf-3* were grown according to the protocol described in chapter 5 and placed at either 25°C or 26°C from the L1 stage. Movement was recorded using the INVAPP imaging system on day 7. Figure 6.4 shows that the introduction of the *rrf-3* mutation into the ZAAT-expressing strain has little effect on the growth/motility deficient. Z3RF worms continue to display a significantly reduced movement phenotype when cultured at 25°C and 26°C when compared with the control *rrf-3* background strain. Experiments were performed in biological triplicate.

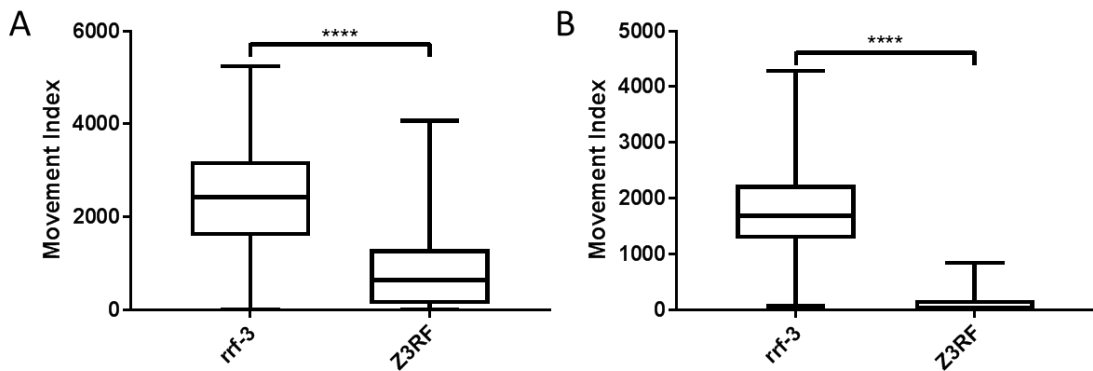


**Figure 6.4.** Z3RF worms display a lower movement index when grown at higher temperatures compared to *rrf-3* worms. (A) Z3RF have significantly impaired growth/motility (represented by the movement index) compared with *rrf-3* when cultured at 25°C (unpaired t test, \*\*\*\* indicates  $P<0.0001$ ). (B) Growth and/or motility of Z3RF is reduced even further when cultured at 26°C (unpaired t test, \*\*\*\* indicates  $P<0.0001$ ). Data shown is based on  $n=3$ . Plots produced in GraphPad Prism v.7.

#### 6.4.3 RNAi feeding protocol method development

A significant amount of time was spent developing the protocol of RNAi library screening previously described in this chapter. A number of screening parameters were systematically investigated in turn to develop the method finally adopted. Examples of considerations include: the concentration of NGM used in the wells of the 96-well plates; the amount of bacterial suspension seeded into the wells; the number of worms dispensed to each well; plate drying time of both steps; incubation time of the plates containing dsRNA-expressing bacteria and then containing both bacteria and worms; the optimum day of imaging and also the most effective and efficient method of imaging. Many of the outcomes of these individual investigations were assessed by eye, for example, drying time was measured by the appearance of cracks in NGM in the wells and amount of bacterial suspension seeded by how quickly the worms exhausted the food source. Another important concern was contamination within the wells which can arise easily in a multi-step high-throughput screen; bacterial contamination of the plates being a particular apprehension as it could result in reduced RNAi uptake. Significant steps were taken to identify the source of such contamination and to avoid it, which in itself was a lengthy process. In order to ensure the smooth effective running of a potentially highly variable, long and laborious library screen it was important to balance many of these parameters together, thus the protocol in Figure 6.1 was developed.

#### 6.4.4 Confirmation of functional RNAi by the detection of dumpy phenotype worms in the screen

To increase confidence in finding hit genes, it was important to validate the RNAi screen to confirm that the RNAi knock down was in fact silencing genes sufficiently. This was achieved by searching through the plates by eye for any obvious phenotypic changes in the animals. A very clear dumpy phenotype was observed in animals from two corresponding wells from the control and test plates (Figure 6.5). The RNAi clone present in both wells was mapped to the

gene *lin-41*. *Lin-41* is a heterochronic gene required for temporal control of specific postembryonic cell fates [302]. It encodes a Ring finger-B box-Coiled Coil (RBCC) protein, which is a member of the NHL family of proteins (named after NCL-1, HT2A and Lin-41) [303]. RNAi targeting of *lin-41* has been known to give rise to the dumpy phenotype when using worms with the *rrf-3* background [304]. The presence of dumpy worms in wells containing the bacterial clone producing dsRNA complementary to *lin-41* confirms the silencing activity of the RNAi.

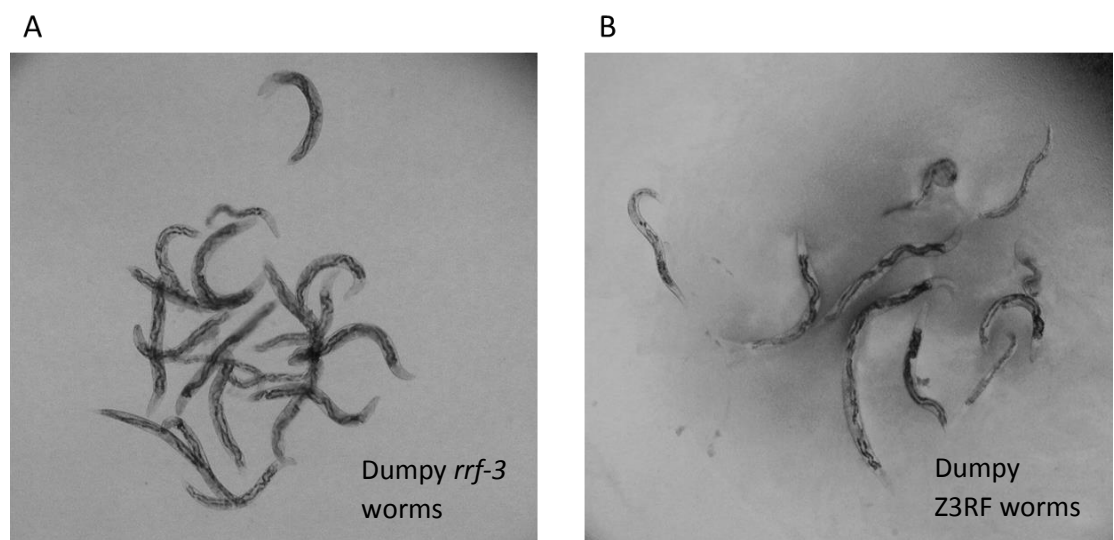


**Figure 6.5.** The presence of dumpy phenotype worms in corresponding wells from the *rrf-3* control plate (A) and the Z3RF plate (B) confirms RNAi silencing activity.

#### 6.4.5 The primary RNAi screen of *C. elegans* chromosomes I and II identified a number hit genes

The RNAi bacterial feeding library screening of chromosomes I and II was undertaken using the *rrf-3* and Z3RF worm strains according to the protocol outlined previously in the methods section of this chapter. Bacterial clones expressing dsRNA complementary to genes in chromosomes I and II were fed to the worms from the L1 stage in 96-well NGM (+IPTG) plates. Plates were incubated for 3 days at 26.5°C to ensure a robust growth/motility deficient

phenotype and to counter any temperature drop that could potentially arise from opening and closing the incubator. On day 3, the wells were flooded with S-basal and the swimming of the worms was quantified using the INVAPP/Paragon imaging system. Swimming was favoured for imaging over crawling as it facilitated faster imaging of the plates (swimming takes 7s to image 1 plate, crawling takes 10s). Each gene was tested on both strains in replicates of 4. The RNAi bacterial library is split into 384-well plates; there are 8 plates covering chromosome I and 9 plates covering chromosome II. Each plate represents a separate experiment and different worm populations; thus each plate has been plotted separately (Figure 6.6 and 6.7).

The median movement index from the 4 replicates of both the *rrf-3* and Z3RF strains were compared on the same plots (Figure 6.6 and 6.7). This enabled identification of hits that improved or worsened the mutant (Z3RF) growth/movement phenotype without greatly affecting the control (*rrf-3*) phenotype. Hit genes were considered as either “improving/rescuing in part” of the Z3RF growth/motility deficit phenotype, or “worsening/exacerbating” of the phenotype. The genes of interest which were considered to improve Z3RF movement but had little effect on *rrf-3* therefore would be positioned in the top centre-right hand corner. Genes which were considered to worsen the phenotype of the Z3RF strain, without affecting the movement of the *rrf-3* strain would be identified in the bottom centre-right part of the plot. Hits were selected by varying the movement index threshold of both strains to highlight genes which obviously by eye fell into these ranges, which was guided in part by the generation of an ellipse denoting a 0.95 normal confidence interval. The gene labels on the plots in Figures 6.6 and 6.7 represent the well of the 384-well Ahringer bacterial RNAi library plate. The hit wells can be mapped back to the original library plate to identify the gene. The lists of hit improving and worsening genes along with their human orthologs are supplied in Supplementary Tables 1 and 2.

There are a number of genes which can be observed in the very bottom left hand corner of each plot in Figures 6.6 and 6.7. These are wells where very little movement has been detected for both strains. The reasons for this could be two-fold; dsRNA produced by bacteria in these wells could result in lethal RNAi phenotypes or the wells could in fact be blanks and contain no bacteria. The RNAi library contains some blank wells as not all genes were successfully cloned into bacteria, but the space was left for potential future expansion of the library. Regardless of the reason, the fact that a low level of movement has been detected in corresponding wells of both strains suggests that a similar effect is occurring to both the *rrf-3* and the Z3RF worms. This is an expected outcome of an RNAi screen and serves to validate the screening protocol.

The spread of the points on the plots representing movement index values for the two strains is also confirmatory of a valid screen. Varying amount of motility for both strains is expected, but the general clustering of movement values suggests that parameters of the screen such as counting and dispensing the worms as well as the screening conditions such as temperature are robust.

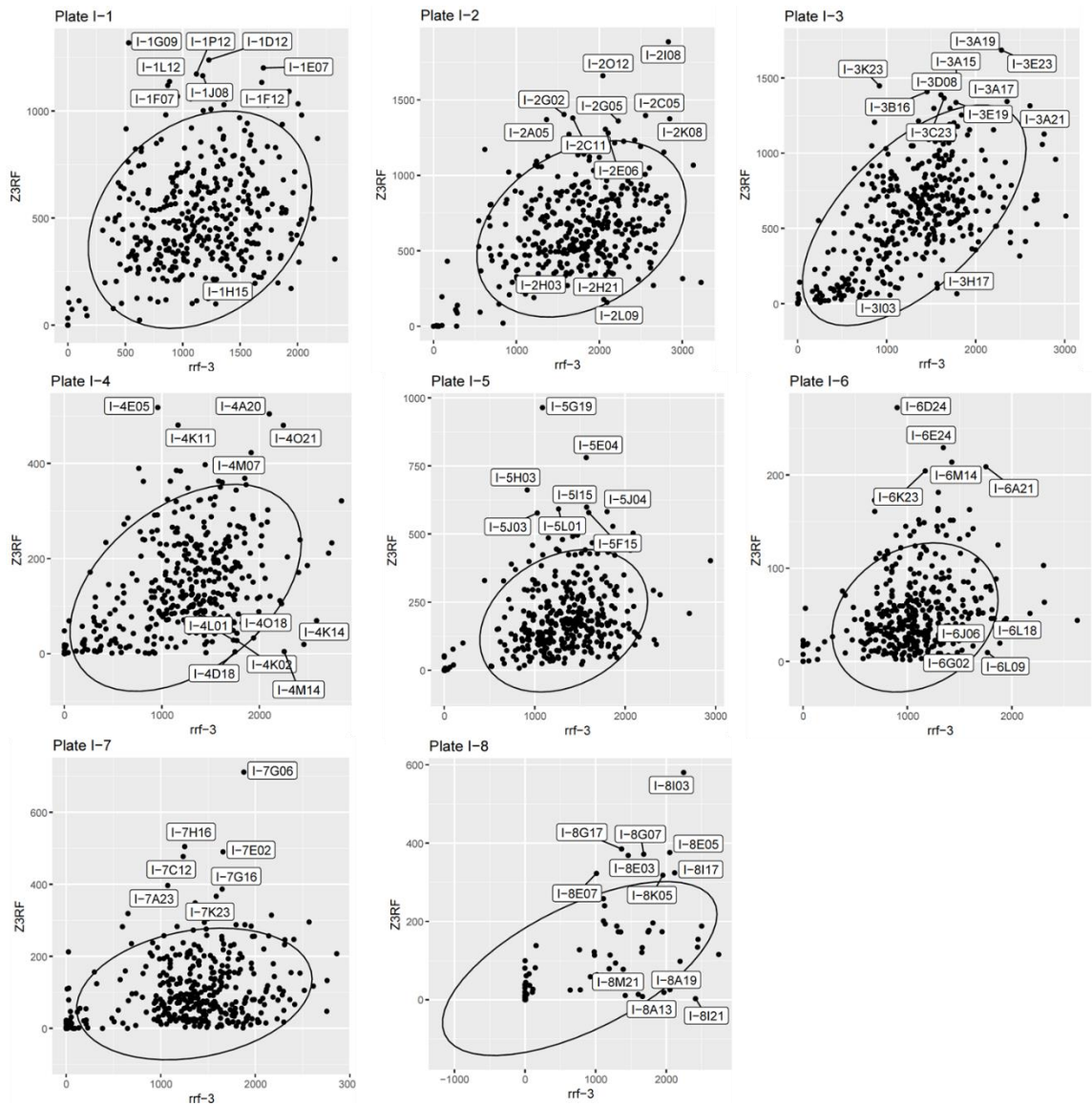


**Figure 6.6.** Identifying RNAi hits from chromosome I. Each plot represents one 384-well plate from the Ahringer library. The median of 4 replicates of each gene is plotted as a single point for both *rrf-3* and Z3RF strains. Hits in the top centre-right area are genes considered to improve the Z3RF growth/motility but have little effect on the *rrf-3* movement. Hits at the bottom are genes considered to worsen the growth/motility deficit in the Z3RF strain without affecting *rrf-3* motility. Gene labels are the positions on the 384-well plate. The ellipse denotes a 0.95 normal confidence interval. Plots produced in R.

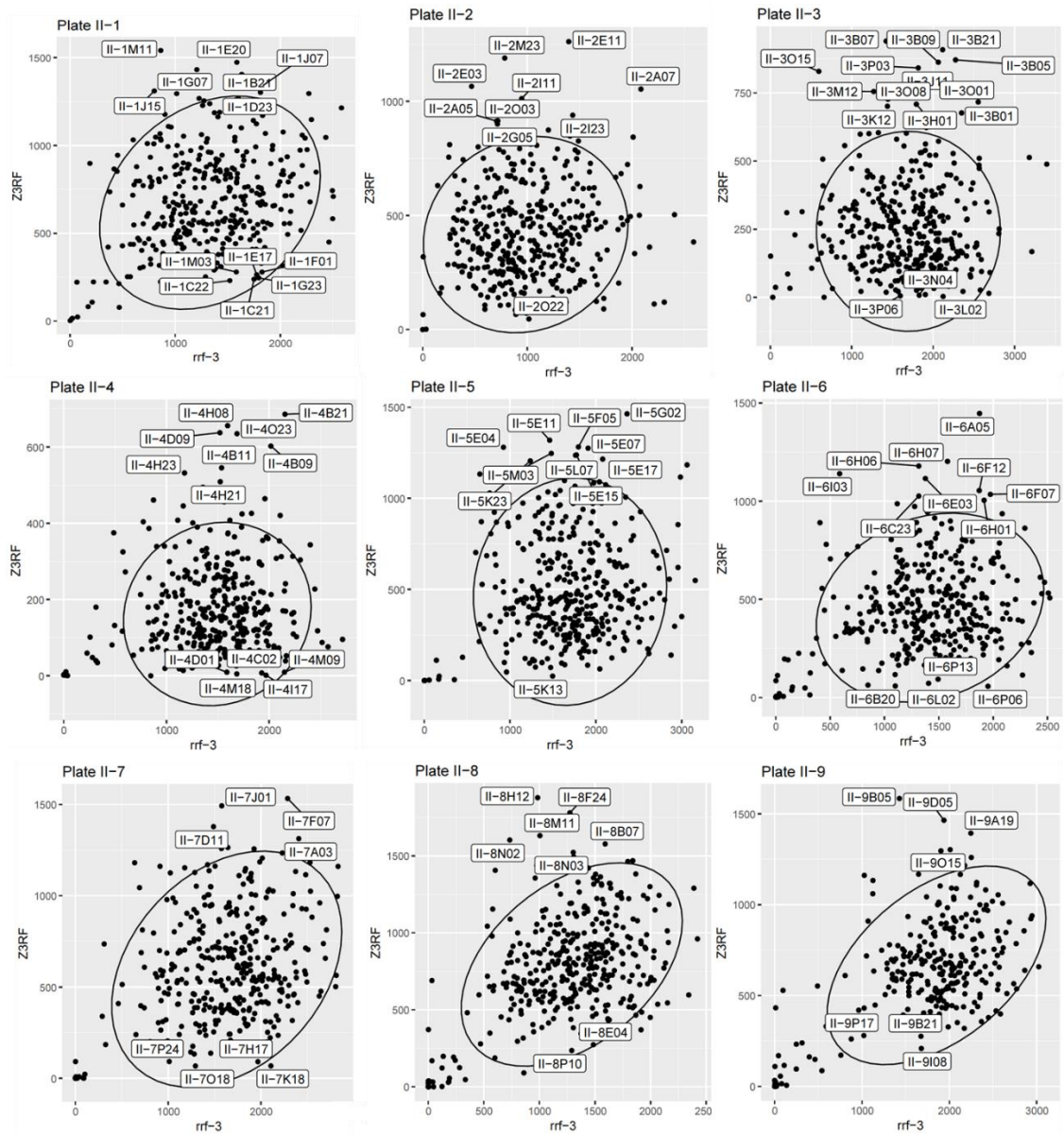


**Figure 6.7.** Identifying RNAi hits from chromosome II. Each plot represents one 384-well plate from the Ahringer library. The median of 4 replicates of each gene is plotted as a single point for both *rrf-3* and Z3RF strains. Hits in the top centre-right area are genes considered to improve the Z3RF growth/motility but have little effect on the *rrf-3* movement. Hits at the bottom are genes considered to worsen the growth/motility deficit in the Z3RF strain without affecting *rrf-3* motility. Gene labels are the positions on the 384-well plate. The ellipse denotes a 0.95 normal confidence interval. Plots produced in R.

#### 6.4.6 Analysis of the hit genes from the RNAi screen did not reveal any common pathways but did reveal a set of genes with gene ontology terms enriched against the background of chromosomes I and II

It is important to state at the outset that the RNAi screen carried out above was a primary screen and due to time constraints, no hit genes were re-screened. This means that the hits generated from the screening of chromosomes I and II are primary hits and should be considered thus; the analysis carried out on them is for informative purposes and before any strong conclusions can be made a secondary screen would be performed to confirm the hits.

The sets of genes identified from the RNAi screen as either improving or worsening of the growth/motility deficient Z3RF phenotype were interrogated for any genes which had roles in shared molecular pathways. The improving and worsening lists were submitted separately and jointly into The Database for Annotation, Visualisation and Integrated Discovery (DAVID) Bioinformatics Resource v6.8 [305]. This search revealed no significant convening of any hits on specific molecular pathways apart from general ion transport mechanisms.

In order to assess the enrichment of gene ontology (GO) terms which were significantly over-represented in the set of improving and worsening genes, the Gene Set Enrichment Analysis (GSEA) tool on WormBase was used

(<https://www.wormbase.org/tools/enrichment/tea/tea.cgi>) [306, 307]. GO or GSEA tools address the question: given that the set of improving or worsening genes were identified out of a whole set (chromosomes I and II) tested, then are the hit genes a random sample of the whole set tested. GO terms in WormBase are defined by the activity of the gene product. The lists of hit genes were uploaded separately and jointly along with a list of all background genes in chromosomes I and II. Using a hypergeometric statistical method, the tool results show all significantly enriched GO terms. The resulting list of GO terms are determined as significant by a Q value  $< 0.1$  and are ranked by their P values (the Q value is a false discovery rate adjusted P value). Inputting the improving set of genes did not reveal any significantly enriched terms.

Inputting the worsening set of gene hits resulted in the significant GO terms found in Table 6.1.

A common theme of transmembrane transport and ion channel activity can be concluded.

GO term	Expected frequency	Observed frequency	Enrichment fold change	P value	Q value
Passive transmembrane transporter activity	0.99	6	6.1	6.2e-5	0.0076
Transmembrane transport	2.3	9	3.9	0.00013	0.0079
Substrate-specific channel activity	0.89	5	5.6	0.00027	0.011
Gated channel activity	0.43	3	7	0.00087	0.027
Potassium ion transport	0.32	2	6.3	0.0038	0.093

**Table 6.1.** The significant enrichment of gene ontology (GO) terms for hit genes which were considered to worsen the Z3RF growth/motility deficit phenotype reveals a common theme of transmembrane transport and ion channel activity.

The selection of genes input into the GSEA WormBase tool which correspond to the resulting GO terms in Table 6.1 were identified and their properties can be seen in Table 6.2.

Gene name	Gene product	Function	Expression	Human Orthology	Reference
<i>ggr-1</i>	Predicted member of the GABA/ glycine receptor family of ligand-gated chloride channels	Affects thermotaxis	Expressed in neurons and in the egg-laying muscles.	Glycine receptor alpha 1	Fujiwara et al. (1996) [308]

<i>twk-1</i>	Potassium two pore domain channel	Predicted to have potassium channel activity	Expressed in the hypodermis, nervous system, gonadal sheath cell, and the DTC; <i>twk-1</i> is localized to the plasma membrane.	Potassium two pore domain channel subfamily K member 5, 16 and 17	Meissner et al. (2011) [309]; Salkoff et al. (2001) [310]
<i>unc-29</i>	A non-alpha subunit of the nicotinic acetylcholine receptor (nAChR) superfamily	Required for normal locomotion and egg-laying. Functions as a subunit of a ligand-gated ion channel that likely mediates fast actions of acetylcholine at neuromuscular junctions and in the nervous system	Expressed in body wall muscle	Cholinergic receptor nicotinic beta 1 subunit	Fleming et al. (1997) [311]; Mongan et al. (2002) [312]
<i>lgc-27</i>		Predicted to have extracellular ligand-gated ion channel activity	Expressed in certain interneurons	Cholinergic receptor nicotinic alpha 2 subunit	Wenick et al. (2004) [313]; Jones et al. (2007) [314]; Jones et al. (2008) [315]
<i>mps-2</i>	Single-pass transmembrane proteins that associate with, and regulate, pore-forming ion channels	Required for the normal function of several neurons and thus for normal body touch sensation, chemotaxis to select molecules, osmotic avoidance, and nose-touch	MPS-2 reporter fusions are expressed in the ADF amphid sensory neuron and in the enteric muscle	Related to the vertebrate KCNE proteins, also known as MinK-related peptides (MiRPs)	Park et al. (2005) [316]

<i>inx-12</i>	A protein of the innixin family; innexins are gap junction proteins	May be required to form gap junctions between the excretory canal and hypodermis, thus playing an essential role in osmoregulation	An INX-12::GFP fusion protein is expressed in the excretory canal	Similar function to vertebrate connexins	Phelan and Starich (2001) [317]
<i>vha-10</i>	An ortholog of subunit G of the cytoplasmic (V1) domain of vacuolar proton-translocating ATPase (V-ATPase)	Required for necrosis, (vha-10 (RNAi) suppresses necrotic neurodegeneration)	Predicted cytosolic stator (stalk) component	ATPase H <sup>+</sup> transporting V1 subunit G2	Syntichaki et al. (2005) [318]; Inoue et al. (2005) [319]
<i>T19D12.9</i>		Affected by 1-methylnicotinamide, Rotenone, D-glucose, Resveratrol, Fluoranthene, Chlorpyrifos, and Diazinon (RNA sequencing and microarray studies)	Enriched in the excretory cell and intestine and in neurons including the GABAergic neurons		Camon et al. (2003) [320]
<i>haf-4</i>	A half-molecular ATP-binding cassette (ABC) transporter	Required for the formation of intestinal organelles; for proper growth, normal brood size and for the normal defecation cycle	haf-4 and haf-9 are localized to intestinal organelles and physically interact to form a heterodimer	The half-type ATP-binding cassette (ABC) transporter, TAPL/ABCB9	Schroeder et al. (2007) [321]; Tanji et al. (2013) [322]

**Table 6.2.** Identities and description of genes with GO terms that were significantly enriched in the RNAi screen hit gene list which were considered to worsen the Z3RF mutant phenotype when submitted against a background list of all genes in chromosomes I and II. Information extracted and adapted from WormBase gene entries.

In order to capture additional GO terms that were significantly enriched in the hit gene set, the improving and worsening gene lists were submitted to the GSEA tool together against a background of genes found in chromosomes I and II. The results included GO terms already described in Table 6.1 and genes identified in Table 6.2, but also included supplementary ones. Table 6.3 shows the resulting significant GO terms identified from this joint set and Table 6.4 presents the genes which were defined by those GO terms.

GO term	Expected frequency	Observed frequency	Enrichment fold change	P value	Q value
Passive transmembrane transporter activity	2.7	11	4.1	1.5e-5	0.0044
Transmembrane transport	6.3	17	2.7	7.2e-5	0.0044
Substrate-specific channel activity	2.4	8	3.3	0.00066	0.027

**Table 6.3.** The significant enrichment of gene ontology (GO) terms for hit genes which were considered to improve or to worsen the Z3RF growth/motility deficit phenotype reveals a common theme of transmembrane transport and ion channel activity.

Gene name	Gene product	Function	Expression	Human Orthology	Reference
<i>gon-2</i>	A predicted transmembrane cation channel	Regulates the onset and continuation of post-embryonic mitotic cell divisions in the somatic gonad precursor cells	Excretory cell, gonad, intestine, pharynx, rectal epithelium	Long transient receptor potential channel (LTRPC) subfamily of TRP channels	Harteneck et al. (2000) [323]; West et al. (2001) [324]
<i>kqt-3</i>	One of three <i>C. elegans</i> KCNQ-like potassium channel subunits	Likely functions to regulate cellular excitability	Neurones and intestine	KCNQ1 channel protein	Culetto and Sattelle (2000) [103]; Wei et al.

					(2005) [325]
<i>unc-105</i>	Encodes a muscle degenerin, a mechanosensory membrane channel that is a member of the degenerin ion channel superfamily	Required for normal growth and for normal contraction and organization of muscle	Varying expression profile during development	Similarities to subunits of the mammalian amiloride-sensitive epithelial sodium channel	Sigurdson et al. (1984) [326]; Corey and Garcia-Anoveros (1996) [327]
<i>sol-2</i>	A CUB and LDLa domain-containing type I transmembrane protein	Functions as an auxiliary protein that positively regulates activity of the AMPA-subtype ionotropic glutamate receptor, GLR-1, and thus regulates glutamate-mediated synaptic transmission and behaviour	<i>sol-2::GFP</i> promoter fusion is expressed in head and tail neurons, including command interneurons and neurons that also express GLR-1 and SOL-1	Vertebrate Neto proteins	Wang et al. (2012) [328]
<i>inx-17</i>	Innixin	A gap junction protein	In the intestine-rectal valve, certain interneurons, and the intestine	Analogous to vertebrate connexins	Altun et al. (2009) [329]
<i>C18H9.5</i>		Affected by Mercuric Chloride, Juglone, Indole, 4-bromodiphenyl ether, Levamisole, Cry5B, Quercetin, and	Excretory cell, ventral nerve cord, hypodermis, and male-specific tissues and in the AFD neurons	Solute carrier family 17 (anion/sugar transporter)	Camon et al. (2003) [320]

		Ag nanoparticles			
<i>abch-1</i>		Predicted to have ATP binding activity and ATPase activity	Nervous system, body region, and the reproductive system	Isoform 1 of ATP-binding cassette sub-family G member 8	Camon et al. (2003) [320]
<i>slc-25A42</i>	Solute carrier homolog		Pharynx, head, intestine, and the body wall musculature	Solute carrier family 25 member 42	Camon et al. (2003) [320]

**Table 6.4.** Identities and description of genes with GO terms that were significantly enriched in the RNAi screen hit gene list which were considered to improve or worsen the Z3RF mutant phenotype when submitted against a background list of all genes in chromosomes I and II. Information generated and adapted from gene entries in WormBase.

#### 6.4.7 The correlation between hit genes from this RNAi screen and published RNAi screens of *C. elegans* models of AATD and other protein misfolding disease

RNAi screens have been performed using transgenic *C. elegans* strains modelling a variety of human protein misfolding diseases. These include Huntington's disease (associated with polyglutamine repeats) [330], Parkinson's-like diseases (associated with  $\alpha$ -synuclein mutants) [227], frontotemporal dementia (associated with tau mutants) [331] and motor neurone's disease (associated with SOD1 mutants) [230]. The hit genes identified from these other screens along with the list of genes identified from the RNAi screen using the *C. elegans* model of AATD previously described [111], were inspected for any similarity with the improving or worsening genes identified in the screen described above. Lists from all published screens are submitted in Supplementary Table 3. List comparison identified only one common gene

between the set of hits which improved the growth/motility deficient Z3RF phenotype and the tau mutant frontotemporal dementia model screen [331]: *aex-1*. *Aex-1* encodes a C2 calcium-binding domain protein. *AEX-1* functions in retrograde signalling to regulate presynaptic activity and localisation of the synaptic vesicle fusion protein *UNC-13*. It is required for defecation, locomotion, male mating and egg laying. *AEX-1* is expressed in the intestine and body wall muscles [332, 333].

#### 6.4.8 Investigating human orthologs for the improving and worsening hit genes

To identify human orthologs of hit genes which either improved or worsened the Z3RF impaired growth/motility phenotype, the lists were submitted to the SimpleMine Gene Query tool on WormBase (<https://wormbase.org/tools/mine/simplemine.cgi>). Of 128 phenotype improving genes submitted, 52 returned human orthologs, giving an orthology of 40%. 26 out of 55 of the phenotype worsening genes returned human orthologs giving an orthology of 47%. Both scores are close to and slightly higher than the 35-40% human orthologs predicted to be present in the *C. elegans* genome [334]. This suggests that the improving and worsening hits identified in the screen have an expected level of evolutionary conserved genes. The lists of human ortholog genes are included in Supplementary Tables 1 and 2.

#### 6.4.9 Predicting hit gene product biomolecular and chemical interactions

To understand how the hit phenotype improving and worsening genes and their products could be interacting with biomolecular or chemical partners, the online database resource “Search Tools for Interacting Chemicals” (STITCH) (<http://stitch.embl.de/>) was used. This database integrates information about interactions from metabolic pathways, crystal structures, binding experiments and drug-target relationships and infers information from phenotypic effects, text mining and chemical structure similarity to predict relationships between proteins and proteins and chemicals [335]. It encompasses information on more than

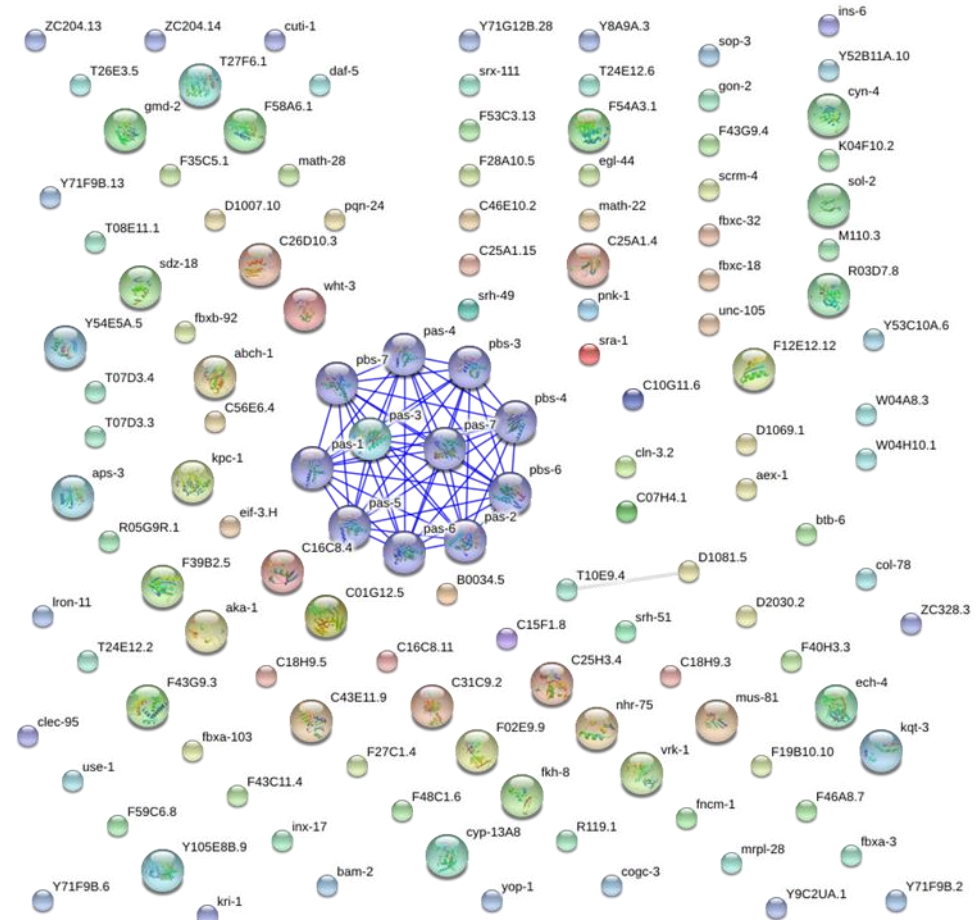
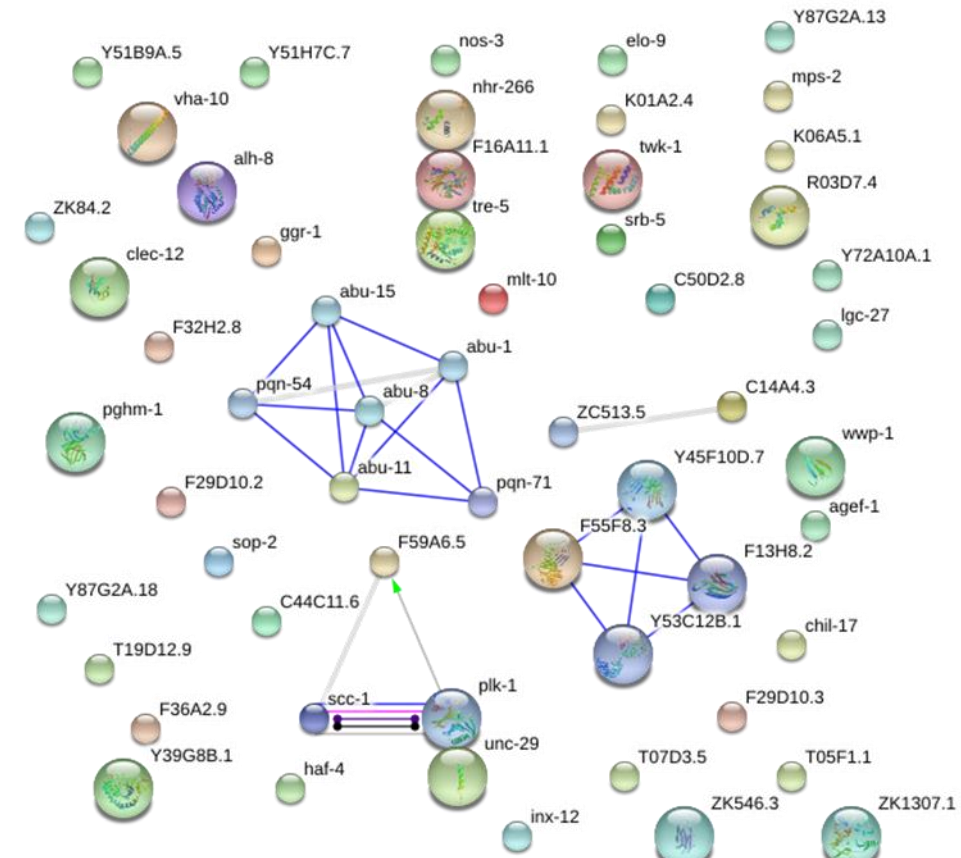
9,600,000 proteins and 430,000 chemicals [336]. Known interactions come largely from manually curated datasets such as DrugBank [337] and Matador [338] and a number of pathway databases such as the Kyoto Encyclopaedia of Genes and Genomes (KEGG) [339] and Reactome [340]. A confidence score in the range of 0 to 0.999 is given to indicate the probability that the predicted interaction exists. For all the following submissions, the highest confidence score of 0.99 was selected.

*C. elegans* hit genes from both the improving list and the worsening list were uploaded to STITCH separately. The resulting predicted interactions can be seen in Figure 6.8A and B respectively. A significant cluster of predicted interactions from the improving gene set (Figure 6.8A) can be seen involving the proteins: PAS-1, PAS-2, PAS-3, PAS-4, PAS-5, PAS-6, PAS-7, PBS-3, PBS-4, PBS-6 and PBS-7 (*pas-3* was the original hit gene). These proteins are subunit components of the proteasome, suggesting that there is a link between the hits generated in the screen and the mechanisms of the proteasome. Since this transgenic *C. elegans* strain is modelling the protein accumulation disorder AATD and it is known that the proteasome plays an important role in the degradation of mutant AAT but not polymeric AAT, the predication of protein binding partners associated with the proteasome is highly plausible. Since these hits were generated by improving the mutant Z3RF phenotype, it suggests that silencing genes associated with the proteasome could in fact have a beneficial impact on the transgenic worm model of AATD.

In the worsening gene set binding prediction schematic (Figure 6.8B); an interesting predicted binding cluster includes: ABU-1, ABU-8, ABU-15. These proteins are all activated during blocked unfolded protein response, a phenomenon known to occur as a result of AAT polymer accumulation within the ER, as discussed previously. Silencing of the *abu-11* gene resulted in a worsening of the mutant Z3RF phenotype suggesting that ABU-11 may help to protect the animal from damage by a misfolded accumulating protein. Other interesting predicted binding

interactions include: PQN-54 and PQN-71 which are both prion-like-(Q/N-rich)-domain-bearing protein family members, although little is known about their function.

The human orthologs corresponding to genes improving or worsening of the mutant phenotype that were generated by the SimpleMine tool in WormBase were also submitted to STITCH for analysis and similar predictions were made as described, due to the orthology. Although chemical interaction predictions for human orthologs would be highly interesting, the results returned none that were particularly striking. Results included: nicotine, testosterone, epibatidine (a toxic analgesic), trehalose, glucose, cholesterol and azimilide; none of which have any clinical relevance apart from azimilide, which activates potassium channels.

**A****B**

**Figure 6.8.** The results of submitting the hit genes which improved the Z3RF mutant phenotype and worsened the Z3RF mutant phenotype to STITCH analysis. STITCH integrates information from structural and phenotypic databases and published literature to suggest potential molecular binding partners. Blue lines indicate predicted biomolecular binding interactions between proteins submitted to the analysis and predicted interacting partners. Large nodes indicate that structural information on the molecule is known. (A) The STITCH output from the list of hits deemed to improve the Z3RF mutant phenotype predicted gene product binding partners with proteins involved in proteasomal degradation. (B) The STITCH output from the list of hit genes deemed to worsen the mutant phenotype predicted gene product binding partners involved in the blocked unfolded response.

## 6.5 Discussion

### 6.5.1 Developing the novel high-throughput genome-wide RNAi screen

Given that the newly generated transgenic ZAAT-expressing *C. elegans* worms displayed a pronounced growth/motility deficit which was measurable using the INVAPP/Paragon motility imaging system and that the RNAi bacterial library was easily available, the opportunity to develop a high-throughput genome-wide RNAi screen was clear. A strong transgenic worm phenotype (characterised in chapter 4 and in Figure 6.4) and the development of a new imaging system, (INVAPP/Paragon, described in chapter 3) made for a powerful combination to identify genes which play a role in AATD but had not been previously associated with disease.

When developing a new high-throughput whole genome RNAi screen, many assay variables need to be carefully investigated and optimised. These include selecting the genetic background of the strain to be screened, method of RNAi, delivery protocol (feeding), temperature and timings of the assay, number of animals to be screened, number of replicates and the method of scoring and quantifying the read out. These variables need to be adjusted specifically for the high throughput 96-well assay plate where small alterations such as in NGM composition, local humidity, amount of food and number of animals can have a large effect on

the measured outcome. A considerable amount of time was devoted to developing the details this RNAi screening protocol which was influenced by two published methods which outline NGM-based screening methods in 96-well plate based assays [341, 342].

To provide the best chance of obtaining strong obvious hits in the RNAi screen and due to the strength of the growth/motility deficit phenotype of the ZAAT worms described in chapter 4 (Figure 4.7A), an RNAi hypersensitive strain was crossed in to the transgenic worm strain. The RNAi hypersensitivity of the deletion mutant strain *rrf-3* is well documented [135], and therefore it was selected to cross with ZAAT. The resulting ZAAT transgenic *rrf-3* mutant strain (termed Z3RF) displayed similar temperature-dependent growth/motility deficiency to the ZAAT strain (Figure 6.4) confirming its suitability for the screen. The presence of dumpy worms in a well containing bacteria expressing dsRNA for *lin-41*, RNAi of which is known to result in a dumpy phenotype [304], served as confirmation that the developed RNAi method was indeed efficiently silencing genes in the animals. This increased confidence in the ability of the screen to identify hit genes which improved the motility phenotype of the transgenic worms.

### 6.5.2 Hit genes from a primary screen of chromosomes I and II with the caveat of required re-screening

The results from the RNAi screen suggest that promising hit genes, which were shown to either improve or worsen the mutant phenotype without affecting the control *rrf-3* motility phenotype, were identified. Importantly, this screen constitutes only the primary screening of chromosomes I and II without any re-testing of the hit genes. In order to confirm these, hit validation comprising of re-screening and feeding transgenic worms with a separate bacteria expressing dsRNA complementary to a different section of the hit gene mRNA would need to be performed. Nevertheless, performing initial, speculative analysis on the hit genes is interesting and possibly allows a directed approach to re-testing.

The primary screening of chromosomes I and II identified 129 hit genes which were deemed to improve the mutant phenotype of the Z3RF worms and 55 hit genes which were shown to worsen the phenotype. Determining the threshold by which these hits were identified from the plots in Figures 6.6 and 6.7 was by eye and rather arbitrary and could therefore benefit from a more methodical calculated approach. The spread of gene motility represented in Figures 6.6 and 6.7 and the identification of improving and worsening genes confirms that the screening method and protocol was suitable and robust.

Gene set enrichment ontology analysis revealed significant enrichment for several GO terms within the hit gene lists, mostly falling within the categories of transmembrane transport and ion channel activity. As proteostasis is an active process, for example, the energy-dependence of the chaperone system [343], it is quite likely that a number of transmembrane transport and ion channel activity mechanisms play a key role in the regulation of misfolded protein such as in AATD. A published example of a relationship between a mutant protein and ion channel activity is that of muscular dystrophy. A causal link was made between hypersensitivity to acetylcholine and the acetylcholinesterase inhibitor, aldicarb in a *C. elegans* *dys-1* mutant model of the disease [103, 344], which is a genetic disorder in which a mutation in the muscular protein dystrophin leads to muscle wasting [345].

One hit gene from this screen, *aex-1*, was also identified in a whole-genome RNAi screen of a *C. elegans* model of tauopathy disorders, which include frontotemporal dementia and Alzheimer's disease [331]. These are disorders of a protein accumulation nature which suggests there could be a connection in the pathways involved. AEX-1, a calcium-binding domain protein expressed in the muscle and intestine, functions in retrograde signalling to regulate presynaptic activity and localisation of the synaptic vesicle fusion protein UNC-13 [332]. Mutants of *aex-1* display neural-defective phenotypes such as defects in defecation and abnormal localisation of UNC-13. Interestingly, these effects are reversed by muscle- or

intestine-specific expression of AEX-1 but not by neuronal-specific expression of AEX-1. This suggests that AEX-1 functions in the muscle and intestine to control neural activities, likely mediated by AEX-5 prohormone convertase [332, 346]. Its role in pathology is unclear, however silencing in the tau worm model worsened the mutant phenotype. Interestingly, RNAi of *aex-1* in the ZAAT worm model improved the mutant phenotype, suggesting that it could be exerting its effect by opposing mechanisms, possibly involving neuronal control. Identifying only one gene similarity between the RNAi screen presented here and other RNAi screens on models of protein misfolding disorders [227, 230, 330, 331] is not surprising as there was little overlap between the screens themselves. However, it could also suggest that this one gene overlap is simply the result of chance, as a higher degree of overlap would be expected if similar pathways and interactions are involved in these disorders.

Identifying the predicted molecular binding partners of the hit gene products using the online database tool STITCH was informative and interesting. STITCH was used by O'Reilly and colleagues to analyse the gene hit list obtained from the whole-genome RNAi screen to identify the drug-target interactions [111]. STITCH has also been used to identify a set of compounds capable of modifying intracellular manganese levels [347]. The STITCH tool predicted gene hit interactions involved in proteasome function and blocked unfolded protein response; both of which are known to be affected by the accumulation of misfolded ZAAT within the ER as previously discussed in chapter 1 [60, 348]. This serves as confirmation of the validity of the RNAi screen and increases confidence in finding authentic hits in the remaining genome to be screened. Of course, it is important to note that these binding partners are predictive and should be considered thus.

### 6.5.3 The originality of this whole genome RNAi screen and its future applications

A number of possible screening methods can be adapted using the basic RNAi protocol; here is presented a unique approach to high-throughput whole-genome phenotypic RNAi screening using a *C. elegans* model of AATD. As previously discussed, the powerful combination of a nematode model of AATD displaying a growth/motility deficit phenotype and the INVAPP/Paragon high-throughput imaging system provides an excellent platform for a genome-wide gene silencing screen. This screen is distinct from that published by O'Reilly and colleagues as the phenotypic element allows the capture of genetic modifiers of disease which act in an orthogonal way to simply reducing fluorescent mutant protein accumulation. Interestingly also, so far there were no commonalities found in the hit genes between the screens, suggesting that there is indeed scope for further RNAi screening studies.

The completion of primary screening on the remaining four *C. elegans* chromosomes is a priority in the following steps of this study. Subsequent to this, the re-testing of all hits identified in the primary screen should be performed in a secondary screen, preferably by a slightly varied method to decisively confirm the hits. Further detailed analysis of pathway commonalities and structural and functional correlation between gene hits can then be executed using the methods outlined above. It is also possible to envisage this method as being useful for high-throughput whole-genome RNAi screening on other *C. elegans* models of human disease which display a growth or motility impaired phenotype.

# Chapter 7 Forward mutagenesis using the transgenic ZAAT *C. elegans* strain

## 7.1 Introduction

### 7.1.1 Forward mutagenesis

Randomly occurring spontaneous genetic mutations occur through a variety of mechanisms and drive diversity and natural selection. In *C. elegans*, mutations can arise from replication and repair errors, endogenous oxidative damage and exogenous environmental impairment [349]. Point mutations, gene duplications and deletions occur at the relatively high rates of  $2 \times 10^{-8}$ ,  $3.4 \times 10^{-7}$  and  $2.2 \times 10^{-7}$  per gene per generation respectively [350, 351]. Experimentally-induced mutagenesis is an important tool in *C. elegans* research for the exploration of gene function. Causal association between mutations and organism phenotypes can provide essential information regarding gene activity. Forward mutagenesis techniques deliver mutations which assist in elucidating the roles of genes which play key roles in biomolecular mechanisms of interest.

There are several advantages of forward mutagenesis over targeted transcription knockdown approaches such as RNAi. First, that it is able to capture the effects of genes which are recalcitrant to RNAi approaches, also given that the RNAi library only covers 72% of the worm genome [267]. Secondly, induced mutations tend to produce stronger consistent phenotypes which are easier to quantify than RNAi phenotypes, which can give variable results [267]. Indeed, a mutant displaying a strong phenotype is considered the gold standard for gene function elucidation.

### 7.1.2 Forward mutagenesis as a screening method

To perform screening of *C. elegans* for spontaneous mutations, prohibitively large numbers of animals would have to be used, however mutation rates can be augmented experimentally by

the deployment of a number of highly mutagenic chemicals, notably EMS and ENU [96, 352].

The use of such agents makes possible large-scale, genetic screening, where a high number of animals are randomly mutagenized, and their phenotypes scored for a desired trait. Scoring involves searching for individual worms which express mutations that suppress or enhance a specific phenotype. For example, Sydney Brenner used forward mutagenesis to elucidate genes resistant to levamisole later found to be the 5 subunits (*lev-1, unc-29, unc-38, unc-63, lev-8*) of its molecular target the levamisole-sensitive nicotinic acetylcholine receptor (nAChR) present on worm body wall muscle [311, 353-355]. The power of such 'chemistry-to-gene' screens [253] is that they identify other genes e.g. *unc-74*, which was subsequently shown to be a chaperone critical for nAChR expression [356]. Screening for resistance to acetylcholinesterase further assisted in identifying many of the genes important in cholinergic synaptic signalling [357]. The human orthologues of which are important in understanding human neuromuscular disorders [358]. Another recent screen involved using forward mutagenesis to elucidate drug targets of anthelmintic compounds in *C. elegans*. The screen involved searching for mutagenized animals which survive exposure to the anthelmintic compound and identified compounds with distinct mechanisms of action from previously characterised anthelmintics [167].

### 7.1.3 Forward mutagenesis screen design

There are some key elements to the design of a successful random mutagenesis screen. First, it is important to clearly characterise and compare in detail both the wild type animal as well as phenotype of interest to be screened, as a robust distinction is needed to maximise the chances of successfully identifying mutants with desired traits. Secondly, it is important to select or design a screening strategy suitable to the particular objectives of the screen. The most common type of forward screen is a simple F2 screen (Figure 7.1). This involves mutagenizing the germ cells of a parental strain (P0) at the L4 larval stage and selecting for

homozygous recessive mutations in the F2 generation of offspring by phenotypic analysis. The F2 generation is normally chosen because the F1 generation will possess many heterozygous mutations [359]. Another critical step in the development of forward mutagenesis protocols is to calculate the number of F2 generation worms that are required to be screened to confidently reach genome saturation – the level at which we can be certain there have been mutations in every gene. A number of variations on this basic screen exist which can be tailored to suit the specific demands of the phenotype. For instance, some phenotypes can only be observed in the second homozygous generation. An example of such was a screen to identify germ-line cell factors which prevent ageing that occurs in somatic cells. In this screen, single F2 generation worms had to be picked for more than ten generations to identify mutants which were sterile after the fourth generation. *Mrt-2* was identified as a result, which encodes a DNA-damage checkpoint protein [360].

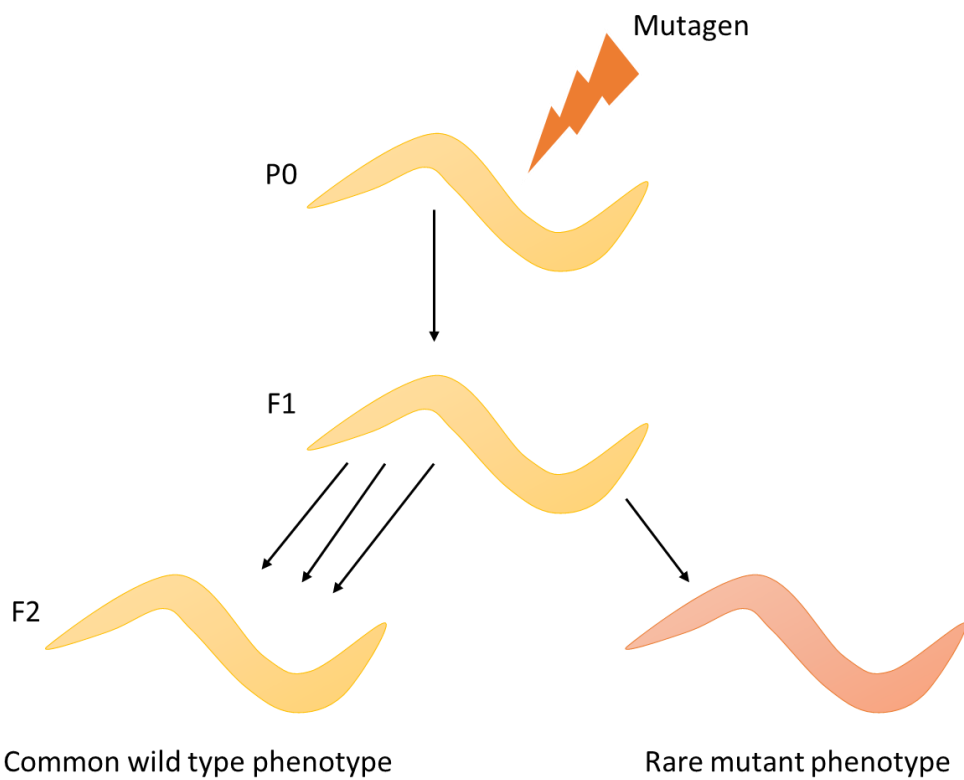


**Figure 7.1.** A simple *C. elegans* forward mutagenesis F2 progeny screen. L4 animals are randomly mutagenized as P0's. The F1 offspring which are heterozygous for mutations are allowed to self, producing the F2 generation which possess homozygous mutations. F2 animals are screened for the rare mutant phenotype. Schematic reproduced from Kutscher and Shaham (2014) [361].

#### 7.1.4 Types of mutagenic agents suitable for use in large-scale genetic screening

In *C. elegans*, random mutations can be induced by exposure to mutagenic agents such as ethyl methanesulfonate (EMS), N-ethyl-nitrosourea (ENU) or trimethylpsoralen with subsequent ultraviolet light activation (TMP/UV). EMS is by far the most widely used mutagen as it is the most potent [362]. It induces a mutation rate of  $2.5 \times 10^{-3}$  mutations/gene/generation with moderate rates of sterility [363]. EMS is an alkylating agent which acts by adding an ethyl group to primary guanine residues thus resulting in its mispairing with thymine during replication [364]. Mutations therefore have a strong bias towards G/C to A/T transitions which commonly lead to generation of stop codons, thus producing

strong loss-of-function or null alleles. EMS can also induce deletions or other chromosomal rearrangements at a rate of approximately 13% [365]. ENU is also a powerful mutagen which creates an array of transversions and transitions. The rate of A/T to G/C transitions is greatly increased with ENU and all codons are equally mutable resulting in the frequent creation of non-null alleles [366]. Treatment with UV/TMP generates all types of un-biased transitions and transversions [362]. The most powerful mutagen is EMS which causes 1.5-2 times more mutations than ENU and upwards of 3 times more mutations than UV/TMP. The type of mutagen selected depends on the desired mutations, ENU generates the greatest diversity of missense mutations but EMS results in more null alleles. Types of common physical irradiation mutagens include gamma, X-ray and UV, which result in major chromosomal rearrangements and generate duplications, inversions, deficiencies and translocations [367]. A number of other chemical and irradiation mutagens can be used to induce a variety of genetic lesions as well as non-directed insertional mutagenesis using transposons. This method involves DNA sequences that can insert and displace into a genome aided by a transposase enzyme encoded by the transposon. Mutant alleles are generated that are tagged with a transposon which can then be used to identify the mutated gene. There are however several drawbacks to this method, such as multiple copies of each transposon in the genome complicating the identification of mutagenic insertion and poor insertional efficiency [361].

### 7.1.5 Mapping the mutations

Classical mutant mapping is achieved by two- or three- point mapping with genetic markers or by mapping with deficiencies and duplications. The former method relies on the measure of genetic distance or recombination frequency between the gene to be mapped and clear phenotypic mutants (with known mutation landmark sites) [367]. Using this method, the region containing the mutation can be quickly determined, however fine mapping is difficult due to the low number of landmark mutants [368]. Moreover, interaction between the gene to

be mapped and the landmark gene greatly convolute the process. Mapping results from deficiencies (which refer to specific deleted regions within the chromosomes) and duplications (most similarly resemble extrachromosomal arrays) can be obscure and vague [369]. Thus, single nucleotide polymorphism (SNP) mapping techniques are generally favoured.

#### 7.1.5.1 SNP mapping

SNP mapping relies on the sequence divergence of the N2 *Bristol* reference strain (most commonly used in research) and the CB4856 *Hawaiian* strain [370]. Due to the geographical separation of the two strains and millions of years of evolutionary drift, SNPs arise around every 1000 base pair and include substitutions, insertions or deletions. These can be detected by restriction digests or sequencing. SNP mapping involves crossing the CB4856 into the mutant strain and selecting for the homozygous mutation in the F2 offspring to produce mutants with a CB4856 background. F2 animals which display the mutant phenotype are pooled and evaluated by sequencing or digests and evaluated by their recombination frequency [371]. If the mutation is close in proximity to a given SNP, the probability of a recombination event at that locus is low, therefore the locus around that SNP is likely to have an over-represented N2 background compared with other areas which will display equally represented CB4856 and N2 polymorphisms [372, 373]. SNP mapping revolutionised mutational identification, however it is not without limitations. The CB4856 strain was shown to have 141 deletions erasing 483 genes from its genome [374]; additionally, genetic incompatibility and phenotypic variation of mutants in the N2 and *Hawaiian* background has been blamed for producing confusing results [375].

#### 7.1.5.2 Next generation mapping approaches

The mapping strategies described are multi-step processes relying on acquiring and analysing a large number of recombinants. It would take several weeks or months to define a finely-mapped mutation locus and following this, a considerable amount of work remained to

identify the phenotype-causing mutation. Two next generation technologies have revolutionised genetic mapping: array comparative genome hybridisation (ACGH) and next generation sequencing (NGS). ACGH uses high density oligonucleotide microarrays to detect sequence polymorphism insertions/deletions in the entire genome or sections of interest. This technique is fast, requires only one genetic cross between the *Hawaiian* and N2 mutant and can detect heterozygous deletions as small as 141bp [374]. The advent of NGS represented a paradigm shift for mutational mapping. Whole genome sequencing of the mapping population identifies the frequency of the mutant allele and its localisation to a chromosome. Subtracting background strain variants and other variants from mutants in the screen allows filtration of the homozygous variants in the mapping region. Mutations are prioritised based on the selected mutagen biases. Candidate mutations are then validated experimentally to confirm the causal mutation[376]. Consequently, is now possible to simultaneously map and identify all genetic variations in the genome of the mutant strain, dramatically reducing the amount of time to identify a causal mutation.

#### 7.1.6 Forward mutagenesis screening using a *C. elegans* model of human disease

In the first mutagenesis screens, Sydney Brenner identified mutants due to visible phenotypes, such as those which resulted in the characterisation of the uncoordinated (*unc*) class of genes as well as mutations which caused small bodies, blistered cuticles, twitching muscles, long or dumpy bodies and forked heads [96]. Although these discoveries were interesting in the field of *C. elegans*, they also had wider consequences for human disease research. For example, the characterisation of the gene *unc-2* and the pathways in which it was involved, led to the discovery of the requirement of UNC-2 for the desensitisation to dopamine and serotonin [298]. This in turn has implications in the pathology of migraine, which is often associated with low levels of serotonin [377].

Moreover, coupling the power of forward genetic screens and *C. elegans* models of human disease has been an extremely fruitful venture. In no field has this been exemplified better than in the research of neurodegenerative disease, examples of which have been previously discussed in chapter 4. An instance of the strength of this research combination was an EMS screen performed on a Q-40-expressing *C. elegans* model of polyglutamine accumulation disease; a group of disorders which include Huntington's disease and spinocerebellar ataxia [378]. These diseases are characterised by the abnormal expansion of CAG triplets (encoding glutamine) which cause the protein to aggregate, usually in neurones. The forward mutagenesis screen identified MOAG-4, revealed to be a general aggregation-promoting factor in the polyglutamine accumulation model. Inactivation of MOAG-4 improved polyglutamine-associated aggregation and toxicity; an effect which was conserved in human orthologs SERF1A and SERF2 [379].

Taken together, forward mutagenic screens using *C. elegans* models of human disease are a powerful method of identifying genes and pathways not previously implicated in such disorders. Given the efficiency of classic mutagenic methods and recent developments in mapping-by-sequencing, forward screening has vast potential to elucidate new information on the molecular pathogenesis of protein accumulation disorders such as AATD and could lead to novel small molecule targets.

## 7.2 Aims

1. To develop and undertake a novel forward mutagenesis screening method using the newly generated *C. elegans* model of AATD described in chapter 4.
2. The screening protocol will be based on a simple F2 screening method using the highly potent EMS as the chemical mutagen.

3. F2 homozygous mutants will be scored by eye and individuals (and their progeny) which displayed an improved growth/motility phenotype will be selected and evaluated using the INVAPP/Paragon imaging system.
4. Candidate mutants will be assessed for their transgene expression level to ensure that it was being expressed normally. Following this, mutants that display the expected transgene expression levels will be investigated to identify their causative mutations using the mapping-by-sequencing method.

## 7.3 Methods

### 7.3.1 EMS mutagenesis

This protocol was adapted from *C. elegans*: A Practical Approach by Ian Hope [380] and is shown schematically in Figure 7.2. Five NGM plates each containing approximately 300 L4 Z-AAT-expressing *C. elegans* were washed using S-basal. The worm containing solution was transferred to a 15ml falcon tube and centrifuged at 1721 X g for 30s. The supernatant was removed and the worm pellet washed with S-basal twice more by resuspending and centrifuging. The supernatant was removed leaving 3ml of worm solution. EMS is a toxic chemical, all handling of EMS and EMS-containing solutions and glass/plastic-ware was performed inside a fume hood. In a separate 15ml falcon tube, 20 $\mu$ l ethylmethanesulfonic acid, ethyl ester, Sigma #M- 0880 (EMS) was added to 1ml S-basal and shaken until no longer cloudy. The 3ml worm solution was transferred into the tube containing the EMS solution (47mM final concentration). The solution was swirled every 30min for 4h at RT. The worms were then allowed to settle to the bottom of the tube and the supernatant was removed and placed in an EMS waste container. The worms were washed twice with 3ml S-basal and the supernatant collected each time into the waste container. The worms were transferred in a few drops of S-basal to the edge of a lawn on an NGM plate and allowed to recover for ~1h. All solutions and tips containing EMS were deactivated by addition of excess 2M NaOH then

disposed of safely in the sink or in the phenol disposal refuse. Approximately 40 L4 animals were picked to a fresh NGM plate and left for 24h.

The following day, 40 adult worms were picked to individual plates as P0's and allowed to lay eggs for 24h. The adults were then picked to separate plates and allowed to lay eggs for 24h. Approximately 100 F1s hatched on each plate, total 80 plates. The F1s were allowed to grow to adulthood and begin laying eggs. Before many eggs hatched, the adults were washed/vacuumed off the plates leaving the eggs adhered to the NGM. The plates were incubated at either 25°C or 26°C to ensure a strong mutant phenotype as previously characterised in chapter 4. F2s were inspected every day subsequently by eye, and any animals displaying an improved phenotype (better growth, movement, general health which indicate full or partial rescue of the mutant phenotype) were picked to a fresh plate and its offspring observed.

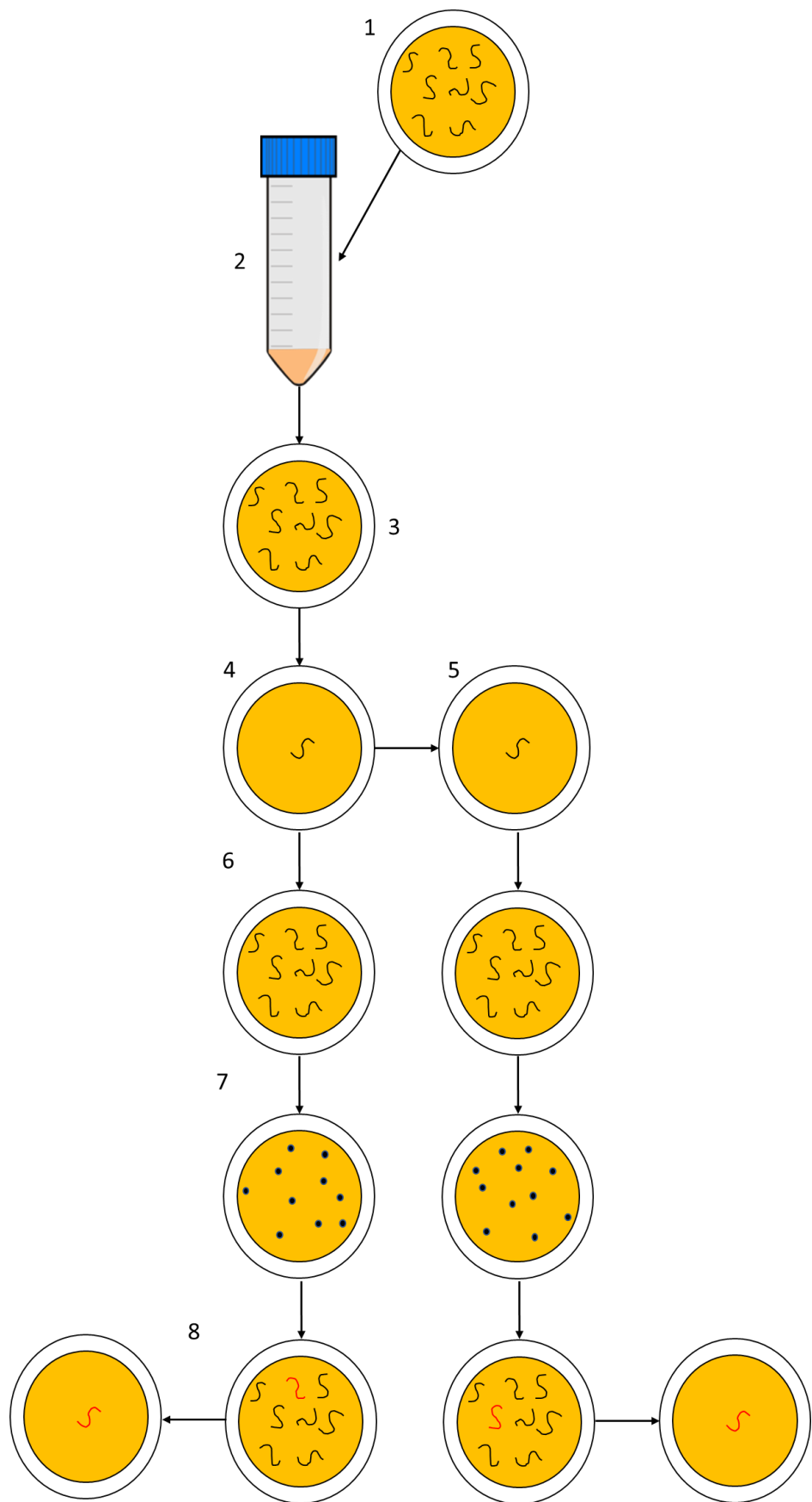


**Figure 7.2.** (1) Five plates containing many L4 ZAAT-expressing *C. elegans* were washed with S-basal. (2) The worm suspension was mixed with an S-basal solution containing EMS and incubated with swirling at room temperature for 4h. (3) Worms were placed on an NGM plate and allowed to recover for 1h before approximately 40 L4 animals were picked to a fresh plate and left for 24h. (4) The 40 adult worms were picked to individual plates as P0's and allowed to lay eggs for 24h. (5) The animals were then picked to a second plate and allowed to continue laying eggs. (6) The F1 progeny of these worms were allowed to grow to adulthood until there were many eggs on the plates. (7) The adult worms were washed/vacuumed off the plates leaving the eggs adhered to the NGM. Plates were incubated at either 25°C or 26°C. (8) Hatched F2 progeny were screened for any improvement to the growth/motility phenotype.

### 7.3.2 RT-qPCR

Approximately 40 L4/adult worms were picked into a DNA-free Eppendorf tubes containing 50µl DI H<sub>2</sub>O and 2µl glycogen. 200µl of Trizol was added to the tubes. The tubes were vortexed vigorously for 5s before being transferred to the -80°C freezer overnight.

#### 7.3.2.1 Isolating RNA and reverse transcription

The tubes were taken from the freezer and immediately immersed in a 65°C water bath for 90s, then vortexed for a few seconds before being left at room temperature for 15min. 40µl of chloroform was added to the tubes which were then shaken vigorously for 15s by hand in a fume hood. The tubes were left at room temperature for 2-3min before being spun in a microcentrifuge at maximum speed (16.1 X g) for 10min. From this step onward, all pipette tips and Eppendorf tubes used were RNase-free. The clear aqueous phase was removed from the solutions and placed in a fresh Eppendorf tube. 100µl isopropanol was added to the tubes before vortexing gently for a few seconds. The tubes were placed on ice for 10min then centrifuged at 4°C, maximum speed for 10min. The liquid was carefully removed from the pellet. 200µl of 70% v/v ethanol was added to the pellet then centrifuged at 4°C, maximum

speed for 6min. The liquid was carefully removed from the pellet which was then allowed to air dry for approximately 1h. The pellet was re-suspended in 10 $\mu$ l DI H<sub>2</sub>O.

Reverse transcription was performed using a SuperScript<sup>TM</sup> VILO<sup>TM</sup> Master Mix kit (Invitrogen, Carlsbad, California). Briefly, the 10 $\mu$ l RNA suspension was mixed with 4 $\mu$ l of SuperScript<sup>TM</sup> VILO<sup>TM</sup> Master Mix and 6 $\mu$ l of DI H<sub>2</sub>O. The tubes were incubated at 25°C for 10min, followed by incubation at 42°C for 60min and finally 85°C for 5min to terminate the reaction. The resulting cDNA was stored at -20°C.

### 7.3.2.2 qPCR reactions

The cDNA concentration was measured by nanodrop and diluted to between 1-10ng/ $\mu$ l. The components of the qPCR reactions were added to the PCR plates as follows: 2 $\mu$ l cDNA solution, 300mM forward and reverse primers (either housekeeping gene or Tag-RFP primers), 10 $\mu$ l SYBR<sup>®</sup> Green PCR Master Mix and DI H<sub>2</sub>O up to 20 $\mu$ l. Plates were sealed and placed in an Eppendorf real plex Mastercycler<sup>®</sup> pro (Hamburg, Germany). The thermocycler was programmed for a two-step qPCR reaction for 40 cycles shown in Table 7.1.

Step	AmpliTaq Gold <sup>®</sup> Polymerase Activation	PCR	
	Hold	CYCLE (40 cycles)	
Temp.	95°C	95°C	60°C
Time	10min	15s	1min
Volume	20 $\mu$ l		

**Table 7.1.** Cycling conditions for the qPCR reactions

## 7.4 Results

### 7.4.1 Selected EMS mutants display an improved growth/motility phenotype at higher temperatures compared with Z AAT-expressing worms

In order to search for novel genetic modifiers of the *C. elegans* line expressing the mutant form of the human protein, ZAAT, a forward genetic screen was performed using the transgenic worms. EMS was selected as the mutagen due to its high potency for generating useful null mutants. L4 larva (P0 generation) were exposed to EMS and consequently allowed to self-fertilise to produce the F1 generation containing heterozygous mutations. The F1 generation were also allowed to self-fertilise to produce the F2 generation bearing homozygous mutations. The F2 generation were placed at either 25°C or 26°C from the egg stage and scored for any improvement to the growth/movement phenotype at L4/adult stage. Scoring was performed by eye under a microscope and any individual animals that showed a potential rescued phenotype was transferred to a separate NGM plate. Approximately 160,000 F2 offspring were screened by this method.

Once a mutant F2 worm was selected it was placed at 25°C for further evaluation of the potentially improved growth/motility phenotype. If the mutant produced offspring that appeared healthy and grew and moved well compared to ZAAT-expressing worms at that temperature, that strain was considered a candidate for possessing a mutation which rescues the effects of ZAAT-accumulation within the worms. To quantify this improved growth/motility phenotype, one candidate mutant was picked to an NGM plate (day 1) and placed at 25°C for one week. The plate was then imaged using the INVAPP imaging system on day 7. Figure 7.3 reveals that all the mutants display an increase in growth, reproduction and motility to varying degree when compared to ZAAT transgenic worms when incubated at a higher temperature. The mutant strain C1 had the lowest level of motility rescue compared with ZAAT-expressing worms.

The letter preceding the worm strain denotes the plate that the F2 progeny was selected from, and the number denotes the original individual animal that was selected. For example, all strains beginning with A were selected from the same plate but differing individual worms. It is likely that mutants selected from the same plate could possess the same mutation as they would have arisen from the same parent worm.

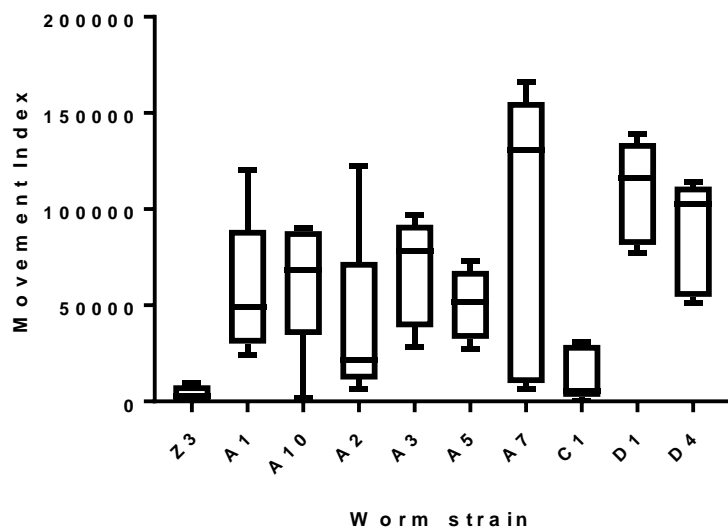


**Figure 7.3.** Candidate ZAAT transgenic *C. elegans* mutants display an increase in growth/motility when grown at 25°C compared with ZAAT-expressing worms. 1 L4 worm was picked to an NGM plate and incubated for 7 days before imaging using the INVAPP imaging system. n=5, box and whiskers plot: central line in box represents the median, box extends from the 25<sup>th</sup> to 75<sup>th</sup> percentiles and whiskers represent minimum and maximum values. Data plotted in GraphPad Prism v.7.

#### 7.4.2 EMS-induced mutant strains display a decrease in fluorescent ZAAT accumulation

To investigate whether the improvement in growth and/or motility observed in the mutant transgenic strains correlated with a decrease in accumulation of ZAAT, the strains were examined by microscopy. Three L4 worms of all mutant strains and the ZAAT strain were

picked to separate NGM plates and incubated at 25°C for approximately 1 week. Progeny were selected at random for imaging.

A high level of fluorescent ZAAT accumulation can be observed in the transgenic ZAAT-expressing strain when cultured at higher temperatures (Figure 4.2) as previously discussed in chapter 4. Very little fluorescence can be seen in panels displaying strains A and strain C1 (Figure 7.4B-G and 7.4H). This suggests that there is almost no ZAAT protein accumulation within the muscle of these worm strains. Some fluorescence can be observed in strains D1 and D4 (Figure 7.4I and J respectively) however this level is decreased when compared to the ZAAT-expressing strain. The improved growth/motility phenotype is likely the result of a decrease in ZAAT protein accumulation within the worm muscle.

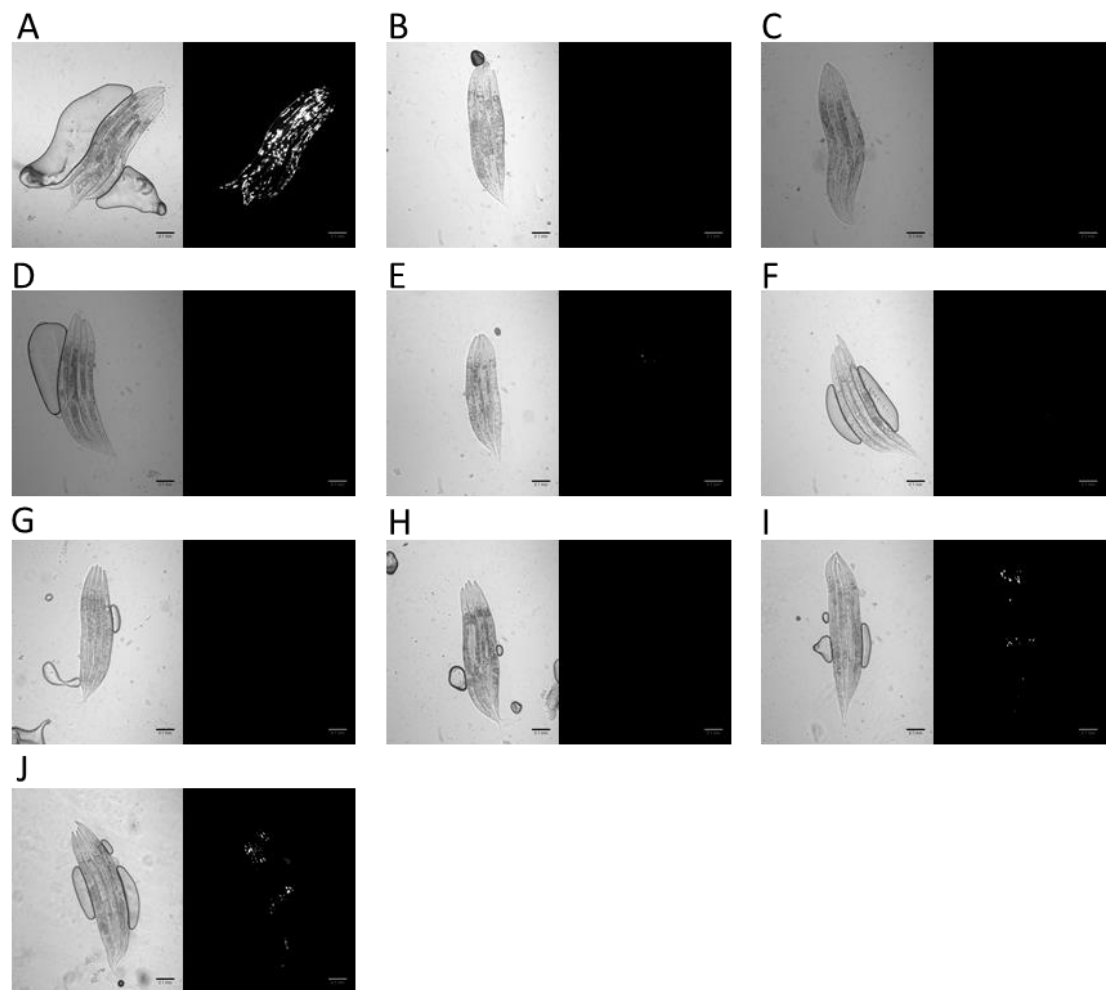


**Figure 7.4.** Bright field and corresponding fluorescent images of ZAAT transgenic and EMS-induced mutant ZAAT worm strains incubated at 25°C. Fluorescence indicates accumulation of Tag-RFP labelled ZAAT. Panels represent the following worm strains: A: ZAAT, B: A1, C: A2, D: A3, E: A5, F: A7, G: A10, H: C1, I: D1, J: D4. Bright field exposure: 15ms, fluorescent exposure: 150ms. Scale bar = 0.1mm.

#### 7.4.3 Measuring ZAAT transgene expression in the candidate mutant strains

The purpose of undertaking a forward mutagenesis screen was to identify mutants which improved the growth/motility of the ZAAT-expressing *C. elegans* worms and that the causative mutations could yield insights into the role of novel pathways or biological components which confer protection to the transgenic worms. However, it is also possible that the causative

mutations exert their protective effect by simply modifying the expression of the ZAAT transgene. It was therefore important to investigate whether there was any silencing of the ZAAT transgene occurring within the candidate mutant strains. This was achieved by measuring the expression level of the ZAAT transcript relative to two housekeeping genes by qPCR.

The qPCR technique allows for the quantification of DNA (or RNA that has been converted to cDNA via reverse transcription) in real time by measuring the fluorescent signal resulting from the random intercalation of a fluorescent probe (SYBR) into the strand of DNA during a polymerase chain reaction. DNA is quantified by plotting fluorescence against PCR amplification cycle number. A threshold for fluorescent detection is determined by 3-5 times the standard deviation of the signal above the background. The threshold cycle (C<sub>t</sub>) is given by the number of cycles at which the fluorescent signal surpasses the threshold. C<sub>t</sub> values for the transgene are subtracted from the average C<sub>t</sub> values from two housekeeping genes to quantify transgene expression [381].

It was first necessary to identify two endogenous genes which were the most stably expressed across all mutant strains and the ZAAT strain. A set of endogenous genes were identified from the literature as candidate housekeeping genes (Table 7.2.) These genes are constitutive genes required for basic cellular function and expressed in numerous cell types and tissues. They are known to display consistent expression levels between strains.

Gene name	Forward primer	Reverse primer	Product size
<i>ama-1</i>	CCTACGATGTATCGAGGCCAA	CCTCCCTCCGGTGTAAATAATG	139
<i>cdc-42</i>	CTGCTGGACAGGAAGTTACG	CTCGGACATTCTCGAATGAAG	111
<i>pmp-3</i>	GTTCCCGTGTTCATCACTCAT	ACACCGTCGAGAAGCTGTAGA	115
<i>Y45F10D.4</i>	GTCGCTTCAAATCAGTTCAGE	GTTCTTGTCAAGTGATCCGACA	139
<i>unc-15</i>	GTCCGAGTCCGTAACAATGC	ATGAGGTGAAGGCTGGACTC	108
<i>rla-1</i>	GTCTACGCTGCTCTCATCCT	CGAAGAGTCCTGCCAGTAT	115
Tag-RFP	ATCAAGGAGGCCGACAAAGA	GCCATTAAGTTGTGCCCCA	99

**Table 7.2.** Primers used for endogenous *C. elegans* genes to be tested for use as housekeeping genes in qPCR. Primer sequences for *ama-1*, *cdc-42*, *pmp-3* and *Y45F10D.4* were taken from Hoogewijs et al. (2008)[382]; all other primers were designed using Primer3 and synthesised by Invitrogen.

All candidate housekeeping genes were investigated by qPCR and the coefficient of variation (CV) calculated from the Ct values for each gene (Table 7.3). The two genes with the lowest CV values were then selected as housekeeping genes, *ama-1* and *unc-15*.

Endogenous gene	Coefficient of variation
<i>pmp-3</i>	4.62
<i>cdc-42</i>	7.73
<i>rla-1</i>	16.45
<i>ama-1</i>	1.08
<i>Y45F</i>	3.14
<i>unc-15</i>	2.01

**Table 7.3.** The coefficient of variation for each endogenous gene calculated from Ct values generated by qPCR. The two genes with the lowest Ct values are highlighted.

Once the two housekeeping genes had been identified, qPCR was performed on all strains using the primers specific for Tag-RFP. Ct values for *ama-1* and *unc-15* along with Tag-RFP were used to calculate relative transgene expression in all mutant strains and the ZAAT strain. Figure 7.5 reveals that the expression of the ZAAT transgene is lowered in all mutant strains at both 20° and 24°C when compared with ZAAT-expressing worms. This indicates that the ZAAT transgene is being silenced in the mutant strains. The mutations resulting in the improvement of the motility phenotype are therefore likely causing a reduction in transgene expression rather than by a pathologically relevant mechanism. The data in Figure 7.5 represent two biological repeats which suggests that the results are conclusive.

The expression levels of strains selected from the same plate i.e. which potentially arose from the same parent show a high degree of similarity. For example, the expression levels of all “A” strains are approximately 0.5 and the expression levels of the “D” strains are approximately 1. This suggests that the causative mutations could be the same in strains that arose from the same plate and likely from the same parent animal.

Interestingly, the expression data correlates well with the microscopy images presented in Figure 7.4. Expression levels of “A” and “C” strains are the lowest, which coincides with undetectable fluorescent signal (Figure 7.4 B-H), suggesting that very little ZAAT protein accumulation is likely due to low protein expression. Whereas expression levels in the “D” strains are slightly higher, coinciding with observable fluorescent protein accumulation within the animals (Figure 7.4 I-J). This again reinforces the reliability of the transgene expression results determined by qPCR.

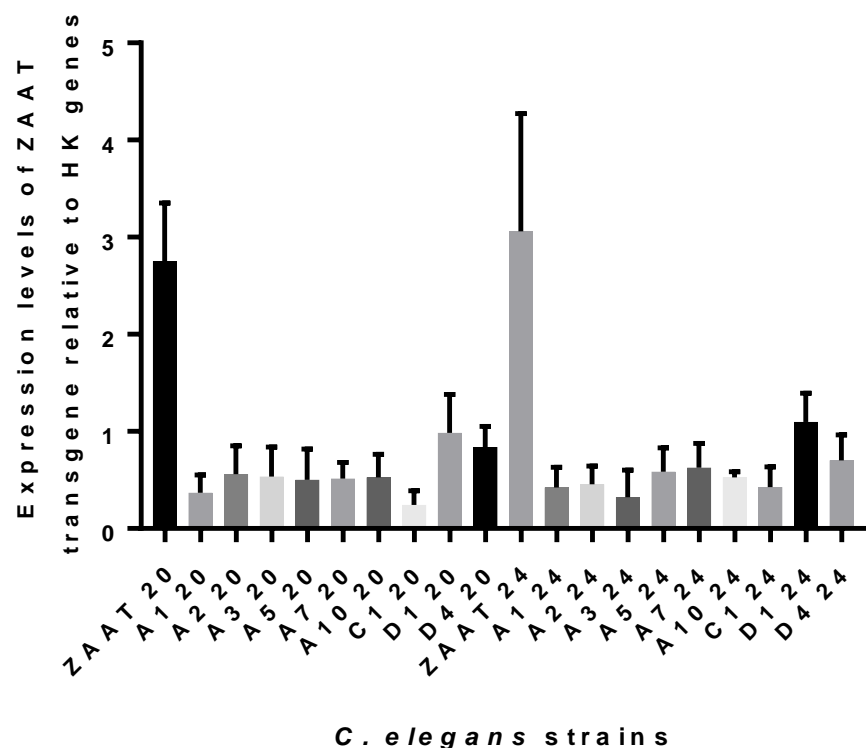


**Figure 7.5.** Expression levels of the ZAAT transgene in mutant strains and unmutated ZAAT worms relative to expression levels of housekeeping (HK) endogenous genes *ama-1* and *unc-15* when cultured at 20°C and 24°C. Mutant strains all derived from individual F2 animals selected in the EMS screen, prefix letters denote the F2 plate from which they were selected e.g. all strains beginning with ‘A’ were selected from the same plate. Expression of the transgene is reduced in all mutant strains compared with ZAAT worms at 20°C and 24°C. n=2, error bars represent SEM. Data plotted in GraphPad v.7.

## 7.5 Discussion

### 7.5.1 The forward mutagenesis screening protocol for ZAAT worms was robust and capable of identifying mutants with an improved motility phenotype

The aim of this study was to develop and execute a forward mutagenesis screen on the newly generated *C. elegans* model of AATD (previously described in chapter 4) to search for genetic modifiers not previously associated with disease. This was a novel approach as there are no such examples in the published literature. There were clear successes in the development and execution of this mutagenesis screen. The screening protocol was robust and permitted the identification of ZAAT *C. elegans* mutants which displayed an improved growth/motility phenotype. Nine mutants with varying degrees of phenotypic improvement were selected from the screen and characterised, as can be seen by the motility profiles in Figure 7.3. As outlined in detail by Jorgensen and Mango (2002) [359], the key to forward screening success lies in the appropriate design of the screening method. The protocol developed for this screen, including conditions such as worm strain, temperature and stage of temperature shift, which were thoroughly investigated prior to beginning the screen, were suitable for identifying candidate mutants.

The microscopy data corresponded well with the motility analysis of the candidate EMS-induced mutants (Figure 7.4). All mutant strains showed a reduction in fluorescent ZAAT signal when compared with the un-mutated ZAAT strain. This confirmed that the improvement in growth/motility was indeed the result of reduced ZAAT accumulation within the mutant worm muscle.

### 7.5.2 Limitations of the forward screen

Identifying candidate mutants with an improved growth/motility phenotype was a positive outcome from the forward genetic screen, however upon evaluating transcript levels of the

transgene by qPCR, it was revealed that each mutant showed a decrease in transgene expression (Figure 7.5). The decrease in transgene expression levels coincided with the motility data and microscopy images, suggesting that the decrease in ZAAT transgene expression was in fact the cause of the low ZAAT protein accumulation and the improvement in growth/motility of the transgenic animals. As the causative mutations in the candidate mutants are not known, they are likely to be mutations that result in somatic transgene silencing. A number of RNAi phenotypes have been documented to result in somatic transgene silencing; these include knock down of *rba-1*, *npp-9*, *uri-1* and *sin-3* among others [383]; mutations in any of which could result in this effect. When selecting ZAAT mutants which have an improved growth/motility phenotype, the eye is naturally drawn to those which display a dramatic effect and mutants with a silenced transgene would likely fall into this category. It would therefore be prudent to scrutinise the F2 population of mutated ZAAT worms for more subtle phenotypic changes and err on the side of caution, picking individuals with a less pronounced rescued motility.

Given these potentially subtle phenotypic changes in ZAAT mutants, the practicalities of a manual screen could become laborious, resulting in researcher fatigue and failure to detect mutants with a rescued phenotype. Considering elements of this novel EMS mutagenesis screen which could be automated could lead to improved screening efficiency and success. Screens making use of the Complex Object Parametric Analyser and Sorter (COPAS™) Biosorter have overcome some of these issues [384, 385]. Sorting individual F2 mutagenised worms into wells of 96-well plates and using the INVAPP/Paragon imaging system to identify mutants with improved growth/motility would drastically reduce the screening time and labour. This could lead to near mutational saturation of the worm genome and could identify mutants with causative mutations that are pathologically relevant to AATD.

### 7.5.3 Future applications of the novel forward mutagenic screen on ZAAT-expressing *C. elegans*

The forward mutagenesis screen on a novel *C. elegans* model of AATD described in this chapter represents a new method of screening for genetic modifiers of the disease. Following success in identifying individual ZAAT-expressing worms which displayed an improved growth/motility phenotype, and the progress made towards improving the screening technique (including sourcing use of a COPAS™ Biosorter to improve animal sorting); this method has great potential for capturing mutants whose causative mutations have greater relevance for AATD pathology in future screens. It paves the way for the potential elucidation of new genes and pathways not previously associated with AATD.

## Chapter 8 Final conclusions and future perspectives

### 8.1 The urgent need for novel treatments for AATD

The genetic disorder AATD results in extensive liver and lung damage due to the toxic aggregation of mutant ZAAT protein within hepatocytes, and the lack of circulating functional protein respectively [7]. Patients with AATD currently have limited treatment options, with liver transplantation being the only effective course of therapeutic action [48]. The need for novel treatments for AATD is therefore indisputable. Despite a deep understanding of the AAT protein and its role in causing the disease, much of its impact on cellular pathology and the mechanisms of injury are still poorly understood. The aim of this study was to characterise a novel *C. elegans* model of AATD, using a newly developed high-throughput imaging platform, INVAPP, to develop and perform chemical and genetic screens in order to identify novel modulators of disease.

### 8.2 The capabilities of the INVAPP/Paragon system for large scale chemical and genetic screening

An invertebrate automated phenotyping platform (INVAPP) used in combination with the Paragon algorithm represents a novel opportunity to image and quantify growth and movement of parasitic nematodes and potentially other invertebrate organisms as well as *C. elegans* models of human disease in multi-well plate settings. The key advantage of the INVAPP/Paragon system lies in the speed with which imaging can be performed, making it particularly valuable in large-scale chemical or genetic screens [168]. In chapter 3 of this study, these capabilities were demonstrated by the screening of an open-source library of drugs on *C. elegans* for anthelmintic activity. The successful identification of small molecules with anthelmintic properties confirmed the future application of this system for further screens of larger libraries to search for additional compounds with potential therapeutic application. Furthermore, the development of bespoke algorithms for the organisms to be screened, such

as mosquitoes and other parasites, widens the application of INVAPP/Paragon to the search for novel treatments for a number of vector-borne diseases. The capacity to quantify *C. elegans* phenotypes, in terms of growth and motility using the INVAPP/Paragon system also extended its usefulness to screening nematode models of human disease.

### 8.3 A novel *C. elegans* model of AATD

The newly generated and characterised *C. elegans* model of AATD described in chapter 4, expressed the mutant form of AAT (ZAAT) within its muscle cells. It displayed temperature-dependent accumulation of ZAAT, which correlated with a growth/motility impaired phenotype. This deficient phenotype was scorable using the INVAPP/Paragon system, permitting the possibility of using the model in high-throughput screening to search for novel genetic and chemical modifiers of AATD. The purpose of identifying such modifiers was two-fold, first to find potentially therapeutic drugs or drug targets and secondly to further elucidate the cellular mechanisms of AATD particularly with regard to cell damage. Phenotypic screening of a growth/motility deficit is advantageous over simply searching for modulators of accumulation (as has been previously reported [109-112]) as it widens the scope of the screen to capture drugs or genes which act orthogonally to simply blocking mutant ZAAT aggregation. Three such screens were developed and carried out.

### 8.4 Library-scale chemical screening of a *C. elegans* model of AATD

A method for a small molecule screen was developed and performed in a pilot fashion for a small library of 960 compounds. Growth/motility was used as a read-out which was quantified using INVAPP. No chemical hits were identified; however, the screening protocol was robust and certainly paves the way for use in a larger screen of more compounds in the future. Typically, small molecule screens involve tens of thousands of compounds which greatly enhances the probability of identifying hit compounds. The collaboration between the

Lomas/Sattelle group and the chemistry group at Oxford, which has already led to the discovery of two new classes of chemistry with anthelmintic activity, will expedite progression on this approach to search for a new small molecule therapy for AATD. The employment of novel libraries consisting of compounds with new chemistries, natural products or re-purposed drugs could also aid the discovery of efficacious compounds. Future investment in the development of worms which are highly permeable to chemicals, but which display improved overall physical health could also be fruitful in identifying efficacious drugs using the *C. elegans* model of AATD [105].

## 8.5 Genome-scale RNAi screening of a *C. elegans* model of AATD

A protocol for an RNAi knock down genome-wide screen was developed and used to screen 2 out of 6 *C. elegans* chromosomes. The screen yielded several interesting hits, which will require re-testing and validating. The success of the screen in identifying potential hits confirms the usefulness of this method in finding genes, which play a role in AATD but have not been previously associated with disease. It will be fruitful to continue this screen to completed genome level in order to capture as many possible hits as possible. Hits will then need to be validated and assessed for their potential role in the disorder, using some of the gene analysis tools outlined in the chapter. Given the recent FDA approval for Patisiran (Alnylam), an RNAi treatment for transthyretin or amyloidosis, there is a renewed enthusiasm for gene silencing as treatments for human disease, and indeed for the use of *C. elegans* in the discovery of such treatments given that RNAi was first fully elucidated in the worm [263].

## 8.6 A forward genetic screen applied to a *C. elegans* model of AATD

An EMS-based forward genetic screen using the *C. elegans* model of AATD was set up. The screen yielded a selection of mutants which displayed improved growth and motility compared with the ZAAT strain. However, upon examination of the transgene transcript levels, it was

found that each mutant had a reduced level of ZAAT expression which was resulting in the improved phenotype. Whilst this result was disappointing, it revealed that using the forward mutagenesis method developed in this study, it was indeed possible to identify animals with an improved phenotype. This is encouraging for the future use of such mutagenesis screens to search for additional ZAAT worms with induced mutations which display an improved phenotype. This approach could enable the identification of novel genes not previously associated with AATD. As the qPCR protocol was also developed in this study, animals selected from the screen could be rapidly assessed for the expression of the ZAAT transgene to eliminate those that displayed transgene silencing from further study.

## 8.7 Cell and gene therapy for AATD

The recent interest and developments in gene therapy to treat human disease, show that there is great potential for its possible therapeutic use in AATD, with one such therapy reaching a phase II trial [128]. However, essential improvements required in vector design and excessive development costs pose challenges to the progress towards treatments for patients. The improvement in manufacturing technologies is likely to decrease cost in future and could speed up advancement in the field [386]. Gene therapy using CRISPR/Cas9 is another exciting AATD treatment endeavour. Although the challenges of off-target genome-editing as well as large deletions and DNA repair mechanism damage require resolution before it is considered a viable treatment option [132]. The potential combination of cell and gene therapy using genetically corrected then engrafted patient hiPSCs also presents a promising new therapeutic approach, as it addresses both lung and liver components of disease [48]. However, substantial work is required to ascertain whether this method can be successfully translated into a treatment for patients of AATD.

## 8.8 Conclusions

Taken together the work contained in this thesis study has involved describing and demonstrating the capabilities of a novel imaging system adapted for high-throughput large scale screening. The INVAPP/Paragon system has applications in anthelmintic drug discovery as well as in the screening of nematode models of human disease. The imaging system was validated by screening an open source small molecule library from the MMV. A newly generated *C. elegans* model of the genetic disease AATD was characterised and used in three newly developed chemical and genetic screens including a small molecule screen, a whole-genome RNAi screen and an EMS-induced forward mutagenesis screen. Each screen showed advantages and limitations, however they all present potential for future application in the continuing search for novel AATD treatments and in advancing insight into the disease.

## Bibliography

1. Irving, J.A., et al., *Phylogeny of the serpin superfamily: implications of patterns of amino acid conservation for structure and function*. Genome Res, 2000. **10**(12): p. 1845-64.
2. Gettins, P.G., *Keeping the serpin machine running smoothly*. Genome Res, 2000. **10**(12): p. 1833-5.
3. Clarke, E.P., et al., *A collagen-binding protein in the endoplasmic reticulum of myoblasts exhibits relationship with serine protease inhibitors*. J Biol Chem, 1991. **266**(26): p. 17230-5.
4. Hammond, G.L., et al., *Primary structure of human corticosteroid binding globulin, deduced from hepatic and pulmonary cDNAs, exhibits homology with serine protease inhibitors*. Proc Natl Acad Sci U S A, 1987. **84**(15): p. 5153-7.
5. Huang, J., et al., *Expression and purification of functional human alpha-1-Antitrypsin from cultured plant cells*. Biotechnol Prog, 2001. **17**(1): p. 126-33.
6. Ohlsson, K., *Neutral leucocyte proteases and elastase inhibited by plasma alpha 1 - antitrypsin*. Scand J Clin Lab Invest, 1971. **28**(3): p. 251-3.
7. Gooptu, B., J.A. Dickens, and D.A. Lomas, *The molecular and cellular pathology of  $\alpha$ 1-antitrypsin deficiency*. Trends in Molecular Medicine, 2014. **20**(2): p. 116-127.
8. Venembre, P., et al., *Secretion of  $\alpha$ 1-antitrypsin by alveolar epithelial cells*. FEBS Letters, 1994. **346**(2): p. 171-174.
9. Geboes, K., et al., *Morphological identification of alpha-1-antitrypsin in the human small intestine*. Histopathology, 1982. **6**(1): p. 55-60.
10. Pääkkö, P., et al., *Activated neutrophils secrete stored alpha 1-antitrypsin*. American Journal of Respiratory and Critical Care Medicine, 1996. **154**(6): p. 1829-1833.
11. Cohen, A.B., *Interrelationships between the Human Alveolar Macrophage and Alpha-1-Antitrypsin*. The Journal of Clinical Investigation, 1973. **52**(11): p. 2793-2799.
12. Archibald, A.L., et al., *High-level expression of biologically active human alpha 1-antitrypsin in the milk of transgenic mice*. Proc Natl Acad Sci U S A, 1990. **87**(13): p. 5178-82.
13. Lodish, H.F., et al., *Hepatoma secretory proteins migrate from rough endoplasmic reticulum to Golgi at characteristic rates*. Nature, 1983. **304**(5921): p. 80-3.
14. Duvoix, A., Roussel, BD., Lomas, DA., *Molecular pathogenesis of alpha-1-antitrypsin deficiency*. Revue des Maladies Respiratoires, 2014. **31**(10): p. 992-1002.
15. Bode, W. and R. Huber, *Natural protein proteinase inhibitors and their interaction with proteinases*. Eur J Biochem, 1992. **204**(2): p. 433-51.
16. Hunt, L.T. and M.O. Dayhoff, *A surprising new protein superfamily containing ovalbumin, antithrombin-III, and alpha 1-proteinase inhibitor*. Biochem Biophys Res Commun, 1980. **95**(2): p. 864-71.
17. Huntington, J.A., R.J. Read, and R.W. Carrell, *Structure of a serpin-protease complex shows inhibition by deformation*. Nature, 2000. **407**(6806): p. 923-926.
18. Mashiba, S., et al., *In vivo complex formation of oxidized alpha(1)-antitrypsin and LDL*. Arterioscler Thromb Vasc Biol, 2001. **21**(11): p. 1801-8.

19. Pettersen, E.F., et al., *UCSF Chimera--a visualization system for exploratory research and analysis*. J Comput Chem, 2004. **25**(13): p. 1605-12.
20. Elliott, P.R., et al., *Topography of a 2.0 Å structure of alpha1-antitrypsin reveals targets for rational drug design to prevent conformational disease*. Protein Sci, 2000. **9**(7): p. 1274-81.
21. Laurell, C.B. and S. Eriksson, *The electrophoretic alpha1-globulin pattern of serum in alpha1-antitrypsin deficiency*. 1963. Copd, 2013. **10 Suppl 1**: p. 3-8.
22. Sveger, T., *Liver disease in alpha1-antitrypsin deficiency detected by screening of 200,000 infants*. N Engl J Med, 1976. **294**(24): p. 1316-21.
23. Silverman, E.K., et al., *Alpha-1-antitrypsin deficiency. High prevalence in the St. Louis area determined by direct population screening*. Am Rev Respir Dis, 1989. **140**(4): p. 961-6.
24. Dafforn, T.R., et al., *A kinetic mechanism for the polymerization of alpha1-antitrypsin*. J Biol Chem, 1999. **274**(14): p. 9548-55.
25. Lomas, D.A., et al., *The mechanism of Z alpha 1-antitrypsin accumulation in the liver*. Nature, 1992. **357**(6379): p. 605-607.
26. Lomas, D.A., et al., *Effect of the Z mutation on the physical and inhibitory properties of alpha 1-antitrypsin*. Biochemistry, 1993. **32**(2): p. 500-8.
27. Yamasaki, M., et al., *Crystal structure of a stable dimer reveals the molecular basis of serpin polymerization*. Nature, 2008. **455**(7217): p. 1255-8.
28. Ekeowa, U.I., et al., *Defining the mechanism of polymerization in the serpinopathies*. Proceedings of the National Academy of Sciences, 2010. **107**(40): p. 17146-17151.
29. Yamasaki, M., et al., *Molecular basis of alpha1-antitrypsin deficiency revealed by the structure of a domain-swapped trimer*. EMBO Rep, 2011. **12**(10): p. 1011-7.
30. Dickens, J.A. and D.A. Lomas, *Why has it been so difficult to prove the efficacy of alpha-1-antitrypsin replacement therapy? Insights from the study of disease pathogenesis*. Drug Design, Development and Therapy, 2011. **5**: p. 391-405.
31. Salahuddin, P., *Genetic variants of alpha1-antitrypsin*. Curr Protein Pept Sci, 2010. **11**(2): p. 101-17.
32. Sifers, R.N., et al., *A frameshift mutation results in a truncated alpha 1-antitrypsin that is retained within the rough endoplasmic reticulum*. Journal of Biological Chemistry, 1988. **263**(15): p. 7330-7335.
33. Kroeger, H., et al., *Endoplasmic Reticulum-associated Degradation (ERAD) and Autophagy Cooperate to Degrade Polymerogenic Mutant Serpins*. Journal of Biological Chemistry, 2009. **284**(34): p. 22793-22802.
34. Eriksson, S., J. Carlson, and R. Velez, *Risk of cirrhosis and primary liver cancer in alpha 1-antitrypsin deficiency*. N Engl J Med, 1986. **314**(12): p. 736-9.
35. Lindblad, D., K. Blomenkamp, and J. Teckman, *Alpha-1-antitrypsin mutant Z protein content in individual hepatocytes correlates with cell death in a mouse model*. Hepatology, 2007. **46**(4): p. 1228-35.
36. Lomas, D.A., et al., *Alpha 1-antitrypsin Siiyama (Ser53-->Phe). Further evidence for intracellular loop-sheet polymerization*. J Biol Chem, 1993. **268**(21): p. 15333-5.

37. Lomas, D.A. and R.W. Carrell, *Serpinopathies and the conformational dementias*. Nat Rev Genet, 2002. **3**(10): p. 759-768.
38. Lieberman, J., B. Winter, and A. Sastre, *Alpha 1-antitrypsin Pi-types in 965 COPD patients*. Chest, 1986. **89**(3): p. 370-3.
39. Elliott, P.R., D. Bilton, and D.A. Lomas, *Lung Polymers in Z  $\alpha$ 1-Antitrypsin Deficiency-related Emphysema*. American Journal of Respiratory Cell and Molecular Biology, 1998. **18**(5): p. 670-674.
40. Parmar, J.S., et al., *Polymers of alpha(1)-antitrypsin are chemotactic for human neutrophils: a new paradigm for the pathogenesis of emphysema*. Am J Respir Cell Mol Biol, 2002. **26**(6): p. 723-30.
41. Taggart, C., et al., *Oxidation of either methionine 351 or methionine 358 in alpha 1-antitrypsin causes loss of anti-neutrophil elastase activity*. J Biol Chem, 2000. **275**(35): p. 27258-65.
42. Stone, H., A. Pye, and R.A. Stockley, *Disease associations in alpha-1-antitrypsin deficiency*. Respir Med, 2014. **108**(2): p. 338-43.
43. Janus, E.D., N.T. Phillips, and R.W. Carrell, *Smoking, lung function, and alpha 1-antitrypsin deficiency*. Lancet, 1985. **1**(8421): p. 152-4.
44. Dauriat, G., et al., *Functional results of unilateral lung volume reduction surgery in alpha1-antitrypsin deficient patients*. Int J Chron Obstruct Pulmon Dis, 2006. **1**(2): p. 201-6.
45. Wewers, M.D., et al., *Replacement therapy for alpha 1-antitrypsin deficiency associated with emphysema*. N Engl J Med, 1987. **316**(17): p. 1055-62.
46. Gadek, J.E., et al., *Replacement therapy of alpha 1-antitrypsin deficiency. Reversal of protease-antiprotease imbalance within the alveolar structures of PiZ subjects*. J Clin Invest, 1981. **68**(5): p. 1158-65.
47. Gotzsche, P.C. and H.K. Johansen, *Intravenous alpha-1 antitrypsin augmentation therapy for treating patients with alpha-1 antitrypsin deficiency and lung disease*. Cochrane Database Syst Rev, 2010(7): p. Cd007851.
48. Ghouse, R., et al., *Mysteries of alpha1-antitrypsin deficiency: emerging therapeutic strategies for a challenging disease*. Dis Model Mech, 2014. **7**(4): p. 411-9.
49. Kemmer, N., et al., *Alpha-1-antitrypsin deficiency: outcomes after liver transplantation*. Transplant Proc, 2008. **40**(5): p. 1492-4.
50. Hood, J.M., et al., *Liver transplantation for advanced liver disease with alpha-1-antitrypsin deficiency*. N Engl J Med, 1980. **302**(5): p. 272-5.
51. Jain, A.B., et al., *Effect of liver transplant on pulmonary functions in adult patients with alpha 1 antitrypsin deficiency: 7 cases*. Exp Clin Transplant, 2010. **8**(1): p. 4-8.
52. Bertolotti, A., et al., *Dynamic interaction of BiP and ER stress transducers in the unfolded-protein response*. Nature Cell Biology, 2000. **2**: p. 326.
53. Shen, J., et al., *ER stress regulation of ATF6 localization by dissociation of BiP/GRP78 binding and unmasking of Golgi localization signals*. Dev Cell, 2002. **3**(1): p. 99-111.
54. McCaffrey, K. and I. Braakman, *Protein quality control at the endoplasmic reticulum*. Essays Biochem, 2016. **60**(2): p. 227-235.

55. Cabral, C.M., et al., *Processing by endoplasmic reticulum mannosidases partitions a secretion-impaired glycoprotein into distinct disposal pathways*. J Biol Chem, 2000. **275**(32): p. 25015-22.
56. Kruse, K.B., J.L. Brodsky, and A.A. McCracken, *Characterization of an ERAD gene as VPS30/ATG6 reveals two alternative and functionally distinct protein quality control pathways: one for soluble Z variant of human alpha-1 proteinase inhibitor (A1PiZ) and another for aggregates of A1PiZ*. Mol Biol Cell, 2006. **17**(1): p. 203-12.
57. Wang, Y. and D.H. Perlmutter, *Targeting intracellular degradation pathways for treatment of liver disease caused by alpha1-antitrypsin deficiency*. Pediatr Res, 2014. **75**(1-2): p. 133-9.
58. Perlmutter, D.H., *The role of autophagy in alpha-1-antitrypsin deficiency: a specific cellular response in genetic diseases associated with aggregation-prone proteins*. Autophagy, 2006. **2**(4): p. 258-63.
59. Greene, C.M. and N.G. McElvaney, *Z alpha-1 antitrypsin deficiency and the endoplasmic reticulum stress response*. World J Gastrointest Pharmacol Ther, 2010. **1**(5): p. 94-101.
60. Hidvegi, T., et al., *Accumulation of mutant alpha1-antitrypsin Z in the endoplasmic reticulum activates caspases-4 and -12, NFkappaB, and BAP31 but not the unfolded protein response*. J Biol Chem, 2005. **280**(47): p. 39002-15.
61. Lawless, M.W., et al., *Activation of Endoplasmic Reticulum-Specific Stress Responses Associated with the Conformational Disease Z  $\alpha$ 1-Antitrypsin Deficiency*. The Journal of Immunology, 2004. **172**(9): p. 5722-5726.
62. Ordóñez, A., et al., *Endoplasmic reticulum polymers impair luminal protein mobility and sensitize to cellular stress in alpha1 - antitrypsin deficiency*. Hepatology, 2013. **57**(5): p. 2049-2060.
63. Davies, M.J., et al., *Neuroserpin polymers activate NF-kappaB by a calcium signaling pathway that is independent of the unfolded protein response*. J Biol Chem, 2009. **284**(27): p. 18202-9.
64. Teckman, J.H. and A. Jain, *Advances in alpha-1-antitrypsin deficiency liver disease*. Curr Gastroenterol Rep, 2014. **16**(1): p. 367.
65. Rashid, S.T., et al., *Modeling inherited metabolic disorders of the liver using human induced pluripotent stem cells*. J Clin Invest, 2010. **120**(9): p. 3127-36.
66. Yusa, K., et al., *Targeted gene correction of alpha1-antitrypsin deficiency in induced pluripotent stem cells*. Nature, 2011. **478**(7369): p. 391-4.
67. Davidson, M.D., B.R. Ware, and S.R. Khetani, *Stem cell-derived liver cells for drug testing and disease modeling*. Discov Med, 2015. **19**(106): p. 349-58.
68. Lomas, D.A., J.R. Hurst, and B. Gooptu, *Update on alpha-1 antitrypsin deficiency: New therapies*. J Hepatol, 2016. **65**(2): p. 413-24.
69. McCracken, A.A. and K.B. Kruse, *Selective protein degradation in the yeast exocytic pathway*. Mol Biol Cell, 1993. **4**(7): p. 729-36.
70. Werner, E.D., J.L. Brodsky, and A.A. McCracken, *Proteasome-dependent endoplasmic reticulum-associated protein degradation: an unconventional route to a familiar fate*. Proc Natl Acad Sci U S A, 1996. **93**(24): p. 13797-801.

71. Brodsky, J.L., et al., *The requirement for molecular chaperones during endoplasmic reticulum-associated protein degradation demonstrates that protein export and import are mechanistically distinct*. J Biol Chem, 1999. **274**(6): p. 3453-60.

72. McCracken, A.A., et al., *Yeast mutants deficient in ER-associated degradation of the Z variant of alpha-1-protease inhibitor*. Genetics, 1996. **144**(4): p. 1355-62.

73. Palmer, E.A., et al., *Differential requirements of novel A1PiZ degradation deficient (ADD) genes in ER-associated protein degradation*. J Cell Sci, 2003. **116**(Pt 11): p. 2361-73.

74. Li, X., et al., *beta-Subunit appendages promote 20S proteasome assembly by overcoming an Ump1-dependent checkpoint*. Embo j, 2007. **26**(9): p. 2339-49.

75. Scott, C.M., et al., *ADD66, a gene involved in the endoplasmic reticulum-associated degradation of alpha-1-antitrypsin-Z in yeast, facilitates proteasome activity and assembly*. Mol Biol Cell, 2007. **18**(10): p. 3776-87.

76. Joly, P., et al., *ERAD defects and the HFE-H63D variant are associated with increased risk of liver damages in Alpha 1-Antitrypsin Deficiency*. PLoS One, 2017. **12**(6): p. e0179369.

77. Christianson, J.C., et al., *OS-9 and GRP94 deliver mutant alpha1-antitrypsin to the Hrd1-SEL1L ubiquitin ligase complex for ERAD*. Nat Cell Biol, 2008. **10**(3): p. 272-82.

78. Feng, L., et al., *Ubiquitin ligase SYVN1/HRD1 facilitates degradation of the SERPINA1 Z variant/alpha-1-antitrypsin Z variant via SQSTM1/p62-dependent selective autophagy*. Autophagy, 2017. **13**(4): p. 686-702.

79. Belorgey, D., et al., *Mutant Neuroserpin (S49P) that causes familial encephalopathy with neuroserpin inclusion bodies is a poor proteinase inhibitor and readily forms polymers in vitro*. J Biol Chem, 2002. **277**(19): p. 17367-73.

80. Guadagno, N.A. and E. Miranda, *Polymer toxicity in neurodegeneration FENIB*. Oncotarget, 2017. **8**(22): p. 35490-35491.

81. Rubin, G.M., et al., *Comparative genomics of the eukaryotes*. Science, 2000. **287**(5461): p. 2204-15.

82. Brand, A.H. and N. Perrimon, *Targeted gene expression as a means of altering cell fates and generating dominant phenotypes*. Development, 1993. **118**(2): p. 401-15.

83. Miranda, E., et al., *The intracellular accumulation of polymeric neuroserpin explains the severity of the dementia FENIB*. Hum Mol Genet, 2008. **17**(11): p. 1527-39.

84. Yamamoto, M.T., *Drosophila Genetic Resource and Stock Center; The National BioResource Project*. Exp Anim, 2010. **59**(2): p. 125-38.

85. Sifers, R.N., et al., *Tissue specific expression of the human alpha-1-antitrypsin gene in transgenic mice*. Nucleic Acids Res, 1987. **15**(4): p. 1459-75.

86. Carlson, J.A., et al., *Accumulation of PiZ alpha 1-antitrypsin causes liver damage in transgenic mice*. J Clin Invest, 1989. **83**(4): p. 1183-90.

87. Weiner, W., *The Biology of the Laboratory Mouse*. Journal of Clinical Pathology, 1957. **10**(3): p. 288-288.

88. Giovannoni, I., et al., *Alpha-1-antitrypsin deficiency: from genoma to liver disease. PiZ mouse as model for the development of liver pathology in human*. Liver International, 2015. **35**(1): p. 198-206.

89. Rudnick, D.A., et al., *Analyses of hepatocellular proliferation in a mouse model of alpha-1-antitrypsin deficiency*. Hepatology, 2004. **39**(4): p. 1048-55.

90. An, J.K., et al., *Quantitative isolation of alpha1AT mutant Z protein polymers from human and mouse livers and the effect of heat*. Hepatology, 2005. **41**(1): p. 160-7.

91. Hidvegi, T., et al., *An autophagy-enhancing drug promotes degradation of mutant alpha1-antitrypsin Z and reduces hepatic fibrosis*. Science, 2010. **329**(5988): p. 229-32.

92. Mueller, C., et al., *Sustained miRNA-mediated knockdown of mutant AAT with simultaneous augmentation of wild-type AAT has minimal effect on global liver miRNA profiles*. Mol Ther, 2012. **20**(3): p. 590-600.

93. Barrangou, R., et al., *CRISPR provides acquired resistance against viruses in prokaryotes*. Science, 2007. **315**(5819): p. 1709-12.

94. Borel, F., et al., *Editing out five Serpina1 paralogs to create a mouse model of genetic emphysema*. Proc Natl Acad Sci U S A, 2018. **115**(11): p. 2788-2793.

95. Sun, X., et al., *Disease phenotype of a ferret CFTR-knockout model of cystic fibrosis*. J Clin Invest, 2010. **120**(9): p. 3149-60.

96. Brenner, S., *The genetics of Caenorhabditis elegans*. Genetics, 1974. **77**(1): p. 71-94.

97. Sulston, J.E. and H.R. Horvitz, *Post-embryonic cell lineages of the nematode, Caenorhabditis elegans*. Dev Biol, 1977. **56**(1): p. 110-56.

98. White, J.G., et al., *The structure of the nervous system of the nematode Caenorhabditis elegans*. Philos Trans R Soc Lond B Biol Sci, 1986. **314**(1165): p. 1-340.

99. National Research Council (US) Committee on Developmental Toxicology, *Scientific Frontiers in Developmental Toxicology and Risk Assessment*. 2000, Washinton, USA: National Academies Press (US).

100. Ruvkun, G. and O. Hobert, *The Taxonomy of Developmental Control in Caenorhabditis elegans*. Science, 1998. **282**(5396): p. 2033-2041.

101. Corsi, A., B. Wightman, and M. Chalfie, *A Transparent window into biology: A primer on Caenorhabditis elegans*, in *WormBook: The Online Review of C. elegans Biology*, WormBook: Pasadena (CA).

102. Hulme, S.E. and G.M. Whitesides, *Chemistry and the worm: Caenorhabditis elegans as a platform for integrating chemical and biological research*. Angew Chem Int Ed Engl, 2011. **50**(21): p. 4774-807.

103. Culetto, E. and D.B. Sattelle, *A role for Caenorhabditis elegans in understanding the function and interactions of human disease genes*. Hum Mol Genet, 2000. **9**(6): p. 869-77.

104. Burns, A.R., et al., *A predictive model for drug bioaccumulation and bioactivity in Caenorhabditis elegans*. Nat Chem Biol, 2010. **6**(7): p. 549-57.

105. Partridge, F.A., et al., *The C. elegans glycosyltransferase BUS-8 has two distinct and essential roles in epidermal morphogenesis*. Dev Biol, 2008. **317**(2): p. 549-59.

106. Voisine, C., J.S. Pedersen, and R.I. Morimoto, *Chaperone networks: tipping the balance in protein folding diseases*. Neurobiol Dis, 2010. **40**(1): p. 12-20.

107. Schipanski, A., et al., *A novel interaction between aging and ER overload in a protein conformational dementia*. Genetics, 2013. **193**(3): p. 865-76.

108. Silverman, R.M., et al., *The aggregation-prone intracellular serpin SRP-2 fails to transit the ER in Caenorhabditis elegans*. Genetics, 2015. **200**(1): p. 207-19.

109. Long, O.S., et al., *A C. elegans model of human  $\alpha$ 1-antitrypsin deficiency links components of the RNAi pathway to misfolded protein turnover*. Human Molecular Genetics, 2014. **23**(19): p. 5109-5122.

110. Gosai, S.J., et al., *Automated high-content live animal drug screening using C. elegans expressing the aggregation prone serpin alpha1-antitrypsin Z*. PLoS One, 2010. **5**(11): p. e15460.

111. O'Reilly, L.P., et al., *A genome-wide RNAi screen identifies potential drug targets in a C. elegans model of alpha1-antitrypsin deficiency*. Hum Mol Genet, 2014. **23**(19): p. 5123-32.

112. Li, J., et al., *Fluphenazine reduces proteotoxicity in C. elegans and mammalian models of alpha-1-antitrypsin deficiency*. PLoS One, 2014. **9**(1): p. e87260.

113. O'Reilly, L.P., et al., *Worming our way to novel drug discovery with the Caenorhabditis elegans proteostasis network, stress response and insulin-signaling pathways*. Expert Opin Drug Discov, 2014. **9**(9): p. 1021-32.

114. Murphy, C.T. and P.J. Hu, *Insulin/insulin-like growth factor signaling in C. elegans*. 2005, WormBook: The Online Review of C. elegans Biology [Internet]: WormBook.

115. Cummings, E.E., et al., *Deficient and Null Variants of SERPINA1 Are Proteotoxic in a Caenorhabditis elegans Model of alpha1-Antitrypsin Deficiency*. PLoS One, 2015. **10**(10): p. e0141542.

116. Mallya, M., et al., *Small molecules block the polymerization of Z alpha1-antitrypsin and increase the clearance of intracellular aggregates*. J Med Chem, 2007. **50**(22): p. 5357-63.

117. Alam, S., et al., *Preventing and reversing the cellular consequences of Z alpha-1 antitrypsin accumulation by targeting s4A*. J Hepatol, 2012. **57**(1): p. 116-24.

118. Engin, F. and G.S. Hotamisligil, *Restoring endoplasmic reticulum function by chemical chaperones: an emerging therapeutic approach for metabolic diseases*. Diabetes Obes Metab, 2010. **12 Suppl 2**: p. 108-15.

119. Burrows, J.A., L.K. Willis, and D.H. Perlmutter, *Chemical chaperones mediate increased secretion of mutant alpha 1-antitrypsin (alpha 1-AT) Z: A potential pharmacological strategy for prevention of liver injury and emphysema in alpha 1-AT deficiency*. Proc Natl Acad Sci U S A, 2000. **97**(4): p. 1796-801.

120. Teckman, J.H., *Lack of effect of oral 4-phenylbutyrate on serum alpha-1-antitrypsin in patients with alpha-1-antitrypsin deficiency: a preliminary study*. J Pediatr Gastroenterol Nutr, 2004. **39**(1): p. 34-7.

121. Bouchecareilh, M., et al., *Histone deacetylase inhibitor (HDACi) suberoylanilide hydroxamic acid (SAHA)-mediated correction of alpha1-antitrypsin deficiency*. J Biol Chem, 2012. **287**(45): p. 38265-78.

122. Kaushal, S., et al., *Rapamycin reduces intrahepatic alpha-1-antitrypsin mutant Z protein polymers and liver injury in a mouse model*. Exp Biol Med (Maywood), 2010. **235**(6): p. 700-9.

123. Mahadeva, R., et al., *6-mer peptide selectively anneals to a pathogenic serpin conformation and blocks polymerization. Implications for the prevention of Z alpha(1)-antitrypsin-related cirrhosis*. J Biol Chem, 2002. **277**(9): p. 6771-4.

124. Tafaleng, E.N., et al., *Induced pluripotent stem cells model personalized variations in liver disease resulting from alpha1-antitrypsin deficiency*. Hepatology, 2015. **62**(1): p. 147-57.

125. Guo, S., et al., *Antisense oligonucleotide treatment ameliorates alpha-1 antitrypsin-related liver disease in mice*. J Clin Invest, 2014. **124**(1): p. 251-61.

126. Hazari, Y.M., et al., *Alpha-1-antitrypsin deficiency: Genetic variations, clinical manifestations and therapeutic interventions*. Mutat Res, 2017. **773**: p. 14-25.

127. Li, C., et al., *Combination therapy utilizing shRNA knockdown and an optimized resistant transgene for rescue of diseases caused by misfolded proteins*. Proc Natl Acad Sci U S A, 2011. **108**(34): p. 14258-63.

128. Flotte, T.R., et al., *Phase 2 clinical trial of a recombinant adeno-associated viral vector expressing alpha1-antitrypsin: interim results*. Hum Gene Ther, 2011. **22**(10): p. 1239-47.

129. Song, C.Q., et al., *In Vivo Genome Editing Partially Restores Alpha1-Antitrypsin in a Murine Model of AAT Deficiency*. Hum Gene Ther, 2018. **29**(8): p. 853-860.

130. Shen, S., et al., *Amelioration of Alpha-1 Antitrypsin Deficiency Diseases with Genome Editing in Transgenic Mice*. Hum Gene Ther, 2018. **29**(8): p. 861-873.

131. Bjursell, M., et al., *Therapeutic Genome Editing With CRISPR/Cas9 in a Humanized Mouse Model Ameliorates alpha1-antitrypsin Deficiency Phenotype*. EBioMedicine, 2018. **29**: p. 104-111.

132. Roy, B., et al., *CRISPR/Cascade 9-Mediated Genome Editing-Challenges and Opportunities*. Front Genet, 2018. **9**: p. 240.

133. Ding, J., et al., *Spontaneous hepatic repopulation in transgenic mice expressing mutant human alpha1-antitrypsin by wild-type donor hepatocytes*. J Clin Invest, 2011. **121**(5): p. 1930-4.

134. Stiernagle, T., *C. elegans: A Practical Approach*. The C. elegans Research Community ed. 2006: WormBook.

135. Simmer, F., et al., *Loss of the putative RNA-directed RNA polymerase RRF-3 makes C. elegans hypersensitive to RNAi*. Curr Biol, 2002. **12**(15): p. 1317-9.

136. Strange, K., *Drug Discovery in Fish, Flies, and Worms*. Ilar J, 2016. **57**(2): p. 133-143.

137. Croston, G.E., *The utility of target-based discovery*. Expert Opinion on Drug Discovery, 2017. **12**(5): p. 427-429.

138. Zheng, W., N. Thorne, and J.C. McKew, *Phenotypic screens as a renewed approach for drug discovery*. Drug Discov Today, 2013. **18**(21-22): p. 1067-73.

139. Swinney, D.C. and J. Anthony, *How were new medicines discovered?* Nat Rev Drug Discov, 2011. **10**(7): p. 507-19.

140. Borsari, C., et al., *Target-based approaches for the discovery of new antimycobacterial drugs*. Drug Discovery Today, 2017. **22**(3): p. 576-584.

141. Lechartier, B., et al., *Tuberculosis drug discovery in the post-post-genomic era*. EMBO Mol Med, 2014. **6**(2): p. 158-68.

142. Gawad, J. and C. Bonde, *Decaprenyl-phosphoryl-ribose 2'-epimerase (DprE1): challenging target for antitubercular drug discovery*. Chem Cent J, 2018. **12**(1): p. 72.

143. Vanover, K.E., et al., *Pharmacological and behavioral profile of N-(4-fluorophenylmethyl)-N-(1-methylpiperidin-4-yl)-N'-(4-(2-methylpropyloxy)phenylmethyl) carbamide (2R,3R)-dihydroxybutanedioate (2:1) (ACP-103), a novel 5-hydroxytryptamine(2A) receptor inverse agonist*. J Pharmacol Exp Ther, 2006. **317**(2): p. 910-8.

144. Weiner, D.M., et al., *5-hydroxytryptamine2A receptor inverse agonists as antipsychotics*. J Pharmacol Exp Ther, 2001. **299**(1): p. 268-76.

145. Gao, M., et al., *Chemical genetics strategy identifies an HCV NS5A inhibitor with a potent clinical effect*. Nature, 2010. **465**(7294): p. 96-100.

146. Nutescu, E.A. and N.L. Shapiro, *Ezetimibe: a selective cholesterol absorption inhibitor*. Pharmacotherapy, 2003. **23**(11): p. 1463-74.

147. Altmann, S.W., et al., *Niemann-Pick C1 Like 1 protein is critical for intestinal cholesterol absorption*. Science, 2004. **303**(5661): p. 1201-4.

148. Moffat, J.G., et al., *Opportunities and challenges in phenotypic drug discovery: an industry perspective*. Nat Rev Drug Discov, 2017. **16**(8): p. 531-543.

149. Burns, A.R., et al., *Caenorhabditis elegans is a useful model for antihelminthic discovery*. Nat Commun, 2015. **6**: p. 7485.

150. Tritten, L., A. Silbereisen, and J. Keiser, *In vitro and in vivo efficacy of Monepantel (AAD 1566) against laboratory models of human intestinal nematode infections*. PLoS Negl Trop Dis, 2011. **5**(12): p. e1457.

151. Tritten, L., O. Braissant, and J. Keiser, *Comparison of novel and existing tools for studying drug sensitivity against the hookworm Ancylostoma ceylanicum in vitro*. Parasitology, 2012. **139**(3): p. 348-57.

152. Buckingham, S.D., F.A. Partridge, and D.B. Sattelle, *Automated, high-throughput, motility analysis in Caenorhabditis elegans and parasitic nematodes: Applications in the search for new antihelmintics*. Int J Parasitol Drugs Drug Resist, 2014. **4**(3): p. 226-32.

153. Ahringer, J., *Turn to the worm!* Curr Opin Genet Dev, 1997. **7**(3): p. 410-5.

154. Nutting, C.S., et al., *Analysis of nematode motion using an improved light-scatter based system*. PLoS Negl Trop Dis, 2015. **9**(2): p. e0003523.

155. Silbereisen, A., L. Tritten, and J. Keiser, *Exploration of novel in vitro assays to study drugs against Trichuris spp*. J Microbiol Methods, 2011. **87**(2): p. 169-75.

156. Smout, M.J., et al., *A novel high throughput assay for antihelminthic drug screening and resistance diagnosis by real-time monitoring of parasite motility*. PLoS Negl Trop Dis, 2010. **4**(11): p. e885.

157. Wangchuk, P., et al., *Identification of lead chemotherapeutic agents from medicinal plants against blood flukes and whipworms*. Sci Rep, 2016. **6**: p. 32101.

158. Wangchuk, P., et al., *Compounds Derived from the Bhutanese Daisy, Ajania nubigena, Demonstrate Dual Anthelmintic Activity against Schistosoma mansoni and Trichuris muris*. PLoS Negl Trop Dis, 2016. **10**(8): p. e0004908.

159. Buckingham, S.D. and D.B. Sattelle, *Strategies for automated analysis of C. elegans locomotion*. Invert Neurosci, 2008. **8**(3): p. 121-31.

160. Buckingham, S.D. and D.B. Sattelle, *Fast, automated measurement of nematode swimming (thrashing) without morphometry*. BMC Neurosci, 2009. **10**: p. 84.

161. Marcellino, C., et al., *WormAssay: a novel computer application for whole-plate motion-based screening of macroscopic parasites*. PLoS Negl Trop Dis, 2012. **6**(1): p. e1494.
162. Storey, B., et al., *Utilization of computer processed high definition video imaging for measuring motility of microscopic nematode stages on a quantitative scale: "The Worminator"*. Int J Parasitol Drugs Drug Resist, 2014. **4**(3): p. 233-43.
163. Preston, S., et al., *Practical and low cost whole-organism motility assay: A step-by-step protocol*. Mol Cell Probes, 2016. **30**(1): p. 13-7.
164. Preston, S., et al., *Low cost whole-organism screening of compounds for anthelmintic activity*. Int J Parasitol, 2015. **45**(5): p. 333-43.
165. Preston, S., et al., *Screening of the 'Pathogen Box' identifies an approved pesticide with major anthelmintic activity against the barber's pole worm*. Int J Parasitol Drugs Drug Resist, 2016. **6**(3): p. 329-334.
166. Mathew, M.D., N.D. Mathew, and P.R. Ebert, *WormScan: a technique for high-throughput phenotypic analysis of *Caenorhabditis elegans**. PLoS One, 2012. **7**(3): p. e33483.
167. Mathew, M.D., et al., *Using *C. elegans* Forward and Reverse Genetics to Identify New Compounds with Anthelmintic Activity*. PLoS Negl Trop Dis, 2016. **10**(10): p. e0005058.
168. Partridge, F.A., et al., *An automated high-throughput system for phenotypic screening of chemical libraries on *C. elegans* and parasitic nematodes*. Int J Parasitol Drugs Drug Resist, 2018. **8**(1): p. 8-21.
169. Edelstein, A.D., et al., *Advanced methods of microscope control using muManager software*. J Biol Methods, 2014. **1**(2).
170. Malo, N., et al., *Statistical practice in high-throughput screening data analysis*. Nat Biotechnol, 2006. **24**(2): p. 167-75.
171. Martin, R.J., *gamma-Aminobutyric acid- and piperazine-activated single-channel currents from *Ascaris suum* body muscle*. Br J Pharmacol, 1985. **84**(2): p. 445-61.
172. Maizels, R.M. and D.A. Denham, *Diethylcarbamazine (DEC): immunopharmacological interactions of an anti-filarial drug*. Parasitology, 1992. **105 Suppl**: p. S49-60.
173. Martin, R.J., A.P. Robertson, and H. Bjorn, *Target sites of anthelmintics*. Parasitology, 1997. **114 Suppl**: p. S111-24.
174. Driscoll, M., et al., *Genetic and molecular analysis of a *Caenorhabditis elegans* beta-tubulin that conveys benzimidazole sensitivity*. J Cell Biol, 1989. **109**(6 Pt 1): p. 2993-3003.
175. Cully, D.F., et al., *Cloning of an avermectin-sensitive glutamate-gated chloride channel from *Caenorhabditis elegans**. Nature, 1994. **371**(6499): p. 707-11.
176. Caffrey, C.R., *Chemotherapy of schistosomiasis: present and future*. Curr Opin Chem Biol, 2007. **11**(4): p. 433-9.
177. Ritz, C. and J.C. Streibig, *Bioassay Analysis Using R*. 2005, 2005. **12**(5): p. 22.
178. Holden-Dye, L. and R.J. Walker, *Anthelmintic drugs*. WormBook, 2007: p. 1-13.
179. Kuntz, A.N., et al., *Thioredoxin glutathione reductase from *Schistosoma mansoni*: an essential parasite enzyme and a key drug target*. PLoS Med, 2007. **4**(6): p. e206.

180. Debnath, A., et al., *A high-throughput drug screen for *Entamoeba histolytica* identifies a new lead and target*. *Nat Med*, 2012. **18**(6): p. 956-60.

181. Sharlow, E.R., et al., *Auranofin is an apoptosis-simulating agent with in vitro and in vivo anti-leishmanial activity*. *ACS Chem Biol*, 2014. **9**(3): p. 663-72.

182. Bulman, C.A., et al., *Repurposing auranofin as a lead candidate for treatment of lymphatic filariasis and onchocerciasis*. *PLoS Negl Trop Dis*, 2015. **9**(2): p. e0003534.

183. Kwok, T.C., et al., *A small-molecule screen in *C. elegans* yields a new calcium channel antagonist*. *Nature*, 2006. **441**(7089): p. 91-5.

184. Satyendra, R.V., et al., *Synthesis, in vitro antioxidant, antihelmintic and molecular docking studies of novel dichloro substituted benzoxazole-triazolo-thione derivatives*. *Eur J Med Chem*, 2011. **46**(7): p. 3078-84.

185. da Silva-Alves, D.C., et al., *Larvicalid isoxazoles: Synthesis and their effective susceptibility towards *Aedes aegypti* larvae*. *Bioorg Med Chem*, 2013. **21**(4): p. 940-7.

186. Tatipaka, H.B., et al., *Substituted 2-phenylimidazopyridines: a new class of drug leads for human African trypanosomiasis*. *J Med Chem*, 2014. **57**(3): p. 828-35.

187. Nare, B., et al., *Discovery of novel orally bioavailable oxaborole 6-carboxamides that demonstrate cure in a murine model of late-stage central nervous system african trypanosomiasis*. *Antimicrob Agents Chemother*, 2010. **54**(10): p. 4379-88.

188. Jacobs, R.T., et al., *SCYX-7158, an orally-active benzoxaborole for the treatment of stage 2 human African trypanosomiasis*. *PLoS Negl Trop Dis*, 2011. **5**(6): p. e1151.

189. Jones, D.C., et al., *Genomic and Proteomic Studies on the Mode of Action of Oxaboroles against the African Trypanosome*. *PLoS Negl Trop Dis*, 2015. **9**(12): p. e0004299.

190. Elewski, B.E., et al., *Efficacy and safety of tavaborole topical solution, 5%, a novel boron-based antifungal agent, for the treatment of toenail onychomycosis: Results from 2 randomized phase-III studies*. *J Am Acad Dermatol*, 2015. **73**(1): p. 62-9.

191. Rock, F.L., et al., *An antifungal agent inhibits an aminoacyl-tRNA synthetase by trapping tRNA in the editing site*. *Science*, 2007. **316**(5832): p. 1759-61.

192. Akama, T.J., Kurt; Plattner, Jacob J.; Pulley, Shon Roland; White, William Hunter; Zhang, Yong-Kang; Zhou, Yasheen; *1-hydroxy-benzooxaboroles as Antiparasitic Agents*. 2014.

193. Zhang, Y.-k., et al., *Boron-containing Small Molecules as Antihelminth Agents*. . 2011.

194. Palencia, A., et al., *Cryptosporidium and Toxoplasma Parasites Are Inhibited by a Benzoxaborole Targeting Leucyl-tRNA Synthetase*. *Antimicrob Agents Chemother*, 2016. **60**(10): p. 5817-27.

195. Palencia, A., et al., *Discovery of Novel Oral Protein Synthesis Inhibitors of *Mycobacterium tuberculosis* That Target Leucyl-tRNA Synthetase*. *Antimicrob Agents Chemother*, 2016. **60**(10): p. 6271-80.

196. Sonoiki, E., et al., *Antimalarial Benzoxaboroles Target *Plasmodium falciparum* Leucyl-tRNA Synthetase*. *Antimicrob Agents Chemother*, 2016. **60**(8): p. 4886-95.

197. Zheng, W., W. Sun, and A. Simeonov, *Drug repurposing screens and synergistic drug-combinations for infectious diseases*. *Br J Pharmacol*, 2018. **175**(2): p. 181-191.

198. Pollastri, M.P. and R.K. Campbell, *Target repurposing for neglected diseases*. *Future Med Chem*, 2011. **3**(10): p. 1307-15.

199. Liu, C.T., J.W. Tomsho, and S.J. Benkovic, *The unique chemistry of benzoxaboroles: current and emerging applications in biotechnology and therapeutic treatments*. Bioorg Med Chem, 2014. **22**(16): p. 4462-73.

200. Nwaka, S., et al., *Advancing drug innovation for neglected diseases-criteria for lead progression*. PLoS Negl Trop Dis, 2009. **3**(8): p. e440.

201. Hotez, P., *Forgotten People, Forgotten Diseases: the Neglected Tropical Diseases and Their Impact on Global Health and Development*. Second ed. ed. 2013, Washington, DC: ASM Press.

202. Sales, N. and S. Love, *Resistance of Haemonchus sp. to monepantel and reduced efficacy of a derquantel / abamectin combination confirmed in sheep in NSW, Australia*. Vet Parasitol, 2016. **228**: p. 193-196.

203. Kaletta, T. and M.O. Hengartner, *Finding function in novel targets: C. elegans as a model organism*. Nat Rev Drug Discov, 2006. **5**(5): p. 387-98.

204. Mello, C. and A. Fire, *DNA transformation*. Methods Cell Biol, 1995. **48**: p. 451-82.

205. Mello, C.C., et al., *Efficient gene transfer in C.elegans: extrachromosomal maintenance and integration of transforming sequences*. Embo j, 1991. **10**(12): p. 3959-70.

206. Praitis, V., et al., *Creation of low-copy integrated transgenic lines in Caenorhabditis elegans*. Genetics, 2001. **157**(3): p. 1217-26.

207. Frokjaer-Jensen, C., et al., *Single-copy insertion of transgenes in Caenorhabditis elegans*. Nat Genet, 2008. **40**(11): p. 1375-83.

208. Yoshina, S., et al., *Locus-specific integration of extrachromosomal transgenes in C. elegans with the CRISPR/Cas9 system*. Biochem Biophys Rep, 2016. **5**: p. 70-76.

209. Evans, T.C., *Transformation and microinjection*. 2006: WormBook, ed. The C. elegans Research Community, WormBook.

210. Nagarajan, A., et al., *A Fluorescence Resonance Energy Transfer Assay For Monitoring alpha-Synuclein Aggregation in a Caenorhabditis Elegans Model For Parkinson's Disease*. CNS Neurol Disord Drug Targets, 2015. **14**(8): p. 1054-68.

211. Siddiqui, S.S., et al., *C. elegans as a model organism for in vivo screening in cancer: effects of human c-Met in lung cancer affect C. elegans vulva phenotypes*. Cancer Biol Ther, 2008. **7**(6): p. 856-63.

212. Dosanjh, L.E., et al., *Behavioral phenotyping of a transgenic Caenorhabditis elegans expressing neuronal amyloid-beta*. J Alzheimers Dis, 2010. **19**(2): p. 681-90.

213. Wahlby, C., et al., *An image analysis toolbox for high-throughput C. elegans assays*. Nat Methods, 2012. **9**(7): p. 714-6.

214. Lui, J.H., D.V. Hansen, and A.R. Kriegstein, *Development and evolution of the human neocortex*. Cell, 2011. **146**(1): p. 18-36.

215. Farias, G., et al., *Mechanisms of tau self-aggregation and neurotoxicity*. Curr Alzheimer Res, 2011. **8**(6): p. 608-14.

216. Lublin, A.L. and S. Gandy, *Amyloid-beta oligomers: possible roles as key neurotoxins in Alzheimer's Disease*. Mt Sinai J Med, 2010. **77**(1): p. 43-9.

217. Kraemer, B.C., et al., *Neurodegeneration and defective neurotransmission in a Caenorhabditis elegans model of tauopathy*. Proc Natl Acad Sci U S A, 2003. **100**(17): p. 9980-5.

218. McCormick, A.V., et al., *Dopamine D2 receptor antagonism suppresses tau aggregation and neurotoxicity*. *Biol Psychiatry*, 2013. **73**(5): p. 464-71.

219. Lublin, A.L. and C.D. Link, *Alzheimer's disease drug discovery: in vivo screening using *Caenorhabditis elegans* as a model for beta-amyloid peptide-induced toxicity*. *Drug Discov Today Technol*, 2013. **10**(1): p. e115-9.

220. Link, C.D., *Expression of human beta-amyloid peptide in transgenic *Caenorhabditis elegans**. *Proc Natl Acad Sci U S A*, 1995. **92**(20): p. 9368-72.

221. Fay, D.S., et al., *In vivo aggregation of beta-amyloid peptide variants*. *J Neurochem*, 1998. **71**(4): p. 1616-25.

222. Link, C.D., et al., *Gene expression analysis in a transgenic *Caenorhabditis elegans* Alzheimer's disease model*. *Neurobiol Aging*, 2003. **24**(3): p. 397-413.

223. Wu, Y., et al., *Amyloid-beta-induced pathological behaviors are suppressed by *Ginkgo biloba* extract EGb 761 and ginkgolides in transgenic *Caenorhabditis elegans**. *J Neurosci*, 2006. **26**(50): p. 13102-13.

224. Treusch, S., et al., *Functional links between Abeta toxicity, endocytic trafficking, and Alzheimer's disease risk factors in yeast*. *Science*, 2011. **334**(6060): p. 1241-5.

225. Lublin, A., et al., *FDA-approved drugs that protect mammalian neurons from glucose toxicity slow aging dependent on cbp and protect against proteotoxicity*. *PLoS One*, 2011. **6**(11): p. e27762.

226. Spillantini, M.G. and M. Goedert, *The alpha-synucleinopathies: Parkinson's disease, dementia with Lewy bodies, and multiple system atrophy*. *Ann N Y Acad Sci*, 2000. **920**: p. 16-27.

227. van Ham, T.J., et al., *C. elegans model identifies genetic modifiers of alpha-synuclein inclusion formation during aging*. *PLoS Genet*, 2008. **4**(3): p. e1000027.

228. Hamamichi, S., et al., *Hypothesis-based RNAi screening identifies neuroprotective genes in a Parkinson's disease model*. *Proc Natl Acad Sci U S A*, 2008. **105**(2): p. 728-33.

229. Oeda, T., et al., *Oxidative stress causes abnormal accumulation of familial amyotrophic lateral sclerosis-related mutant SOD1 in transgenic *Caenorhabditis elegans**. *Hum Mol Genet*, 2001. **10**(19): p. 2013-23.

230. Wang, J., et al., *An ALS-linked mutant SOD1 produces a locomotor defect associated with aggregation and synaptic dysfunction when expressed in neurons of *Caenorhabditis elegans**. *PLoS Genet*, 2009. **5**(1): p. e1000350.

231. Neumann, M., et al., *Ubiquitinated TDP-43 in frontotemporal lobar degeneration and amyotrophic lateral sclerosis*. *Science*, 2006. **314**(5796): p. 130-3.

232. Grice, S.J., et al., *Invertebrate models of spinal muscular atrophy: insights into mechanisms and potential therapeutics*. *Bioessays*, 2011. **33**(12): p. 956-65.

233. Joyce, P.I., et al., *SOD1 and TDP-43 animal models of amyotrophic lateral sclerosis: recent advances in understanding disease toward the development of clinical treatments*. *Mamm Genome*, 2011. **22**(7-8): p. 420-48.

234. Sleigh, J.N., et al., *A novel *Caenorhabditis elegans* allele, smn-1(cb131), mimicking a mild form of spinal muscular atrophy, provides a convenient drug screening platform highlighting new and pre-approved compounds*. *Hum Mol Genet*, 2011. **20**(2): p. 245-60.

235. O'Reilly, L.P., et al., *C. elegans in high-throughput drug discovery*. *Adv Drug Deliv Rev*, 2014. **69-70**: p. 247-53.

236. Giacometto, J. and L. Segalat, *High-throughput screening and small animal models, where are we?* *Br J Pharmacol*, 2010. **160**(2): p. 204-16.

237. Miranda, E., et al., *A novel monoclonal antibody to characterize pathogenic polymers in liver disease associated with alpha1-antitrypsin deficiency*. *Hepatology*, 2010. **52**(3): p. 1078-88.

238. Qu, D., et al., *Degradation of a mutant secretory protein, alpha1-antitrypsin Z, in the endoplasmic reticulum requires proteasome activity*. *J Biol Chem*, 1996. **271**(37): p. 22791-5.

239. Kamimoto, T., et al., *Intracellular inclusions containing mutant alpha1-antitrypsin Z are propagated in the absence of autophagic activity*. *J Biol Chem*, 2006. **281**(7): p. 4467-76.

240. Sveger, T., *Prospective study of children with alpha 1-antitrypsin deficiency: eight-year-old follow-up*. *J Pediatr*, 1984. **104**(1): p. 91-4.

241. Primhak, R. and M. Tanner, *Alpha-1 antitrypsin deficiency*. *Archives of Disease in Childhood*, 2001. **85**(1): p. 2-5.

242. Zhang, J.H., T.D. Chung, and K.R. Oldenburg, *A Simple Statistical Parameter for Use in Evaluation and Validation of High Throughput Screening Assays*. *J Biomol Screen*, 1999. **4**(2): p. 67-73.

243. Gravato-Nobre, M.J., et al., *Multiple genes affect sensitivity of *Caenorhabditis elegans* to the bacterial pathogen *Microbacterium nematophilum**. *Genetics*, 2005. **171**(3): p. 1033-45.

244. Jones, A.K., et al., *A Cys-loop mutation in the *Caenorhabditis elegans* nicotinic receptor subunit UNC-63 impairs but does not abolish channel function*. *J Biol Chem*, 2011. **286**(4): p. 2550-8.

245. Engel, A.G. and S.M. Sine, *Current understanding of congenital myasthenic syndromes*. *Curr Opin Pharmacol*, 2005. **5**(3): p. 308-21.

246. Lehner, B., J. Tischler, and A.G. Fraser, *RNAi screens in *Caenorhabditis elegans* in a 96-well liquid format and their application to the systematic identification of genetic interactions*. *Nat Protoc*, 2006. **1**(3): p. 1617-20.

247. Petrascheck, M., X. Ye, and L.B. Buck, *An antidepressant that extends lifespan in adult *Caenorhabditis elegans**. *Nature*, 2007. **450**(7169): p. 553-6.

248. Petrascheck, M., X. Ye, and L.B. Buck, *A high-throughput screen for chemicals that increase the lifespan of *Caenorhabditis elegans**. *Ann N Y Acad Sci*, 2009. **1170**: p. 698-701.

249. Cooper, J.F. and J.M. Van Raamsdonk, *Modeling Parkinson's Disease in *C. elegans**. *J Parkinsons Dis*, 2018. **8**(1): p. 17-32.

250. Braungart, E., et al., *Caenorhabditis elegans MPP+ model of Parkinson's disease for high-throughput drug screenings*. *Neurodegener Dis*, 2004. **1**(4-5): p. 175-83.

251. Marvanova, M. and C.D. Nichols, *Identification of neuroprotective compounds of *caenorhabditis elegans* dopaminergic neurons against 6-OHDA*. *J Mol Neurosci*, 2007. **31**(2): p. 127-37.

252. Artal-Sanz, M., L. de Jong, and N. Tavernarakis, *Caenorhabditis elegans: a versatile platform for drug discovery*. *Biotechnol J*, 2006. **1**(12): p. 1405-18.

253. Jones, A.K., S.D. Buckingham, and D.B. Sattelle, *Chemistry-to-gene screens in Caenorhabditis elegans*. *Nat Rev Drug Discov*, 2005. **4**(4): p. 321-30.

254. Wang, G. and V. Reinke, *A C. elegans Piwi, PRG-1, regulates 21U-RNAs during spermatogenesis*. *Curr Biol*, 2008. **18**(12): p. 861-7.

255. Gent, J.I., et al., *A Caenorhabditis elegans RNA-directed RNA polymerase in sperm development and endogenous RNA interference*. *Genetics*, 2009. **183**(4): p. 1297-314.

256. Aitlhadj, L. and S.R. Sturzenbaum, *The use of FUdR can cause prolonged longevity in mutant nematodes*. *Mech Ageing Dev*, 2010. **131**(5): p. 364-5.

257. Angeli, S., et al., *A DNA synthesis inhibitor is protective against proteotoxic stressors via modulation of fertility pathways in Caenorhabditis elegans*. *Aging (Albany NY)*, 2013. **5**(10): p. 759-69.

258. Schwendeman, A.R. and S. Shaham, *A High-Throughput Small Molecule Screen for C. elegans Linker Cell Death Inhibitors*. *PLoS One*, 2016. **11**(10): p. e0164595.

259. Leung, C.K., et al., *An ultra high-throughput, whole-animal screen for small molecule modulators of a specific genetic pathway in Caenorhabditis elegans*. *PLoS One*, 2013. **8**(4): p. e62166.

260. Bae, Y.K., et al., *An in vivo C. elegans model system for screening EGFR-inhibiting anti-cancer drugs*. *PLoS One*, 2012. **7**(9): p. e42441.

261. Falchi, F., F. Caporuscio, and M. Recanatini, *Structure-based design of small-molecule protein-protein interaction modulators: the story so far*. *Future Med Chem*, 2014. **6**(3): p. 343-57.

262. Zheng, S.Q., et al., *Drug absorption efficiency in Caenorhabditis elegans delivered by different methods*. *PLoS One*, 2013. **8**(2): p. e56877.

263. Fire, A., et al., *Potent and specific genetic interference by double-stranded RNA in Caenorhabditis elegans*. *Nature*, 1998. **391**(6669): p. 806-11.

264. Tabara, H., A. Grishok, and C.C. Mello, *RNAi in C. elegans: soaking in the genome sequence*. *Science*, 1998. **282**(5388): p. 430-1.

265. Timmons, L. and A. Fire, *Specific interference by ingested dsRNA*. *Nature*, 1998. **395**(6705): p. 854.

266. *Genome sequence of the nematode C. elegans: a platform for investigating biology*. *Science*, 1998. **282**(5396): p. 2012-8.

267. Kamath, R.S. and J. Ahringer, *Genome-wide RNAi screening in Caenorhabditis elegans*. *Methods*, 2003. **30**(4): p. 313-21.

268. Bernstein, E., et al., *Role for a bidentate ribonuclease in the initiation step of RNA interference*. *Nature*, 2001. **409**(6818): p. 363-6.

269. Carthew, R.W. and E.J. Sontheimer, *Origins and Mechanisms of miRNAs and siRNAs*. *Cell*, 2009. **136**(4): p. 642-655.

270. Ahlquist, P., *RNA-dependent RNA polymerases, viruses, and RNA silencing*. *Science*, 2002. **296**(5571): p. 1270-3.

271. Daka, A. and D. Peer, *RNAi-based nanomedicines for targeted personalized therapy*. *Adv Drug Deliv Rev*, 2012. **64**(13): p. 1508-21.

272. Yang, W.Q. and Y. Zhang, *RNAi-mediated gene silencing in cancer therapy*. Expert Opin Biol Ther, 2012. **12**(11): p. 1495-504.

273. Seyhan, A.A., *RNAi: a potential new class of therapeutic for human genetic disease*. Hum Genet, 2011. **130**(5): p. 583-605.

274. Sijen, T., et al., *Secondary siRNAs result from unprimed RNA synthesis and form a distinct class*. Science, 2007. **315**(5809): p. 244-7.

275. Pak, J. and A. Fire, *Distinct populations of primary and secondary effectors during RNAi in C. elegans*. Science, 2007. **315**(5809): p. 241-4.

276. Zhang, C. and G. Ruvkun, *New insights into siRNA amplification and RNAi*. RNA Biology, 2012. **9**(8): p. 1045-1049.

277. Alcazar, R.M., R. Lin, and A.Z. Fire, *Transmission dynamics of heritable silencing induced by double-stranded RNA in Caenorhabditis elegans*. Genetics, 2008. **180**(3): p. 1275-88.

278. Gu, S.G., et al., *Amplification of siRNA in Caenorhabditis elegans generates a transgenerational sequence-targeted histone H3 lysine 9 methylation footprint*. Nat Genet, 2012. **44**(2): p. 157-64.

279. Feng, X. and S. Guang, *Small RNAs, RNAi and the inheritance of gene silencing in Caenorhabditis elegans*. J Genet Genomics, 2013. **40**(4): p. 153-60.

280. Rechavi, O. and I. Lev, *Principles of Transgenerational Small RNA Inheritance in Caenorhabditis elegans*. Curr Biol, 2017. **27**(14): p. R720-r730.

281. Houri-Ze'evi, L., et al., *A Tunable Mechanism Determines the Duration of the Transgenerational Small RNA Inheritance in C. elegans*. Cell, 2016. **165**(1): p. 88-99.

282. Winston, W.M., C. Molodowitch, and C.P. Hunter, *Systemic RNAi in C. elegans requires the putative transmembrane protein SID-1*. Science, 2002. **295**(5564): p. 2456-9.

283. Timmons, L., D.L. Court, and A. Fire, *Ingestion of bacterially expressed dsRNAs can produce specific and potent genetic interference in Caenorhabditis elegans*. Gene, 2001. **263**(1-2): p. 103-12.

284. Kennedy, S., D. Wang, and G. Ruvkun, *A conserved siRNA-degrading RNase negatively regulates RNA interference in C. elegans*. Nature, 2004. **427**(6975): p. 645-649.

285. Fraser, A.G., et al., *Functional genomic analysis of C. elegans chromosome I by systematic RNA interference*. Nature, 2000. **408**(6810): p. 325-30.

286. Gonczy, P., et al., *Functional genomic analysis of cell division in C. elegans using RNAi of genes on chromosome III*. Nature, 2000. **408**(6810): p. 331-6.

287. Maeda, I., et al., *Large-scale analysis of gene function in Caenorhabditis elegans by high-throughput RNAi*. Curr Biol, 2001. **11**(3): p. 171-6.

288. Piano, F., et al., *RNAi analysis of genes expressed in the ovary of Caenorhabditis elegans*. Curr Biol, 2000. **10**(24): p. 1619-22.

289. Kamath, R.S., et al., *Systematic functional analysis of the Caenorhabditis elegans genome using RNAi*. Nature, 2003. **421**(6920): p. 231-7.

290. Conrad, C. and D.W. Gerlich, *Automated microscopy for high-content RNAi screening*. J Cell Biol, 2010. **188**(4): p. 453-61.

291. Colaiacovo, M.P., et al., *A targeted RNAi screen for genes involved in chromosome morphogenesis and nuclear organization in the *Caenorhabditis elegans* germline*. *Genetics*, 2002. **162**(1): p. 113-28.

292. Khabirova, E., et al., *The TRiC/CCT chaperone is implicated in Alzheimer's disease based on patient GWAS and an RNAi screen in Abeta-expressing *Caenorhabditis elegans**. *PLoS One*, 2014. **9**(7): p. e102985.

293. Boutros, M. and J. Ahringer, *The art and design of genetic screens: RNA interference*. *Nat Rev Genet*, 2008. **9**(7): p. 554-66.

294. Rual, J.F., et al., *Toward improving *Caenorhabditis elegans* phenome mapping with an ORFeome-based RNAi library*. *Genome Res*, 2004. **14**(10b): p. 2162-8.

295. Ni, Z. and S.S. Lee, *RNAi screens to identify components of gene networks that modulate aging in *Caenorhabditis elegans**. *Brief Funct Genomics*, 2010. **9**(1): p. 53-64.

296. Prudencio, M. and M.J. Lehmann, *Illuminating the host - how RNAi screens shed light on host-pathogen interactions*. *Biotechnol J*, 2009. **4**(6): p. 826-37.

297. Nijwening, J.H. and R.L. Beijersbergen, *Using large-scale RNAi screens to identify novel drug targets for cancer*. *IDrugs*, 2010. **13**(11): p. 772-7.

298. Sin, O., H. Michels, and E.A. Nollen, *Genetic screens in *Caenorhabditis elegans* models for neurodegenerative diseases*. *Biochim Biophys Acta*, 2014. **1842**(10): p. 1951-1959.

299. Wang, D. and G. Ruvkun, *Regulation of *Caenorhabditis elegans* RNA interference by the daf-2 insulin stress and longevity signaling pathway*. *Cold Spring Harb Symp Quant Biol*, 2004. **69**: p. 429-31.

300. Duchaine, T.F., et al., *Functional proteomics reveals the biochemical niche of *C. elegans* DCR-1 in multiple small-RNA-mediated pathways*. *Cell*, 2006. **124**(2): p. 343-54.

301. Zhuang, J.J. and C.P. Hunter, *Tissue specificity of *Caenorhabditis elegans* enhanced RNA interference mutants*. *Genetics*, 2011. **188**(1): p. 235-7.

302. Del Rio-Albrechtsen, T., et al., *Novel gain-of-function alleles demonstrate a role for the heterochronic gene lin-41 in *C. elegans* male tail tip morphogenesis*. *Dev Biol*, 2006. **297**(1): p. 74-86.

303. Slack, F.J., et al., *The lin-41 RBCC gene acts in the *C. elegans* heterochronic pathway between the let-7 regulatory RNA and the LIN-29 transcription factor*. *Mol Cell*, 2000. **5**(4): p. 659-69.

304. Simmer, F., et al., *Genome-wide RNAi of *C. elegans* using the hypersensitive rrf-3 strain reveals novel gene functions*. *PLoS Biol*, 2003. **1**(1): p. E12.

305. Huang da, W., B.T. Sherman, and R.A. Lempicki, *Systematic and integrative analysis of large gene lists using DAVID bioinformatics resources*. *Nat Protoc*, 2009. **4**(1): p. 44-57.

306. Lee, R.Y.N., et al., *WormBase 2017: molting into a new stage*. *Nucleic Acids Res*, 2018. **46**(D1): p. D869-d874.

307. Angeles-Albores, D., et al., *Tissue enrichment analysis for *C. elegans* genomics*. 2016. **17**(1): p. 366.

308. Fujiwara, M., T. Ishihara, and I. Katsura, *Ligand-gated chloride channel is necessary for correct thermotaxis*, in *Worm Breeder's Gazette*. 1996. p. 1.

309. Meissner, B., et al., *Determining the sub-cellular localization of proteins within *Caenorhabditis elegans* body wall muscle*. *PLoS One*, 2011. **6**(5): p. e19937.

310. Salkoff, L., et al., *Evolution tunes the excitability of individual neurons*. Neuroscience, 2001. **103**(4): p. 853-9.

311. Fleming, J.T., et al., *Caenorhabditis elegans levamisole resistance genes lev-1, unc-29, and unc-38 encode functional nicotinic acetylcholine receptor subunits*. J Neurosci, 1997. **17**(15): p. 5843-57.

312. Mongan, N.P., et al., *Novel alpha7-like nicotinic acetylcholine receptor subunits in the nematode Caenorhabditis elegans*. Protein Sci, 2002. **11**(5): p. 1162-71.

313. Wenick, A.S. and O. Hobert, *Genomic cis-regulatory architecture and trans-acting regulators of a single interneuron-specific gene battery in C. elegans*. Dev Cell, 2004. **6**(6): p. 757-70.

314. Jones, A.K., et al., *The nicotinic acetylcholine receptor gene family of the nematode Caenorhabditis elegans: an update on nomenclature*. Invertebrate neuroscience : IN, 2007. **7**(2): p. 129-131.

315. Jones, A.K. and D.B. Sattelle, *The cys-loop ligand-gated ion channel gene superfamily of the nematode, Caenorhabditis elegans*. Invertebrate Neuroscience, 2008. **8**(1): p. 41-47.

316. Park, K.H., et al., *A family of K<sup>+</sup> channel ancillary subunits regulate taste sensitivity in Caenorhabditis elegans*. J Biol Chem, 2005. **280**(23): p. 21893-9.

317. Phelan, P. and T.A. Starich, *Innexins get into the gap*. Bioessays, 2001. **23**(5): p. 388-96.

318. Syntichaki, P., C. Samara, and N. Tavernarakis, *The vacuolar H<sup>+</sup>-ATPase mediates intracellular acidification required for neurodegeneration in C. elegans*. Curr Biol, 2005. **15**(13): p. 1249-54.

319. Inoue, T., et al., *Structure and regulation of the V-ATPases*. J Bioenerg Biomembr, 2005. **37**(6): p. 393-8.

320. Camon, E., et al., *The Gene Ontology Annotation (GOA) project: implementation of GO in SWISS-PROT, TrEMBL, and InterPro*. Genome Res, 2003. **13**(4): p. 662-72.

321. Schroeder, L.K., et al., *Function of the Caenorhabditis elegans ABC transporter PGP-2 in the biogenesis of a lysosome-related fat storage organelle*. Mol Biol Cell, 2007. **18**(3): p. 995-1008.

322. Tanji, T., et al., *Co-operative function and mutual stabilization of the half ATP-binding cassette transporters HAF-4 and HAF-9 in Caenorhabditis elegans*. Biochem J, 2013. **452**(3): p. 467-75.

323. Harteneck, C., T.D. Plant, and G. Schultz, *From worm to man: three subfamilies of TRP channels*. Trends Neurosci, 2000. **23**(4): p. 159-66.

324. West, R.J., et al., *The C. elegans gon-2 gene encodes a putative TRP cation channel protein required for mitotic cell cycle progression*. Gene, 2001. **266**(1-2): p. 103-10.

325. Wei, A.D., A. Butler, and L. Salkoff, *KCNQ-like potassium channels in Caenorhabditis elegans. Conserved properties and modulation*. J Biol Chem, 2005. **280**(22): p. 21337-45.

326. Sigurdson, D.C., G.J. Spanier, and R.K. Herman, *Caenorhabditis elegans deficiency mapping*. Genetics, 1984. **108**(2): p. 331-45.

327. Corey, D.P. and J. Garcia-Anoveros, *Mechanosensation and the DEG/ENaC ion channels*. Science, 1996. **273**(5273): p. 323-4.

328. Wang, R., et al., *The SOL-2/Neto auxiliary protein modulates the function of AMPA-subtype ionotropic glutamate receptors*. *Neuron*, 2012. **75**(5): p. 838-50.

329. Altun, Z.F., et al., *High resolution map of *Caenorhabditis elegans* gap junction proteins*. *Dev Dyn*, 2009. **238**(8): p. 1936-50.

330. Nollen, E.A., et al., *Genome-wide RNA interference screen identifies previously undescribed regulators of polyglutamine aggregation*. *Proc Natl Acad Sci U S A*, 2004. **101**(17): p. 6403-8.

331. Kraemer, B.C., et al., *Molecular pathways that influence human tau-induced pathology in *Caenorhabditis elegans**. *Hum Mol Genet*, 2006. **15**(9): p. 1483-96.

332. Doi, M. and K. Iwasaki, *Regulation of retrograde signaling at neuromuscular junctions by the novel C2 domain protein AEX-1*. *Neuron*, 2002. **33**(2): p. 249-59.

333. Thomas, J.H., *Genetic analysis of defecation in *Caenorhabditis elegans**. *Genetics*, 1990. **124**(4): p. 855-72.

334. Shaye, D.D. and I. Greenwald, *OrthoList: a compendium of *C. elegans* genes with human orthologs*. *PLoS One*, 2011. **6**(5): p. e20085.

335. Kuhn, M., et al., *STITCH: interaction networks of chemicals and proteins*. *Nucleic Acids Research*, 2008. **36**(Database issue): p. D684-D688.

336. Szklarczyk, D., et al., *STITCH 5: augmenting protein-chemical interaction networks with tissue and affinity data*. *Nucleic Acids Research*, 2016. **44**(Database issue): p. D380-D384.

337. Law, V., et al., *DrugBank 4.0: shedding new light on drug metabolism*. *Nucleic Acids Res*, 2014. **42**(Database issue): p. D1091-7.

338. Gunther, S., et al., *SuperTarget and Matador: resources for exploring drug-target relationships*. *Nucleic Acids Res*, 2008. **36**(Database issue): p. D919-22.

339. Kanehisa, M., et al., *Data, information, knowledge and principle: back to metabolism in KEGG*. *Nucleic Acids Res*, 2014. **42**(Database issue): p. D199-205.

340. Croft, D., et al., *The Reactome pathway knowledgebase*. *Nucleic Acids Res*, 2014. **42**(Database issue): p. D472-7.

341. O'Rourke, E.J., A.L. Conery, and T.I. Moy, *Whole-animal high-throughput screens: the *C. elegans* model*. *Methods Mol Biol*, 2009. **486**: p. 57-75.

342. Squiban, B., et al., *Quantitative and Automated High-throughput Genome-wide RNAi Screens in *C. elegans**. *Journal of Visualized Experiments : JoVE*, 2012(60): p. 3448.

343. Díaz-Villanueva, J.F., R. Díaz-Molina, and V. García-González, *Protein Folding and Mechanisms of Proteostasis*. *Int J Mol Sci*, 2015. **16**(8): p. 17193-230.

344. Bessou, C., et al., *Mutations in the *Caenorhabditis elegans* dystrophin-like gene dys-1 lead to hyperactivity and suggest a link with cholinergic transmission*. *Neurogenetics*, 1998. **2**(1): p. 61-72.

345. Guiraud, S., et al., *The Pathogenesis and Therapy of Muscular Dystrophies*. *Annu Rev Genomics Hum Genet*, 2015. **16**: p. 281-308.

346. Nonet, M.L., *AEXpulsing a retrograde signal*. *Neuron*, 2002. **33**(2): p. 155-6.

347. Kumar, K.K., et al., *Cellular manganese content is developmentally regulated in human dopaminergic neurons*. *Sci Rep*, 2014. **4**: p. 6801.

348. Perlmutter, D.H., *Alpha-1-antitrypsin deficiency: importance of proteasomal and autophagic degradative pathways in disposal of liver disease-associated protein aggregates*. Annu Rev Med, 2011. **62**: p. 333-45.

349. Denver, D.R., et al., *A genome-wide view of *Caenorhabditis elegans* base-substitution mutation processes*. Proc Natl Acad Sci U S A, 2009. **106**(38): p. 16310-4.

350. Denver, D.R., et al., *High mutation rate and predominance of insertions in the *Caenorhabditis elegans* nuclear genome*. Nature, 2004. **430**(7000): p. 679-82.

351. Lipinski, K.J., et al., *High spontaneous rate of gene duplication in *Caenorhabditis elegans**. Curr Biol, 2011. **21**(4): p. 306-10.

352. Muller, H.J., *ARTIFICIAL TRANSMUTATION OF THE GENE*. Science, 1927. **66**(1699): p. 84-7.

353. Lewis, J.A., et al., *Cholinergic receptor mutants of the nematode *Caenorhabditis elegans**. J Neurosci, 1987. **7**(10): p. 3059-71.

354. Culetto, E., et al., *The *Caenorhabditis elegans* unc-63 gene encodes a levamisole-sensitive nicotinic acetylcholine receptor alpha subunit*. J Biol Chem, 2004. **279**(41): p. 42476-83.

355. Towers, P.R., et al., *The *Caenorhabditis elegans* lev-8 gene encodes a novel type of nicotinic acetylcholine receptor alpha subunit*. J Neurochem, 2005. **93**(1): p. 1-9.

356. Boulin, T., et al., *Functional reconstitution of *Haemonchus contortus* acetylcholine receptors in *Xenopus* oocytes provides mechanistic insights into levamisole resistance*. Br J Pharmacol, 2011. **164**(5): p. 1421-32.

357. Nguyen, M., et al., **Caenorhabditis elegans* mutants resistant to inhibitors of acetylcholinesterase*. Genetics, 1995. **140**(2): p. 527-35.

358. Millar, N.S., *RIC-3: a nicotinic acetylcholine receptor chaperone*. British Journal of Pharmacology, 2008. **153**(Suppl 1): p. S177-S183.

359. Jorgensen, E.M. and S.E. Mango, *The art and design of genetic screens: *caenorhabditis elegans**. Nat Rev Genet, 2002. **3**(5): p. 356-69.

360. Ahmed, S. and J. Hodgkin, *MRT-2 checkpoint protein is required for germline immortality and telomere replication in *C. elegans**. Nature, 2000. **403**(6766): p. 159-64.

361. Kutscher, L.M. and S. Shaham, *Forward and reverse mutagenesis in *C. elegans**. WormBook, 2014: p. 1-26.

362. Flibotte, S., et al., *Whole-genome profiling of mutagenesis in *Caenorhabditis elegans**. Genetics, 2010. **185**(2): p. 431-41.

363. Gengyo-Ando, K. and S. Mitani, *Characterization of mutations induced by ethyl methanesulfonate, UV, and trimethylpsoralen in the nematode *Caenorhabditis elegans**. Biochem Biophys Res Commun, 2000. **269**(1): p. 64-9.

364. Coulondre, C. and J.H. Miller, *Genetic studies of the lac repressor. III. Additional correlation of mutational sites with specific amino acid residues*. J Mol Biol, 1977. **117**(3): p. 525-67.

365. Anderson, P., *Mutagenesis*. Methods Cell Biol, 1995. **48**: p. 31-58.

366. De Stasio, E.A. and S. Dorman, *Optimization of ENU mutagenesis of *Caenorhabditis elegans**. Mutat Res, 2001. **495**(1-2): p. 81-8.

367. Boulin, T. and O. Hobert, *From genes to function: the C. elegans genetic toolbox*. Wiley Interdiscip Rev Dev Biol, 2012. **1**(1): p. 114-37.

368. Fay, D., *Genetic mapping and manipulation: chapter 1--Introduction and basics*. WormBook, 2006: p. 1-12.

369. Fay, D., *Genetic mapping and manipulation: chapter 6--Mapping with deficiencies and duplications*. WormBook, 2006: p. 1-3.

370. Wicks, S.R., et al., *Rapid gene mapping in Caenorhabditis elegans using a high density polymorphism map*. Nat Genet, 2001. **28**(2): p. 160-4.

371. Hu, P.J., *Whole genome sequencing and the transformation of C. elegans forward genetics*. Methods, 2014. **68**(3): p. 437-40.

372. Fay, D. and A. Bender, *Genetic mapping and manipulation: chapter 4--SNPs: introduction and two-point mapping*. WormBook, 2006: p. 1-7.

373. Davis, M.W., et al., *Rapid single nucleotide polymorphism mapping in C. elegans*. BMC Genomics, 2005. **6**: p. 118.

374. Maydan, J.S., et al., *Efficient high-resolution deletion discovery in Caenorhabditis elegans by array comparative genomic hybridization*. Genome Res, 2007. **17**(3): p. 337-47.

375. Seidel, H.S., M.V. Rockman, and L. Kruglyak, *Widespread genetic incompatibility in C. elegans maintained by balancing selection*. Science, 2008. **319**(5863): p. 589-94.

376. Doitsidou, M., S. Jarriault, and R.J. Poole, *Next-Generation Sequencing-Based Approaches for Mutation Mapping and Identification in Caenorhabditis elegans*. Genetics, 2016. **204**(2): p. 451-474.

377. Kindt, K.S., et al., *Serotonin promotes G(o)-dependent neuronal migration in Caenorhabditis elegans*. Curr Biol, 2002. **12**(20): p. 1738-47.

378. Blum, E.S., A.R. Schwendeman, and S. Shaham, *PolyQ disease: misfiring of a developmental cell death program?* Trends Cell Biol, 2013. **23**(4): p. 168-74.

379. Falsone, S.F., et al., *SERF protein is a direct modifier of amyloid fiber assembly*. Cell Rep, 2012. **2**(2): p. 358-71.

380. Hope, I.A., *C. elegans: A Practical Approach*. 1999, Oxford: Oxford University Press.

381. Bustin, S.A., et al., *The MIQE guidelines: minimum information for publication of quantitative real-time PCR experiments*. Clin Chem, 2009. **55**(4): p. 611-22.

382. Hoogewijs, D., et al., *Selection and validation of a set of reliable reference genes for quantitative sod gene expression analysis in C. elegans*. BMC Mol Biol, 2008. **9**: p. 9.

383. Kim, J.K., et al., *Functional genomic analysis of RNA interference in C. elegans*. Science, 2005. **308**(5725): p. 1164-7.

384. Pulak, R., *Techniques for analysis, sorting, and dispensing of C. elegans on the COPAS flow-sorting system*. Methods Mol Biol, 2006. **351**: p. 275-86.

385. Doitsidou, M., et al., *Automated screening for mutants affecting dopaminergic-neuron specification in C. elegans*. Nat Methods, 2008. **5**(10): p. 869-72.

386. Collins, M. and A. Thrasher, *Gene therapy: progress and predictions*. Proc Biol Sci, 2015. **282**(1821): p. 20143003.

## Supplementary Table 1

Genes found to improve the ZAAT *C. elegans* mutant phenotype and their human orthologues

WormBase ID	Worm gene name	Human Orthologue ID	Human gene name
WBGene00023314	H31G24.2		
WBGene00020087	R119.1		
WBGene0001231	eif-3.H	ENSG00000147677	EIF3H
WBGene00016602	mus-81	ENSG00000172732	MUS81
WBGene00016607	C43E11.9	ENSG00000132603	NIP7
WBGene00219754	linc-85		
WBGene00020306	T07D3.3		
WBGene00002139	inx-17		
WBGene00000540	cln-3.2	ENSG00000188603	CLN3
WBGene00017854	F27C1.4		
WBGene00018908	fncm-1		
WBGene00017007	D1007.10		
WBGene00004113	pqn-24		
WBGene00007631	wht-3	ENSG00000160179	ABCG1
WBGene00018599	F48C1.6		
WBGene00003924	pas-3	ENSG00000041357	PSMA4
WBGene00022460	use-1	ENSG00000053501	USE1
WBGene00004068	pnk-1	ENSG00000157881	PANK4
WBGene00022593	ZC328.3	ENSG00000023171	GRAMD1B
WBGene00005274	srh-51		
WBGene00202057	C10G11.16		
WBGene00020414	T10E9.4		
WBGene00008412	D2030.2	ENSG00000166855	CLPX
WBGene00000084	aex-1		
WBGene00019395	K04F10.2	ENSG00000047578	KIAA0556
WBGene00005272	srh-49		
WBGene00172093	21ur-15496		
WBGene00022591	cuti-1		
WBGene00015686	C10G11.6		
WBGene00013955	kri-1	ENSG00000001631	KRIT1
WBGene00009667	F43G9.4		
WBGene00009666	slc-25A42	ENSG00000181035	SLC25A42
WBGene00008532	dpt-1	ENSG00000254986	DPP3
WBGene00014731	F02E9.8		
WBGene00001651	gon-2	ENSG00000083067	TRPM3
WBGene00008383	D1081.5		
WBGene00007706	N.A.	ENSG00000104177	MYEF2
WBGene00199495	C25A1.18		
WBGene00010327	F59C6.8		
WBGene00013927	clec-95		

WBGene00007713	C25A1.15		
WBGene00009750	F46A8.7		
WBGene00219950	F46A8.13		
WBGene00002232	kpc-1	ENSG00000115257	PCSK4
WBGene00008681	scrm-4	ENSG00000231213	PLSCR5
WBGene00013129	Y52B11A.10	ENSG00000146909	NOM1
WBGene00012102	T27F6.1		
WBGene00012038	T26E3.5		
WBGene00013137	Y53C10A.6		
WBGene00010166	gmd-2	ENSG00000112699	GMDS
WBGene00010587	sol-2		
WBGene00000165	aps-3	ENSG00000157823	AP3S2
WBGene00013200	Y54E5A.5	ENSG00000102390	PBDC1
WBGene00013693	Y105E8B.9	ENSG00000169919	GUSB
WBGene00014964	Y105E8B.10		
WBGene00012238	W04A8.3		
WBGene00009556	F39B2.5	ENSG00000170677	SOCS6
WBGene00008612	fbxa-103		
WBGene00022128	Y71F9B.6	ENSG00000149679	CABLES2
WBGene00022126	Y71F9B.2	ENSG00000144559	TAMM41
WBGene00022127	yop-1	ENSG00000129625	REEP5
WBGene00004946	sop-3		
WBGene00000237	bam-2		
WBGene00022131	Y71F9B.13		
WBGene00022121	cogc-3	ENSG00000136152	COG3
WBGene00022129	Iron-11	ENSG00000178772	CPN2
WBGene00022163	Y71G12B.28		
WBGene00017036	D1069.1		
WBGene00021030	W04H10.1		
WBGene00020796	mrpl-28	ENSG00000086504	MRPL28
WBGene00017873	F28A10.5		
WBGene00016303	fbxc-32		
WBGene00016307	fbxc-18		
WBGene00020307	T07D3.4	ENSG00000106692	FKTN
WBGene00018442	sdz-18		
WBGene00018438	btb-6		
WBGene00022564	ZC204.14		
WBGene00020357	T08E11.1		
WBGene00020363	fbxa-3		
WBGene00022563	ZC204.13		
WBGene00016717	math-22		
WBGene00018102	math-28		
WBGene00021172	Y8A9A.3		
WBGene00006002	srx-111		
WBGene00020775	T24E12.6		
WBGene00015849	C16C8.11		

WBGene00018756	plpp-1.1	ENSG00000067113	PLPP1
WBGene00016708	C46E10.2		
WBGene00044693	fbxb-92		
WBGene00086558	F12E12.12	ENSG00000087076	HSD17B14
WBGene00015842	C16C8.4		
WBGene0003665	nhr-75		
WBGene00017589	F19B10.10		
WBGene00020772	T24E12.2		
WBGene00015005	B0034.5		
WBGene00016113	eif-2D	ENSG00000143486	EIF2D
WBGene0002089	ins-6		
WBGene00019022	F58A6.1	ENSG00000104823	ECH1
WBGene0001208	egl-44	ENSG00000074219	TEAD2
WBGene00017895	vrk-1	ENSG00000105053	VRK3
WBGene0001440	fkh-8	ENSG00000198815	FOXJ3
WBGene00018251	F40H3.3		
WBGene00015797	C15F1.8		
WBGene00019906	R05G9R.1		
WBGene00016003	C18H9.5		
WBGene00000101	aka-1	ENSG00000157077	ZFYVE9
WBGene00016972	C56E6.4		
WBGene00016002	C18H9.3	ENSG00000204120	GIGYF2
WBGene00016973	abch-1		
WBGene00006832	unc-105	ENSG00000162572	SCNN1D
WBGene00000654	col-78	ENSG00000019169	MARCO
WBGene00005042	sra-16		
WBGene00007744	C26D10.3	ENSG00000121350	PYROXD1
WBGene00010913	M110.3		
WBGene00005027	sra-1		
WBGene00007421	C07H4.1		
WBGene00012421	Y9C2UA.1		
WBGene00000880	cyn-4	ENSG00000100023	PPIL2
WBGene00010992	R03D7.8	ENSG00000172531	PPP1CA
WBGene00001153	ech-4	ENSG00000198721	ECI2
WBGene00011674	cyp-13A8	ENSG00000106258	CYP3A5
WBGene00002235	kqt-3	ENSG00000053918	KCNQ1
WBGene00007836	C31C9.2	ENSG00000092621	PHGDH
WBGene00009390	F35C5.1		
WBGene00018381	F43C11.4		
WBGene00018781	F54A3.2	ENSG00000175216	CKAP5
WBGene00000901	daf-5	ENSG00000188779	SKOR1
WBGene00007245	C01G12.5	ENSG00000087076	HSD17B14

## Supplementary Table 2

Genes found to worsen the ZAAT *C. elegans* mutant phenotype and their human orthologues

WormBase ID	Worm gene name	Human Orthologue ID	Human gene name
WBGene00002134	inx-12		
WBGene00006919	vha-10	ENSG00000213760	ATP6V1G2
WBGene00018891	F55F8.3	ENSG00000275464	FP565260.1
WBGene00018993	nhr-266		
WBGene00006656	twk-1	ENSG00000164626	KCNK5
WBGene00019429	K06A5.1		
WBGene00008876	F16A11.1	ENSG00000159579	RSPRY1
WBGene00009345	F32H2.8		
WBGene00009251	F29D10.2		
WBGene00009252	F29D10.3		
WBGene00009456	F36A2.9	ENSG00000163803	PLB1
WBGene00006765	unc-29	ENSG00000170175	CHRN1
WBGene00011488	nra-2	ENSG00000125912	NCLN
WBGene00013604	Y87G2A.18	ENSG00000089486	CDIP1
WBGene00013601	Y87G2A.13	ENSG00000064545	TMEM161A
WBGene00012386	agef-1	ENSG00000066777	ARFGEF1
WBGene00012103	clec-12	ENSG00000163815	CLEC3B
WBGene00007654	C17H1.1		
WBGene00022144	pghm-1	ENSG00000145730	PAM
WBGene00001814	haf-4	ENSG00000250264	AL669918.1
WBGene00007009	wwp-1	ENSG00000123124	WWP1
WBGene00022202	Y72A10A.1		
WBGene00019279	K01A2.4		
WBGene00019282	mps-2		
WBGene00016811	C50D2.8	ENSG00000108848	LUC7L3
WBGene00020308	T07D3.5		
WBGene00015646	mlt-10		
WBGene00000034	abu-11		
WBGene00006611	tre-5	ENSG00000118094	TREH
WBGene00022283	lgc-27	ENSG00000120903	CHRNA2
WBGene00174962	21ur-10128		
WBGene00004737	scc-1	ENSG00000164754	RAD21
WBGene00022650	ZK84.2		
WBGene00005070	srp-5		
WBGene00200157	C27D6.13		
WBGene00019087	F59A6.5	ENSG00000122966	CIT
WBGene00017392	basl-2		
WBGene00022760	ZK546.3		
WBGene00020583	T19D12.9		
WBGene00014910	Y51B9A.t1		

WBGene00013087	Y51B9A.5		
WBGene00173449	21ur-13955		
WBGene00201542	Y51B9A.13		
WBGene00011159	chil-17		
WBGene00014244	ZK1307.1		
WBGene00003785	nos-3		
WBGene00000114	alh-8	ENSG00000119711	ALDH6A1
WBGene00010990	tceb-3	ENSG00000183791	ELOA3
WBGene00001586	ggr-1	ENSG00000145888	GLRA1
WBGene00007556	C14A4.3	ENSG00000086848	ALG9
WBGene00004945	sop-2		
WBGene00206479	C44C11.6		
WBGene00012722	Y39G8B.1	ENSG00000151632	AKR1C2
WBGene00021785	Y51H7C.7	ENSG00000197223	C1D
WBGene00001247	elo-9	ENSG00000119915	ELOVL3

### Supplementary Table 3

Gene hits identified from other RNAi screens on *C. elegans* models of protein misfolding disorders

Wang et al. (2009)	Nollen et al. (2004)	van Ham et al. (2008)	Kraemer et al. (2006)	O'Reilly et al. (2014)
hsf-1	alg-1	cdh-7	Y38H8A.3	B0218.5
C30C11.4	phi-2	rcq-5	C09D4.3	age-1
dnj-19	phi-3	mcm-7	F52B5.2	B0393.6
F08H9.4	hel-1	pri-2	Y18D10A.5	bre-3
stc-1	mog-5	col-139	T17E9.1	baf-1
CCT-4	phi-4	vha-15 (phi-52)	F38H4.9	tag-342
CCT-5	phi-5	ndx-4	F48E8.5	tes-1
W07G4.4	phi-6	cyp-34A7	K09C6.8	otub-4
sel-10	phi-7	sulp-6	R74.3	jud-4
rbx-1	phi-8	fbp-1	K09C4.3b	adm-2
C27A12.6	phi-9	spp-10	Y53C10A.12	nuc-1
Y54E10BR.4	phi-10	lpd-6	F26D10.3	lin-39
F30A10.10	prp-8	paf-1	T09B4.10	rpl-21
uba-2	phi-11	lagr-1	T20D3.6	lec-9
ubc-9	phi-12	math-24	F31D4.3	C17C3.5
gei-17	phi-13	ymel-1	F46G10.3	cab-1
C05C8.7	sap-49	ubc-12	F53F8.1	rege-1
R10D12.10	snr-1	fbxb-93	C14C11.6	C33A12.3
H18N23.2	snr-2	efk-1	K10C8.1	exc-5
T09B4.1	snr-3	puf-4	T22A3.5	gop-3
F13H10.4	snr-4	srb-2	F53B6.4	atgp-2
fut-4	snr-5	rsp-7	F31E8.6	ire-1
bli-3	snr-7	mdt-17	F38H4.7	bicd-1

pdi-2	uaf-2	uaf-2	T24C4.1	sams-1
C30H7.2	phi-14	Y48G1A_53.a	F56H1.5	bath-42
dbl-1	ama-1	str-13	F21F8.3	unc-79
dat-1	lpd-1	srbc-59	Y102A5C.8	prmn-1
srd-56	skp-1	mab-20	Y37A1B.15	mob-2
trpa-1	nhr-23	ZK355.h	F11C7.3	F10E7.11
rrc-1	nhr-61	let-2	C13D9.8	sri-65
nhr-119	hlh-13	spe-26	F47G6.1	dmd-6
acy-3	lir-1	sir-2.1	D2030.10	F14D2.2
H43I07.2	mep-1	ins-28	T05C12.2	pab-2
Y65B4A.1	ntl-1	hgrs-1 (pqn-9)	E01A2.3	F21D5.3
C23H3.3	phi-15		B0511.12	tag-353
rsp-2	phi-16		C07G1.5	F28B12.1
lsm-3	cky-1		C42C1.15	F31D4.8
emb-4	gei-13		M04G12.3	acs-4
Y71H10B.1	egl-45		F55F3.2	odr-8
ZK54.1	eif-2		C24A11.9	btb-16
F53F1.2	eif-3		F47G4.7	hrp-1
H12D21.4	phi-17		B0304.3	rps-8
C01G12.8	phi-18		LLC1.3	alg-1
C06E4.6	eft-1		C37H5.3	str-223
top-1	eft-2		F10D2.9	F53H1.4
div-1	eft-4		K12B6.2	ztf-1
his-6	phi-19		F47G6.3	fut-3
his-8	phi-20		Y18D10A.1	H06I04.3
col-158	phi-21		C50E3.12	ubl-1
col-176	lpd-7		B0310.6	H32C10.1
W02A11.1	rpl-2		W06B11.3	bcat-1
pqn-68	rpl-5		F31B12.2	nhr-88
rab-11.2	rpl-6		C04B4.2	K08D10.1
tba-8	rpl-7		C03B1.2	nhr-71
pha-4	phi-22		T18D3.6	K11H12.8
pqn-38	rpl-8		R106.1	sago-1
C26E1.2	rpl-10		C30G4.2	abl-1
Y57A10B.6	rpl-11		Y52B11B.1	aak-1
T20D3.3	rpl-13		Y53H1C.3	vdac-1
R144.3	rpl-14		C24H12.9	R08C7.1
F38E11.6	rpl-15		F34D6.5	R08C7.12
nrf-6	rpl-17		F52C6.6	R09F10.3
lpd-3	rpl-18		F55C12.7	cls-2
T25G12.3	rpl-19		T28D9.11	daf-16
F44E5.3	rpl-20		F59G1.2	got-1.2
lin-42	rpl-21		B0513.6	hum-5
T20D3.6	rpl-22		C32H11.3	T03F6.3
C29E6.4	rpl-23		F36H1.4	kgb-1
R04E5.7	rpl-24		T04C9.3	T07A9.8

K09B11.3	rpl-26		R13A1.8	T07E3.4
T07C4.3	rpl-31		C03G6.5	sri-43
fbxb-54	rpl-35		H14N18.3	T14G8.4
C16C8.13	rpl-39		R02D5.3	T19D12.1
C18E9.7	rpl-42		Y113G7B.4	T20B12.3
C47G2.5	rpa-0		C56E6.1	pygl-1
lin-49	rps-5		C56E6.1	nol-58
mdt-17	rps-1			sknr-1
F09C8.2	rps-0			W03G1.5
H40L08.3	rps-3			cacn-1
F56C11.5	rps-2			nhr-41
F56G4.4	rps-10			mat-1
	rps-12			sec-23
	rps-14			pap-1
	rps-15			mrg-1
	rps-16			clec-8
	rps-18			orc-4
	rps-19			Y39B6A.27
	rps-21			tgt-2
	rps-26			hrpu-1
	ars-2			Y43F8B.12
	cct-1			snrp-200
	cct-2			nlp-21
	cct-4			cdh-12
	cct-5			Y75B7B.2
	cct-6			acs-5
	cct-7			fbxa-19
	hsp-1			pals-17
	hsp-6			daf-41
	rme-8			npr-29
	phi-23			dve-1
	ran-1			sar-1
	ran-4			srh-209
	imb-3			ppg-3
	imb-5			ZK512.1
	npp-8			
	tbb-2			
	act-2			
	act-4			
	dhc-1			
	tba-1			
	tba-2			
	phi-24			
	phi-25			
	apt-1			
	apt-3			

	rab-1			
	rab-5			
	tfg-1			
	nsf-1			
	phi-26			
	phi-27			
	phi-28			
	phi-29			
	phi-30			
	phi-31			
	pas-4			
	pas-6			
	pbs-1			
	pbs-2			
	pbs-3			
	pbs-4			
	pbs-5			
	rpn-6			
	rpn-8			
	rpn-11			
	rpt-5			
	phi-32			
	uba-1			
	phi-33			
	ptc-1			
	ptc-3			
	acn-1			
	lit-1			
	vha-12			
	dab-1			
	phi-34			
	phi-35			
	phi-36			
	asb-2			
	atp-2			
	phi-37			
	phi-38			
	phi-39			
	phi-40			
	phi-41			
	dpy-14			
	let-767			
	phi-42			
	phi-43			
	phi-44			
	phi-45			

	bli-3			
	phi-46			
	phi-47			
	phi-48			
	phi-49			
	phi-50			
	phi-51			
	vha-5			
	vha-6			
	vha-8			
	phi-52			
	phi-53			
	phi-54			
	phi-55			
	phi-56			
	phi-57			
	phi-58			
	phi-59			
	phi-60			
	phi-61			
	phi-62			
	phi-63			
	sym-5			
	ama-1			
	ama-1			
	frs-2			
	frs-2			